Studies of the growth, structure and some electrical properties of heavy rare earth dihydride films.

by

Mohammad Sayeedur Rahman Khan

A thesis submitted for the degree of Doctor of Philosophy in the University of London.

Department of Physics
Royal Holloway College

July, 1976.

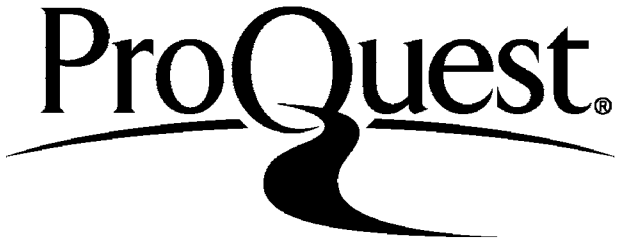

A B S T R A C T

Conditions have been established for the epitaxial growth, by vacuum evaporation at 10^{-6} torr, of single crystal films of the dihydrides of gadolinium, terbium, dysprosium, holmium and erbium, on the cube, dodecahedral and octahedral faces of rock salt. The film structures have been investigated by electron microscopy and diffraction. Lattice parameter measurements on single crystal and polycrystalline specimens indicate that thin films($<200\text{Å}$) are face-centred-cubic dihydrides whereas thick films($>900\text{Å}$) are dominated by hexagonal close-packed metallic structure. Films of intermediate thickness exhibit a mixed (f.c.c. dihydride and h.c.p. metal) phase.

The effects, on the structure of Gd and Tb dihydride films, of such parameters as substrate nature and temperature, vacuum environment, annealing and hydrogen treatment have been studied. Some nucleation and decoration studies have been conducted for gadolinium and terbium dihydrides.

The electrical resistivity and temperature coefficient of resistance of polycrystalline films of the dihydrides of gadolinium, terbium, dysprosium, holmium and erbium, grown on glass slides, have been measured in vacuo. Resistivity measurements on the dihydride films, made in the temperature range $77^{\circ}K$ to $573^{\circ}K$ indicate generally metallic conduction characteristics. Studies of the changes of resistivity on annealing the dihydride films in the presence of a stream of hydrogen gas support the conclusion that the films become converted to semiconducting trihydrides having negative temperature coefficient of resistance.

INTRODUCTORY REMARKS

The main objectives of the work described in this thesis were to

i) study the structural change with thickness of the various hydride films in the range 80 - 1000Å, grown from heavy rare earth metals,

ii) establish the conditions for growing epitaxial single crystal films,

iii) measure the resistivity and temperature coefficient of resistance, in situ, of the films 'as grown' and when treated with hydrogen and finally

iv) correlate the structural studies with the resistivity measurements.

Chapter 1 describes the existing theories of epitaxy and nucleation. The structures and non-stoichiometry of heavy rare earth dihydrides are discussed in chapter 2. Chapter 3 describes the theory of electrical conduction in thin films and reviews the reported work on electrical properties of rare earth dihydrides. The preparation of epitaxial single crystal dihydride films of Gd, Tb, Dy, Ho and Er is described in chapter 4. Chapter 5 describes the structures of the films grown from Gd, Tb, Dy, Ho and Er. The investigations of some growth parameters of GdH_2 and TbH_2 films are reported in chapter 6. Chapter 7 describes the experimental details of the electrical measurements of the films. The electrical resistivity and temperature coefficient of resistance of the films grown from Gd, Tb, Dy, Ho and Er are discussed in chapter 8. Chapter 9 comprises the conclusions, discussions and suggestions for further work.

ACKNOWLEDGEMENTS

I wish to express my gratitude to Dr. R.F. Miller for his supervision, guidance, encouragement and helpful discussions throughout the course of this work. My thanks are also due to Mr. R.P. May, Mr. M. Thyer and Mr. J. Williams of the technical staff of the Physics Department, Royal Holloway College. I would like to thank Mr. R.B. Inwood for supplying me some gadolinium and terbium films grown in ultra high vacuum system.

I am indebted to my parent organisation, University of Rajshahi (Bangladesh) for granting me study leave and also to The British Council for awarding me the scholarship under the Technical Assistance Training Scheme. Mrs. M.J. Delancy also deserves my thanks for typing the thesis.

I wish to thank my wife KUMU for patiently helping me in the preparation of readable manuscript and drawing some of the graphs. Finally I must express my deepest sympathy for my little daughter 'KASHFI', who missed all the parental love and affections during the long period of her isolation.

CONTENTS

Page

Page

CHAPTER 1.

THEORIES OF EPITAXY AND NUCLEATION

1.1. Introduction

The phenomenon of epitaxy has been known for over a century and is the basis of the most commonly used process that leads to the growth of single crystalline films. The term epitaxy ("arrangement on") was introduced by Royer (1928) to denote the phenomenon of the oriented or single crystalline growth of one crystal upon another such that there exist crystallographic relations between the overgrowth and the substrate. An epitaxial film is a single crystal or well oriented collection of crystallites, in the form of thin films, grown by the deposition of the material of interest on to a substrate of different material. In general, the substrate will itself be a single crystal or well oriented assembly of crystallites.

Interest in epitaxy was first aroused when it was noticed by mineralogists that two different naturally occuring crystal species sometimes grew together with some definite and unique orientation relationship, as revealed by their external forms. These observations led to attempts to reproduce the effect artificially, during crystal growth from solution, and the first recorded successful attempts was reported by Frankenheim (1836), who demonstrated the now well-known case of the parallel oriented growth of sodium nitrate on calcite. The other means of the crystal growth by which epitaxy can be produced in the laboratory are, electrodeposition (Cochrane, 1936), chemical action

(Aminoff and Broome, 1936), sputtering (Finch and Quarrell, 1933), condensation from the vapour phase (Bruck, 1936). The later technique, especially in the form of vacuum deposition, has proved to have wide application and is the most commonly used technique today.

In early days, the subject of epitaxy was restricted because the crystals had to be grown (growth from solution was the only readily available technique for preparing samples) such that their orientation could be determined by optical microscopy, which was the only observational technique available, and the understanding of a crystal structure was very rudimentary, since there were no techniques available for structure analysis. But with the discovery of X-ray diffraction in 1912 and electron diffraction in 1927, further progress in this subject has been dominated by the influence of a succession of new experimental techniques, especially those for making structural observations on crystals. Although Davisson and Germer (1927) started with low energy electron diffraction (LEED), Thomson and Reid (1927) initiated the high energy electron diffraction (HEED), which was by far the more practical technique and began to be applied to the study of epitaxy. HEED involved reflection diffraction (RHEED) as well as transmission through thin films. The advantages of electron diffraction were quite clear. First, it was possible to examine extremely thin layers of overgrowths prepared by a variety of methods. Second, orientation could be determined from internal crystal structure rather than external morphology. With the appearance of new and improved electron microscopes in the mid 1950s, the study of epitaxy was given a completely new

impetus. By means of transmission technique (TEM), it was possible to obtain a wealth of new information on the nucleation, growth and structure of thin films. Comprehensive reviews of the electron microscope work on epitaxy have been given by Pashley (1956, 1965), Matthews (1967) and recently by Pashley (1975).

1.2. Theories of Epitaxy.

The occurrence of epitaxy in thin films has received considerable theoretical treatment which can broadly be classified into two groups: (1) older theories, based on the geometrical fittings between the lattices of the deposit and the substrate and (2) current theories, based on the nucleation process. A critical review of the older theories is given by Pashley (1956). A brief discussion of the various theories is given below.

1.2.1. Older Theories

Royer (1928) put forward a set of rules for epitaxy and stated that epitaxy requires a small misfit between the deposit film and the substrate. The percentage misfit is expressed as 100 (b-a)/a, where a and b represent the network spacings in the substrate and the film, respectively. This misfit rule is not generally valid, since there are numerous examples of epitaxy occurring with very large misfits (Schulz, 1951, 1952). The general conclusion is that a small misfit may be important but is not an essential condition for epitaxy. Menzer (1938) attempted to explain the occurrence of epitaxy with large misfits by a mechanism based on the concept that an epitaxial layer corresponding to a good fit occurs during the initial growth stage, and subsequent growth gives rise to different orientations. However,

other examples such as Kirchner (1938), Uyeda (1942), Raether (1946, 1951) prove the invalidity of this concept.

The theory put forward by Bruck (1936) and Engel (1952, 1953) postulates that there exists a minimum epitaxial temperature, for complete epitaxy and that the occurrence of orientation depends upon the misfit between the film and the substrate. This theory also has no general validity, since the results on epitaxy (Pashley, 1959) indicate that the epitaxial temperature for a particular film-substrate system varies over a wide range depending upon the conditions of film formation.

According to the Frank and Van der Merwe (1949 a,b) theory, the initial stage of growth of an epitaxial film is the formation of an immobile monolayer, homogeneously deformed to fit on the substrate so as to have the same spacing as the substrate. This is called a 'Pseudomorphic monolayer' and is said to occur provided the misfit is less than a certain critical value, i.e. about 14%. Once this epitaxial monolayer forms, a thick epitaxial film can then grow by repetition of the process, the lattice deformation reducing with successive layers. This pseudomorphic film would undergo some transition at a certain growth stage to give a strain-free bulk deposit which would remain epitaxial. A critical discussion by Pashley (1956) has shown that the concept of pseudomorphism has no valid experimental confirmation, since various investigators have reported for and against the concept. For example, Cochrane (1936) observed the evidence of modified spacings in electrodeposited layers of nickel and cobalt on single

crystals of copper and Miyake (1938) also found the similar results for Sb_2O_4 formed on stibnite (Sb_2S_3), and both of them attributed this as the effects of pseudomorphic growth. On the other hand, the works of Finch and Quarrell (1933), Lucas (1951) and Newman and Pashley (1955) proved against the above concept. At a later stage also the same conflicting results persisted. Jones (1965) has shown by field-emission microscopy that the first few atomic layers of cobalt deposit on tungsten in ultra-high vacuum (uhv) are pseudomorphic and Jesser and Matthews (1967) also produced the evidence for the pseudomorphic growth of iron and cobalt on copper (001) surface and chromium on nickel (001) surface in uhv. However, these results are in contradiction with those of Schlier and Farnsworth (1968) who found no evidence of such a layer by the LEED technique. Newman and Pashley (1955) and Freedman (1962) observed that although the film material becomes strained, its lattice parameters do not exactly match those of the corresponding unstrained bulk material.

1.2.2. Current Theories

The theories discussed above do not provide adequate explanation of epitaxial growth, since they are all based on unsuitable models for the growth of the initial nuclei of the deposit. The general current concepts of epitaxial film growth in the light of nucleation theory are described below.

Pashley (1956) recognised the importance of nucleation in the epitaxial growth of thin films in his critical discussion of the theories of epitaxy. He pointed out that the occurrence of epitaxy depends upon the formation of oriented nuclei, and that

a detailed understanding of epitaxial process depends upon the factors controlling the orientation of these nuclei. Hirth and Pound (1963 a,b) and Hirth etal (1964) have dealt with the theory of capillarity model for heterogeneous nucleation and have considered the relation of nucleation theory to epitaxy. They have predicted that the orientations of the nuclei are not the critical requirements for epitaxy of thin films. The critical requirement is that a particular orientation has a lower free energy of formation (and hence occurs in greatest numbers) and a much higher nucleation rate than any other orientation. It is suggested that high substrate temperatures and low supersaturations are the requisites for epitaxy.

Moazed (1966) has considered the application of the theory of heterogeneous nucleation to epitaxy, and has shown that the main conditions in heterogenous nucleation which lead to epitaxial nucleus formation are:

i. High substrate temperatures - a decrease in substrate temperature decreases the ratio of epitaxial nucleation rate to random nucleation rate.

ii. Low supersaturations - at low supersaturations only preferred sites can act as nucleation sites, while at high supersaturations, random nucleation is more likely.

The capillarity model nucleation theory has proved to be satisfactory for experimental conditions where the critical nucleus is large. There are many cases, however, involving the condensation of vapours on solid surfaces, where the critical nucleus may involve only a few atoms. It is then desirable to use the atomistic model of nucleation for the interpretation of

nucleation effects. Rhodin and Walton (1962, 1964), Walton etal (1963), Walton (1962 a,b) and Rhodin (1966) have extended the nucleation theory to include very small nuclei by treating the clusters as simple macromolecules and they conclude that the nucleus with the fewest atoms has the highest probability of being stable. It is shown that the critical nucleus for a (111) stable orientation is just a pair of adsorbed stoms, for a (100) orientation it is three atoms, and for the rarely observed (110) orientation it is four atoms. This explains why (100) and (111) orientation occur in the f.c.c. metals when grown on rock salt. Rhodin and Walton (1964) and Shirai and Fukada (1962) have considered that there are at least two mechanisms by which a particular orientation may be favoured:

i. The critical nucleus which leads to the orientation is adsorbed more strongly than any other.

ii. The critical nucleus which leads to some other orientation is strongly and energetically favoured, but subsequent growth of the cluster requires the addition of atoms in unfavourable positions. Thus a deposit with the orientation can nucleate but may not be able to grow.

It appears that a most likely mechanism for favouring one of two equally probable orientations of nuclei is by preferential recrystallization during coalescence. The experimental results of Matthews (1965) support this view point. In situ electron microscopy studies by Pashley etal (1964) and Pashley (1965) have demonstrated the mode of nucleation and the way in which the nuclei develop into a continuous film. The observations have

revealed two important process - "liquid-like" coalescence of nuclei and islands, and recrystallization of islands. It is seen that recrystallization occurs during coalescence of nuclei and islands, and the orientation of the initial nuclei therefore plays a determining role in the final film orientation.

The theoretical treatments of the preceding sections indicate that the following factors which contribute to the formation of epitaxial films should be given careful consideration:

i. Nucleation orientation: initial occurrence of a large number of one type of nuclei with a high growth rate.

ii. Growth orientation: initially there may be many types of nuclei, but a preferred rate of growth of one type may dominate the final film orientation.

iii. Recrystallization: This process occurs after initial nucleation and growth, leading to a film structure with a state of lower free energy. The orientation of the initial nuclei will therefore have a dominant role in providing the final orientation.

It is expected that epitaxy will occur by the combination of these processes. The contribution of the preferred nucleation and growth of structured nuclei to epitaxial growth as proposed by Rhodin and Walton (1962, 1964) appears to be generally applicable. However, the contribution of preferred recrystallization during coalescence to epitaxial-film formation (Pashley 1965 and Pashley et al, 1964), may be considered to be a more important factor than that proposed by Rhodin and Walton. Although these treatments are not quite adequate to explain all the experimentally observed features of epitaxial-film growth, they seem to provide a valuable basis

for developing a more detailed understanding of the epitaxial growth process.

1.3. Conditions for epitaxial-film formation.

As indicated before, a small misfit is important but not an essential criterion for the occurence of epitaxy. In epitaxial growth, a well-defined crystal plane of the deposit grows parallel to the exposed plane of the substrate. If the substrate surface is faceted, the overgrowth will grow parallel to the facets. A match of symmetry at the film-substrate interface is an important factor in determining what orientation is preferred, although sometimes symmetries are not matched; e.g. a threefold symmetrical (111) plane can grow on a fourfold (100) substrate plane. In many cases the observed orientation is not that which corresponds to the best possible geometrical fitting along one lattice row at the film-substrate interface. This is the general situation with regard to the fit between the crystal lattices of the film and the substrate. In order to obtain epitaxy, it is necessary to control deposition parameters as well as the substrate parameters. The important substrate and deposition parameters that must be optimized for the growth of epitaxial single-crystal films will be considered in the following sections.

1.4. Nature of Substrate.

It is necessary to use single crystalline substrates for the epitaxial-film growth. The choice of the substrates is dictated by a number of factors, such as (a) compatibility of crystal structure, i.e. crystal symmetry, crystal orientation, and lattice parameter; (b) freedom from surface strain and cleavage steps; (c) chemical inertness at deposition temperature; and (d)

compatibility of thermal-expansion coefficients between the film material and the substrate. There are however, exceptions to most of these conditions; e.g. (i) f.c.c. metals can be grown on mica, and (ii) cleavage steps enhance nucleation (Rhodin 1966).

The substrate preparation can have an important influence on epitaxial temperature and film orientation. Important factors to be considered include substrate orientation, surface topography and surface cleanliness. Surface topography such as surface steps or microfacets can have a direct influence on film orientation. However, it has not been conclusively shown that they have a determining role in epitaxy. Basset etal (1959) have shown that there is no difference in orientation between gold nuclei formed on steps on rock salt and those formed in between the steps. Epitaxial temperatures vary, depending upon whether the substrate is cleaved in air or in ultra-high vacuum (Sella and Trillat, 1964).

1.5. Substrate Temperature.

Bruck (1936) concluded, from experiments on f.c.c. metals and rock salt, that there is a critical substrate temperature below which perfect epitaxy cannot occur. However, it is now generally recognised that the epitaxial temperature varies widely for different film-substrate combinations, and is influenced by other variables such as substrate surface preparation, deposition rate, and surface contamination (Jaunet and Sella 1964, Stirland 1966, and Matthews, 1965). The substrate temperature together with the deposition rate is sometimes involved in determining whether a film is single crystalline, polycrystalline, or amorphous.

Increasing the substrate temperature cleans the substrate surface by the desorption of contaminants, and provides the activation energy required for the deposited atoms to take up positions for alignment with the substrate lattice. Higher temperature also increases the surface and volume diffusion for accommodating the misfits which develop when neighbouring nuclei grow together. In general, increasing the substrate temperature improves epitaxy for a variety of film-substrate combinations, and for various methods of film formation. Since the film growth is influenced by many deposition parameters, it is difficult to define a precise value for the epitaxial temperature.

1.6. Deposition rate and film thickness.

The temperature at which epitaxy occurs is dependent on the deposition rate. It decreases with increasing rate. A higher deposition rate can lead to a rise in substrate temperature, thus favouring epitaxy, and can have effect on the coalescence of nuclei, as shown by Matthews (1965). As agglomeration increases, the film becomes electrically continuous at a higher average thickness called the critical thickness. The critical thickness increases with the deposition rate but approaches a constant value at sufficiently high rates when high supersaturations produces more stable nuclei because of interaction between vapour atoms (Chopra and Randlett, 1968). At a slower rate, the gas content of the film may be thickness dependent, and can result in a higher ratio of contamination to the film, which could favour epitaxy (Shinozaki and Sato, 1965 and Matthews, 1965).

In epitaxial deposition, an orientation is usually maintained up to a certain thickness beyond which further deposition leads to poor orientation and eventually random orientation (Spielmann, 1965 and Khan, 1969). The loss of good orientation is due to the development of twins, stacking faults, and other defects, which are not generally present in the initial stages. The orientation can, however, improve with increasing film thickness, as has been shown in the growth of silver on mica (Pashley 1959, Matthews, 1962). This improvement in orientation is ascribed to reorientation of the initial nuclei.

1.7. Contamination.

The presence of impurities in a vacuum system has a strong influence on epitaxial growth of thin films. The main sources of contamination are contaminants brought into the system on the substrate surface, residual contaminant gases as vapours in the vacuum system, and gases released from the source material or the heater material. An important effect of contamination is the loss of adequate adherence of the deposited film. Contamination of a clean surface by exposure to air has been shown to influence the orientation of an epitaxial film. The effect of contamination is to increase the number of initial nuclei, which causes them to coalescence early in film growth, thereby influencing the orientation of a continuous film (Matthews, 1965a, 1965b, Matthews and Grunbaum, 1964 and Matthews, 1966). Minute amounts of any contamination may influence the nucleation behaviour of thin film.

It can be concluded from the preceding sections that any theory of epitaxy must explain the following experimental facts:

(a) A particular value of lattice misfit or the best-fit geometrical matching of lattice is neither a necessary nor a sufficient condition. (b) Pseudomorphism or constraining of the lattice of the deposit by the substrate, if present, is not required for obtaining epitaxial growth. (c) Epitaxy appears at the earliest stages of film growth by three dimensional nucleation, although orientation changes with subsequent growth may also result by reorientation or recrystallization on coalescence of differently oriented nuclei. (d) For a given material and suitable deposition conditions such as low rate and high deposition temperature, epitaxy or at least partial epitaxy is generally possible on single crystal substrates of a variety of crystal structures and different types of atomic bonds. The orientation, degree of perfection, vary with different substrate materials for the same deposit and vice versa.

1.8. Theory of Nucleation.

In general, there are two processes into which this topic is normally divided, namely homogeneous and heterogeneous nucleation. The former refers to nucleation which takes place at random within a phase. However, it is found that nuclei form preferentially at free surfaces within the system, the surface acting as catalysts; the process is known as heterogeneous nucleation. Since it is obvious that the deposition of thin films upon a substrate as used in the work reported in this thesis is governed by heterogeneous nucleation, the theory of homogeneous nucleation is just touched as a preliminary. Heterogeneous nucleation theory can be explained on the basis of two important models: the capillarity model and the atomistic model.

1.8.1. Heterogeneous nucleation theory based on capillarity model.

A homogeneous nucleation theory which takes into account the total free energy of formation of a cluster of adatoms was postulated by Volmer and Weber (1925), and Becker and Doring (1935). It was later extended to heterogeneous nucleation by Volmer (1939) and to the particular shapes of clusters in a thin film case by Pound etal (1954, 1963). In this theory, clusters (also called embryos, or subcritical nuclei) are formed by collisions of adatoms on the substrate surface, and in the vapour phase if supersaturation is sufficiently high. They develop initially with an increase in free energy until a critical size is reached, above which growth continues with a decrease in free energy. If one assumes that bulk thermodynamical quantities can be ascribed to the properties of clusters, the Gibbs free energy of formation of a spherical cluster of radius r, given by the sum of the surface energy (to create a surface) and the volume energy of condensation, is

$$\Delta G_0 = 4\pi r^2 \sigma_{cv} + \frac{4}{3}\pi r^3 \Delta G_v \quad \ldots\ldots\ldots\ldots (1)$$

Here, σ_{cv} is the condensate-vapour interfacial free energy and $\Delta G_v = \left(\frac{-KT}{V}\right) \ln \left(\frac{p}{pe}\right)$ is the Gibbs free energy difference per unit volume of phase of molecular volume V condensed from the supersaturated vapour of pressure p to the equilibrium pressure pe ($p/pe \equiv S$ is the supersaturation), the value r^* corresponding to the critical nucleus, is determined by maximizing (1) to give

$$r^* = \frac{-2\sigma_{cv}}{\Delta G_v} = \frac{2\sigma_{cv} V}{KT \ln\left(\frac{p}{pe}\right)} \quad \ldots\ldots\ldots\ldots (2)$$

This is the radius of the critical nucleus clusters smaller than

r^* are unstable, while larger aggregates grow to become stable deposits.

If the critical nucleus is cap-shaped, its contact angle in a condensate (c) - vapour (v) - substrate (s) system is determined by Young's equation for the minimization of the surface free energies

$$\sigma_{cv}\cos\theta = \sigma_{sv} - \sigma_{sc} \quad \ldots\ldots\ldots\ldots\ldots (3)$$

By rewriting Gibbs free energy term ΔG_v in terms of the various surface energies, one obtains

$$\Delta G_o = \frac{1}{3}\pi r^3 \Delta G_v (2 - 3\cos\theta + \cos^3\theta) + 2(1 - \cos\theta)\pi r^2 \sigma_{cv}$$

$$+ \pi r^2 \sin\theta (\sigma_{sc} - \sigma_{sv}) \quad \ldots\ldots\ldots\ldots\ldots (4)$$

The value of r^* is still given by equ. (2) for any value of $\theta > 0$. The critical value of ΔG_o is now given by

$$\Delta G^* = \frac{16}{3}\pi \frac{\sigma_{cv}^3}{\Delta G_v^2} \phi(\theta) \quad \ldots\ldots\ldots\ldots\ldots (5)$$

where $\phi(\theta) = \frac{1}{4}(2 - 3\cos\theta + \cos^3\theta)$.

It has been noted that with increasing supersaturation (e.g., with higher melting point materials and lower substrate temperature, r^* decreases ; that is a large number of smaller-sized stable nuclei are formed. This variation is, however, insignificant since, on the basis of the present theory, the calculated value of r^* for most cases is of atomic dimensions.

When $\theta = 0$, $\Delta G^* = 0$, so that there is no activation barrier to the nucleation of the condensed phase. For $\theta = 180^\circ$, $\phi(\theta) = 1$, and the foreign interface is inactive in the nucleation process, ΔG^* is dependent on θ. Chakraverty and Pound (1964)

showed that for $\theta < 45^0$, and $50^0 < \theta < 105^0$, clusters will form, with a smaller ΔG^*, at steps rather than on the flat surfaces. Thus, the concentration of critical nuclei at steps would be increased relative to that on flat surfaces, yielding the well known surface decoration effect. Electrostatic charges present on the vapour atoms or adsorption sites may also lower ΔG^*, thus facilitating the condensation process.

The nucleation rate I is proportional to the product of the concentration, $N^* = No \exp(-\Delta G^*/KT)$, of the critical nuclei, and the rate Γ at which molecules join the critical nuclei by a diffusion process. Here, No is the density of adsorption sites. Thus,

$$I = Z\,(2\pi r^* \sin\theta)\,\Gamma\, N^* \qquad \ldots\ldots\ldots\ldots\ldots\ldots(6)$$

where $2\pi r^* \sin\theta$ is the periphery of the critical nucleus and Z is the Zeldovich correction factor to take into account the departure from equilibrium due to nucleation and the fact that some of the nuclei would decay. Now, the diffusion process yields

$$\Gamma = N_1 a_0 \nu' \exp\left(\frac{Qd}{KT}\right) \qquad \ldots\ldots\ldots\ldots\ldots\ldots(7)$$

where a_0 is the separation between adsorption sites, ν' is a frequency of the order 10^{12} per sec, Qd is the activation energy for surface diffusion, and N_1 is the density of adatoms defined by $N_1 = R\tau_s$ (τ_s is the mean stay time of adatom), so that

$$N_1 = \frac{R}{\nu} \exp\left(\frac{Qdes}{KT}\right) \qquad \ldots\ldots\ldots\ldots\ldots\ldots(8)$$

Here, R is the rate of incidence of single atoms from the vapour (called "impingement flux") and Qdes is the energy of desorption of single atoms from the substrate. If we assume $\nu \sim \nu'$, we obtain the following expression for I by using equs. (6), (7), and (8),

$$I = \frac{4\pi b_{cv}}{\Delta G_v} \sin\theta \, R a_o N_o \exp\left(\frac{Q_{des} - Q_d - \Delta G^*}{KT}\right) \text{ --------- (9)}$$

1.8.2. Heterogeneous nucleation theory based on atomistic model.

The size of the critical nucleus, as suggested by the capillarity theory, is typically of atomic dimensions involving a few atoms, consequently, the applicability of the capillarity model and the use of bulk thermodynamical quantities for such small clusters are questionable. These difficulties may be overcome by writing the partition functions and potential energies for the reacting species and products. An approximate analysis which considered the energies and bonds of nucleation clusters treated as macromolecules was given by Walton and Rhodin (1963, 1964). Accordingly, at low substrate temperatures or very high supersaturations, the critical nuclus may be a single atom which will form a pair with another atom by random occurrence to become a stable cluster and grow spontaneously. The stability of a pair is derived from an assumed one bond per atom. At higher substrate temperature, a pair of atoms may no longer be a stable cluster.

The nucleation rate in this theory is again proportional to $N^*\Gamma$. If one assumes that the vibrational partition functions are unity, and takes En as the energy required to dissociate the n-adatom cluster into n single atoms adsorbed on the surface, the general expression for the nucleation rate of critical nuclei with n* atoms is

$$I = R a_o^2 N_o \left(\frac{R}{\nu N_o}\right)^{n^*} \exp\left[\frac{(n^*+1) Q_{des} - Q_d + E_{n^*}}{KT}\right] \text{ ---- (10)}$$

It is noted that, with increasing size (i.e. n*) of the critical nucleus, the nucleation rate and temperature dependence increases

as R^{n^*+1}. A stability transition from an n* to an n*+1 atom cluster with increasing substrate temperature may be found by equating the two corresponding expressions in equ. (10). For example, a transition from a 2- to a 3-atom cluster occurs at

$$T = \frac{Q_{des} + \frac{1}{2} E_3}{K \ln(R/\nu) N_o} \qquad \ldots\ldots\ldots\ldots\ldots\ldots (11)$$

In view of the similarity of the basic principles, it is not surprising to find a similarity between equs. (9) and (10) of the capillarity and the atomistic models, respectively. By applying macroscopic data to the atomistic model, Lewis (1967) and Lewis and Campbell (1967) made a detailed theoretical comparison of the results of nucleation process derived from the two theories. It was shown that, because of the difference in the value of supersaturation for small nuclei, the capillarity model predicts a relatively larger size for the critical nucleus and a lower nucleation rate. The fact that the idealized shapes of the capillarity model give higher cluster energies, smaller critical nuclei, and a higher nucleation rate compensates for this difference. In general, however, the two models exhibit a wide agreement with each other.

1.9. Conclusion.

The theory of heterogeneous nucleation provides the basis for interpretation of the influence of the degree of supersaturation, of a temperature of transition for epitaxy to occur and of the state of the nucleating surface, on epitaxy for a given condensate-substrate combination. A frame work for the quantitative correlation of these primary variables is provided by both the capillarity model and by the atomistic model approaches. The role of nucleation in epitaxy has already been described in section 1.2.2.

CHAPTER 2.

THE STRUCTURES AND NON-STOICHIOMETRY OF HEAVY RARE EARTH DIHYDRIDES

2.1. Introduction.

The rare earths are those elements from atomic numbers 57 to 71 in the periodic table. They are broadly classified into two groups : light rare earths (Lanthanum, Cerium, Praseodymium, Neodymium and Europium) and heavy rare earths (Samarium, Gadolinium, Terbium, Dysprosium, Holmium, Erbium, Thulium, Ytterbium and Lutetium). The metals Gd, Tb, Dy, Ho and Er all have the hexagonal close-packed structure. Among the heavy rare earths, our interest is concerned with the dihydrides of Gd, Tb, Dy, Ho and Er. In this chapter we discuss the structures of these hydrides in bulk and thin film forms. Since the data on thin film dihydrides are few, we first discuss briefly the bulk materials.

2.2. Non-Stoichiometry of composition.

The non-stoichiometry which characterizes the rare earth hydrogen systems leads to difficulties in nomenclature. Following an imperfect, but accepted practice, the face-centred-cubic phase which includes the $MH_{2.0}$ (M stands for metal) composition is referred to as the dihydride phase. The term trihydride is used in a corresponding way in connection with the Gd-H system, for example, for the phase which includes $GdH_{3.0}$. The principal features of the phase diagrams of Gd-H are shown in Figure 2.1. The wide range of composition of the dihydride phase extending both above and below $MH_{2.0}$ is a distinguishing and important feature of the rare earth hydrides, for which significant deviations from the whole number stoichiometry seem to be the rule. Compounds of definite composition do exist, but the ratios of hydrogen atoms to metal atoms are not the whole numbers

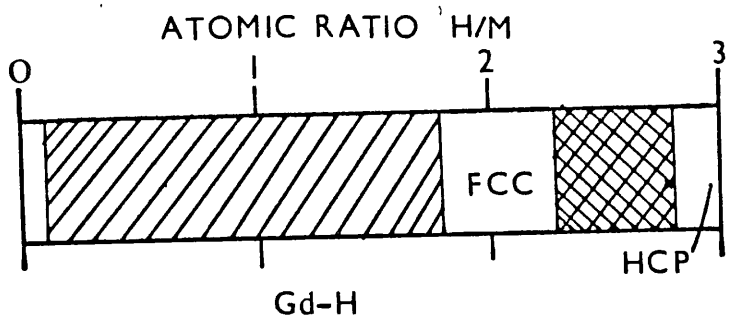

Figure 2.1. Essential featurs of the phase relation Gd-H. Hatched areas refer to two-phase metal-dihydride region. Cross hatched area refers to two-phase dihydride-trihydride region. Blank regions are single phase metal with dissolved hydrogen, dihydride or trihydride.

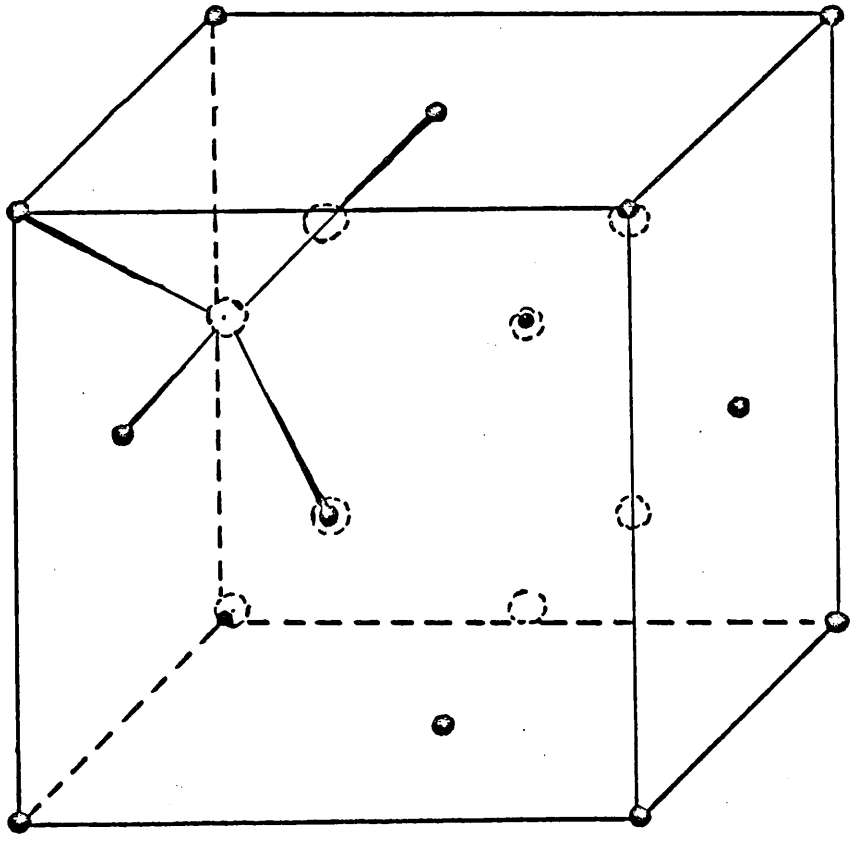

Figure 2.2. Fluorite-type metal dihydride structures; the filled and shaded circles denote metal atoms(ions); the dashed open circles denote hydrogen atoms(or ions). The relative radii shown are representative of the hydride anion model of metallic hydride.

usually expected for chemical compounds.

2.3. Preparation of the bulk rare earth hydrides.

The hydrides of the rare earth metals in bulk form are generally prepared by heating the metals in hydrogen gas. The following procedure was employed by Pebler and Wallace (1962) in preparing the rare earth hydrides. A sample ($\sim$0.4 gm) was cut from the metal (99% purity), polished and washed successively with CCl_4, acetone and ether. After weighing, the sample was introduced into the preparation train (vacuum system and appropriate gas metering equipment) and evacuated to high vacuum ($\sim 10^{-6}$ torr) for at least 4 hours. It was then heated gradually to the range 200 - 500°c and hydrogen was admitted. Hydrides with compositions approximating the dihydride usually formed quite rapidly. Desired compositions were obtained by adding measured amount of gas. After attaining the desired composition, the temperature was reduced and the sample was annealed at 200°c for about 4 hours. All the pressure - temperature - composition data for the rare earth-hydrogen system were obtained with a glass vacuum system consisting of a reaction bulb, a McLeod gauge or a mercury manometer for measuring the pressure of hydrogen over the sample in the reaction bulb, and a means for producing and measuring the amount of hydrogen admitted to the reaction bulb.

2.4. Previous work on structures and non-stoichiometry of bulk rare earth hydrides.

In 1956 Sturdy and Mulford conducted what appears to have been the first investigation of a heavy rare earth hydrogen system. They found by X-ray diffraction, the usual f.c.c. dihydride. This phase, was observed to exist from $GdH_{1.8}$ to $GdH_{2.3}$. The dihydride has a fluorite-type structure (shown in Figure 2.2) with a lattice parameter, $a_0 = 5.303$ A°. At higher hydrogen concentrations a second phase

appeared, in which the Gd ion cores were in a h.c.p. arrangement. The two-phase (metal-dihydride) region extended from $GdH_{2.3}$ to $GdH_{2.85}$, above which only the hexagonal phase existed upto $GdH_{2.91}$, the highest concentration obtained in their study. Mulford (1958) predicted similar behaviour for all the heavy rare earths except Eu and Yb. A crystallographic study of the phases which exist in the gadolinium-hydrogen system has been made by Ellinger (1956). A brief description of the data which he obtained has been given by Sturdy and Mulford (1956). They made six samples of gadolinium hydride of varying hydrogen content and Debye patterns of these samples were examined by Ellinger. The composition and phases present are given in table 2.1.

Table 2.1. Results of X-ray examinations.

Composition	phases present
$GdH_{0.64}$	Gd + cubic dihydride
$GdH_{1.08}$	Gd + cubic dihydride
$GdH_{1.72}$	Gd + cubic dihydride
$GdH_{1.93}$	cubic dihydride only
$GdH_{2.45}$	cubic dihydride + hexagonal trihydride
$GdH_{2.91}$	hexagonal trihydride only

Pebler and Wallace (1962) concentrated their experimental effort largely on five metals Sm, Dy, Ho, Tm and Nd. The others were examined only to the extent necessary to establish that their behaviour is subsequently the same as that of their more thoroughly investigated neighbours in the periodic table. In all cases powder diffraction patterns were obtained for the metal containing varying amounts of

hydrogen. The patterns were analysed to ascertain whether the system was single phase or heterogeneous and to determine the structure(s) of the phase or phases present. When the sharpness and intensities of the lines permitted, lattice parameters were evaluated. The results obtained are summarized in Figs. 2.3 and 2.4 and in talbe 2.2. The metallic phase co-existing with H_oH_2 was examined and its lattice parameters were found to be indistinguishable from those of pure holmium. It is also to be noted regarding Fig.2.3 that in some cases (for example, the Dy-H system) a number of compositions were examined and the phase boundaries could be located within fairly narrow limits. Erbium-hydrogen system was studied by Mulford (1959) and found that erbium dihydride has fluorite and trihydride has the hexagonal structure. For the samarium-, terbium, dysprosium, holmium,- erbium-, thulium - and lutetium-hydrogen systems a hydride phase was observed in the MH_2 - MH_3 composition range (Bos and Gayer, 1966) Each of these higher hydrides displayed a hexagonal close-packed arrangement of metal atoms; in each case the density was less than that of the corresponding dihydride. The existence of hexagonal close-packed trihydrides of the heavier rare earth metals had also been observed by Goffinberry and Ellinger (1957), Mulforf (1958) and Yakel etal (1959). The lattice parameters of $TbH_{2.95}$ were reported by Yakel etal (1959) and are in good agreement with those of Pebler and Wallace. The lattice parameters and crystal structures of di-and trihydrides gf Gd, Tb, Dy, Ho and Er according to Sturdy and Mulford (1956) and Pebler and Wallace (1962) are given in talbe 2.2.

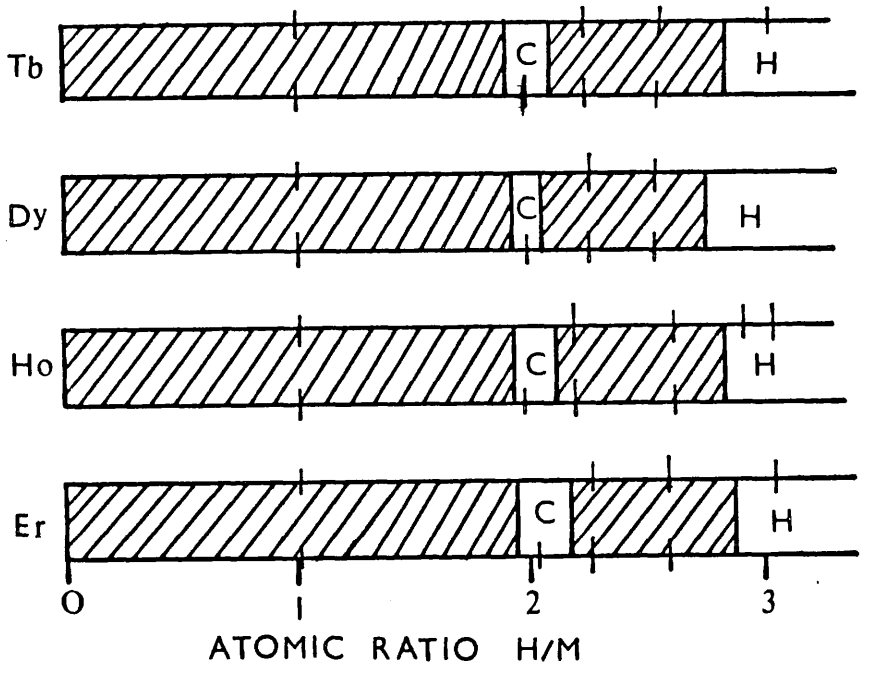

Figure 2.3. Phase relationships in rare earth hydrogen systems. The single phase regions based on the dihydrides(cubic) and trihydrides(hexagonal) are indicated by C and H,respectively. Regions in which two phases co-exist are cross hatched.Compositions for which diffraction patterns were obtained are indicated by the vertical line or lines: ⫲ ,two phase; ⫟ ,single cubic phase; ⫠ ,single hexagonal phase.

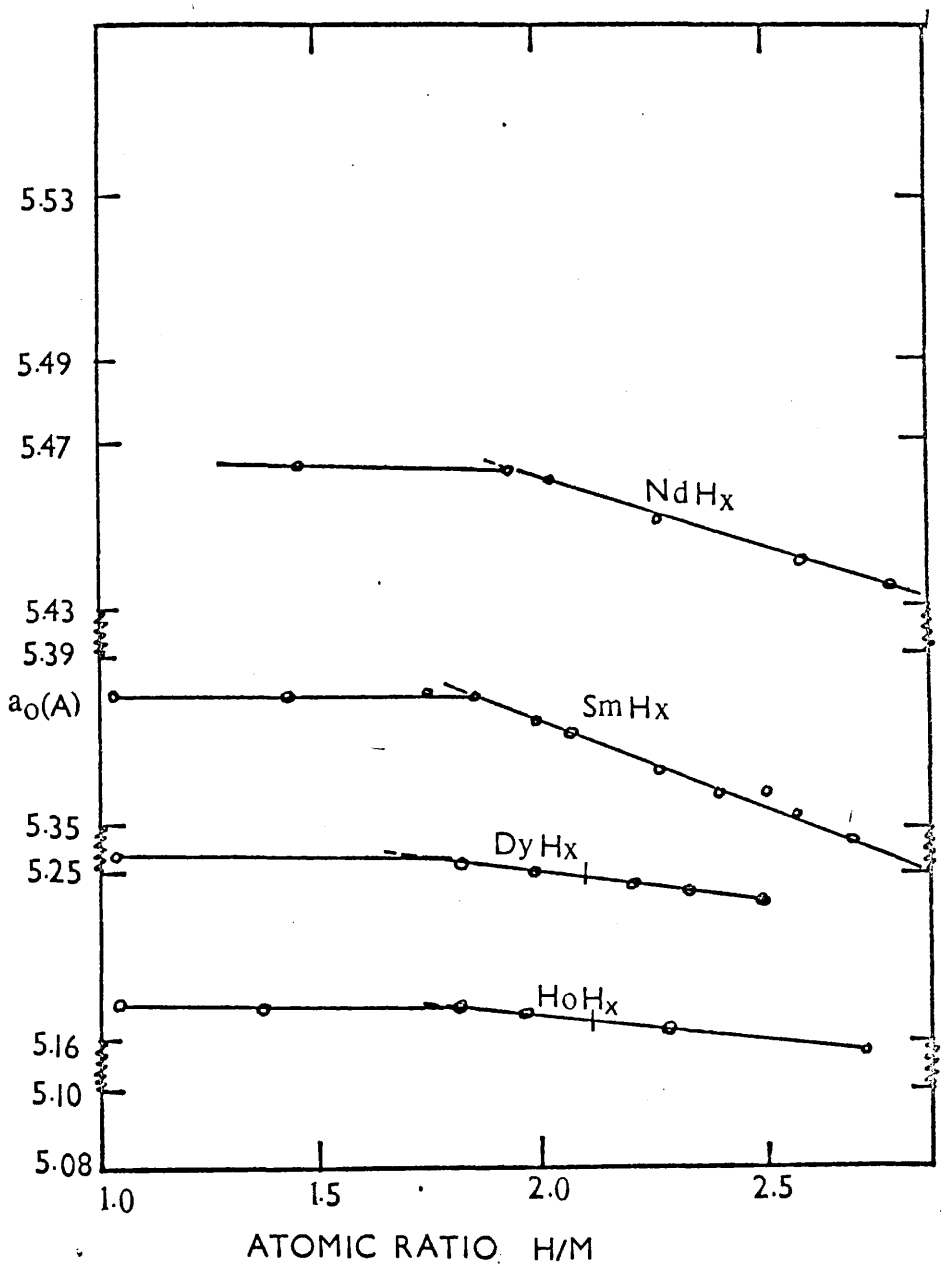

Figure 2.4. Lattice spacings Vs. gross composition for rare earth hydrogen system :

Table 2.2.

Crystal structures and lattice parameters of heavy rare earth hydrides.

Metal	Dihydride		Trihydride	
	Structure	Parameter (A^0)	Structure	Parameters (A^0)
Gd	F.C.C.	a_o = 5.303	H.C.P.	a = 3.73 c = 6.71
Tb	F.C.C.	a_o = 5.246	H.C.P.	a = 3.700 c = 6.658
Dy	F.C.C.	a_o = 5.201	H.C.P.	a = 3.671 c = 6.615
H_o	F.C.C.	a_o = 5.165	H.C.P.	a = 3.642 c = 6.560
Er	F.C.C.	a_o = 5.123	H.C.P.	a = 3.621 c = 6.526

Table 2.3.

Room temperature phase limits of some rare earth hydrides.

Metal	Phase limits of the cubic dihydride, H/M	Phase limits of the hexagonal trihydride, H/M
Gd	1.82 - 2.3	2.85 - 3.0
Tb	1.90 - 2.15	2.81 - 3.0
Dy	1.94 - 2.08	2.86 - 3.0
H_o	1.95 - 2.24	2.64 - 3.0
Er	1.95 - 2.31	2.82 - 3.0

The dihydrides of Gd, Tb, Dy, H_o and Er accommodate additional hydrogen up to a definite concentration and then undergo a phase transformation to a structure in which the metal atoms form a hexagonal lattice. The maximum hydrogen to metal ratio which each hydride can attain before formation of the hexagonal phase (Libowitz, 1965) is shown in tables 2.3. The hexagonal phases also have variable composition as can be seen in the table. There is also a difference between the hydrides of the light rare earths (La, Ce, Pr and Nd hydrides) and the heavy ones (Gd, Tb, Dy, H_o, Er, Tm and Lu hydrides). The light rare earths form trihydrides with no change in structure by merely filling the octahedral sites in the flourite structure with hydrogen atoms (Holley etal, 1955 and Kubota Wallace, 1962). The octahedral sites of the heavy rare earths are also occupied initially, but, before the composition MH_3 is reached, the lattice transforms to a hexagonal structure. This difference is reflected in the schematic phase diagrams for the light and heavy rare earth-hydrogen systems in Figure 2.5.

The contraction in lattice parameter for the dihydride phase with increasing hydrogen content, to which attention has been directed (Rossi, 1934 and Mulford and Holley, 1955) also is revealed by the results in Fig. 2.4. Contraction is quite pronounced for Pr-H, Nd-H and Sm-H but much less so for the heavy rare earth hydrides. In Dy-H system, for example, the dihydride phase extends only upto about $DyH_{2.08}$. Above this the system is two phase and the contraction of the cubic form should be fixed. Thus the lattice parameter should be invariant with gross composition when $H/Dy > 2.08$. The slight dependence on gross composition in the two phase region for this and the H_o-H system is probably due to slight departure from equilibrium conditions. The contraction of the lattice parameter may be explained

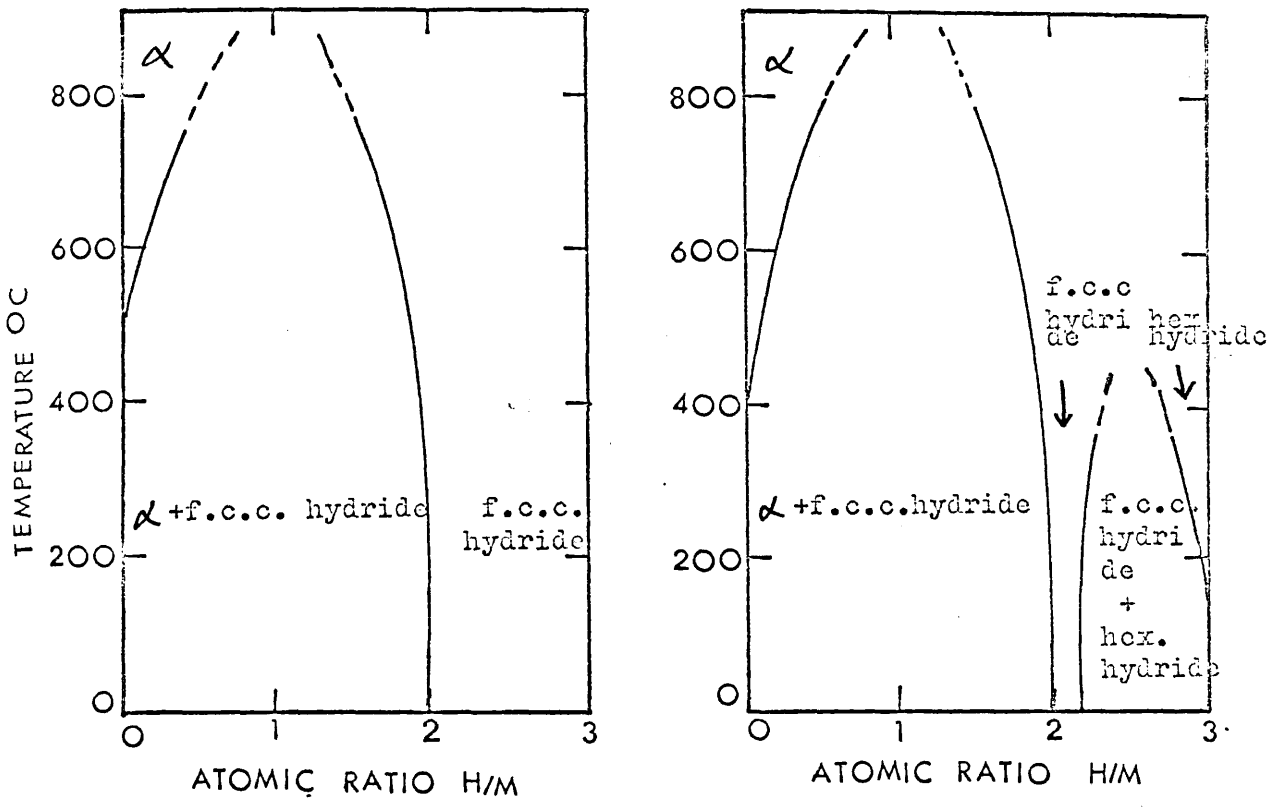

(a) La,Ce,Pr,Nd

(b) Sm,Gd,Dy,Tb,Ho,Er,Tm,Lu

Figure 2.5. Schematic phase diagrams of the rare earth-hydrogen systems.

(Pebler and Wallace, 1962) by the removal of electrons from the conduction band to form hydrogen anions (anion model of conduction is discussed in section 3.2, chapter 3).

2.5. Structure of heavy rare earth thin film dihydrides.

The formation of heavy rare earth dihydride films caused confusions among various groups of workers over the past years. Several workers have reported the observation of cubic phases formed by the vacuum deposition of various rare earth metals which in bulk form have the hexagonal close-packed structure.

Murr (1967) obtained a face-centred-cubic phase when erbium was vacuum deposited on rock salt and attributed this structure to P-type semi conducting oxide Er_0. He calculated the lattice parameter of the observed f.c.c. phase (which he claimed to be ErO) to be $a_o = 5.12A^o$, which agrees absolutely with ErH_2 but not with Er_0. On the other hand he compared the lattice parameters of ErN or NaCl with the observed phase but did not take into account the possibility of ErH_2 which also has f.c.c. structure.

Rai and Srivastava (1971) deposited gadolinium on rock salt substrate and claimed that the NaCl-type face centred cubic structure they observed was due to GdO. They measured the lattice parameter of the observed phase to be $5.50 \pm 0.03A^o$. Their claim was mainly based on Murr's (1967) result on Er_0. They investigated the possibility of GdN and NaCl but did not check for hydride. Later, Bist and Srivastava (1971) and Bist, Kumar and Srivastava (1972) evaporated a preheated mixture of Gd and Gd_2O_3 on formvar-coated grids to obtain what they claimed was GdO having the face-centred-cubic structure of ZnS. The lattice parameter measurement gave a value of $a_0 = 5.24 \pm 0.05A^o$, which differs markedly from that of Rai and Srivastava. Srivastava, although a common author of the three previous papers,

did not discuss the variation of the values of lattice parameters which were obtained in different cases but always attributed as GdO. They omitted to investigate the possibility of the observed phase as hydrides of the metal.

Curzon and Chlebeck (1972) vacuum deposited thin films of erbium both on rock salt and carbon, and found that thin films ($\sim$ 140A°) had face-centred-cubic structure whereas thick films (>195A°) had the hexagonal-close-packed structure of the metal in bulk form. This led them to believe that the face-centred-cubic structure of the thin film was due to a new metallic phase and not to a rare earth metal monoxide as claimed by Murr. Materials in the form of thin film sometimes occur with crystal structure which differ from those of the normal bulk structures (Chopra etal,1967, Schrey etal, 1970, Otsuka and Wayman,1967, Wawner etal, 1969 and Grunbaum and Kremer,1968). This happens for very thin films depending on the influence of the evaporation parameters such as, evaporation rate, degree of vacuum, mode of deposition, and nature and temperature of the substrates etc.

Later on Curzon and Chlebek (1973a) extended their work on other heavy rare earth metals Gd, Tb, Dy, Ho, Er and Tm, and came to the same conclusion claiming the observed f.c.c. phases in thin films as metallic. Thicker films contained both f.c.c. and h.c.p. structures and thickest films (>195A° for Er, thickness for other metals were not measured) had the normal h.c.p. bulk structure. The increased values of the lattice parameters which they obtained were explained as oxygen contamination. Again Curzon and Chlebek (1973b) showed, by temperature dependence of electrical conductivity measurements and later (1973c) by weight increase analysis, that the face-centred-cubic phases were not p-type semi conducting

monoxides, and concluded that these phases were in fact rare earth metals.

Gasgnier et al(1974) have pointed out that the lattice parameters of the face-centred-cubic phases under discussion are consistent,within experimental error, with the face-centred-cubic dihydrides of the rare earth metals and should not be mistaken for a rare earth monoxide or for a f.c.c. phase of the metal. This,together with the facts that hydrogen is present in conventional vacuum systems and the rare earth metals readily combine with hydrogen strongly support the explanation based on dihydrides. Gasgnier et al studied most of the rare earth metals including Gd,Tb,Dy,Ho and Er and observed that in thin films ($<300\mathring{A}$) they form f.c.c. dihydrides;thickest films ($>1000\mathring{A}$) have the normal h.c.p. structure of the bulk metals,and in the intermediate thickness range both f.c.c. dihydrides and h.c.p. metallic phases co-exist. This being so, Curzon and Singh(1975a),studied Ytterbium which is chemically similar to those already mentioned and its dihydride has orthorhombic structure instead of face-centred-cubic.This orthorhombic structure can be easily distinguished from the normal face-centred-cubic bulk form of Yb at room temperature but does resemble a known hexagonal-close-packed form of the metal.In view of the work of Gasgnier et al and the result of their later work(1975a)on Ytterbium,Curzon and Singh were convinced and supported the suggestion made by Gasgnier et al that the face-centred-cubic phase previously attributed to thin films of Gd,Tb,Dy,Ho and Er are in fact due to the dihydrides of these metals and regretted (private correspondence)that the formation of ErH_2 should have been considered as a possibility in their previous works(1973b,1973c).In order to reconfirm Gasgnier's and their own results,Curzon and Singh(1975b)evaporated Eu,Gd,Tb,Dy,Ho,Er,and Yb in the presence of H_2 gas and showed that Gd, Tb, Dy,Ho and Er combined readily with H_2 and that dihydrides of these metals were formed.

Both ordinary and ultra-high vacuum systems have been used by most of the workers, and all of them studied only polycrystalline films. Hence it was felt worthwhile to study the possibility of growing single crystal films. The single crystal f.c.c. structure is easily distinguishable from the polycrystalline h.c.p. structure and also the lattice parameters could be measured more accurately from the reflection spots in single crystal structures.

CHAPTER 3.

PREVIOUS WORK ON THE ELECTRICAL PROPERTIES OF RARE EARTH DIHYDRIDES AND THE THEORY OF ELECTRICAL CONDUCTION IN THIN FILMS.

3.1. Introduction.

At present there is no work at all on the electrical properties of thin films of the rare earth hydrides. But there have been many investigations on the bulk materials, which will be discussed in the following sections.

Conductivity measurements have been made on most of the rare earth hydrides in bulk form, extensively more works on the light rare earth hydrides than heavier ones. The results for light and heavy rare earth hydrides are however very similar (Heckman, 1969), so that a similar theoretical interpretation for both types of hydrides is to be expected. Some results and discussions on light rare earth hydrides are therefore also mentioned along with heavy rare earth hydrides.

3.2. The 'anionic' and protonic model.'

The electronic properties of rare earth hydrides are usually discussed in the literature (Libowitz, 1965, Bos and Gayer, 1966, Heckman, 1964 and Wallace etal, 1963) in terms of one of the two models, a 'protonic hydrogen model', or an 'anionic hydrogen model'. In the protonic model, the hydrogen contributes an electron to the system's conduction band, while in the anionic model it extracts one. In the anionic model (Fig. 3.1) the hydrogen is regarded as an anion. It introduces two levels below the rare earth metal conduction band and therefore takes one electron from it. The Fermi level is lowered and eventually at MH_3 complete depopulation of the conduction band occurs. In the protonic model the hydrogen is regarded as protonic. Here the hydrogen I-S level is introduced into the metal band structure above

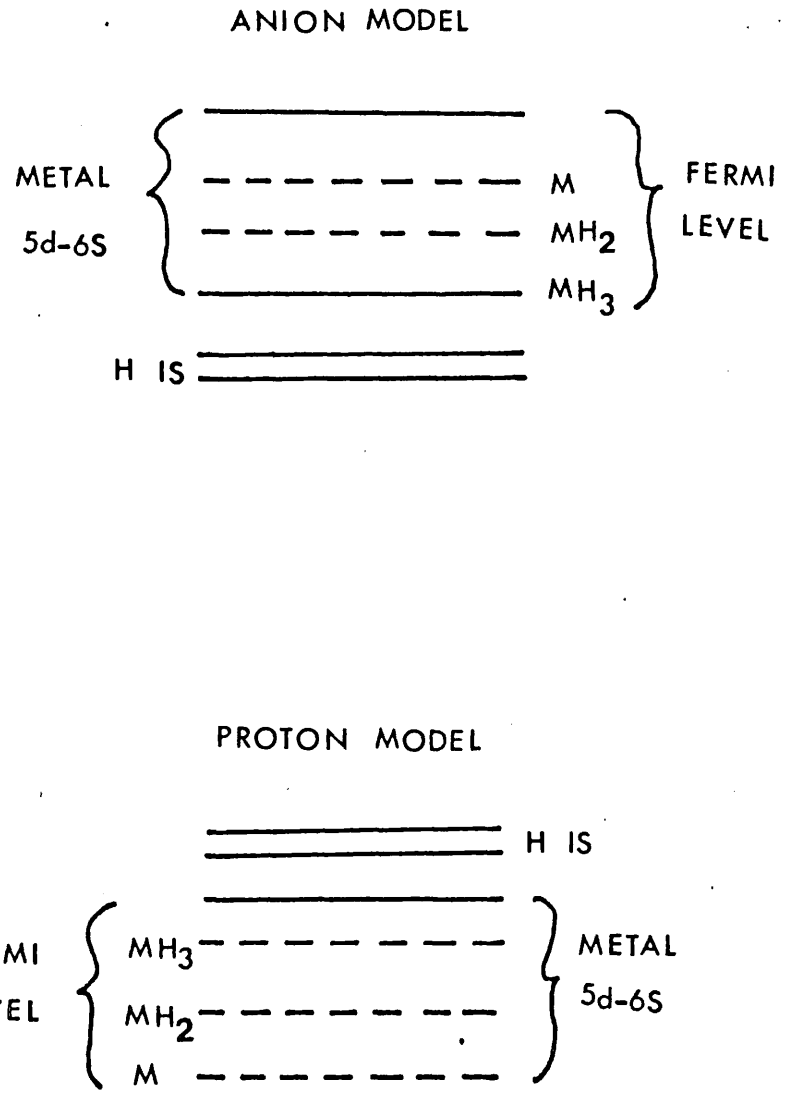

Figure 3.1. Approximate level diagrams for anionic and protonic models showing the position for the hydrogen levels and the Fermi levels relative to metal conduction band.

the conduction band. The hydrogen electron ends up in the conduction band; this raises the Fermi level and causes the number of conduction electrons to increase.

3.3. Existing electrical measurements on bulk rare earth hydrides.

The dihydride f.c.c. phase of Cerium hydride exists for hydrogen concentrations in the range H/c_e = 1.8 - 3.0 (Mulford and Holley 1965). At the lower end of this range the electrical conductivity is comparable to that of a typical metal. As the hydrogen concentration is increased, the conductivity decreases, reaching a low value typical of a semi conductor for hydrogen concentrations in the range $H/c_e = 2.9$ (Stalinski, 1959, Heckman, 1964, 1967). Both the anionic and protonic models provide a satisfactory explanation of this behaviour. In the anionic model, the depletion of the 5d-6s cerium conduction band, caused by the addition of hydrogen, reduces the conduction electron density and thus the conductivity. Since the cerium conduction band originally held three electrons per cerium atom (same is the case with Gd or Tb), the conduction electron density and the conductivity should decrease linearly with increasing hydrogen concentration, reaching zero at H/c_e = 3.0, in agreement with the experimental observations. In the protonic model, the addition of hydrogen and the changing lattice constant (Mueller etal 1968) are thought to cause the conduction band to split into two bands, the lower of which holds six electrons per cerium atom (Libowitz 1965). Since each hydrogen contributes one electron to the conduction band in the protonic model, the lower band would have one hole per cerium atom at H/c_e = 2.0 and would be gradually filled as the hydrogen concentration is increased until it is full for H/c_e = 3.0. As the conductivity would be proportional to the hole density in this case, the protonic model also predicts the observed behaviour of the conductivity as a function of composition.

Experimentally, the conductivity measurements (as will be discussed in the following sections)satisfy both the anionic and protonic models. Hall coefficient measurements for cerium hydride by Heckman (1967) supports the protonic model, which predicts the positive value, although the magnitude is the same for both models. The rare earth hydrogen systems have been the centre of increasing attention, due largely to the extensive non-stoichiometry which they exhibit. There has been speculation, supported by experimental evidence that their electrical properties are directly and significantly related to their hydrogen content. Heckman (1964) measured the resistivity on cerium-hydrogen and gadolinium-hydrogen systems over the composition range CeH_o to $CeH_{2.5}$ and GdH_o to $GdH_{2.13}$. The samples used were polycrystalline bars of the hydrides. Resistivity was measured by conventional four-prove techniques. Voltages were measured potentiometrically and currents were supplied by regulated power supplies. As indicated in Figure 2.1 of Chapter 2, the composition range for which the hydrogen to metal ratio is less than two is predominantly two-phase (metal-dihydride) in Gd-H systems. Figures 3.2 and 3.3 give the conductivity results of Heckman (1964). A few years later Heckman (1969) again measured the conductivity of La-H, Nd-H and Ce-H systems (Figure 3.4) and of Gd-H, H_o-H and Er-H systems (Figure 3.5). Comparing the results of heavy rare earth hydrides (Figure 3.5) with that of light rare earth hydrides (Figure 3.4) one can see substantially the same features.

The conductivities are explained by assuming that the two-phase regions extend only to the maxima in the curves (Figure 2.1 of Chapter 2) i.e., to $GdH_{1.8}$, and thereafter the hydrides are single phase materials of variable composition. The two-phase materials are consequently composed of hydrogen saturated metals and the non-stoichiometric dihydride. An interesting feature of the experimental results is that the dihydride

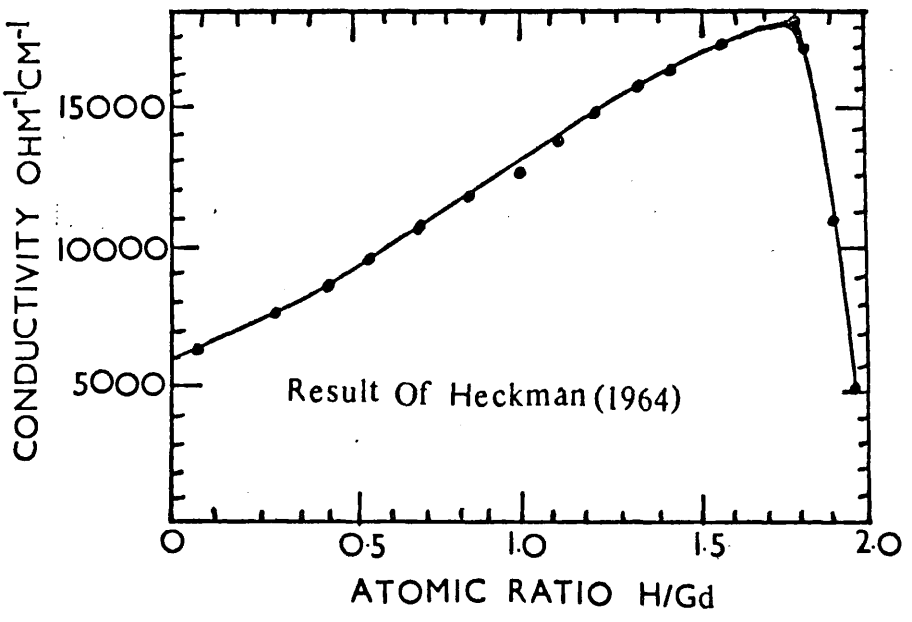

Figure 3.2. Conductivity Vs. composition of $GdH_{0-2.0}$ at room temperature.

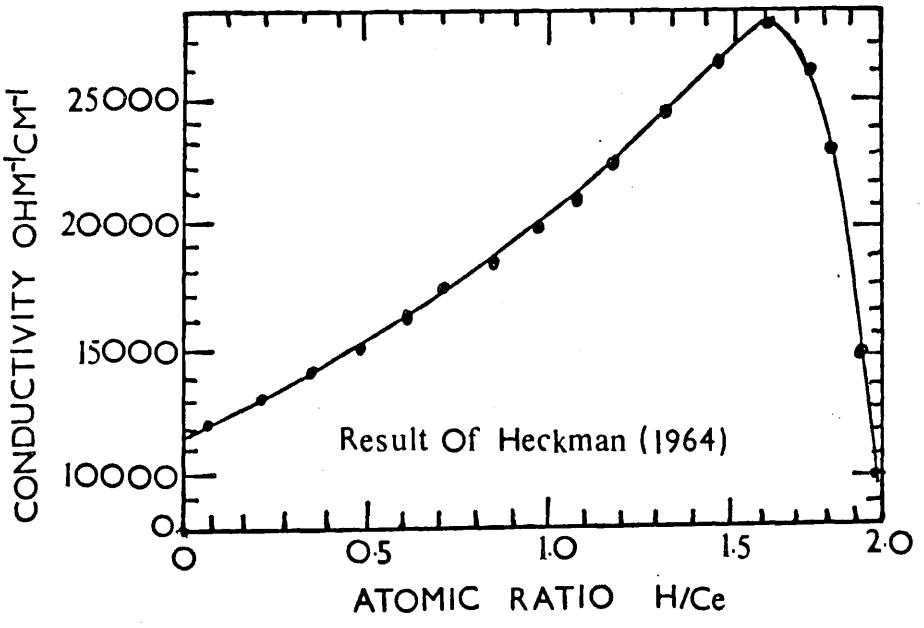

Figure 3.3. Conductivity Vs. composition of $CeH_{0-2.0}$ at room temperature.

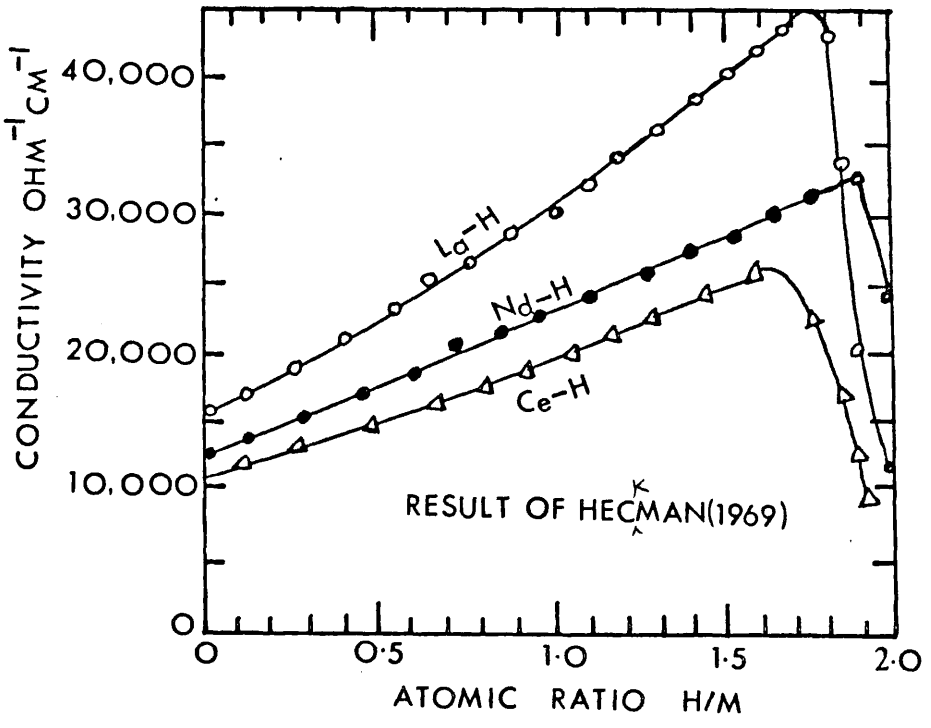

Figure 3.4. Conductivity Vs. composition of La-H, Nd-H and Ce-H for hydrogen to metal ratios from 0 to 2 .

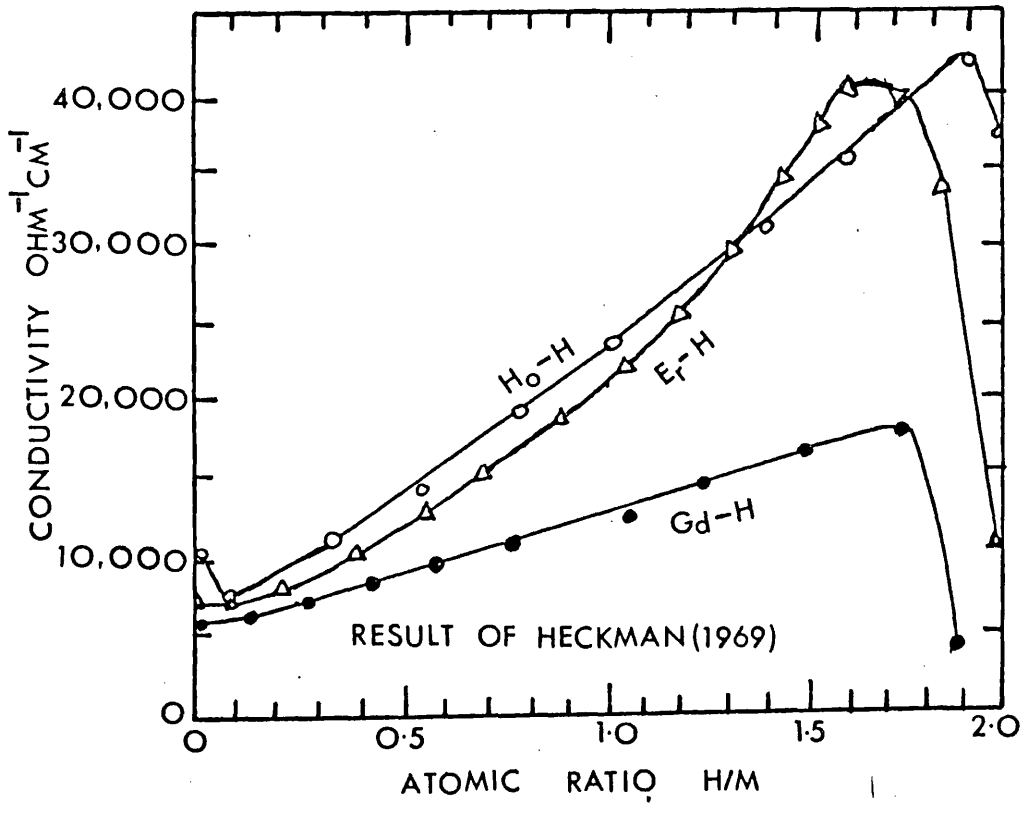

Figure 3.5. Conductivity Vs. composition of Ho-H, Er-H and Gd-H for hydrogen to metal ratios from 0 to 2 .

$GdH_{1.8}$ is a better electrical conductor than is the parent metal. This result may not have been anticipated since electrons in the dihydrides move not only in the presence of the positive metal ion centres as they do in the metals but also, according to the 'anionic model' for these materials, in the presence of an even greater number of negative hydrogen ions. The remarkable extent to which the rare earth dihydride compositions can be varied has already been noted. Fig. 2.1 of chapter 2 shows that the gadolinium dihydride phase can vary from $GdH_{1.8}$ to $GdH_{2.3}$. The conductivities as a function of composition throughout parts of these ranges are shown in Fig. 3.6. Metallic conduction is indicated by the small temperature dependence of conductivity at high temperatures and by the increased conduction at room temperature. This is in agreement with Stalinski's (1959) results for the temperature dependence of conduction in Ce-H. The composition dependence of conduction is the most interesting feature of the data. At high temperatures linear decrements in conduction, with increasing H/M, over sizeable ranges are observed. Nevertheless, the room temperature results are not in any way at variance with those at high temperatures, except that, as is to be expected for metals, conductivities are slightly higher. Extrapolation of the conductivity curve to zero is shown in Fig. 3.6. In the Gd-H system metallic conduction vanishes, according to the extrapolation, at 2.3 H/Gd. The work of Sturdy and Mulford (1956), on this system, has shown at 2.3H/Gd the hexagonal trihydride phase begins to appear with the addition of hydrogen. Fig. 3.7 showing the conductivity results for Er-H (Heckman, 1969) confirms the uniform behaviour across the rare earth series.

Conductivities, as functions of composition and temperature, have been measured for the systems Nd-, Er-, Ho-, and Yb-H by Heckman and Hills (1965). The H/M ratio was varied from 0 to 2.0. The materials are

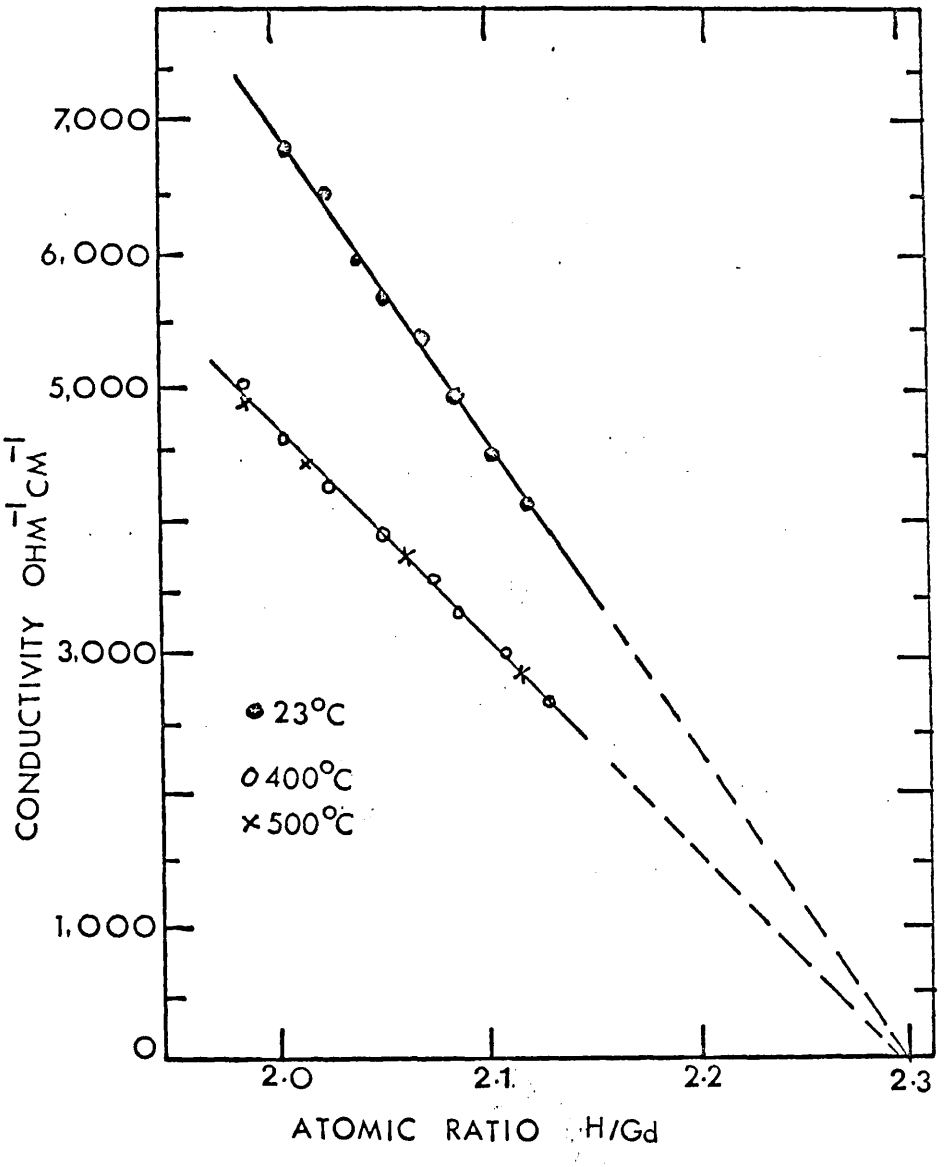

Figure 3.6. Conductivity of gadolinium dihydride Vs composition.

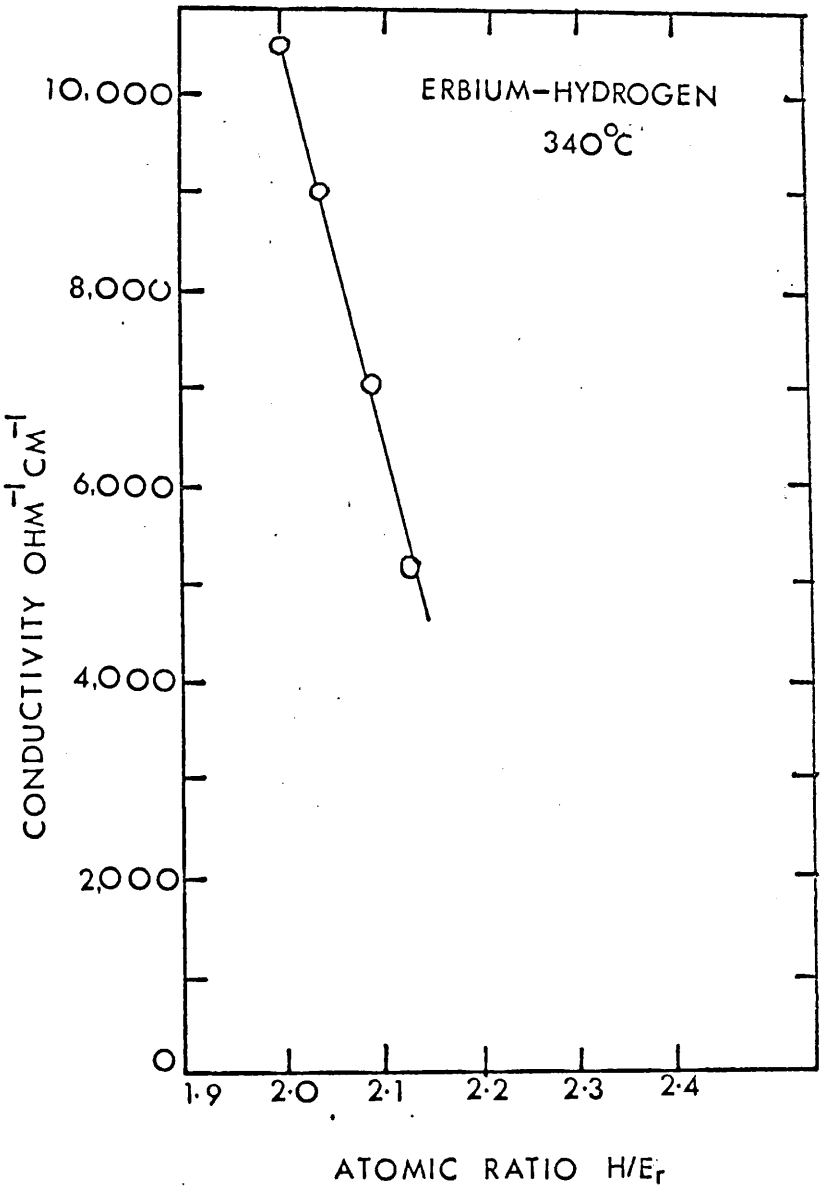

Figure 3.7. Conductivity Vs composition for Er–H 2.0 H/Er 2.15

2-phase throughout most of this region (metal plus dihydride.) For Nd-H, Er-H and H_o-H, the conductivities increase smoothly with hydrogen content throughout the 2-phase region, reaching a miximum in the single phase variable composition dihydrides are metallic, as inferred from the conductivity temperature dependence and, for certain compositions, have substantially higher conductivities than the parent metals. Conductivity maxima (at 25°C) occur at $NdH_{1.9}$, 31000 $(\Omega\text{-cm})^{-1}$, $ErH_{1.8}$, 38000 $(\Omega\text{-cm})^{-1}$, and $HoH_{1.9}$, 40000 $(\Omega\text{-cm})^{-1}$. Heckman (1969) again measured the electrical conductivity of gadolinium dihydrido polycrystalline slabs as a function of temperature and composition. The composition range is $GdH_{2.0}$ to $GdH_{2.2}$ and is single phase, of variable composition. The conduction was found to be metallic. Its composition dependence can be interpreted on the basis of the "anionic model" in which the hydrogen is a negative ion in the lattice, taking its extra electron from the conduction band (Libowitz and Gibb, 1956). The conductivity showed a substantially linear decrease with increasing hydrogen content. By extrapolation, metallic conduction should vanish at approximately $GdH_{2.3}$. In gadolinium hydride, this composition is coincident with a phase boundary between a single cubic region and a two phase region. Typical conductivity in this case was found to be $GdH_{2.1}$, 3.4×10^3 $(\Omega\text{-cm})^{-1}$ at 400°C.

Wallace etal (1963) found that when Dy, Ho and Yb are hydrogenated to saturation, their conductivities diminish by five or more orders of magnitude. Stalinski (1959) also found a similar behaviour for La and Ce, and moreover obtained additional evidence for the non-metallic character of these hydrides by noting that their resistivities decreased with increasing temperature, showing the characteristic of semiconductors. Electrical resistivity measurements on cerium and lanthanum hydrides have been made by Warf and Hardcastle (1961). They reported that the

resistance of $LaH_{2.88}$ decreased with increasing temperature having a value of $-0.006/^{o}C$ for its temperature coefficient of resistivity. Some studies of the electrical resistance of the Ce-H system were carried out on samples in the form of sheets or wires by Daou (1958). The measurements were carried out at 500°C, and the results show that after a slight initial increase, the resistance of samples decreased linearly with increasing hydrogen content until a composition near $CeH_{1.8}$ was reached. At this composition the resistance was 30% less than that of cerium metal. Further absorption of hydrogen led to a rapid increase in the resistance. At room temperature similar results were obtained, but the relative decrease in the resistance was twice as great. Daou (1961) also reported the dependence of the resistivity of non-stoichiometric cerium and praseodymium dihydrides on temperature. For both compounds, the resistivity increased linearly with temperature up to 200°C. Above this temperature the rates of increase of resistivity with temperature became progressively greater. Wallace (1972) indicated that rare earth dihydrides which are metallic conductors, show magnetic ordering at temperatures ranging from $8^{o}K$ for HoH_2 and DyH_2, to $40^{o}K$ for TbH_2.

Hence the results of the electrical measurements of rare earth hydrides (bulk) can be summarised as

(a) dihydrides are metallic and the conductivity varies over the nonstoichiometric composition range of the phase.

(b) trihydrides have semi conducting characteristics.

3.4. <u>The chief characteristics of electrical conduction in thin films</u>.

The results of the conductivity of bulk rare earth dihydrides, as reviewed earlier in section 3.3, revealed the metallic characteristic. Accordingly the theoretical treatment of the conduction mechanism in thin films of these hydrides is summarised on the basis of this characteristic.

The concept of resistivity as an intrinsic property of a metal is meaningful only under the assumption that electrical properties of a given specimen are independent of its shape and size. Experimentally, the conditions under which the resistivity becomes a function of the sample's dimensions are obvious. As long as the distance between the boundaries of the sample are very much greater than the electronic mean free path l_f in the bulk material, the presence of these boundaries will not significantly influence the intrinsic transport properties. However, when one or more dimension approaches l_f, a significant fraction of the electrons will strike and be scattered at the surface rather than in the bulk.

If the surface of the film scatters conduction electrons diffusely (inelastically), thereby artificially limiting the mean free path the resistivity is increased above the bulk value and is a function of the thickness. On the other hand, if electrons are specularly (elastically) reflected from the surface, the resistivity of the film is the same as that of the corresponding bulk material, and is independent of film thickness for an isotropic Fermi surface. This problem has been analysed theoretically by Fuchs (1938) and reviewed by Sondheimer (1952) and Campbell (1966).

3.4.1. Matthiessen's rule.

In interpreting the dependence of resistivity on film thickness it is necessary to consider several factors which contribute to the total resistivity. Electrical resistance in a material may arise from a variety of sources, such as temperature, dissolved impurities and vacancies. Matthiessen's rule states that the resistivity of a given sample will be the simple arithmatical sum of the individual contributions made by all these separate sources of resistance. According to a modified form of Matthiessen's rule the resistivity

ρ_F of a film can be represented by the following equation

$$\rho_F = \rho_T + \rho_d + \rho_s + \rho_m \qquad \ldots\ldots\ldots\ldots\ldots(1)$$

where ρ_T, ρ_d, ρ_s and ρ_m represent the resistivity corresponding to the scattering of the conduction electrons due to thermal vibrations, defects, film surfaces and disordered spins(only in magnetic materials) respectively.

3.4.2. Sheet resistance.

As can be seen from Fig.3.8., the resistance of a rectangular shaped section of film(measured in a direction parallel to the film surface) is given by $R = \frac{\rho}{t} \cdot \frac{l}{b}$ .....(2)

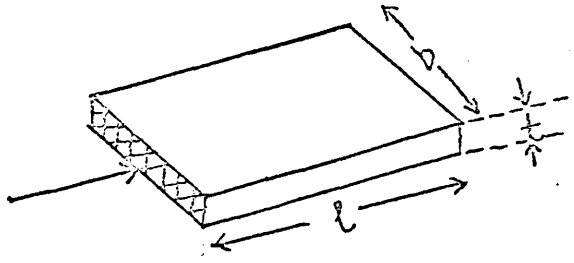

Figure 3.8.Definition of sheet resistance.

If $l = b$, this then becomes $R = \frac{\rho}{t} = R_S$ .....(3)

so that theresistance R_s of one square of film is independent of the size of the square- depending only on resistivity and thickness. The quantity R_s is called the "sheet resistance" of the film and is expressed in ohms per square.

3.4.3. Temperature coefficient of resistance(TCR).

The temperature coefficient of resistance (TCR) α_T, at temperature T, is experimentally determined from the relationship

$$\alpha_T = \frac{R_1 - R_2}{R_T(T_1 - T_2)} \qquad \ldots\ldots\ldots\ldots\ldots(4)$$

where $T_1 > T > T_2$, and the R's are resistance values.

A minimum of three resistance measurements must be made in order to obtain a reliable value for ρ, the third reading being necessary as a check to determine whether the temperature treatment (up or down) has produced any permanent change in this resistance value.

3.4.4. Theory of conduction and resistivity behaviour.

The theory of the conduction mechanism in thin films starts with the analysis of Boltzmann transport equation for electrons (subject to appropriate boundary condition)

$$-\frac{e}{m}\left(E+\frac{1}{c}v\times\bar{H}\right)\nabla_v f+\bar{v}\nabla_r f=\frac{f-f_0}{\tau} \qquad \text{-------(5)}$$

where f = nonequilibrium electronic distribution functions

f_o = electronic distribution at equilibrium

τ = relaxation time for return to equilibrium, a function only of the absolute value of $\bar{v}$, the electron velocity. The other symbols have their usual meaning except that m will be an effective mass rather than the free electron mass. The z axis is taken as perpendicular to the plane of a film of thickness t, and current flows through the film in the x direction. The use of equ. (5) for the investigation of size effects on conductivity depends on the presence of the second term, $\bar{v}\nabla_r f$, which vanishes for bulk material but not in the z direction for a thin film. It is convenient to write

$$f = f_o + f_1 (v, z) \qquad \text{.....(6)}$$

substitution of equ. (6) into (5) gives

$$\frac{eE}{mv_z}\frac{\partial f_0}{\partial v_x}=\frac{\partial f_1}{\partial z}+\frac{f_1}{\tau v_z} \qquad \text{.....(7)}$$

since $\bar{H} = 0$ and $\bar{E}$ is in the x direction

The general solution of equ (7) is of the form

$$f_1(v,z)=\frac{e\tau E}{m}\frac{\partial f_0}{\partial v_x}\left[1+F(v)\exp\left(\frac{-z}{\tau v_z}\right)\right] \qquad \text{.....(8)}$$

where $F(v)$ is an arbitrary function of $\bar{v}$ to be determined by the introduction of the appropriate boundary conditions. To determine $F(v)$ we have to introduce the boundary conditions at the surfaces of a thin film. The simplest assumption is to suppose that every free path is terminated by collision at the surface, so that the scattering is entirely diffuse. The distribution function of the electrons leaving each surface must then be independent of direction. Equation (8) shows that this can be satisfied only if we choose $F(v)$ so that $f_1(v,0) = 0$ for all $\bar{v}$ having $v_z > 0$ (that is, for electrons moving away from the surface $z = 0$), and $f_1(v, t) = 0$ for all v having $v_z < 0$

There are therefore two distribution functions: f_1^+ for electrons with $v_z > 0$, and f_1^- for electrons with $v_z < 0$. In other words

$$f_1^+(v,z) = \frac{e\tau E}{m}\frac{\partial f_0}{\partial v_x}\left[1 - \exp\left(\frac{-z}{\tau v_z}\right)\right] \quad (v_z > 0)$$

$$f_1^-(v,z) = \frac{e\tau E}{m}\frac{\partial f_0}{\partial v_x}\left[1 - \exp\left(\frac{t-z}{\tau v_z}\right)\right] \quad (v_z < 0)$$

The solution to equ. (7) can then be used to calculate $J(z)$, the current density across the film from

$$J = 2e\left(\frac{m}{h}\right)^3 \int v f dv$$

Evaluation of the above integral is facilitated by resorting to polar co-ordinates. Thus, we substitute $v_z = \bar{v}\cos\theta$, and the resulting expression for J is then

$$J(z) = \frac{4\pi e^2 m^2 \tau v^{-3}}{h^3} E \int_0^{\pi/2} \sin^3\theta \left[1 - \exp\left(\frac{-t}{2\lambda\cos\theta}\right)\cosh\left(\frac{t-2z}{2\lambda\cos\theta}\right)\right] d\theta$$

where $\lambda = \tau\bar{v}$ is the mean free path of the electrons. By averaging the current density over all values of z from o to t, an expression can now be derived for σ, the film conductivity:

$$\sigma = \sigma_0 \left[1 - \frac{3}{2K}\int_1^{\infty} \left(\frac{1}{q^3} - \frac{1}{q^5}\right)\left(1 - e^{-KT}\right) dq\right] \qquad \text{.....(9)}$$

where $q = \frac{1}{\cos\theta}$, $K = \frac{t}{\lambda} = \frac{\text{film thickness}}{\text{mean freepath}}$, σ_0 = bulk conductivity value. Approximations can be made to equ. (9) for large and small K:

$$\frac{\sigma}{\sigma_0} = 1 - \frac{3}{8K} \quad (K \gg 1) \qquad \text{.....(10)}$$

$$\frac{\sigma}{\sigma_0} = \frac{3K}{4}\left(\ln\frac{1}{K} + 0.423\right) \quad (K \ll 1) \qquad \text{.....(11)}$$

In determining $F(v)$ in equ. (8), it is more general to allow some function p of the electrons to be elastically scattered (v_x is the same before and after a collision) while the remainder are diffusely scattered, as before. Equations (10) and (11) now become

$$\frac{\sigma}{\sigma_0} = 1 - \frac{3(1-p)}{8K} \quad (K \gg 1) \qquad \text{.....(12)}$$

$$\frac{\sigma}{\sigma_0} = \frac{3K}{4}(1+2p)\left(\ln\frac{1}{K} + 0.423\right) \qquad \text{.....(13)}$$
$$(K, p \ll 1)$$

Similar reasoning may also be applied to determine the effect of film thickness on the temperature coefficient of resistance. The result that one obtains is

$$\frac{\alpha}{\alpha_0} = 1 - \frac{3(1-p)}{8K} \qquad (K \gg 1)$$

$$\frac{\alpha}{\alpha_0} = \frac{1}{\ln\left(\frac{1}{K}\right) + 0.423} \qquad (K \ll 1)$$

CHAPTER 4.

THE PREPARATION OF EPITAXIAL SINGLE CRYSTAL FILMS OF THE DIHYDRIDES OF Gd, Tb, Dy, Ho AND Er.

4.1. Choice of the method.

The various methods of preparing thin solid films may broadly be classified into two separate groups:-

i. chemical methods.

and ii. physical methods.

The principal techniques for the deposition by chemical methods are

(a) Electro deposition

(b) Chemical precipitation

(c) Thermal decomposition from vapour

(d) Explosion of metal wires in an inert gas

(e) Chemical reaction of a metal halide and water vapour to form metal oxide.

physical methods can be divided into

(a) vacuum evaporation of metals and thermally stable compounds

(b) cathodic sputtering of metal or metal oxide in a low pressure glow discharge

The fact that the properties of thin films depend on various deposition parameters (substance to be deposited, the nature of the substrate used, film structure and thickness etc.) must be considered in the choice of a particular technique. Of the above methods, the vacuum evaporation method is simple, clean and very convenient, and is at present the most widely used. The thickness and rate of growth can be controlled to a closer limit with the vacuum evaporation technique. Curzon and Chlebek (1972, 1973, 1974) and Gasgnier etal (1974) found the vacuum evaporation method most suitable for producing heavy rare earth dihydride films,

because the film deposition could be easily controlled over the thickness range 70 - 1000A°. Hence this method was chosen for preparing the films studied in this thesis because of the advantages mentioned above.

4.2. Choice of the substrate.

The crystal structure and formation of films are appreciably influenced by the surface on which they are deposited. Generally, a substrate for thin film growth should satisfy the following requirements:

i. Atomic flatness, smoothness and cleanliness over the area of the specimen. The presence of foreign material on the substrate will affect the sticking co-efficient of the arriving atoms as well as their surface mobility.

ii. No chemical reaction or alloying with the deposit.

iii. Sufficiently low vapour pressure not to interfere with film growth at the temperature required for deposition.

iv. A similar coefficient of thermal expansion to that of the deposit, to minimize thermal stresses in the film.

Additionally, the choice of the substrate for an oriented film depends upon the following factors:

(a) Epitaxy must occur on the substrate.

(b) Since the structure of the film is studied by transmission electron microscopy, it must be possible to remove the film from the substrate.

(c) The melting point of the substrate must be higher than the epitaxial temperature of the materials.

Of course these requirements are very seldom met simultaneously in practice. For the present exercise, the prime requirement was to produce monocrystalline dihydrides of the heavy rare earths. Rock salt was chosen as the substrate because it satisfies most of the above requirements and especially it facilitates the examination of the film by transmission electron microscopy. Cleaved mica and thin carbon films

were also used as substrates for electron microscopic studies of poly crystalline films. Microscope glass slides were chosen to support polycrystalline dihydride films for electrical measurements. Most of the investigation was made into the nature of the rare earth dihydride films grown on (100), (110) and (111) faces of rock salt.

4.3. Preparation of the substrate surface.

4.3.1. Cleaved rock salt.

The rock salt available was artificially grown, and supplied as cleaved 1.5" cubes. The artificial crystal is less hygroscopic than natural specimens, probably due to a higher purity and structural perfection. Rock salt only cleaves easily to form (100) faces, which was done by applying a hammer to a sharp edged knife. Cleaved pieces of about 2-3 mm thick were produced and placed in the vacuum chamber as quickly as possible. They were handled carefully with the tweezer and never touched with naked fingers. These precautions minimized the possibility of contamination, moisture and atmospheric attack.

4.3.2. Polished rock salt.

The (110) and (111) faces of rock salt were cut from 1.5" cubes. This was done by means of a reciprocating band saw formed by a cotton thread under tension, lubricated with water, and driven by a simple arrangement of cranks and pulleys (Fig. 4.1.). Since the cut was required to be a (110) or (111) type of plane, the rock salt cubes were held in jigs especially designed to facilitate this (Fig.4.2.). A brass block with a rectangular 'U' cross-section was milled with a plane face P intersecting the channel, in such a way as to be parallel to a (110) plane of a rock salt cube with cleavage faces clamped to the bottom and one side of the channel. A similar jig was used for cutting (111) planes. The rock salt cube projected so that the band saw passing across the jig face P, cut a (110) or (111) type of plane face on the crystal.

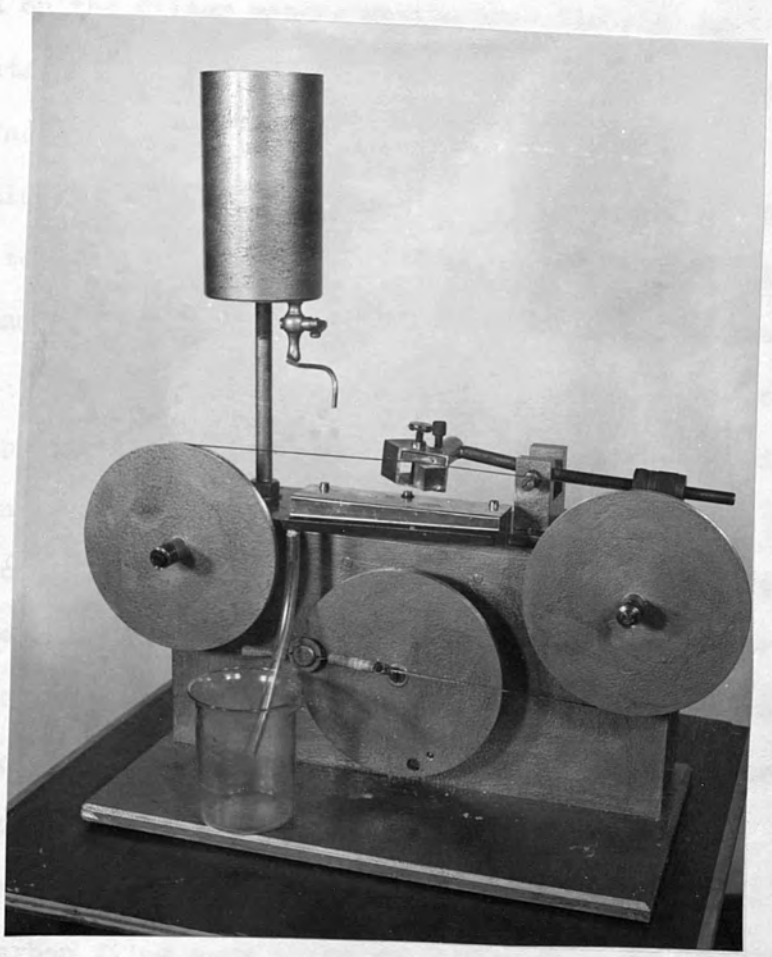

Figure 4.1. Rock salt cutting machine.

When the (111) or (110) face had been cut, any slight saw marks were removed by lightly grinding the face on filter paper moistened with water. This produces a surface which has no macroscopically visible bumps or steps. Grinding continued until the thickness of the slab became about 2-3 mm. satisfactory polishing of the rock salt is essential because films grown on poorly polished surfaces were invariably poorly oriented and mechanically weak. The lower surfaces of the slab were also ground on the filter paper, making them flat, so as to improve thermal contact when, at a later stage, the rock salt was placed on a heated surface.

Polishing was performed on a velvet polishing lap, kept under sufficient tension. The crystal substrate face was moved back and forth by hand for a number of times on a dry portion of the velvet by adding a small amount of putty powder. Then some ethanol was put in another portion of the velvet to make it wet and polishing (back and forth and circular movement) was carried out for about 8-10 minutes until it became very shining and smooth. Care was exercised to avoid any possible dirt while polishing was carried out. This process produced a surprisingly clean surface. Miller (1962) deposited carbon films on such a surface and examined the film in the electron microscope and found no traces of contaminating material.

4.3.3. Carbon films (used as substrates).

Thin carbon films were grown on rock salt in an Edwards 12EA coating unit using a specially designed apparatus (Bradley, 1954). It consists of two pointed carbon rods with the points held lightly together by a tungsten tension spring so that intense local heating occurs in the region of contact. With the carbon rods of about 5 mm diameter an alternating current of 20 amps. was required for evaporation. The rods must be sharply pointed to attain high temperatures and a pencil

sharpener was used for this purpose. Carbon films were then floated off the rock salt and taken onto the copper grids (200 sq.mesh).

4.3.4. Mica substrate.

Tiny shining transparent particles of mica were made by repeatedly cleaving the mica using adhesive tape. The tape was dissolved by immersion in chloroform for about twenty four hours, leaving the mica particles free. These particles are then filtered and placed on copper grids.

4.4. The deposition of the films.

4.4.1. The vacuum system.

The films were prepared by using two separate coating units: Edwards 12EA and Edwards E3. The diameters of the glass bell jars of 12EA and E3 are 12" and 18" respectively. The vacuum chambers were evacuated by means of three-stage water cooled oil vapour diffusion pumps of diameter 4" and 9" respectively, backed by oil rotary pumps. The ultimate pressure of the diffusion pump of 12EA was 5×10^{-6} torr, but the usual operating pressure was $2\text{-}3 \times 10^{-5}$ torr. The operating pressure for E3 was 5×10^{-6} torr. A pirani gauge was used to measure the backing pressure over the range 0.5 to 0.001 torr and a BIRVAC penning guage model T2002 incorporated in the evaporation chamber (E3), covered the range 5×10^{-3} to 1×10^{-7} torr. Since the rare earth metals act as getters for residual gases, the ultimate pressure obtained after effective gettering fell by an order of magnitude.

4.4.2. The evaporation chamber.

Insulated terminals, passing through the base plate of the vacuum chamber, provided electrical access to apparatus in side the bell jar. The filament was supported by thick steel leads. The substrate was placed about 10 cm vertically below the filament on the flat surface

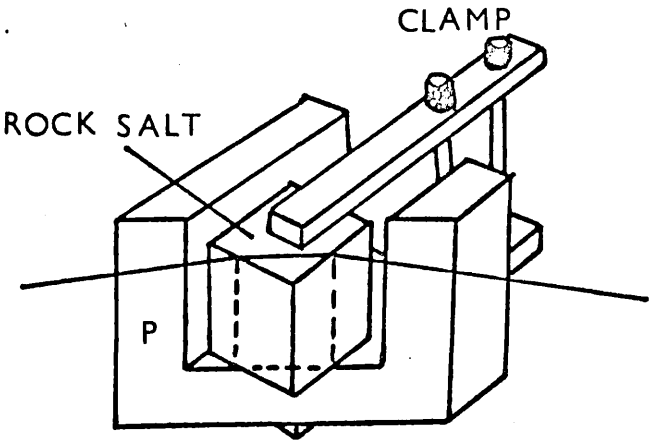

Figure 4.2. Jig used for cutting (110) faces of rock salt.

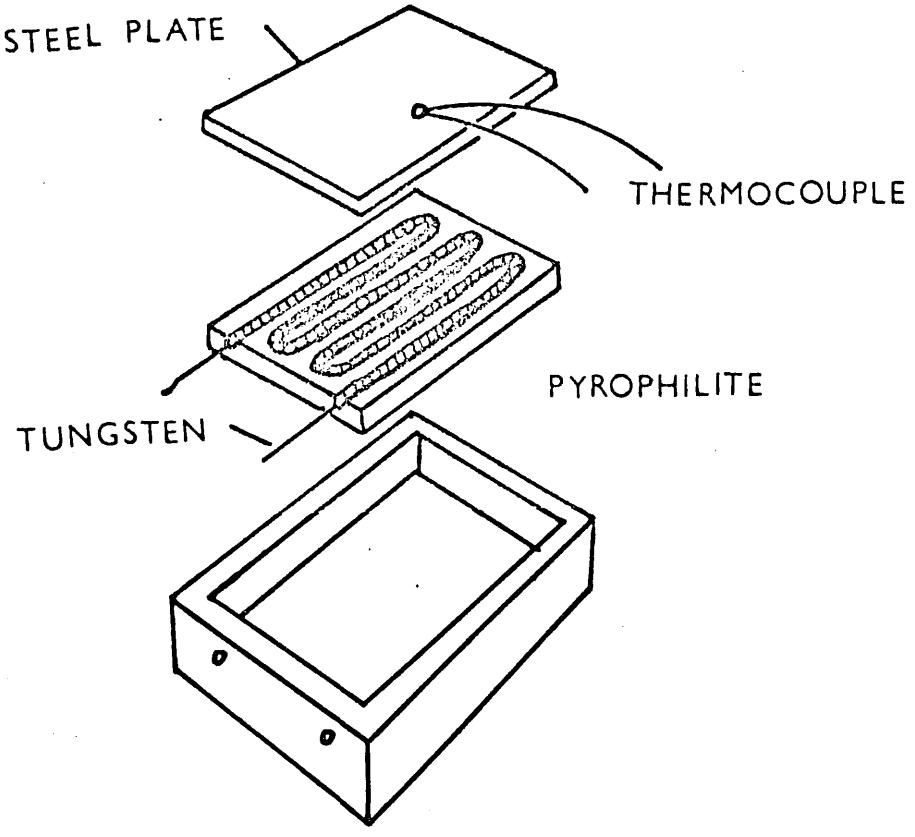

Figure 4.3. The specimen heater.

of an electrically heated stainless steel plate, to which a T_1T_2 thermocouple junction was clamped. The heating element consisted of a flat zig-zag of spirally wound tungsten, supported on a baked pyrophilite base, so as to heat the steel plate uniformly over an area of several times that covered by the rock salt substrate (Figure 4.3.). Alternating current of 0-5 amps. was passed through the heater from a variac transformer with a meter in series. A shutter placed in between the filament and the substrate was operated manually from outside the chamber (Figure 4.4.). A needle valve was fixed to the chamber body which enabled air or H_2 gas to be admitted into the chamber in a finely controlled manner.

4.4.3. The temperature of the substrate surface.

Since it could not be assumed that the temperature of the rock salt surface was the same as that of the heater plate, it was necessary to obtain a calibration in terms of the heater plate temperature. A calibration was therefore obtained in terms of the melting points of various crystalline substances, known to be unreactive with rock salt at the temperature required (table 4.1). Small quantities of these materials were placed on the surface of a typical substrate in vacuo and the temperature of the heater raised, while the crystals were observed through a telescope placed outside the bell jar. By raising the temperature very slowly, and thus allowing the establishment of equilibrium in the rock salt, the thermocouple reading of the heater plate could be calibrated at the known melting points, to within $\pm$ 10°C.

Figure 4.5 shows that there is a considerable difference in temperature between the heater plate and the substrate surface i.e. + 70°C, at 300°C actual temperature. The experiment was repeated with

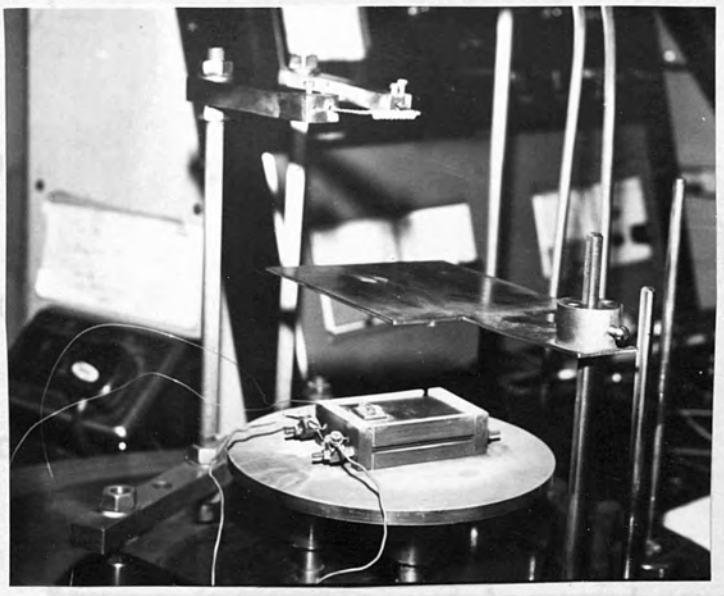

Figure 4.4. Shutter in between the filament and the substrate.

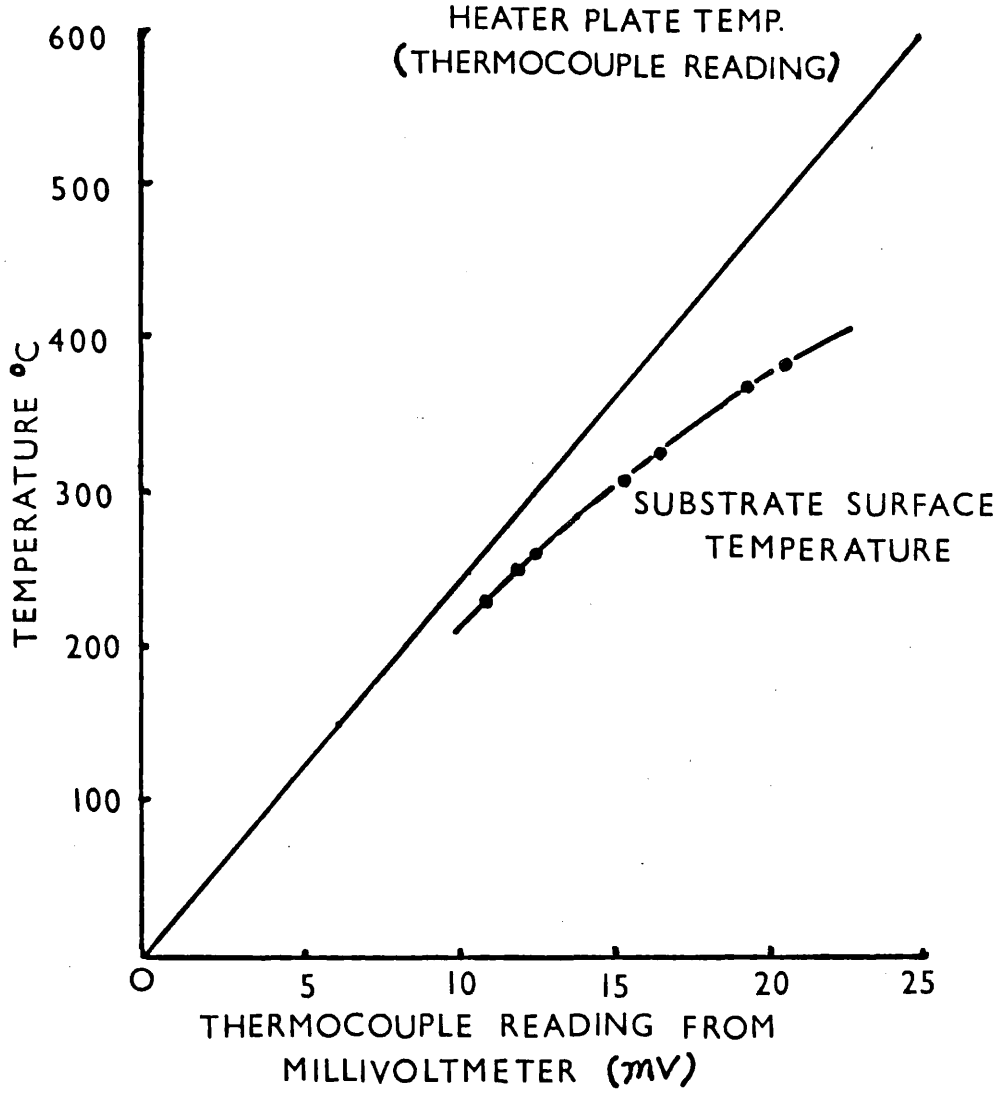

Figure 4.5. Calibration curve for the substrate heater.

other pieces rock salt of similar thickness and different crystal orientations,with the same result. All temperatures mentioned here are therefore true surface temperatures as derived from the calibration curve.

Table 4.1.

Substances used in calibration of substrate surface temperature.

Substance	Melting point ^{0}C
Silver chlorate	230
Sodium dihydrogen phosphate	250
Calcium chloride	260
Sodium nitrate	306
Lead	327
Potassium chlorate	368
Sodium bromate	381

4.4.4. Evaporation procedure.

The substrates were placed in the vacuum chamber immediately after being prepared. The rare earth metals of 99.9% purity were supplied by Koch-Light Ltd.,in the form of wire of 1 mm diameter.They were evaporated from an electrcally heated spirally wound tungsten filament (length~ $2\frac{3}{4}$ cm and internal diameter~ 2 mm)(Fig.4.4.) and the vapour was condensed on rock salt substrate and thin carbon films and transparent cleaved mica supported on copper grids.The distance between the substrate to filament(source) was varied from 8-10cm. The temperature of the substrate was varied from 50^{0}C to 320^{0}C in order to define the epitaxial temperature. The substrates(rock salt) were heated for about four hours before the evaporation. A moveable shutter was used

between the substrate and the source. The shutter had two purposes: firstly, it prevented the metallic vapours from condensing on the substrate until they have gettered the residual gases inside the bell jar and secondly, by successively moving it, films of different thickness could be obtained in the same evaporation.

Prior to evaporation the filament was thoroughly outgassed by passing about 60 amps. a.c. for about ten minutes. The highest melting point of metals studied in this work was H_o and Er, both of which melt a 1500°C. Tungsten melts at 3380°C, so that it appears that contamination of the film by the tungsten filament is unlikely. For evaporation of the metals, alternating current of about 50-60 amps. was passed through the filament. In most cases, the shutter was not removed until the metal vapours have gettered the residual gases. The ultimate pressure prior to evaporation was usually about 5×10^{-6} torr, but after gettering (for Gd) it came down to and remained steady at 6×10^{-7} torr when the film was deposited on the substrate (Fig. 4.6). After the evaporation, the film on the substrate was cooled inside the vacuum to room temperature before it was taken out of the bell jar. For nucleation studies, ultra-thin films of gadolinium and terbium were coated with a thin layer of carbon film, immediately after evaporation.

4.4.5. Removal of the films from the substrate

The rock salt substrate with the film was taken out of the bell jar when it has cooled down to room temperature. By holding with a tweezer, it was then gently lowered into a beaker of distilled water in an inclined position, when the film became separated and floated off as the rock salt dissolved. If the orientation of the film was good, the mechanical coherence of the film and its binding to the substrate was found to be much stronger than for polysrystalline films. The

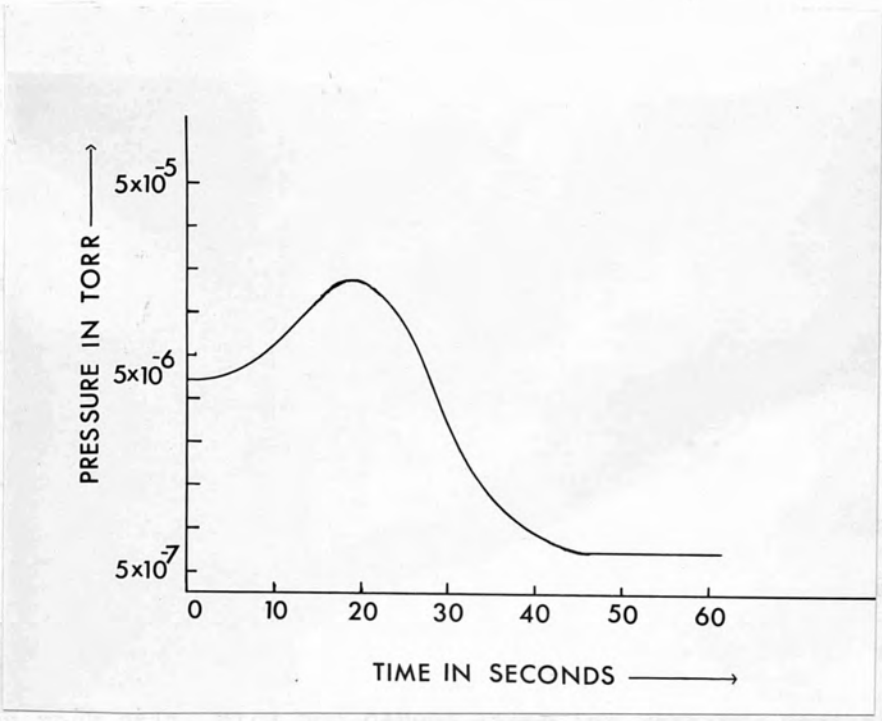

Figure 4.6. Gettering action of Gd.

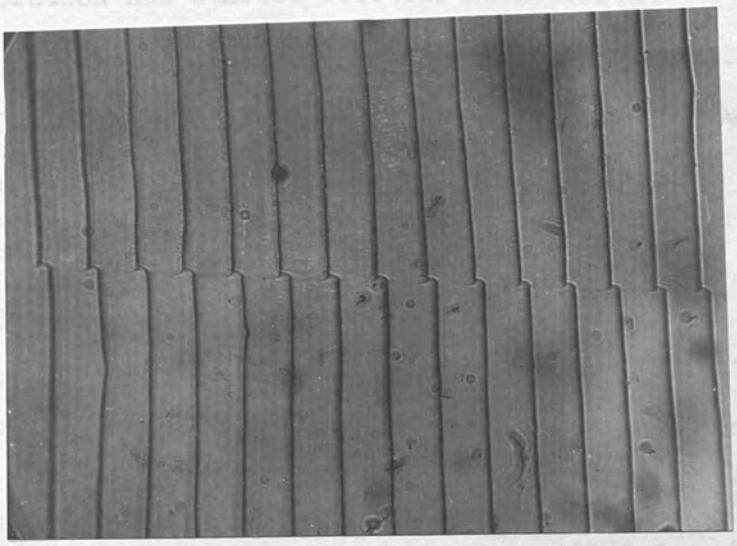

Figure 4.8. Fringe pattern of the multiple-beam interferogram.

attachment of (111) film was the strongest. Frequently the substrates had to be completely dissolved in order to free a film from a (111) face. When the film was free, it was picked up on a clean glass cover slip and transferred to another beaker of distilled water, in order to washoff traces of dissolved sodium chloride from the underneath of the film. Finally it was picked up on copper grids (200 square mesh) for examination in the electron microscope. Extreme care should be exercised in this procedure, otherwise the film might break.

4.4.6. Polycrystalline films.

Polycrystalline films were prepared in the same way as the single crystal films except that the films were deposited on a cold substrate, instead of on a heated one. Polycrystalline films were grown on rock salt, mica and carbon films for electron microscopic studies.

4.5. Films grown after long period of gettering.

In this case the shutter was notremoved for about 5-8 minutes after the evaporation has started i.e. the metal vapour was allowed to condense on the substrate when it has gettered the hydrogen. Although most of the films have been grown after gettering the residual gases, deliberately longer period of gettering was allowed in this particular case.

4.6. Treatment of gadolinium and terbium films with hydrogen.

Gadolinium and terbium films were treated with hydrogen to see its effects on the structure. The performed growth conditions were as follows:

i) Films were grown as usual and then heated at 350°C for about two hours while a stream of H_2 (dry) gas was passing (pressure varied from 0.3 torr to 10^{-5} torr) in a controlled way from a cylinder

through a leak valve.

ii) Films were grown in presence of H_2 gas (pressure 0.5×10^{-5} torr) and some of them were heated up to 350°C.

iii) Films were grown after the chamber was flushed a few times with H_2 (pressure $\sim 10^{-5}$ torr).

iv) It was tried to grow films in H_2 presence at a pressure of $\sim 10^{-3} - 10^{-4}$ torr but did not succeed. The films did not condense well on the substrate and broke into pieces when tried to separate in water.

Films of the thickness range 100 - 900A° were grown under the above circumstances.

4.7. Measurement of film thickness.

The use of Fizeau fringes for thickness measurement is commonly called the Tolansky technique. This technique (Tolansky, 1948) is very convenient and capable of giving the actual thickness with high accuracy. Film thickness measurements in this thesis were carried out by this method. The films were deposited on glass slides, placed by the side of the rock salt (or glass slides for electrical measurements) substrates partly covered by razor blade to get a sharp edge. The razor blade was later removed and an opaque layer of silver ($\sim$ 700A°) deposited over the whole substrate. A step in the silver film of the same thickness as the test film was therefore produced (Fig 4.7.) After removing from the vacuum systems, the step films were brought into contact with a similar glass substrate supporting partially a transparent silver film of about 80% reflectivity and these were clamped together to form a wedge (Fig. 4.7). This was then illuminated with parallel monochromatic light when multiple-beam Fizeau fringes were

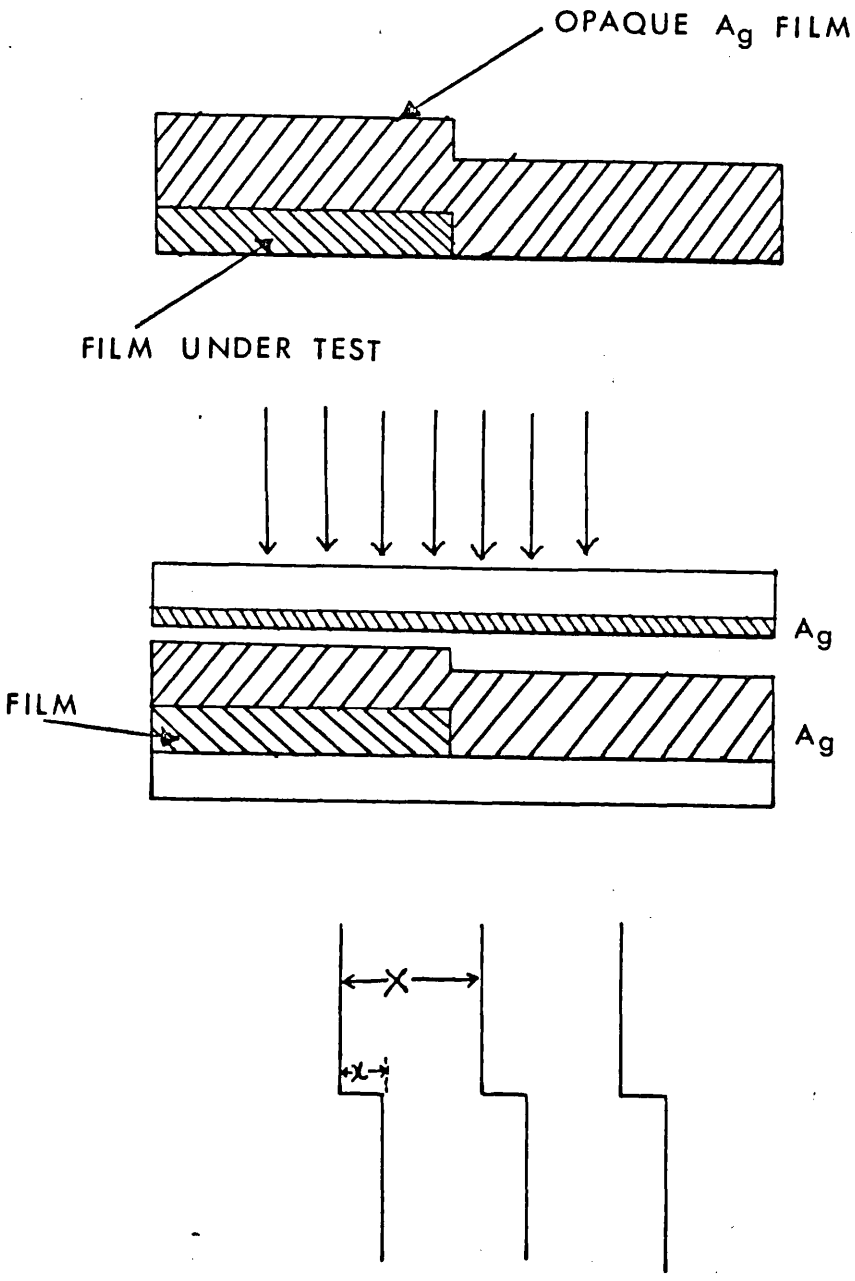

Figure 4.7. Multiple-beam Fizeau fringes.

observed in the microscope.The steps appeared in the fringes and measured accurately by taking photographs.Measuring the step height, the film thickness(t) can be calculated from the known value of wavelength of the light used from the relationship $t = \frac{x}{X} \cdot \frac{\lambda}{2}$ Figure 4.8. shows the appearance of the displaced fringes for a step of 475$\mathring{A}$ gadolinium film.Film thickness as small as 20$\mathring{A}$ and an accuracy of $\pm$ 10$\mathring{A}$ can be measured by this method(Tolansky,1948)

Heavens and Pandeya(1958) applied Tolansky method to iron films,grown epitaxially on rock salt,which had been floated off and mounted on glass. This technique of Heavens and Pandeya was also used in the present work and found satisfactory.

CHAPTER 5.

THE STRUCTURE OF GADOLINIUM, TERBIUM, DYSPROSIUM, HOLMIUM AND ERBIUM DIHYDRIDE FILMS.

5.1. Introduction.

Several workers have reported the observation of cubic phases of rare earth metals formed by vacuum deposition and these structures have been interpreted in different ways as discussed in section 2.4, chapter 2. In this chapter, are described the extensive studies which have been conducted to accurately determine the structures of films of various thickness grown in different epitaxial orientations. The materials examined were Gd, Tb, Dy, Ho and Er. The epitaxial growth from these materials has not been observed before.

The growth and structure of the films grown by the method described in chapter 4, have been studied by using transmission electron microscopy and diffraction. The electron microscopes used were EM-6 and JEM-6A. Electron accelerating voltages of EM-6 were 50 KV, 75KV and 100KV and that of JEM-6A were 50KV, 80KV and 100KV. The optical system of the microscope comprise double condenser lens, an objective and two projectors. The obtainable resolution of the microscopes were in the region of 15Å. The crystal orientation was examined by diffraction of the transmitted electrons, the area of the specimen contributing to the observed pattern being several microns across. Selected area diffraction technique was employed in some instances in order to determine the identity or orientation of small localised features. The d-spacings were measured from the diffraction patterns, using the relationship, $Dd = 2\lambda L$, where D is the ring diameter, d is the interplanar distance, λ is the wavelength of the electrons, L is the effective camera length; the quantity $2L\lambda$ is called the camera constant. The lattice parameters are related to the d-spacings and Miller indices hkl by the expression

$$\frac{1}{d^2} = \frac{h^2 + k^2 + \ell^2}{a_o^2} \quad \text{for f.c.c. system}$$

and $$\frac{1}{d^2} = \frac{4}{3a^2}(h^2 + hk + k^2) + \frac{\ell^2}{c^2} \quad \text{for h.c.p. system,}$$

a_o is the lattice parameter in f.c.c. system and a and c in h.c.p. system. The camera was calibrated by using thallous chloride and gold. Since this work is concerned with the accurate determination of lattice constants, every effort was made to check the camera constant for each set of plates used in the camera. After taking the diffraction pattern on the microscope plates, the ring diameters were measured by using a travelling microscope which has an accuracy of 0.01 mm, a microdensitometer was also used to measure the d-spacings. The thicknesses quoted throughout the work are the average thicknesses.

5.2. Films grown from Gd: structural investigations by electron diffraction.

d-spacings were measured by electron diffraction, for films prepared under different growth conditions and on different substrates.

5.2.1. Films up to 250Å thickness.

i. Epitaxial single crystal films grown on cleaved (100) rock salt. The crystal structure of the film of 200Å is indicated by the diffraction pattern (Fig. 5.1d.). The observed values of the d-spacings are shown in table 1 (in the appendix1)along with the calculated d-spacings of possible structures (f.c.c. GdH_2, f.c.c. Gd and b.c.c. Gd_2O_3). As may be seen from the table all the reflections are consistent with the face-centred-cubic gadolinium dihydride. The d-spacing measurements have been made on a series of films of varying thickness from 70 to 250Å and were found to be in agreement within experimental error (1%) with the values recorded in table 1.

ii. Epitaxial single crystal films deposited on (110) rock salt. The electron diffraction pattern of the film of thickness 180Å is shown in Fig.5.2a. The measured values of the d-spacings are

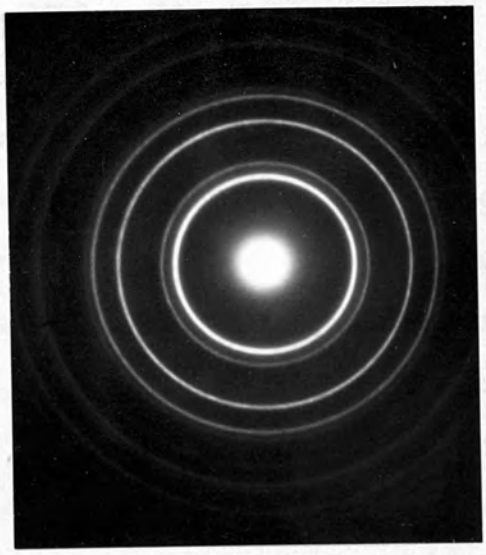

(a) Room Temperature

(b) T = 75°C

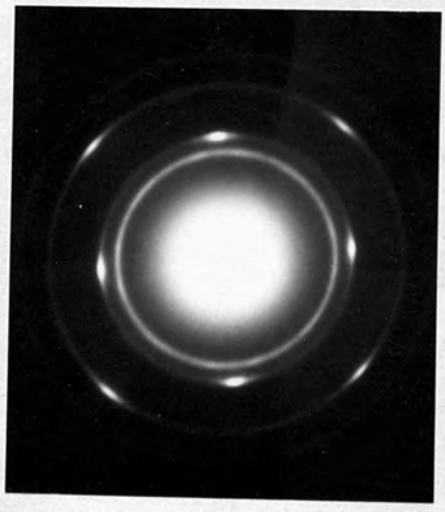

(c) T = 200°C

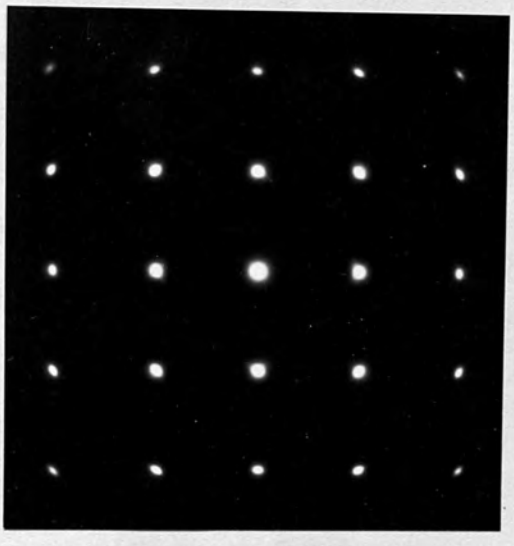

(d) T = 280°C

Fig. 5.1. Electron diffraction patterns of gadolinium dihydride films grown on cleaved rock salt: influence of substrate temperature on orientation.

recorded in table 2 along with the calculated values of f.c.c. GdH_2, f.c.c. Gd and b.c.c. Gd_2O_3. All the values are seen to be in close agreement (within experimental error 1%) with f.c.c. gadolinium dihydride. Not a single reflection corresponded with other structures and hence ruled out their possibilities. Films of varying thickness (70-250Å) were studied and the d-spacings were found to be consistent with the values shown in table 2.

iii. Single crystal films grown on (111) rock salt.

In the (111) orientation of the film only 220 type reflections appeared in the diffraction pattern (Fig. 5.2b). The thickness of the film was 220Å. The measured d-spacings agreed quite well with that of f.c.c. GdH_2 as can be seen from table 3. Because of the symmetry of the diffraction pattern of f.c.c. (111) and h.c.p. (00.1) orientations, the observed d-spacings were compared with h.c.p. (Gd) too. The d-spacings of several other films of the thickness range 70 to 250Å were measured but no significant deviations were observed from the values recorded in table 3.

iv. Polycrystalline films grown on rock salt and on carbon films.

The experimental values of the d-spacings of the films of 150Å deposited on rock salt and carbon films are shown in table 4. The electron diffractions pattern of the films grown on rock salt are shown in Fig. 5.1a. The d-spacings of the film grown on carbon film are shown in bracket. As can be seen from the table, the observed d-spacings are in good agreement with those for f.c.c. dihydrides. The formation of the f.c.c. GdH_2 compound was not affected by the nature of the substrate. A series of films of different thickness from 70 to 250Å were studied, but all had the same structure as f.c.c. GdH_2.

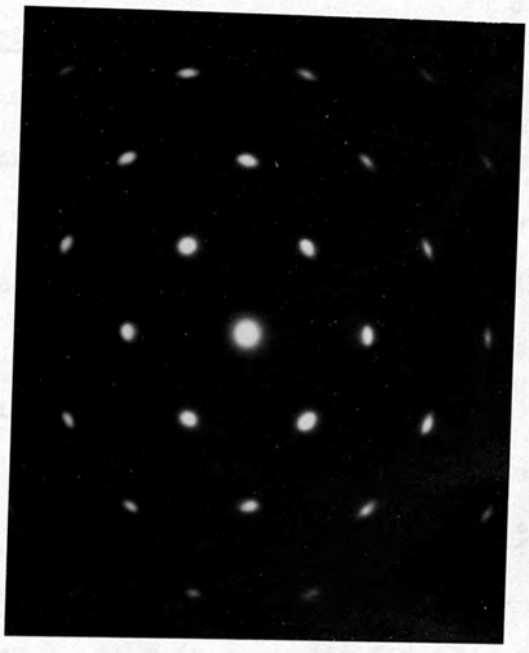

(a) GdH_2 (110), thickness = 180A°

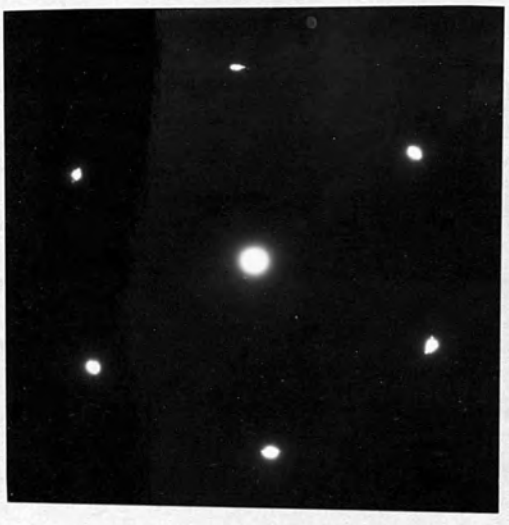

(b) GdH_2(111), thickness = 220A°

Figure.5.2. Electron diffraction patterns of epitaxial single crystal gadolinium dihydride films.

5.2.2. Films of the thickness range 250 - 850Å.

i. Epitaxial single crystal film grown on (100) rock salt.

The crystal structure of the film is clearly seen in the diffraction pattern (Fig. 5.3a) as the co-existence of two phases. The thickness of the film is 450Å. The measured values of the d-spacings are shown in table 5. The indexed pattern of the diffraction pattern is shown in Fig. 5.4a. Comparing the measured values with the calculated d-spacings, it is seen that the structure is composed of two phases - f.c.c. dihydride and h.c.p. metal. The rings (or spots) 1,2,3,4,5, 6 and 7 correspond respectively to 01.0 (h.c.p. Gd), 111 (f.c.c. GdH_2), 00.2 (h.c.p. Gd), 200 (f.c.c. GdH_2), 01.2 (h.c.p. Gd) 220 (f.c.c. GdH_2) and 01.3 (h.c.p. Gd). It may be seen from the diffraction pattern that the debye rings due to h.c.p. structure are faint but they increase in intensity as the thickness increases. The dihydride crystals are also not completely oriented. They deteriorate in orientation as the thickness increases and finally become overlapped by the dominent h.c.p. structure. Films of various thickness (250 - 850Å) were studied and were found to have always mixed phases. Films thicker than 900Å were polycrystalline h.c.p. Gd although the other parameters of epitaxial growth maintained. The d-spacings of the lower indexed reflections sharply define the difference between the two phases (f.c.c. GdH_2 and h.c.p. Gd), but the higher indexed rings or spots are difficult to distinguish from each other because of the close values of their d-spacings.

ii. Epitaxial single crystal films grown on (110) rock salt.

The electron diffraction pattern of 550Å film is shown in Fig. 5.3b. and the observed d-spacings are recorded in table 6. The diffraction pattern clearly indicates the co-existence of two phases. The indexed pattern of the diffraction pattern is shown in Fig.5.4b. Comparing the observed values with the calculated d-spacings, it was found that the

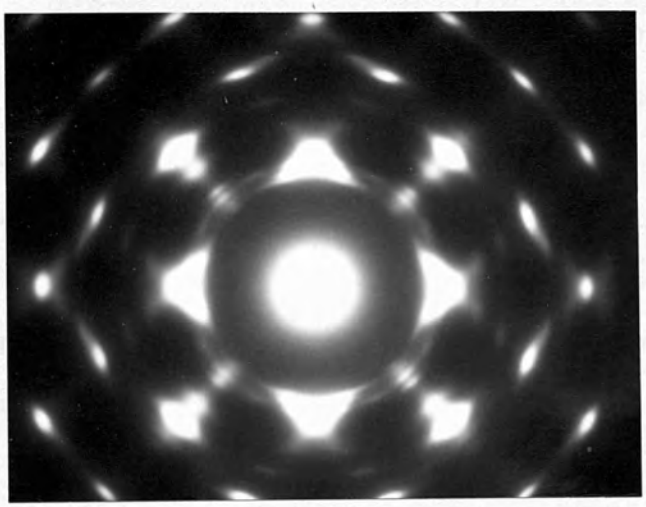

(a) Thickness = 450A°, (100) rock salt substrate

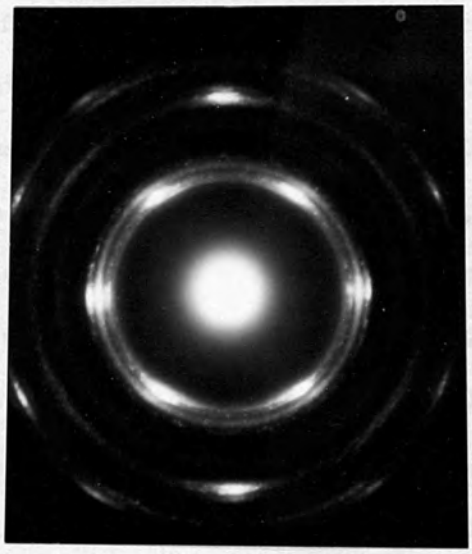

(b) Thickness = 550A°, (110) rock salt substrate

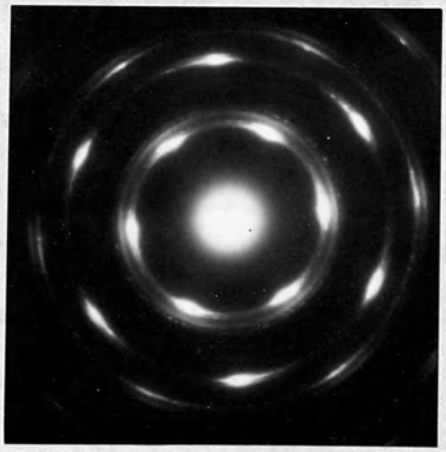

(c) Thickness = 600A°, (111) rock salt substrate

Figure 5.3. Co-existence of f.c.c. gadolinium dihydride and h.c.p. gadolinium in film epitaxially grown on rock salt.

rings 1,2,3,4,5 and 6 correspond respectively to 01.0 (h.c.p.Gd), 111 (f.c.c.GdH_2), 00.2 (h.c.p.Gd), 200 (f.c.c.GdH_2), 01.2 (h.c.p.Gd) and 220 (f.c.c.GdH_2). The ring number 7 corresponds to 11.0 Gd h.c.p. Rings higher indexed than number 7 were not considered in d-spacing measurements because of their closeness together. Films of various thickness (250 - 800Å) were studied and the same structureswere observed, although the intensity of the reflections due to f.c.c. GdH_2 faded out as the thickness increased. Polycrystalline h.c.p. Gd structure appeared above 900Å thickness.

iii. Epitaxial single crystal film grown on (111) rock salt.

The diffraction pattern of 600Å film is shown in Fig. 5.3c. which also indicates the co-existence of two phases. The indexed pattern of the same is shown in Fig.5.4c. Experimental values of the d-spacings are recorded in table 7 along with the calculated values of f.c.c. GdH_2, f.c.c. Gd, h.c.p. GdH_3. On comparison of the observed values with the calculated values in table 7 it is found that the rings, 1,2,3,4,5,6 and 7 are consistent respectively with 01.0 (h.c.p. Gd), 111 (f.c.c. GdH_2), 00.2 (h.c.p. Gd), 200 (f.c.c. GdH_2), 01.2 (h.c.p. Gd), 220 (f.c.c. GdH_2) and 11.0 (h.c.p. Gd). Hence the structure consisted of two phases - f.c.c. GdH_2 and h.c.p. Gd. Measurement of the d-spacings were made on films of various thicknesse's (250-800Å) and the structure always showed a mixture of two phases. As the thickness of the film increased, the intensity of the f.c.c. dihydride spots faded out while that of h.c.p. Gd increased. Finally, the film of thickness above 900Å became completly single crystal (00.1) h.c.p.Gd (Fig. 5.5c). This might have been possible because of the similarity of the crystal structure of (111) substrate and the observed (00.1) orientation.

iv. Polycrystalline film grown on rock salt and on carbon films.

In this case also the structure is composed of two phases - f.c.c. dihydride and h.c.p. metal as seen in the diffraction pattern (Fig.5.5a).

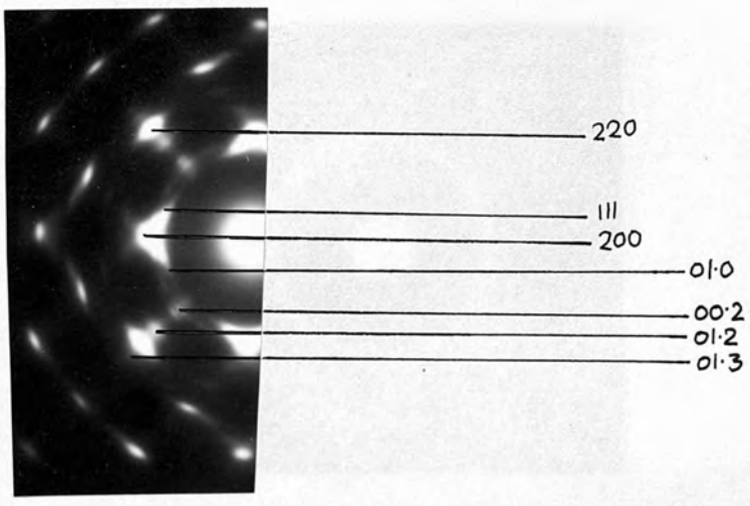

(a) 450A° film grown on (100) rock salt

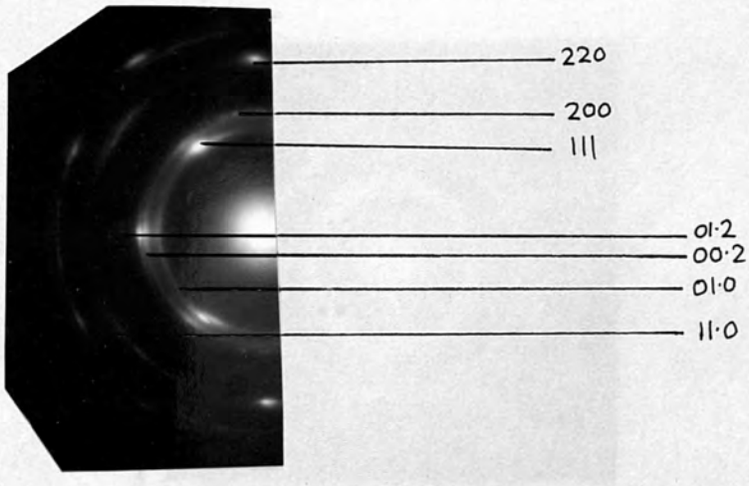

(b) 550A° film grown on (110) rock salt

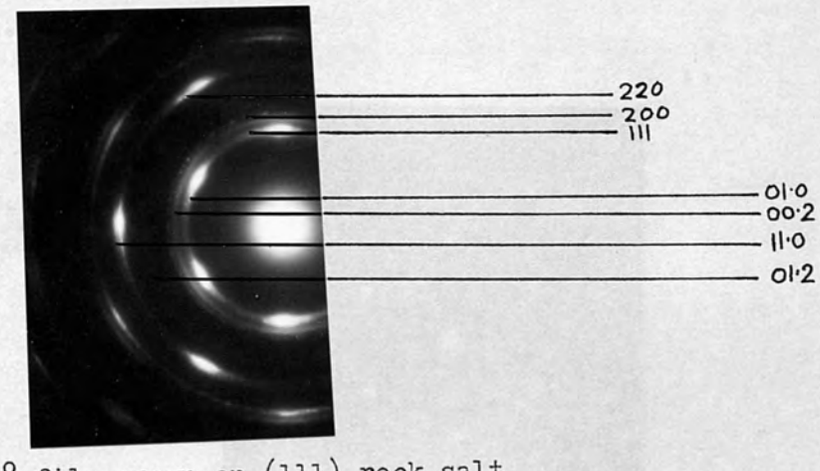

(c) 600A° film grown on (111) rock salt

Figure 5.4. Indexed patterns of Fig. 5.3, showing the co-existence of f.c.c. dihydride and h.c.p. metallic phase.

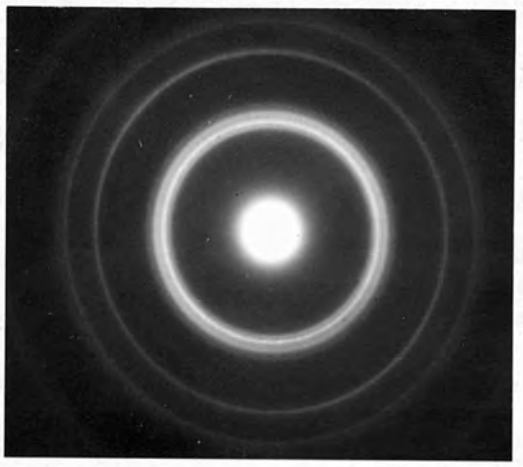

(a) Thickness = 450A°, Polycrystalline film grown on rock salt showing the co-existence of f.c.c. GdH_2 and h.c.p. Gd phase.

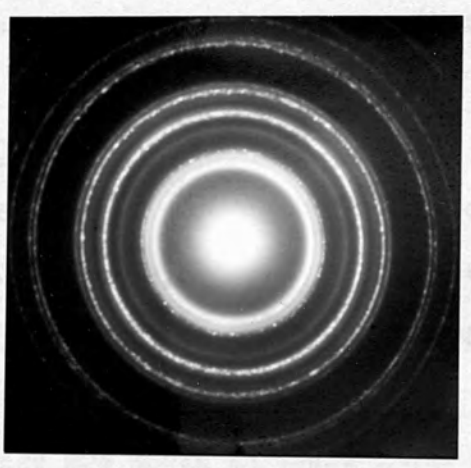

(b) Thickness = 920Å polycrystalline film grown on rock salt showing the h.c.p. structure.

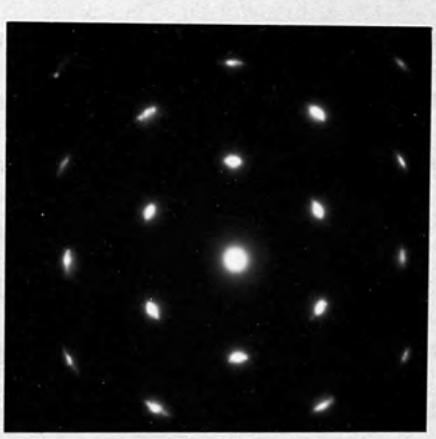

(c) Thickness = 950A°, (00.1) h.c.p. Gd grown on (111) rock salt.

Figure 5.5.

The film thickness is 450Å and was grown on rock salt. The measured d-spacings are shown in table 8. The indexed patterns are also shown in Fig.5.6a. The rings 1,3,5 and 7 correspond respectively to 01.0, 00.2, 01.2 and 11.0 h.c.p. gadolinium and the rings 2,4, and 6 correspond respectively to 111, 200 and 220 f.c.c. GdH_2. Films of different thickness between 250Å to 850Å were studied and found to show the co-existence of two phases (f.c.c. dihydride and h.c.p. Gd). With the increase of the thickness the f.c.c. structure becomes overlapped by the h.c.p. metal and above 900Å thickness, the structure is mainly h.c.p. Gd (Fig. 5.5b.). The d-spacings of the film grown on carbon film are shown in brackets, and indicate very little deviation from those films grown on rock salt.

5.2.3. Films above 900Å thickness.

i. Epitaxial single crystal film grown on (111) rock salt.

The film of about 950Å thick grown on (111) rock salt appeared as single crystal h.c.p. Gd in the (00.1) orientation as may be seen in the diffraction pattern (Fig. 5.5c). The indexed pattern is shown in Fig.5.6c. The measured d-spacings are shown in table 9 and are found consistent with that of h.c.p. Gd. Some very faint reflections due to f.c.c. GdH_2 appeared in the diffraction pattern, though is not clear in the print. The basal plane of orientation was parallel to (111) rock salt surface. Five different films were studied under the same growth conditions and the results obtained were the same.

ii. Polycrystalline film grown on rock salt.

The electron diffraction pattern of 920Å film is shown in Fig.5.5b which is clearly polyscrystalline structure. The experimental values of the d-spacings are shown in table 10. The indexed pattern is shown in Fig. 5.6b. It can be easily seen from Fig.5.6b and table 10 that all the rings except 2 are consistent with h.c.p. gadolinium. The

ring 2 is interpreted as due to f.c.c. 111 gadolinium dihydride, although apparently this ring seemed (from the print) to have merged with ring 1. This has been caused because the intensity of ring 1 has increased with thickness. Five other films of thickness greater than 900Å have been studied and have yielded the same result.

5.3. Films grown from Tb: structural investigations by electron diffraction.

d-spacing measurements of films of various thickness grown from terbium metal on different faces of rock salt and carbon films have been carried out using electron diffraction. Films have been deposited under different growth conditions to study the structural changes.

5.3.1. Films up to 230Å thickness.

i. Epitaxial single crystal films grown on cleaved (100) rock salt. The electron diffraction pattern of 180Å film is shown in Fig.5.7a. and the measured d-spacings are shown in table 11. The calculated values of the d-spacings of f.c.c. TbH_2, f.c.c. Tb and b.c.c. Tb_2O_3 are also shown in the table, as each of them could be claimed as a probable structure. An inspection of the table clearly shows the consistence of the observed values with f.c.c. TbH_2. A series of films of different thickness from 80 to 230Å were studied and found to agree with the values recorded in table 11.

ii. Epitaxial single crystal films deposited on (110) rock salt. The observed values of d-spacings of 200Å film are shown in table 12 and the diffraction pattern of the film is shown in Fig.5.7b. Comparing the observed values with the calculated values, it is seen that they correspond very closely with f.c.c. TbH_2. None of the reflections correspond with any other structures. Films of various thickness from 80 to 230Å were investigated and found to be consistent with f.c.c.

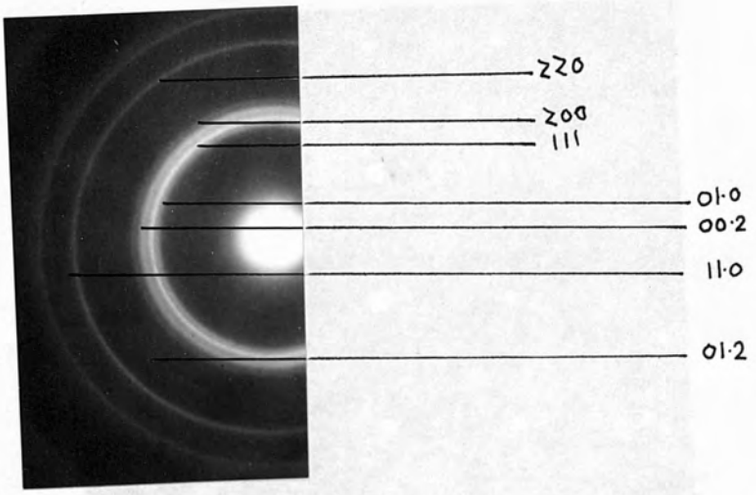

(a) Indexed pattern of Fig. 5.5a

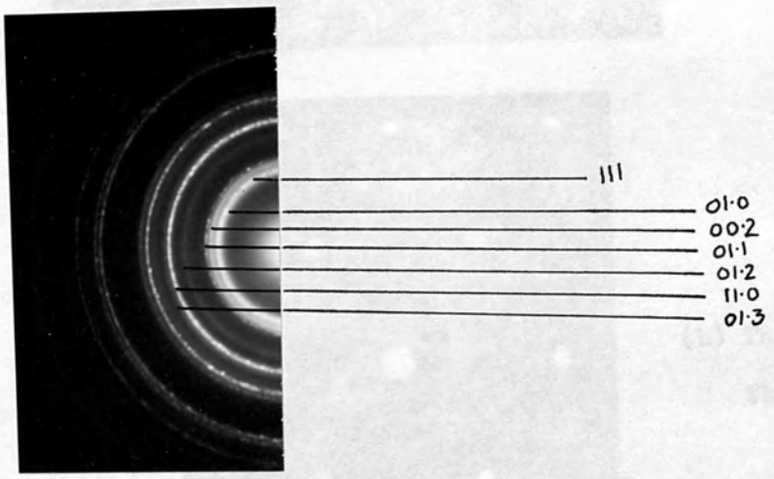

(b) Indexed pattern of Fig. 5.5b.

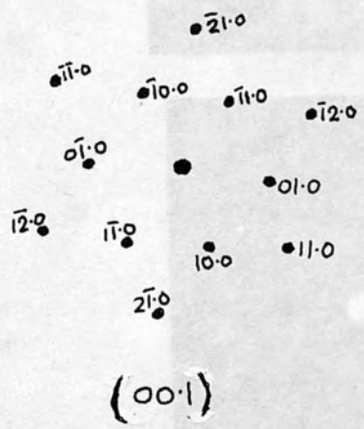

(c) Indexed pattern of Fig. 5.5c.

Figure 5.6. Indexed patterns of Fig. 5.5.

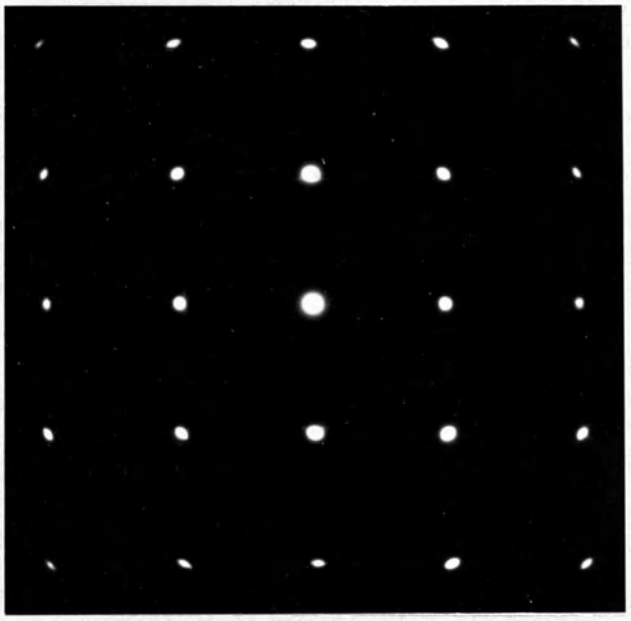

(a) Thickness = 180A°, TbH_2(100).

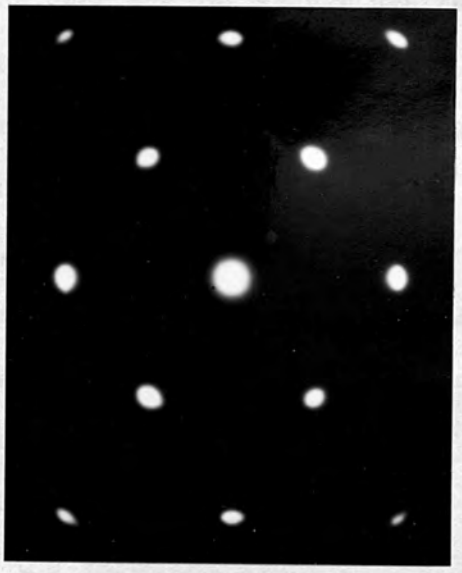

(b) Thickness = 200A°, TbH_2 (110).

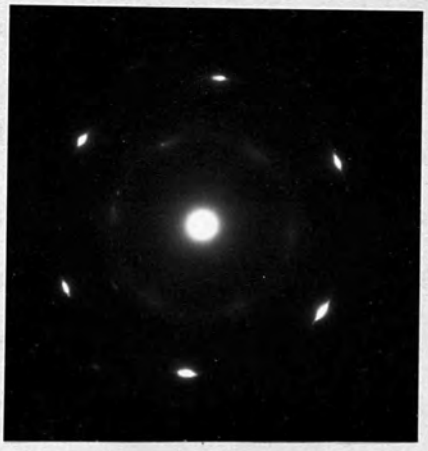

(c) Thickness = 190A°, TbH_2 (111)

Figure 5.7. Electron diffraction pattern of epitaxial single crystal terbium dihydride films grown on rock salt.

terbium dihydride within experimental error (1%).

iii. Epitaxial single crystal films grown on (111) rock salt.

The diffraction pattern of the film of 190Å thick is shown in Fig. 5.7c. and the observed d-spacings are shown in table 13. As may be seen from the diffraction pattern, only 220 reflection appeared. The measured d-spacings agreed quite well with f.c.c. TbH_2. Three other films of varying thickness up to 230Å were also investigated and found to have f.c.c. terbium dihydride structure.

iv. Polycrystalline film grown on rock salt and carbon film.

The diffraction pattern of 200Å polycrystalline film grown on Nacl is shown in Fig.5.8a. and the d-spacings are recorded in table 14.. d-spacings of the film grown on carbon film are shown in the bracket. The observed d-spacings are found to be in good agreement with f.c.c. terbium dihydride. None of the reflections agreed with either h.c.p. Tb or f.c.c. Tb, implying that no material of those structures were present in the film. A series of films of different thickness from 80Å to 230Å were studied to see the structural change. Films up to 230Å thickness always exhibited f.c.c. TbH_2 structure irrespective of the nature of the substrate.

5.3.2. Films of the thickness range 230 to 850Å

i. Epitaxial single crystal film grown on (100) rock salt.

The crystal structure of 650Å thick film is shown in the diffraction pattern (Fig. 5.9a) which indicates the co-existence of two phases. The indexed pattern of the diffraction pattern is shown in Fig.5.10a. The observed d-spacings are recorded in table 15 along with the calculated values of f.c.c. Tb, h.c.p. Tb, f.c.c. TbH_2 and TbH_3. A detailed study of Fig.5.10a and table 15 shows that the film consists of the f.c.c. TbH_2 and h.c.p. Tb. The existence of f.c.c. TbH_2 phase is verified by the presence of 111, 200 and 220 reflections and

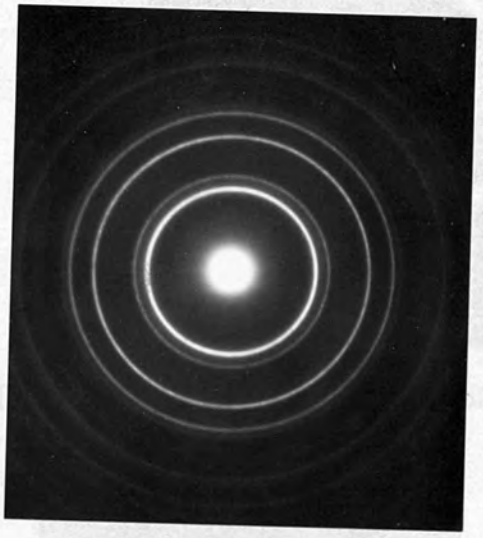

(a) T = 20°C

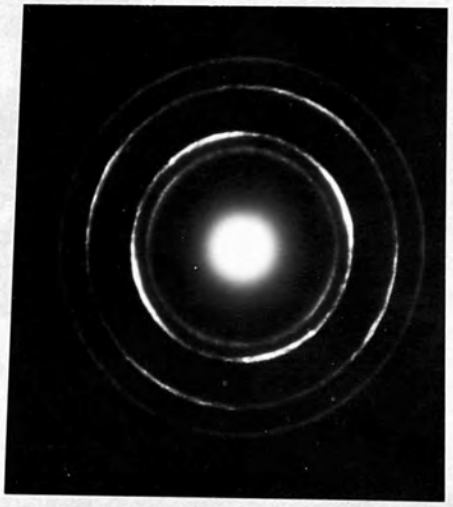

(b) T = 70°C

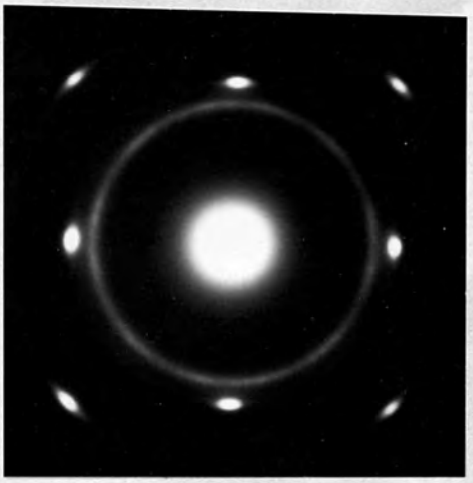

(c) T = 220°C

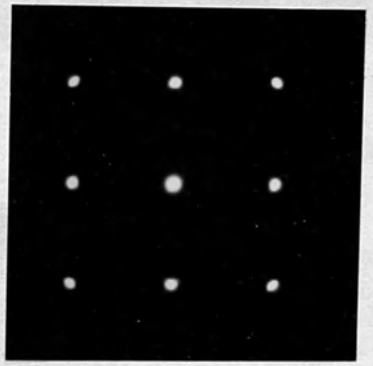

(d) T = 300°C

Figure 5.8. Electron diffraction patterns of f.c.c. terbium dihydride films deposited on cleaved rock salt: influence of the substrate temperature on orientation.

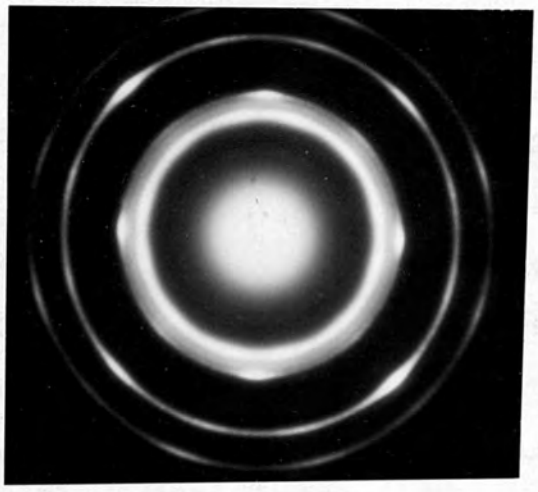

(a) Thickness = 650A°, (100) rock salt substrate.

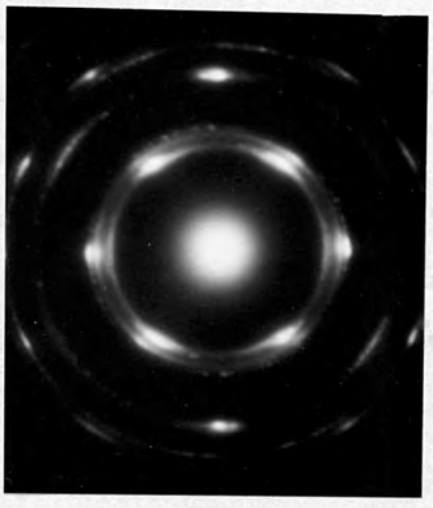

(b) Thickness = 600A°,
(110) rock salt substrate

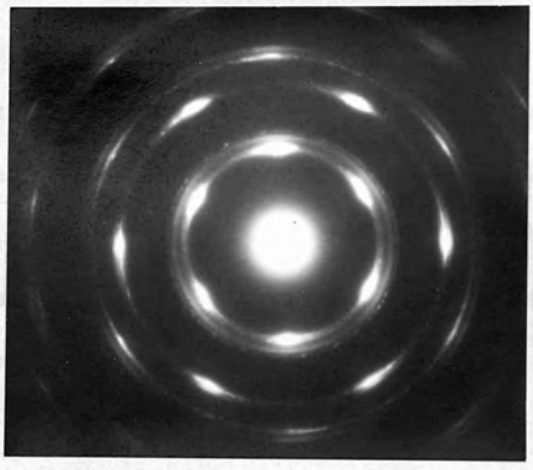

(c) Thickness = 550A°
(111) rock salt substrate

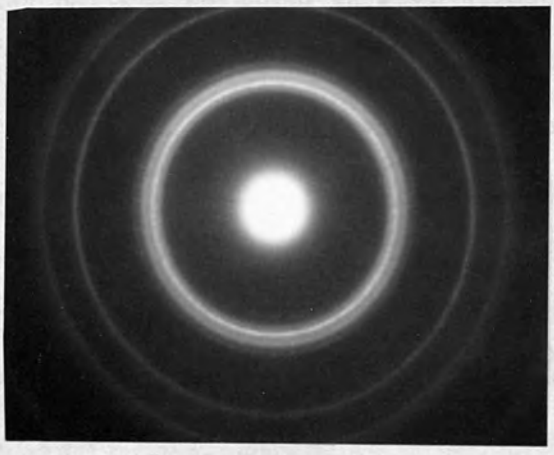

(d) Thickness = 550A°, polycrystalline film grown on rock salt.

Figure 5.9. Co-existence of f.c.c.TbH_2 and h.c.p.Tb in films epitaxially grown on rock salt.

existence of the h.c.p. Tb phase by the 01.0, 00.2 and 01.2 reflections. In the diffraction pattern print the ring 01.2 is very faint, but nevertheless observable. Although the epitaxial growth conditions were maintained, the diffraction pattern shows that the f.c.c. crystallites are not completely oriented. This deterioration in orientation is probably because of the increased thickness. Five films of various thickness from 230 - 850Å have been studied and they always showed the co-existence of the two phases.

ii. Epitaxial single crystal film deposited on (110) rock salt.

The electron diffraction pattern of 600Å film is shown in Fig.5.10b. The experimental values of the d-spacings are recorded in table 16. Comparing the observed values of the d-spacings with the calculated values, it was found that the rings 1,3,5 and 7 correspond respectively to 01.0, 00.2, 01.2 and 11.0 h.c.p. Tb and 2,4 and 6 correspond respectively to 111, 200 and 220 f.c.c. TbH_2. Four other films of the thickness range 230 - 850Å have been studied which also exhibited the presence of mixed phases.

iii. Epitaxial film grown on (111) rock salt.

The electron diffraction pattern of 550Å film is shown in Fig. 5.9c and the indexed pattern is shown in Fig. 5.10d. The observed d-spacings are recorded in table 17. Comparing these values with the calculated values it is found that the composite structure consists of f.c.c. TbH_2 and h.c.p.Tb. The rings 1,3,5 and 7 are due to 01.0, 00.2, 01.2 and 11.0 h.c.p. Tb respectively and the rings 2,4,6 are due to 111, 200 and 220 f.c.c. TbH_2 respectively. Measurement of the d-spacings were also made on films of various thickness from 230Å to 850Å and were found to have mixed phases. Films of thickness above 900Å appeared as single crystal (00.1) h.c.p. Tb as shown in Fig. 5.11a.

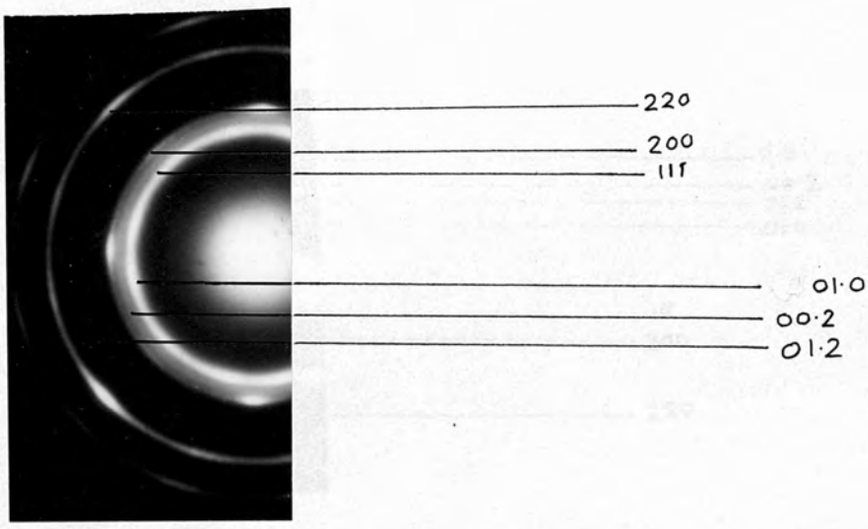

(a) Indexed pattern of Fig. 5.99

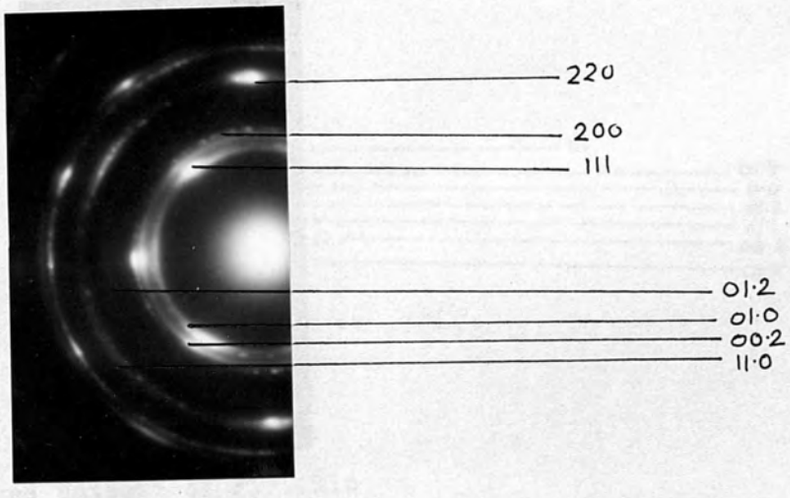

(b) Indexed pattern of Fig. 9b

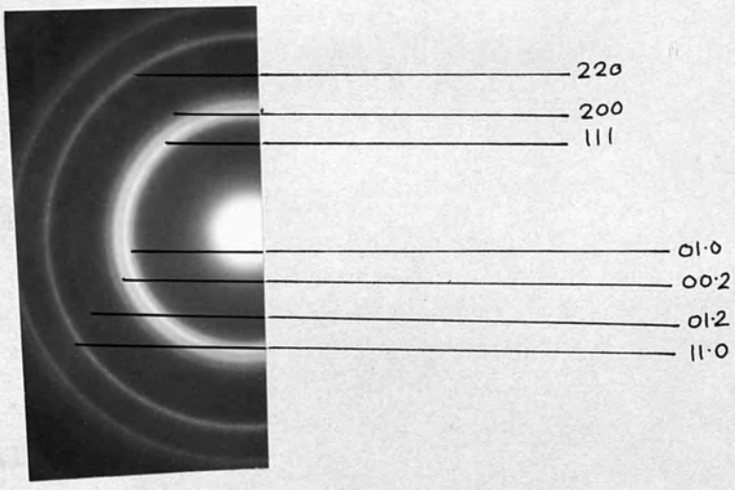

(c) Indexed pattern of Fig. 9d.

Figure 5.10.

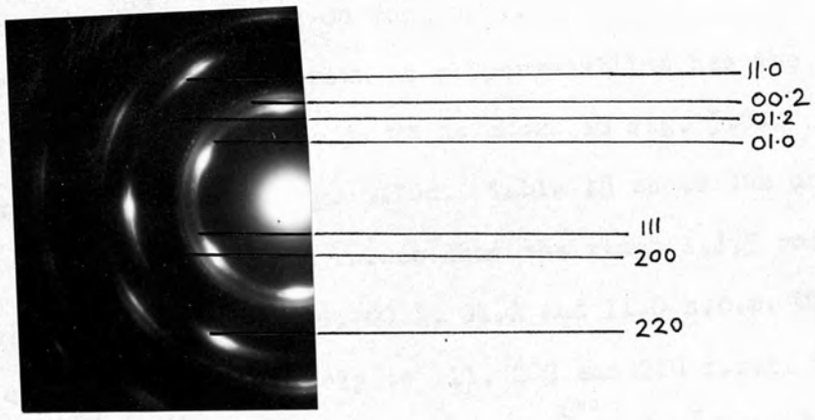

(d) Indexed pattern of Fig. 5.9c

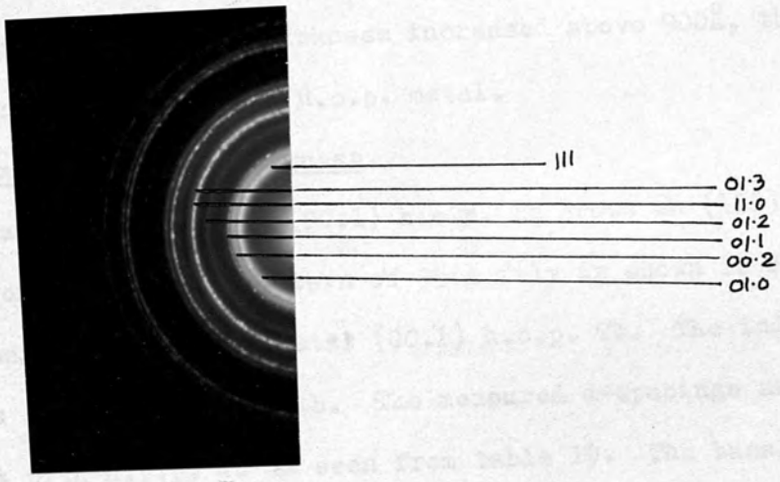

(e) Indexed pattern of Fig.5.11c

Figure 5.10

iv. Polycrystalline film grown on rock salt.

The film of about 500Å thick grown as polycrystalline has the structure composed of f.c.c. TbH_2 and h.c.p. Tb as shown in Fig. 5.9d. The indexed pattern is shown in Fig. 5.10c. Table 18 shows the observed d-spacings with the calculated values that the rings 1,3,5 and 7 correspond respectively to 01.0, 00.2, 01.2 and 11.0 h.c.p. Tb and 2,4 and 6 correspond respectively to 111, 200 and 220 f.c.c. TbH_2. A series of films of various thicknesses from ~~80~~ 230 to 850Å have been studied and found to show the co-existence of f.c.c. dihydride and h.c.p. Tb phases. As the thickness increased above 900Å, the structure was found to be dominated by h.c.p. metal.

5.3.3. Films above 900Å thickness.

i. Epitaxial single crystal (00.1) h.c.p. Tb grown on (111) rock salt.

The electron diffraction pattern of 950Å film is shown in Fig. 5.11a which appeared as single crystal (00.1) h.c.p. Tb. The indexed pattern is shown in Fig. 5.11b. The measured d-spacings are found consistent with h.c.p. Tb as seen from table 19. The basal plane of orientation is parallel to (111) rock salt. The observation of (00.1) Tb was verified by studying four films of similar thickness.

ii. Polycrystalline film of 930Å grown on rock salt.

The electron diffraction pattern of the film is shown in Fig. 5.11c (and indexed pattern is shown in Fig.5.10c), which is predominated by h.c.p. structure of Tb. The observed values of the d-spacings are recorded in table 20, which are consistent with h.c.p. Tb except ring 2. This ring is interpreted as due to 111 f.c.c. dihydride. It was not possible, unfortunately to study films thicker than 980Å or so because such films did not allow the requisite transmission. However, four films up to 950Å thickness have been studied and found to be dominated by h.c.p. terbium.

(a) 950A° (00.1) Tb film grown on (111) rock salt

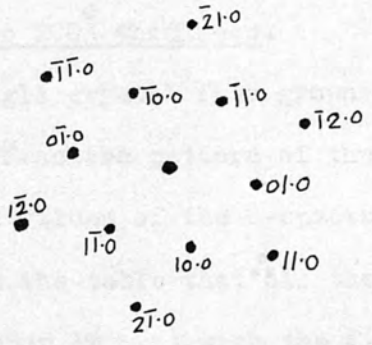

(b) Indexed pattern of Fig. 5.11a.

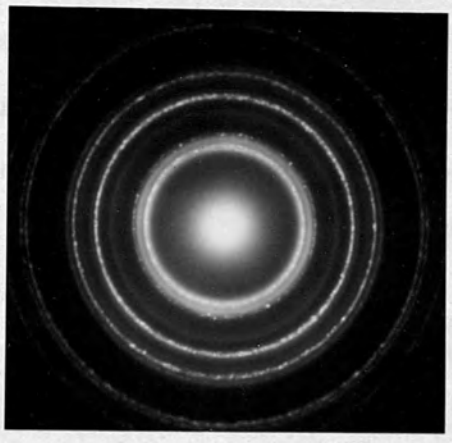

(c) 930A° polycrystalline film grown on rock salt.

Figure 5.11 Diffraction pattern for terbium films.

5.4. Films grown from Dy: structural investigations by electron diffraction.

It has been established from the extensive investigations of films grown from Gd and Tb that at a lower thickness the structure is due to f.c.c. dihydride, at an intermediate thickness both f.c.c. dihydride and metallic h.c.p. phase exist and at higher thickness h.c.p. metallic structure predominates. Although similar results were expected from Dy, H_o and Er films because chemically they are similar, structural investigations were carried out to a lesser extent on these films.

5.4.1. Films upto 200Å thickness.

i. Epitaxial single crystal film grown on (100) rock salt.

The electron diffraction pattern of the film of 170Å is shown in Fig.5.18a and the measured values of the d-spacings are shown in table 21. It may be seen from the table that all the reflections agreed quite well (experimental error 1%) with the f.c.c. dysprosium dihydride. All the films studied up to 200Å thickness showed this structure.

ii. Polycrystalline film of 150Å grown on rock salt.

The experimental values of the d-spacings are shown in table 22; comparing with the calculated values they are found to correspond with f.c.c. dysprosium dihydride. The d-spacing measurements have also been done on the films grown on carbon film and the results obtained were the same. Three films have been studied by varying the thickness up to 200Å but the results did not differ from the above.

5.4.2. Films of the thickness range 200-800Å

i. Epitaxial film grown on (100) rock salt.

The measured values of the d-spacings of 500Å film are shown in table 23. The electron diffraction pattern of the film is similar to that of Figure 5.3a. for gadolinium. The structure is a mixture of

f.c.c. dihydride and h.c.p. metallic phases. It may be seen from the table that the rings 1,2,3,4,5,6 and 7 correspond respectively to 01.0 (h.c.p.Dy), 111 (f.c.c.DyH_2), 00.2 (h.c.p.Dy), 200 (f.c.c.DyH_2), 01.2 (h.c.p.Dy), 220 (f.c.c.DyH_2) and 11.0 (h.c.p.Dy). Variation of thickness in the range 200 - 800Å did not produce any different results.

ii. Polycrystalline film of 500Å grown on rock salt.

The structure of the film as revealed by electron diffraction pattern is similar to that of Fig.5.5a. hence is not shown separately. The measured d-spacings are shown in table 24. on comparison with the calculated values it becomes obvious that the observed d-spacings due to rings 1,2,3,4,5,6 and 7 are consistent respectively to 01.0 (h.c.p.Dy) 111(f.c.c.DyH_2) 00.2 (h.c.p.Dy), 200 (f.c.c.DyH_2), 01.2 (h.c.p.Dy), 220 (f.c.c.DyH_2) and 11.0 (h.c.p.Dy). This structural feature of the co-existence of two phases existed in the thickness range 200-800Å, although it was observed that the intensity of f.c.c. dihydride reflections faded out while that of h.c.p. Dy became stronger as the thickness increased.

5.4.3. Films above 800Å thickness.

The measured values of the d-spacings of 900Å polycrystalline film grown on rock salt are shown in table 25. The diffraction pattern is quite similar to that of Fig.5.5b, hence is not shown separately. Comparing the observed d-spacings with the calculated values, it is seen that all the rings except one correspond with h.c.p. Dy. Ring 2 corresponds to 111 f.c.c. DyH_2. This result is similar to that of Gd and Tb films. Hence the general conclusion is that thicker films are dominated by h.c.p. metallic structure. Epitaxial single crystal films of 900Å were also obtained on (111) rock salt having the (00.1) orientation.

5.5. Films grown from Ho: structural investigations by electron diffraction.

d-spacing measurement of holmium films of different thickness and orientations grown on rock salt and also of polycrystalline films grown on rock salt and carbon films have been made. Since the results obtained are in general agreement with those of Gd and Tb films, the results of only few cases are discussed here. The diffraction patterns also have the similar feature, hence are not put in some cases to avoid unnecessary increase of the volume of the thesis.

5.5.1. Films up to 200Å thickness.

i. Epitaxial single crystal film grown on (100) rock salt.

The electron diffraction patternof 150Å film is shown in Fig. 5.19a and the measured d-spacings are recoreded in table 26. As may be seen from table 26, all the reflections are in good agreement with face-centred-cubic holmium dihydride. Several films of varying thickness between 70Å to 200Å have been studied and found to have f.c.c. HoH_2 structure.

ii. Polycrystalline film grown on rock salt and carbon film.

The measured d-spacings of polycrystalline films grown both on rock salt and carbon film are shown in table 27. The values shown in bracket are due to film grown on carbon. The thickness of the films were about 130Å.on comparison with the calculated values, it is found that the structure is consistent with f.c.c. HoH_2. Three films of different thicknesses up to 200Å were studied having the same result.

5.5.2. Films of the thickness range 200 - 800Å.

i. Epitaxial film grown on (100) rock salt.

The experimentald-spacings of 500Å film grown epitaxially ~~is~~ are shown in table 28. The structure appeared as the co-existence of f.c.c. dihydride and h.c.p. metal. The existence of f.c.c. dihydride is

verified by the appearance of 111, 200 and 220 reflections. The existence of h.c.p. Ho is justified by the presence of 01.0, 00.2, 01.2 and 11.0 reflections. The intensity of the different refelctions varied over the above thickness range, although the overall structure appeared as the mixture of two phases.

ii. Polycrystalline film grown on rock salt.

The measured d-spacings of 450Å film is shown in table 29. The structure is found to consist of both f.c.c. dihydride and h.c.p. metal as seen from the table. The rings 1,3,5 and 7 are due to 01.0, 00.2, 01.2 and 11.0 h.c.p. H_o and 2,4 and 6 correspond to 111, 200 and 220 f.c.c. HoH_2. Films of varying thickness over the range 200 - 800Å have been studied and found to agree with the values recorded in table 29 within experimental error (1%).

5.5.3. Films above 800Å thickness.

The experimental values of the d-spacings of 870Å polycrystalline film grown on rock salt are shown in table 30. It is found on comparison with the measured d-spacings that the structure is predominated by metallic h.c.p. structure. The rings 1,2,3,4,5,6 and 7 correspond respectively to 01.0, 00.2, 01.1, 01.2, 11.0 and 01.3 h.c.p. H_o and only ring 2 is consistent with 111 f.c.c. holmium dihydride. Three other films thicker than 800Å have been studied and found to have the similar structure.

5.6. Films grown from Er: structural investigations by electron diffraction.

In this case also the results of only some typical experiments are discussed, although extensive studies have been made. Since the results were found to follow the trend of the films from Gd and Tb, it was felt unnecessary to elaborate all the details.

5.6.1. Films up to 210Å thickness.

i. Epitaxial single crystal film grown on (100) rock salt.

The crystal structure of 160Å film clearly indicates face-centred-cubic as is seen from the diffraction pattern (Fig. 5.20a). The measured d-spacings are shown in table 31. It is found on comparison of the d-spacings that the structure is consistant with f.c.c.ErH_2. Four films of various thicknesses from 70Å to 210Å have been studied and found to agree with f.c.c. ErH_2.

ii. Polycrystalline films deposited on rock salt and carbon films.

The observed d-spacings of 170Å film grown on rock salt is shown in table 32. As may be seen from the table, the observed d-spacings are consistent with f.c.c.ErH_2. None of the reflections agreed with any other structures. Film thickness variations over the range up to 210Å did not produce any different structure.

5.6.2. Films of the thickness range 210 - 800Å.

i. Epitaxial film grown on (100) rock salt.

The measured values of the d-spacings of 600Å film is shown in table 33. The structure is seen to have a mixture of two phases. The appearance of 111, 200 and 220 reflections indicate the presence of f.c.c. ErH_2 and that of 01.0, 00.2, 01.2 and 11.0 verify the presence of h.c.p. Er metal. Four films of the thickness range 210 - 800Å have been studied and found to show the same structure.

ii. Polycrystalline film deposited on rock salt.

The structure of 550Å film is found to have mixed phases. The observed d-spacings are shown in table 34. These values are seen to be consistent with both f.c.c. dihydride and h.c.p. metal. The rings 1,3,5 and 7 are found to correspond 01.0, 00.2, 01.2 and 11.0 h.c.p. Er respectively and the rings 2,4 and 6 correspond to f.c.c. 111, 200 and 220 ErH_2 respectively. Film of various thickness over the range 210 -

800Å have been studied and found to possess mixed phases.

5.6.3. Films above 800Å thickness.

The observed values of the d-spacings of 900Å polycrystalline film grown on rock salt are shown in table 35. These values are found to correspond with h.c.p. erbium except one. The rings, 1,3,4,5,6 and 7 are found consistent to 01.0, 00.2, 01.1, 01.2, 11.0 and 01.3 h.c.p. Er respectively and ring 2 correspond to 111 face-centred-cubic erbium dihydride. All the films thicker than 800Å were found to be dominated by h.c.p. metallic structure.

5.7. Experimental observations of epitaxial single crystal films.

It is quite convincing from the structural investigations made by electron diffraction in the foregoing section that thin films form the f.c.c. dihydrides of the respective metals and thicker film structures are predominated by h.c.p. bulk structure, while the films of intermediate thickness range show the co-existence of f.c.c. dihydrides and h.c.p. metallic phase. In this section the following observations have been made on the epitaxially growing single crystal dihydride films of Gd, Tb, Dy, H_o and Er.

5.7.1. Gadolinium dihydride films.

i. Influence of the substrate temperature on orientations.

a. Films grown on cleaved (100) rock salt.

Gadolinium dihydride films were prepared on cleaved rock salt substrates which were maintained at elevated temperatures ranging from room temperature to 320°C in order to determine the epitaxial temperature. When prepared by cleaving in air, the rock salt surface usually carries some residual polycrystalline debris, and this was removed by annealing at 450°C for about three hours in a vacuum, after which the substrate was cooled to the deposition temperatures.

The films deposited on cold rock salt substrates were randomly oriented polycrystalline, Fig. 5.1a. An increase in the deposition temperature produced a preferred orientation of some of the crystallites, intensifying the f.c.c. spots on the otherwise uniform rings (Fig.5.1b). Films deposited at 200°C showed even better orientation (Fig.5.1c) with an increase in the intensity and number of reflections. Substantially complete orientations were obtained for substrate temperature of 280°C. The d-spacing measurement of such film is shown in table 1. Figure 5.1d shows the electron diffraction pattern of epitaxial (100) gadolinium dihydride film. The orientation observed was

$$GdH_2(001)\,[100] \,||\, NaCl\,(001)\,[100]$$

No extra spots appeared in the diffraction pattern, which ruled out the possibility of any twins or double diffractions. Deposition at temperatures higher than expitaxial temperature had no effect on orientation but showed deterioration above 400°C.

b) Films grown on polished (100), (110) and (111) rock salts.

The gadolinium dihydride films which were grown directly on polished rock salt faces (100), (110) and (111) at 280°C showed a deterioration in the orientation (Fig. 5.12.). This lack of orientation was evidently due to the rock salt surfaces being disordered by polishing so as to consist of fairly large crystals with little mutual orientation. As in the case of nickel (Miller, 1962), it was found that annealing the substrate at higher temperature (450°C in this work), and then the evaporation at epitaxial temperature (280°C) produced single crystal films in parallel orientation on the (100), (110)and (111) faces. (Fig.5.2). The d-spacing measurement of (110) and (111) films are shown in table 2 and 3 respectively. Evaporation of the films at low temperatures always produced poorly oriented films. Substrate temperatures were varied from room temperature to 300°C to define

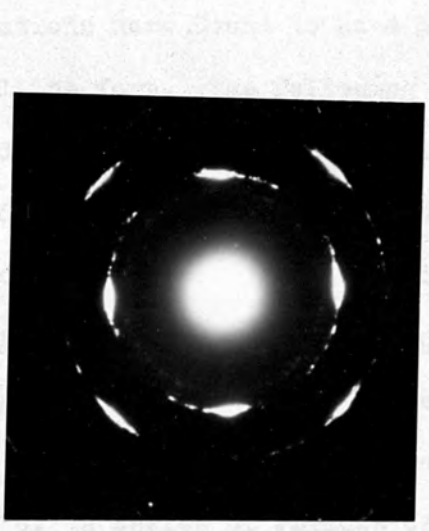

(a) GdH_2 (100)

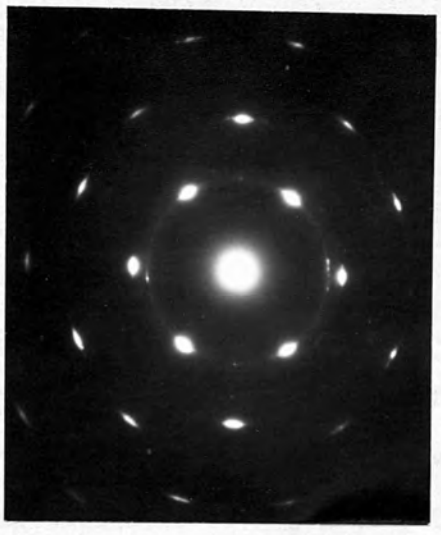

(b) GdH_2 (110)

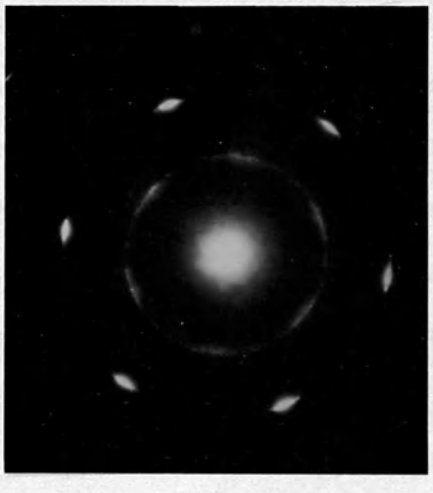

(c) GdH_2 (111)

Figure 5.12. Electron diffraction patterns of GdH_2 films grown on polished rock salt at 280°C without prior annealing.

the epitaxial temperature. The films on the (111) and (110) orientations were found to have much difficulty to grow in perfect crystalline form. The following orientations were observed

GdH_2 (001) [100] || Nacl (001) [100]

GdH_2 (110) [001] || Nacl (110) [001]

GdH_2 (111) [$\bar{1}$10] || Nacl (111) [$\bar{1}$10]

ii. Influence of film thickness on orientation and structure.

The influence of the film thickness on the orientation and structure of the deposit has been investigated with the substrate temperature at 280°C. A series of regions of varying thickness from 30Å to 900Å were obtained by moving the shutter in discrete steps across the substrate surface during deposition. The diffraction patterns of very thin films (~30Å) were even nearly epitaxial with little disorientation. As the thickness was increased to 60Å, the complete orientation was attained. In this case the effect of thickness on orientation was not as great as in the case of f.c.c. metals (Pashley, 1958 and Miller, 1962). The effect of thickness on structure is highly important as is evident from the foregoing sections; so is not discussed here. Thinner films are f.c.c. dihydrides but as the thickness increased, this structure is gradually overlapped by the h.c.p. metallic structure. This feature has also been verified by RHEED in section 6.6., chapter 6.

iii. Influence of the rate of deposition on orientation.

It is well known that the temperature at which epitaxy occurs is dependent on the deposition rate. Hence a wide range of deposition rates were attempted to find a suitable one for the epitaxial growth. Higher deposition rates (400 - 500Å / min.) produced deterioration in the orientation of the film. Very slow evaporation rates (~20Å / min) again produced poor orientation. The optimum deposition rate which gave satisfactory oriented film was found to be 60Å/ min. This moderately

slow evaporation rate might have favoured epitaxy because the film resulted in a higher ratio of contamination (Shinozaki and Sato, 1955, Matthews and Grunbaum, 1965) of the residual hydrogen gas. Influence of the rate of deposition was found to be the same for all the three orientations.

iv. Influence of the substrate temperature on microstructure of the films.

From the electron micrograph of thin film of gadolinium dihydride (Fig.5.13) of about 220Å thick, grown on cleaved rock salt at room temperature, it is seen that the crystallite size was relatively small. This film corresponded to the diffraction pattern of Fig. 5.1. As the substrate temperature was increased and orientation improved, the crystallite size increased (Fig.5.13). But the increament of crystallite size with temperature was found to be smaller than in metallic film (Miller, 1962, Honma and Wayman, 1965). There was no evidence of stacking faults or twinning in the micrograph. Some dislocation loops were found to move when the specimen was irradiated by electron beam. The films grew by the coalescence of small isolated islands and became continuous at a very lower thickness ~80Å. The electron micrographs of epitaxial single crystal (110) and (111) gadolinium dihydride are shown in Figs. 5.14a and 5.14b respectively. Fig.5.15a represent the microstructure of 450Å film (whose diffraction pattern is shown in Fig.5.3a grown epitaxially on (100) rock salt). The electron micrographs of 450Å polycrystalline film which shows the co-existence of f.c.c. dihydride and h.c.p. metallic phase (diffraction pattern, Fig.5.5a) is shown in Fig. 5.15b and that of 920Å polycrystalline h.c.p. gadolinium film is shown in Fig. 5.15c.

5.7.2. Terbium dihydride films.

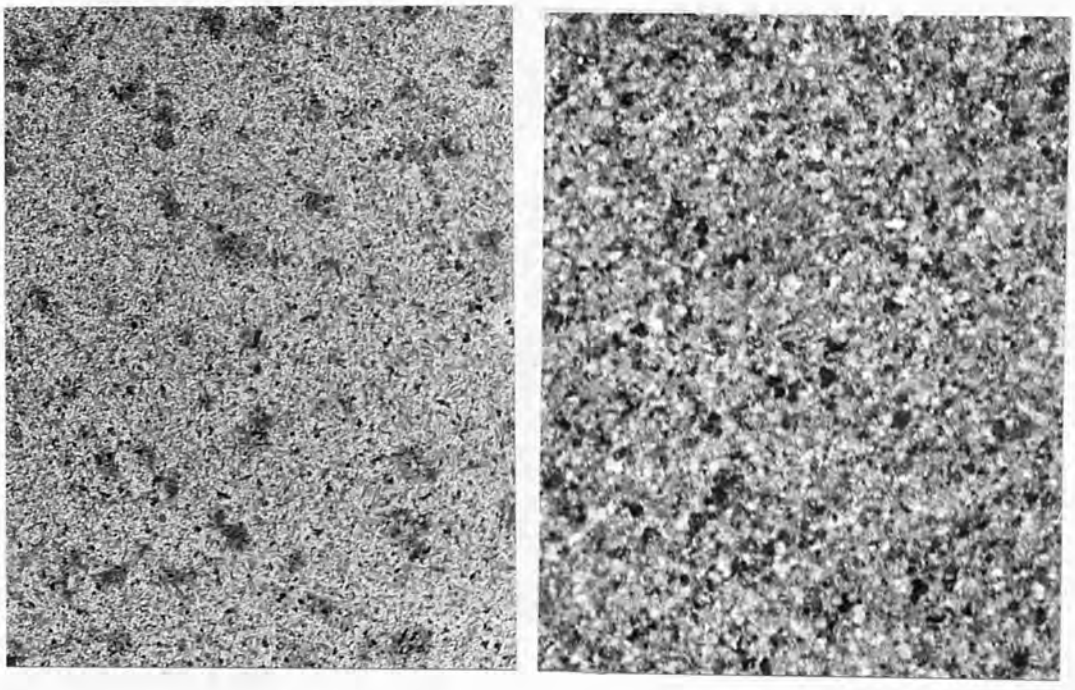

(a) Room temperature (20°C)

(b) T = 75°C

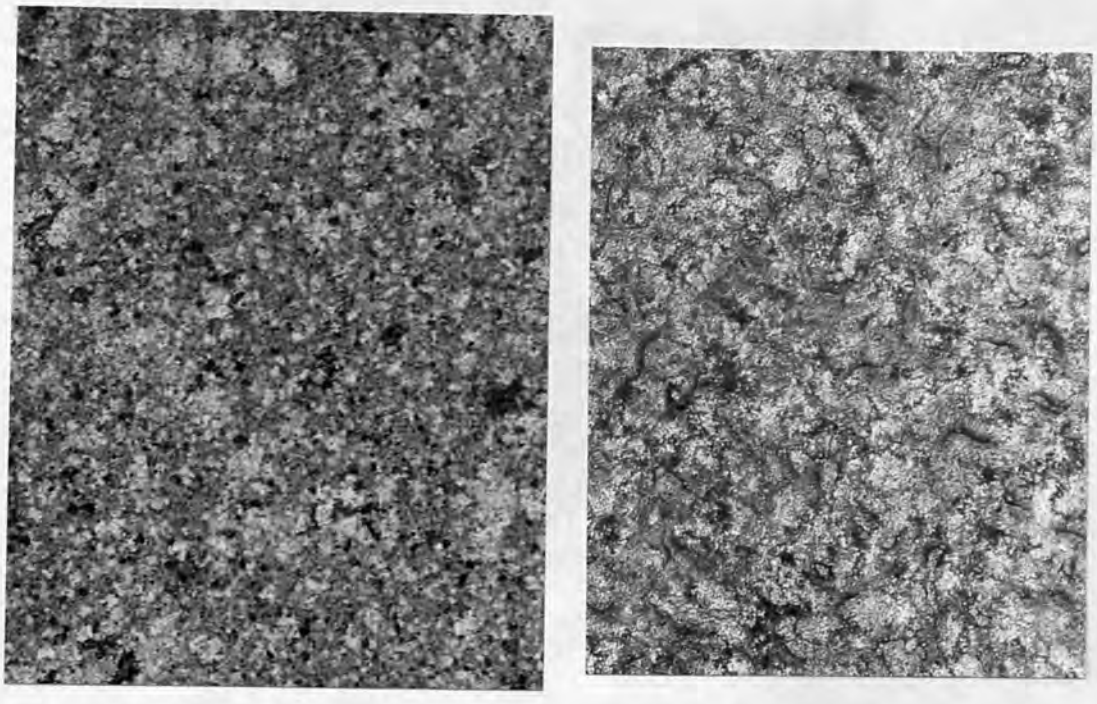

T = 200° C

(d) T = 280°C

Figure 5.13. Gaddlinium dihydride films grown oncleaved rock salt: influence of temperature on microstructure (X 16,000)

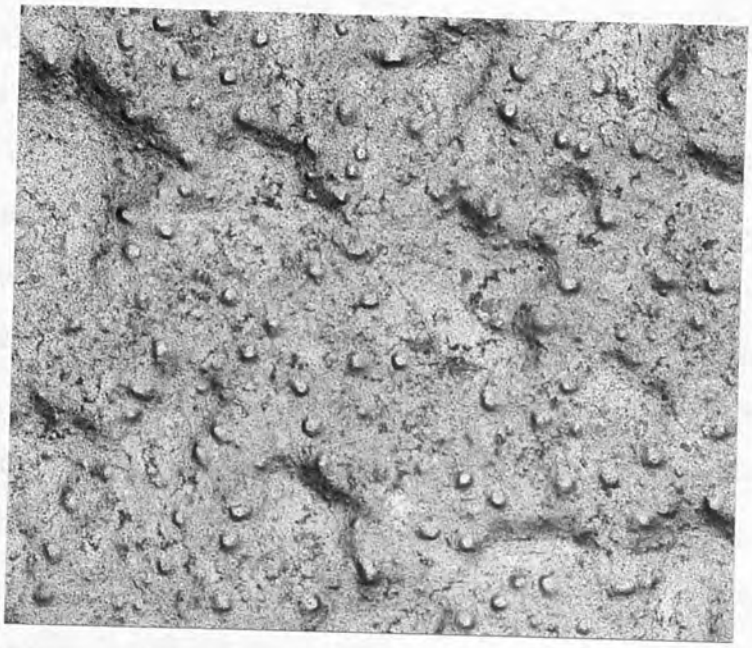

(a) GdH_2 (110)

(b) GdH_2 (111)

Figure 5.14. Electron micrographs of oriented gadolinium dihydride films (X 12,000)

i. Influence of the substrate temperature on orientations.

a. Films grown on cleaved (100) rock salt.

Terbium dihydride films were deposited on cleaved rock salt substrates which were maintained at elevated temperatures ranging from room temperature to 350°C in order to define the epitaxial temperature. Polycrystalline films resulted from deposition on cold rock salt (Fig. 5.8a). As the substrate temperature was increased the orientation improved (Fig. 5.18c) in the same way as the GdH_2 films and substantially complete orientations were obtained for substrate temperature of 300°C. The electron diffraction pattern of epitaxial (100) terbium dihydride film is shown in Fig.5.8d and the measured d-spacings are shown in table 11. The orientation observed was

TbH_2 (001) [100] || Nacl (001) [100]

There were no extra spots apparent in the diffraction pattern. Deposition temperatures between 300 - 400°C had no effect on orientation but higher temperatures caused poorer orientation.

b. Films grown on polished (100), (110) and (111) rock salt.

As in the case of gadolinium dihydride film, there was a deterioration in the orientation of the terbium dihydride films grown directly on polished (100), (110) and (111) rock salt at 300°C. Annealing the substrate at higher temperature (450°C) and then the deposition at epitaxial temperature (300°C) produced single crystal films in parallel orientation. The electron diffraction pattern of epitaxial (110) and (111) film is shown in Figs. 5.7b and 5.7c and the measured d-spacings of the corresponding films are shown in table 12 and 13 respectively. The following orientations were observed

TbH_2 (001) [100] || NaCl (001) [100]

TbH_2 (110) [001] || NaCl (110) [001]

TbH_2 (111) [$\bar{1}$10] || NaCl (111) [$\bar{1}$10]

ii. Influence of film thickness on orientation and structure.

The orientation of the films of varying thickness from 30Å to 850Å have been studied by keeping the substrate temperature at epitaxial value (300°C). It was found that the orientation did not become complete until the thickness reached about 60Å, which indicates that some of the crystallites of the thinner film were randomly oriented. As discussed in section 5.3.2. the orientation of the film thicker than 230Å deteriorated and finally being overlapped by polycrystalline h.c.p. terbium as the thickness increased above 850Å. The phenomenon has been also justified by RHEED studies in section 6.6, chapter 6 .

iii. Influence of the rate of deposition on orientation.

Since the rate of deposition is one of the parameters which define the epitaxial temperature, a wide range of deposition rates were attempted to find a suitable value for the epitxial growth. The optimum deposition rate for the epitaxial growth of the film was determined to be 70Å / min. Higher evaporation rates (200 - 400Å / min.) deteriorated the film orientation. Very slow deposition rates also produced poor orientation. Rate of deposition was not affected by the orientation of the substrates on which films were grown.

iv. Influence of the substrate temperature on the microstructure of the film.

The substrate temperature had the same effect on the microstructure as in the case of GdI_2 (Fig.5.13), i.e. as the temperature was increased the crystallite size increased. The electron micrograph of 180Å epitaxial single crystal terbium dihydride film is shown in Fig.5.16a.

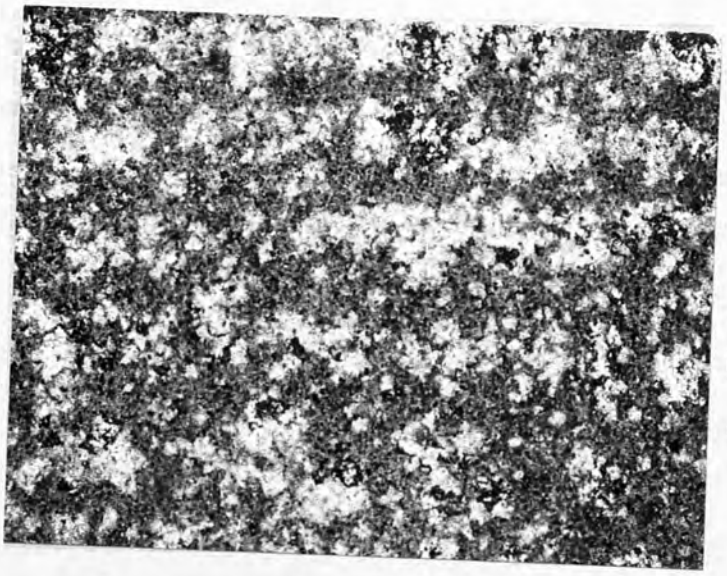

(a) (100), thickness = 450A° (X 20,000)

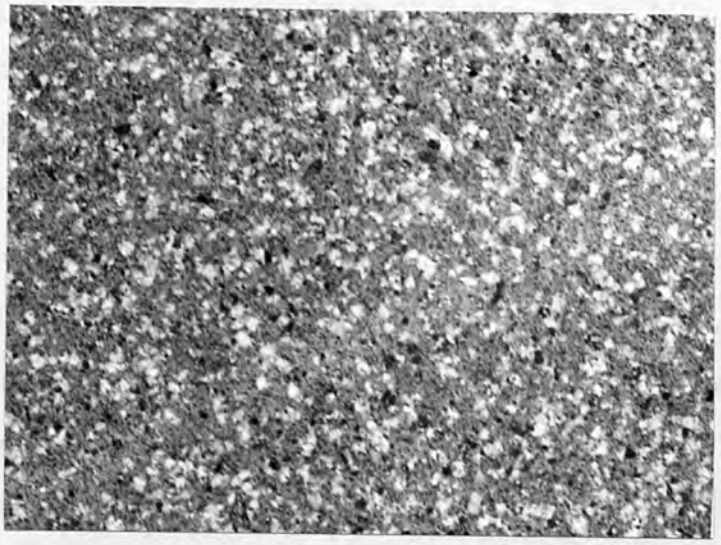

(b) polycrystalline film thickness = 450A° (X 26,000)

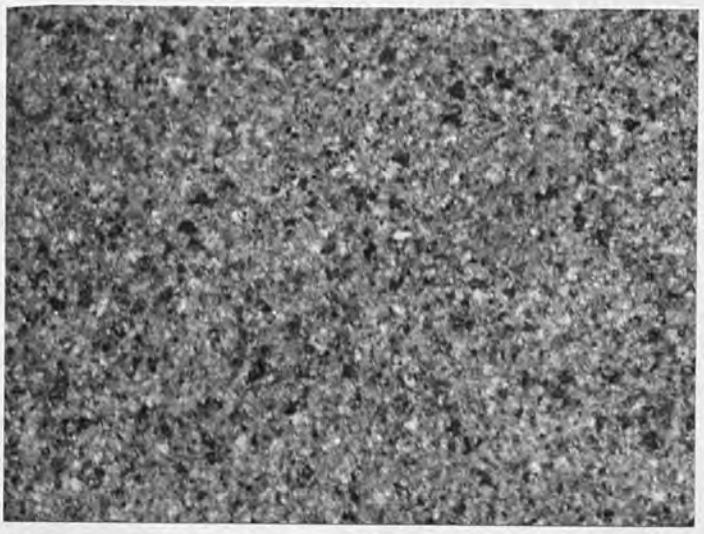

(c) polycrystalline h.c.p. Gd, thickness = 920A° (X 26,000)

Figure 5.15. Electron micrographs of the films grown from Gd on rock salt.

As may be seen from the micrograph, there was no traces of twinning or stacking faults, although the movement of some dislocation loops were observed inside the electron microscope. The crystallite size of the film was reasonably small and film became continuous at a thickness of about only 80Å. Figure 5.16b shows extinction contours in a single crystal TbH_2 film. The electron micrograph of 650Å film grown epitaxially on (100) rock salt which shows the co-existence of both f.c.c. TbH_2 and h.c.p. Tb is shown in Fig. 5.17a. The microstructure of a h.c.p. Tb film of 920Å thick is shown in Fig. 5.17b.

.7.3 Dysprosium, holmium and erbium dihydride films.

i. Influence of the substrate temperature on orientation.

Films of the dihydrides of Dy, H_o and Er have been grown on cleaved (100) and polished (100), (110) and (111) rock salt and the influence of the substrate temperature on the orientation has been studied. It was observed that the degree of orientation depends strongly on the substrate temperature during deposition. The orientations improved with the increase of substrate temperature and complete orientations were obtained for Dy, H_o and Er dihydride at 200°C, 200°C and 215°C respectively. Films grown on cold substrates were found to be randomly oriented polycrystalline. The diffraction patterns of Dy, H_o and Er dihydride films of different orientations (100), (110), (111) are shown in Figures 5.18, 5.19 and 5.20 respectively. The following orientations were observed for each of the dihydrides:

XH_2 (001)[$\bar{1}$00] || Nacl (001)[$\bar{1}$00]

XH_2 (110)[001] || Nacl (110)[001]

XH_2 (111)[$\bar{1}$10] || Nacl (111)[$\bar{1}$10]

(X = Dy, H_o and Er)

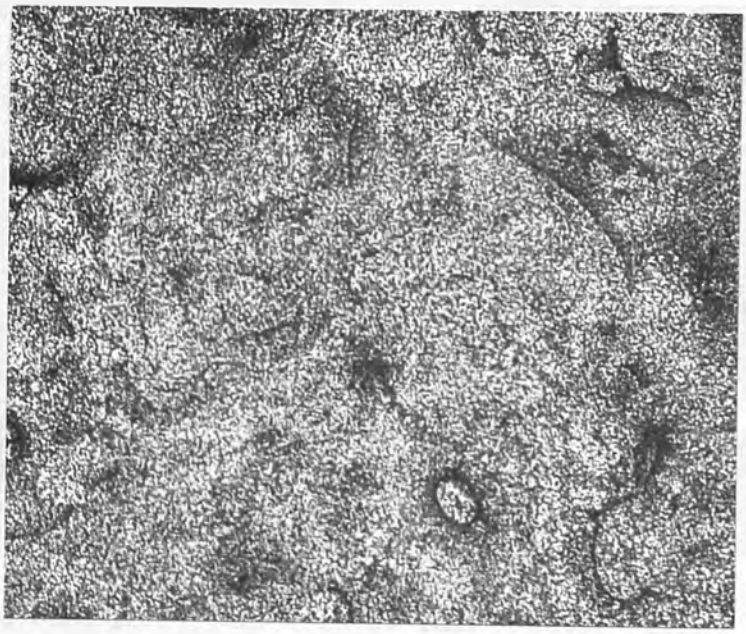

(a) (100), thickness = 180A° (X 16,000)

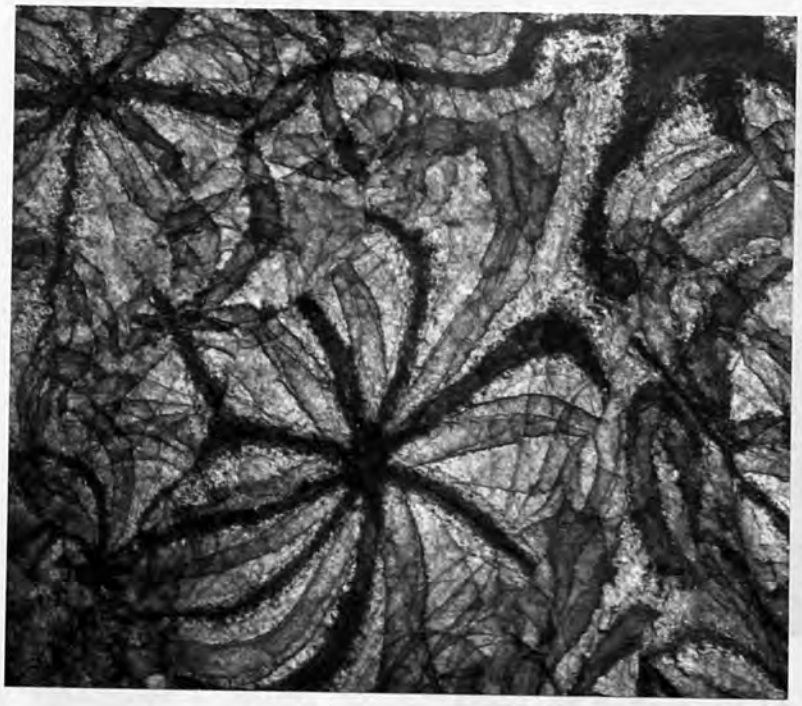

(b) Extinction contours, thickness = 300A° (X 10,000)

Figure 5.16. Electron micrograph of f.c.c. TbH_2 films.

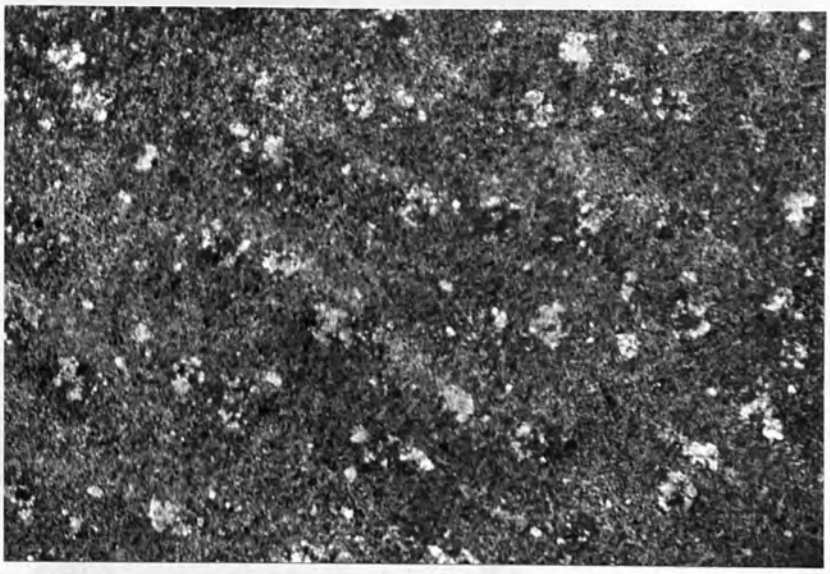

(a) Film thickness = 650A° (f.c.c. TbH_2 + h.c.p. Tb), grown on (100) rock salt (X 12,000)

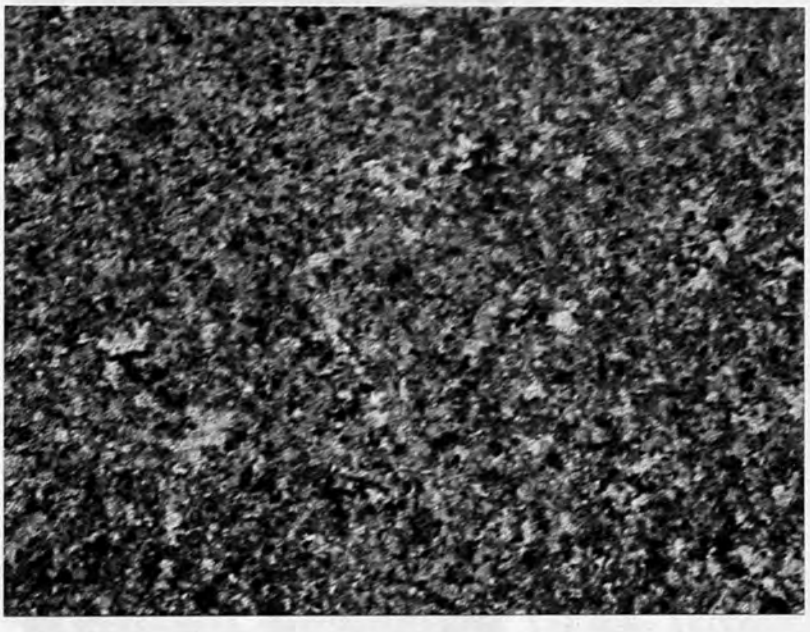

(b) Film thickness = 920A°, polycrystalline h.c.p. Tb (X 30,000)

Figure 5.17. Electron micrographs of films grown from terbium.

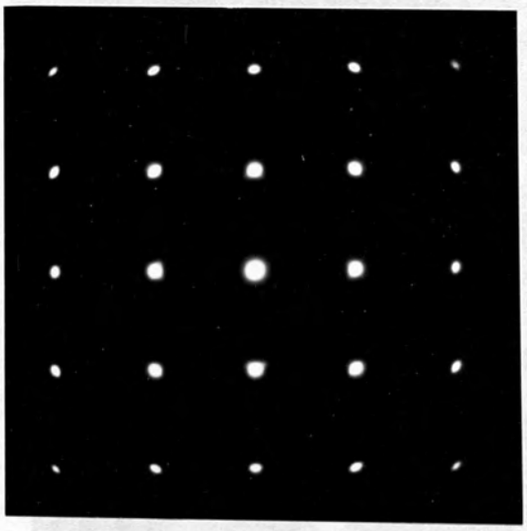

(a) DyH_2 (100)

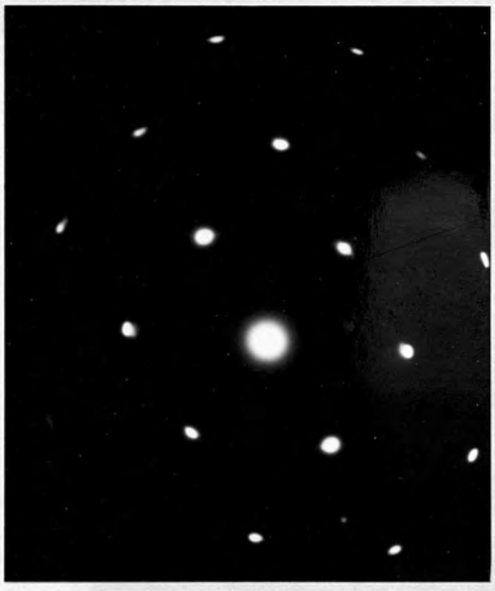

(b) DyH_2 (110)

(c) DyH_2 (111)

Figure 5.18. Electron diffraction patterns of epitaxial DyH_2 films.

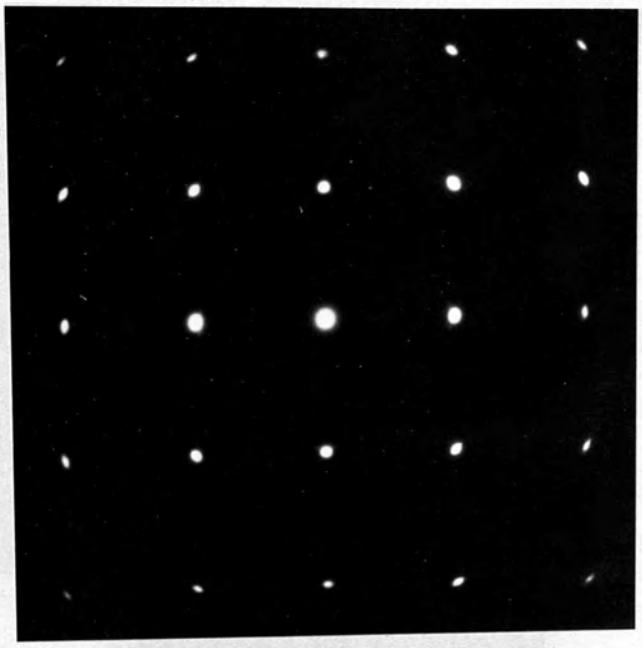

(a) H_oH_2 (100)

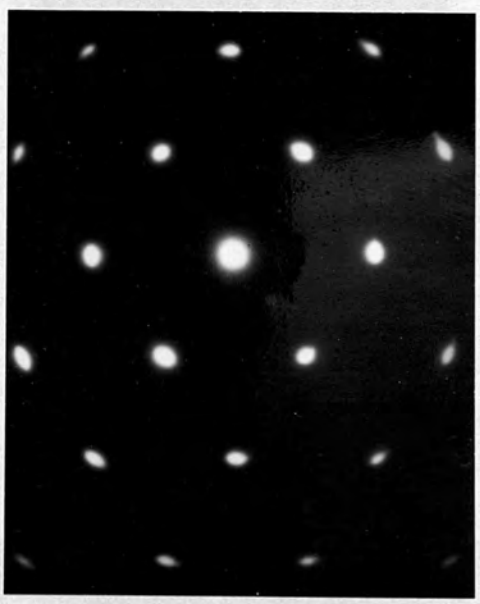

(b) H_oH_2 (110)

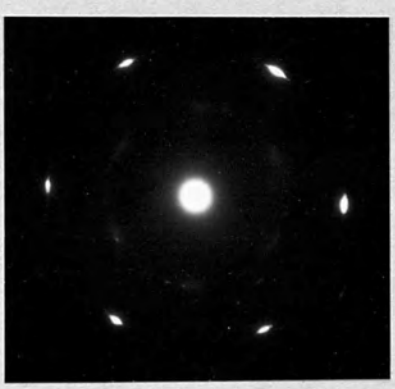

(c) H_oH_2 (111)

Figure 5.19. Electron diffraction patterns of epitaxial single crystal H_oH_2 films.

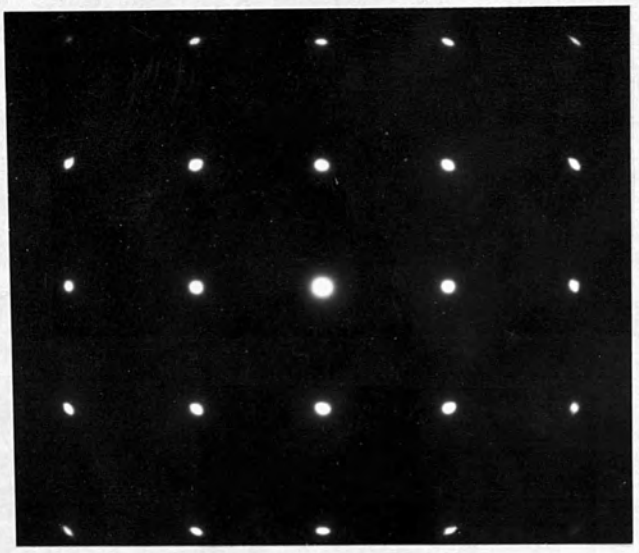

(a) ErH_2 (100)

(b) ErH_2 (110)

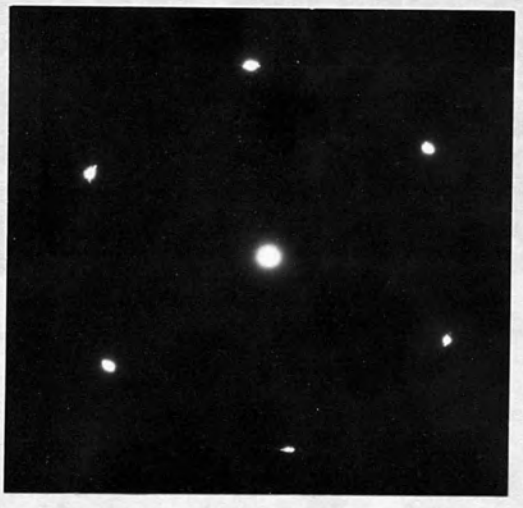

(c) ErH_2 (111)

Figure 5.20. Electron diffraction pattern of epitaxial ErH_2

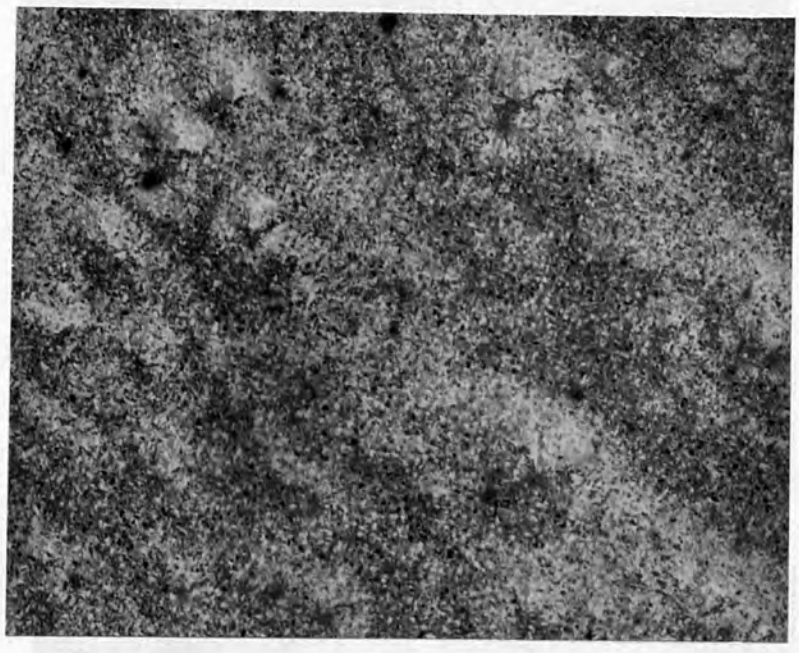

(a) DyH_2 (100), thickness = 170A° (X 10,000)

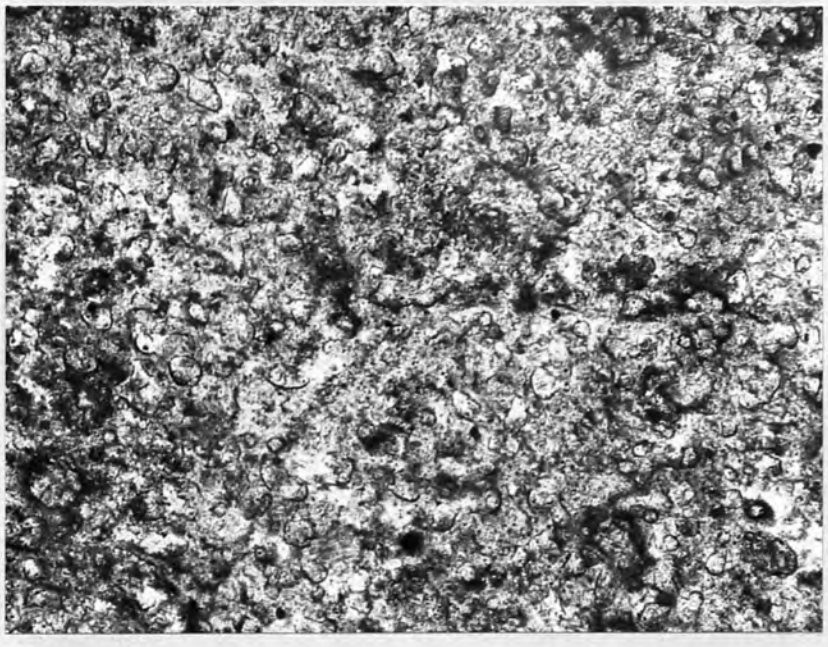

(b) DyH_2 (110), thickness = 200A° (X 30,000)

Figure 5.21. Electron micrographs of dysprosium dihydride films.

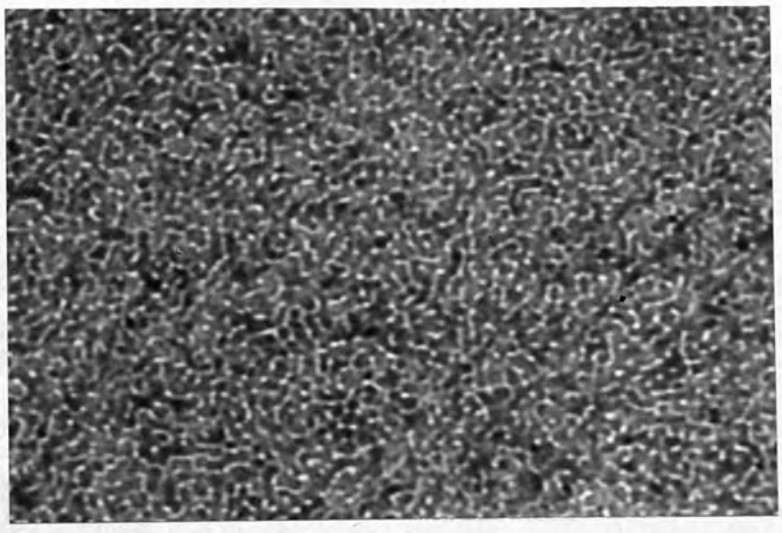

(a) H_oH_2 (100),
discontinuous films

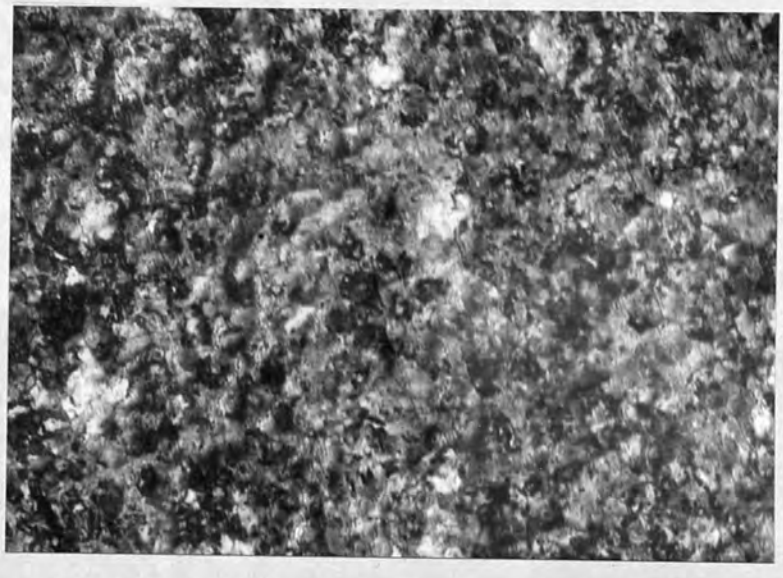

(b) H_oH_2 (100),
continuous film

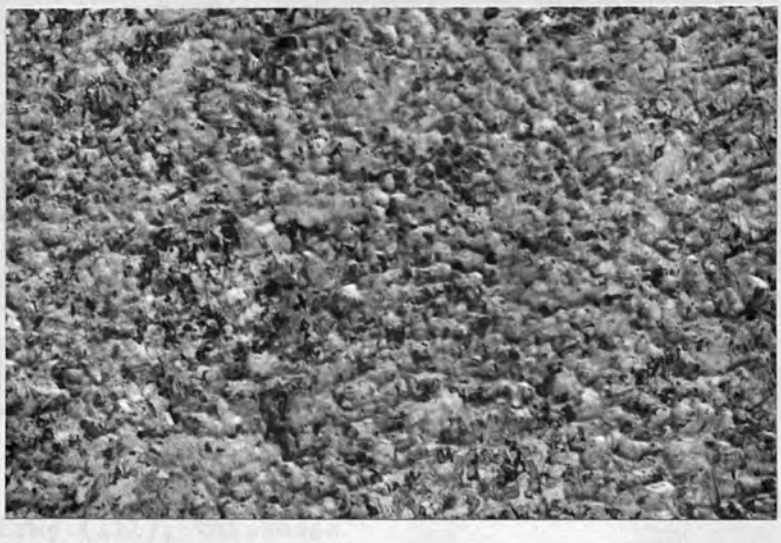

(c) H_oH_2 (111)

Figure 5.22. Electron micrograph of holmium dihydride films (X 20,000)

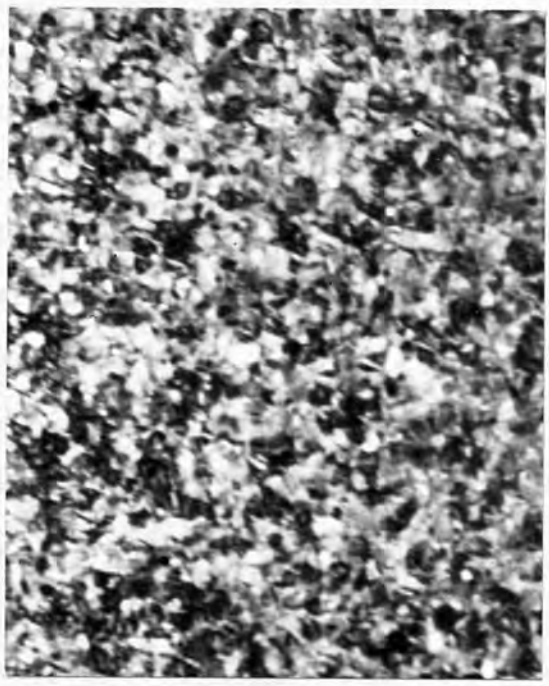

(a) ErH_2 (100), thickness = 200A°

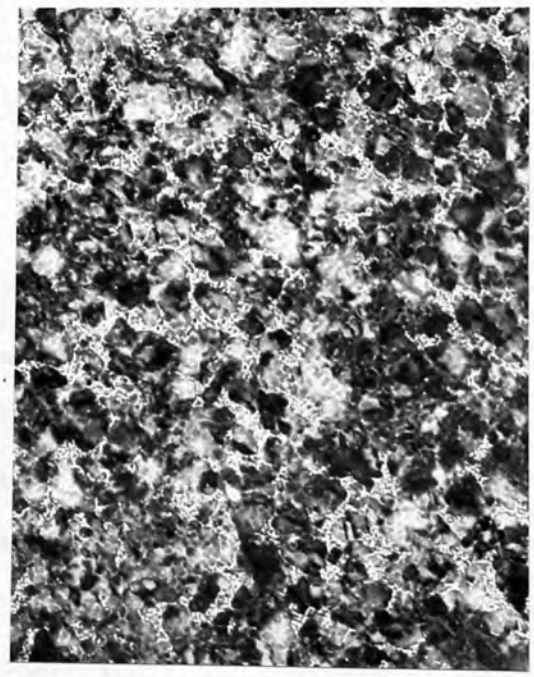

(b) ErH_2 (110), thickness = 190A°.

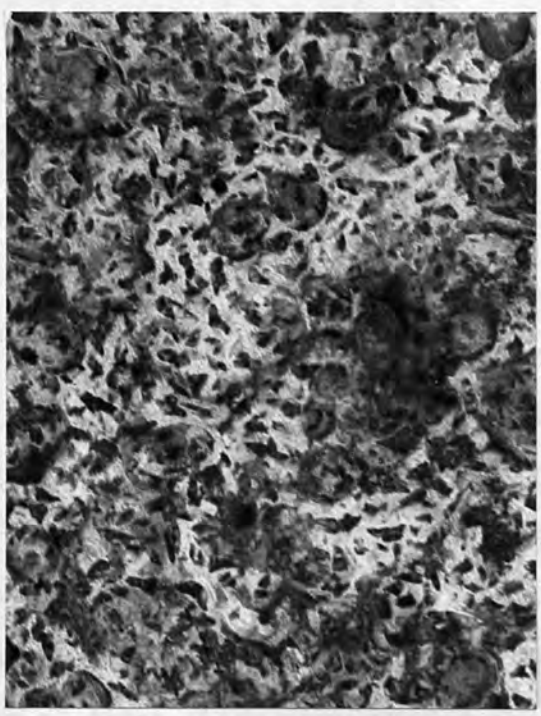

(c) ErH_2 (111), thickness = 180A°

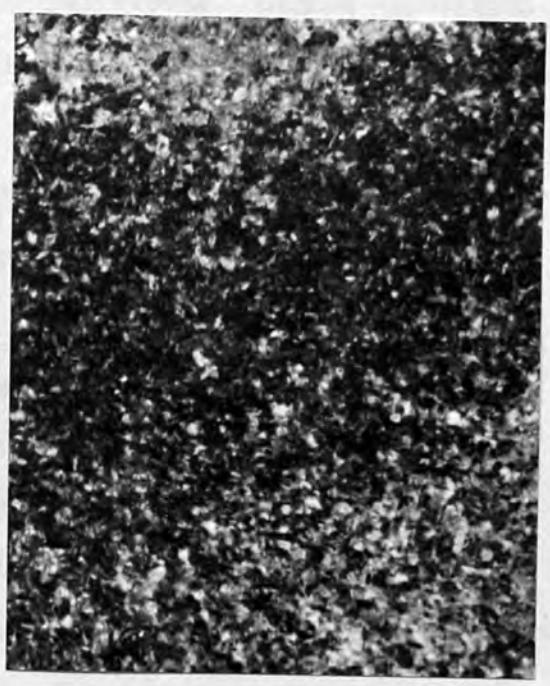

(d) ErH_2 (100), thickness = 270A°, extinction contours.

Figure 5.23. Electron micrographs of ErH2 films (X 20,000)

ii. Influence of film thickness on orientation and structure.

Films of varying thickness from 30Å to 800Å have been studied by electron diffraction in each case keeping the films at their respective epitaxial temperature. It was observed that the orientation improved with the thickness. Complete orientations were not obtained until the thickness reached 70Å, 90Å and 80Å for DyH_2, H_oH_2 and ErH_2 respectively. The structures of the films are highly dependent on thickness as has been shown in sections 5.4, 5.5. and 5.6. Thinner films ($\angle$ 200Å) are f.c.c. dihydrides and thicker films are predominated by h.c.p. metallic structure. This observation was the key one and found to be common to the materials studied.

iii. Influence of the rate of deposition on orientation.

A wide range of deposition rates were attemtped in each case to find out suitable values for the epitaxial growth. Higher deposition rates deteriorated the film orientation as before on the other hand slow evaporation rates produced poor orientation. The optimum deposition rates which produced epitaxial single crystals were 120, 100 and 90Å / minute for DyH_2, H_oH_2 and ErH_2 respectively. The rates of evaporation were the same for all the orientations of the film.

iv. Influence of the substrate temperature on the microstructure of the film.

The crystallite sizes were found to depend on the substrate temperature during deposition following the trend of gadolinium and terbium dihydride i.e. they increased with the increase of temperature. The electron micrograph of 170Å dysprosium dihydride single crystal film grown on (100) rock salt is shown in Fig. 5.21a exhibiting platelike structure. Figure 5.21b shows the microstructure of (110) DyH_2 film of 200Å thickness. Dysprosium dihydride films became continuous at

about 75Å. Holmium dyhidride film was found to be an exception of the series of not becoming continuous up to 110Å thickness. The electron micrograph of a discontinuous (100) H_oH_2 film is shown in Fig. 5.22a. This film generally consisted of numberous 'islands' separated by vacant channels. The initial growth mechanism of holmium dihydride appeared to be different from others. The electron micrographs of (100) and (110) single crystal holmium dihydrides are also shown in Figs. 5.22. Some indications of stacking faults were observed in the micrograph. The micrograph of oriented erbium dihydrides are shown in Fig. 5.23. The dark broad regions in Fig. 5.23d. are extinction contours due to bending of the specimen. Erbium dihydride films became continuous at about 80Å thickness.

5.8. Results and discussions.

The experimental values of the lattice parameters obtained were as follows:

$a_o = 5.308 \pm 0.005$Å for GdH_2

$a_o = 5.250 \pm 0.005$Å for TbH_2

$a_o = 5.206 \pm 0.004$Å for DyH_2

$a_o = 5.170 \pm 0.004$Å for H_oH_2

$a_o = 5.127 \pm 0.004$Å for ErH_2

These values of the lattice parameters are consistent with the face-centred-cubic dihydrides within the experimental accuracy of 1%.

It is well known that the rare earth metals are highly reactive towards hydrogen gas and since hydrogen is one of the most abundant residual gases and most reactive, it can be gettered by the thin films to yield the rare earth dihydrides. Müller, Singh and Surplice (1970, 1972) showed that erbium thin films had exceptional high sorption activity for hydrogen when this gas was by itself or when it was a part of a residual gas mixture. They also observed that

oxygen was absorbed far less, which is also consistent with our observation. Unless the films are heated in air, or inside the electron microscope by a strong electron beam, the possibility of oxidation was practically nil.

The possibility of the formation of GdO and ErO can be easily ruled out (as has been done by Gasgnier etal and Curzon and Singh) for the following reasons. 1) the observed lattice parameters do not agree with any other structures except f.c.c. dihydrides, 2) results of the treatment of the film with hydrogen (Chapter 6) agree with dihydrides not with monoxides, 3) Curzon and Chlebek (1973 a,b) showed by weight increase and electrical resistivity measurements that f.c.c. phase in question was not due to monoxides as claimed by Murr (1967) and Rai and Stivastava (1971) 4) Resluts of our electrical resistivity measurement (Chapter 8) agree with f.c.c. dihydrides and finally 5) correspondence with the rare earth information centre, Iowa State University, U.S.A. revealed that there is no existence of rare earth monoxides in the solid state.

Rare earth trihydrides are formed only when the film is heated in hydrogen as is shown in chapter 6 and the d-spacing measurements also showed the absence of trihydrides. The question of f.c.c. form of the metal is out of hand as may be seen from the measured values of the d-spacings and the results of this film after hydrogen treatment.

CHAPTER 6.

INVESTIGATION OF SOME GROWTH PARAMETERS OF GdH_2 AND TbH_2 FILMS

6.1. Introduction.

The results of the transmission electron diffraction studies presented in chapter 5 indicate that when rare earth metals are evaporated in the vacuo used, the thinner films form as the f.c.c. dihydrides, intermediate thickness produce a mixed (f.c.c. dihydride and h.c.p. metallic) phase, and thicker films consist almost entirely of h.c.p. metal. In order to investigate the nature of these films more fully, a further series of experiments was conducted to determine the effects of

1) Ambient-hydrogen during and after growth. This was done by examining the structure of films grown in ultra-high vacuum, by varying the period of gettering before evaporation, and by introducing additional hydrogen into the system during and after growth.
2) Other contaminants in the films by mass spectrometry analysis.
3) Substrate nature and temperature.
4) Film thickness as an independent parameter (including some nucleation studies).
5) The immediate influence of the substrate, by examining the initial and final film layers by reflection high energy electron diffraction.
6) Oxidation.

6.2. Treatment of gadolinium and terbium films with hydrogen.

i) Films upto 250Å thickness.

Thin films of gadolinium and terbium ($\sim$200Å), grown on rock salt (usually f.c.c. dihydrides) were heated inside the vacuum chamber in presence of a stream of hydrogen for two hours at 300°C (the vacuum before and after admitting hydrogen was 5×10^{-6} torr and $10^{-2} \sim 10^{-3}$ torr respectively). The electron diffraction pattern of the GdH_2 film before

and after treatment with hydrogen is shown in Fig. 6.1a,b. The indexed pattern of the hydrogen treated film is shown in Fig.6.1c. The d-spacing measurements of the film have been carried out as before and are shown in table 36(P-216). Comparing the measured values with the calculated d-spacings it is found that the bulk of the film has been converted to h.c.p. trihydrides. The rings 2,3,4,6 and 8 correspond respectively to 00.2, 01.0, 01.1, 01.2 and 11.0 h.c.p. trihydrides. There was some evidence of oxidation of the film as is verified by the presence of 211 and 510 reflections (ring 1 and 7 respectively) of Gd_2O_3. The appearance of a very faint 200 (ring 5) dihydride reflection indicates that a small amount of the original dihydride still remained unreacted after the hydrogen treatment. As the ring 8 is relatively broad and the d-spacings of 220 dihydride and 11.0 trihydride coincide, it could be due to the superposition of the two. A series of films of Gd and Tb up to 250Å thickness have been investigated in the same way and the results were found consistent with the above. The electron micrograph of the same gadolinium trihydride film is shown in Fig.6.1d.

ii. Film of the thickness range 300 - 800Å

Heating gadolinium and terbium films of the above thickness range (which are usually a mixture of f.c.c. dihydride and h.c.p. metal) in hydrogen causes an increase in the amount of dihydrides. The intensity of the f.c.c. dihydride reflections increased while that of h.c.p. metal decreased, although, they did not actually disappear. The (01.2) metallic reflection was absent after the hydrogen treatment. Although some of the h.c.p. metal was converted to dihydrides, the composite structure of the film remained a mixture of dihydrides and metal. There was no evidence of either oxidation or trihydrides.

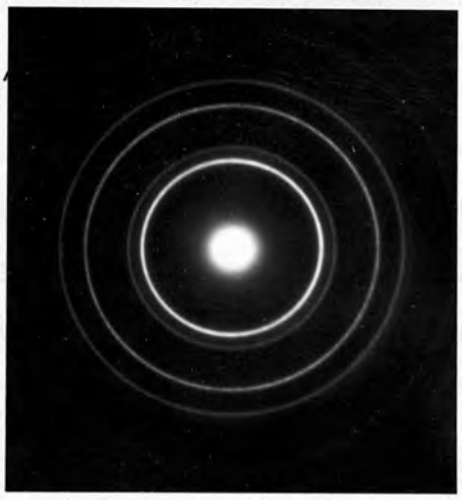

(a) Diffraction pattern of 200Å f.c.c. GdH_2 before heating in H_2

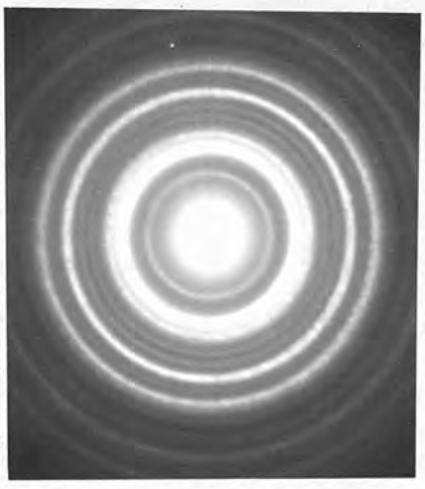

(b) After heating the same film.

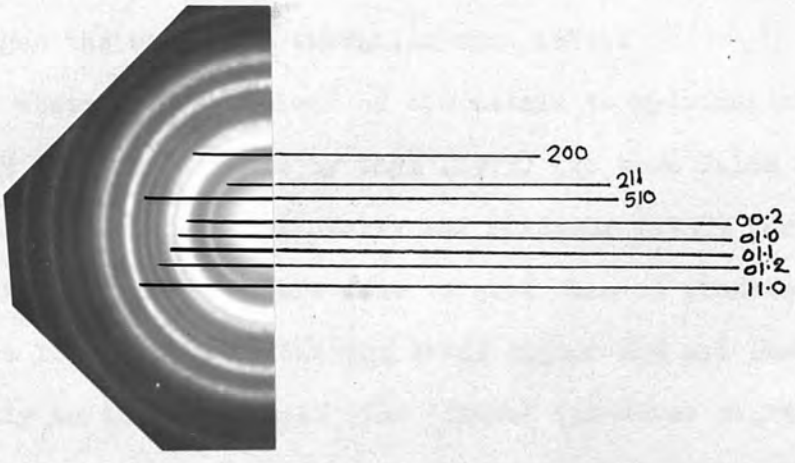

(c) Indexed pattern of Fig. 6.1b.

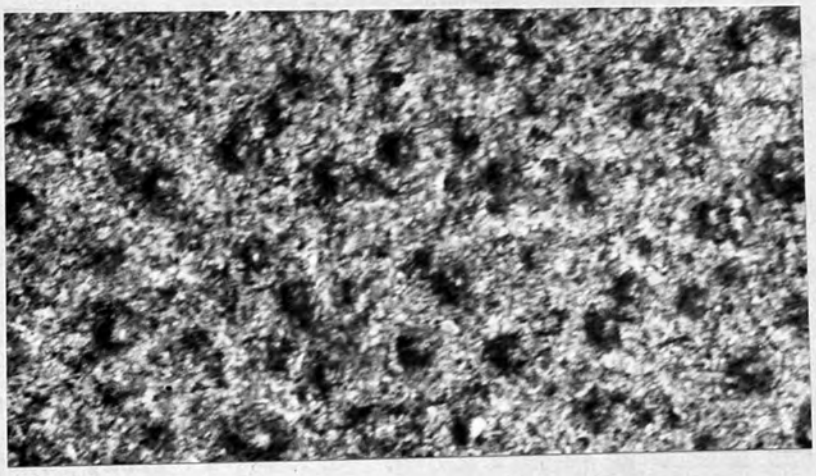

(d) Electron micrograph of 200Å GdH_2 film after treated with H_2 when became converted to GdH_3 (×20,000)

Figure 6.1. Structure of hydrogen treated GdH_2 film.

iii. Films thicker than 850Å

Thick films (~900Å) of gadolinium and terbium, (which are normally dominated by h.c.p. metal) were also examined by electron diffraction, after being treated with hydrogen in the same way. There was no abrupt change in the structure but some rings (111 and 200) due to f.c.c. dihydrides appeared in the diffraction pattern. This means that a small amount of the metal has been converted to dihydrides but the structures as a whole is dominated by h.c.p. metal. Since the film is thick, the reaction is likely to be slow. Very thin films involve a small amount of material and the reaction takes place most readily and changes the structure (Gasgnier etal, 1974).

The observed conversions of the metals to hydrides are in good agreement with those found by Ghys (1973) for thin films and Hardcastle (1961) and Coffinberry and Ellinger (1955) for bulk rare earth metals. Attempts were made to grow film in presence of hydrogen (pressure $10^{-3} \sim 10^{-4}$ torr) but the metal vapour did not condense coherently on the substrate. The 'films' (whatever might have deposited) were very fragile and broke into fine fragments when separated from the rock salt.

6.3. Structure of gadolinium and terbium films grown after longer period of gettering.

Some studies have been made of the structure of the film grown after long periods (6-7 minutes) of gettering, by using a moveable shutter in between the substrate and the source. It may be seen from figure 4.6. that the gadolinium metal vapour gettered the residual hydrogen. (This is contrary to the report by Curzon and Chlebek, 1973, who declared Gd as an exceptional among heavy rare earths in not acting as a getter), and became saturated within a minute, so the film grown after gettering was expected to have metallic structure.

But the investigation by electron diffraction showed that the structure of the film ($\simeq$200Å) was consistent with f.c.c. dihydrides. Thicker films were dominated by h.c.p. metallic structure as usual. It is of course worth noting that the lattice parameter obtained in this case (within experimental accuracy of 1%) was increased by an amount of 0.001Å which is quite in agreement with the non-stoichiometric composition of the dihydrides as discussed in chapter 2, section 2.2. Referring to Fig. 2.4 of chapter 2, it is seen that as the atomic ratio of hydrogen to metal is reduced from 2.0 to 1.9 (within dihydride phase limit of DyH_2), there is a small increament of the lattice parameter. By the gettering action, although the content of hydrogen is slightly reduced, thin coherent films of dihydrides are formed shortly after the metal vapour is deposited.

6.4. Influence of the substrate temperature on the structure of the film.

Thin films of rare earths grown at different temperatures on different substrates have been studied by electron diffraction to see the effect of temperature on the structure. It was observed that the change of structure which takes place at different thickness is not influenced by varying the temperature of the substrate. The only effect of temperature is that when the pitaxial temperature is attained, single crystal films are obtained if other parameters for epitaxial growth are maintained.

6.5. Influence of the substrate nature on the structure of the film.

Studies have been made to see whether the substrate character plays any role in changing the structure of the thin films at different thickness. Films of different thickness grown on mica and on carbon films have been examined by electron diffraction. The

change of the structure which was found at different thickness, was the same as in the case of rock salt substrate. Hence it appears that the formation of f.c.c. dihydrides in thinner films has nothing to do with the rock salt substrate as such. Whatever might be the substrate used, thin films of f.c.c. dihydrides are readily formed as the metal getters the residual hydrogen inside the vacuum plant.

6.6. Reflection high energy electron diffraction (RHEED)

It has been established from the transmission electron diffraction investigations that thin films ($<250\text{Å}$) have f.c.c. dihydride structure and thicker films are dominated by h.c.p. metallic structure. It was not possible to study films thicker than 1000Å because of the transmission problem. Reflection electron diffraction overcomes this difficulty. The main objective of this exercise was to study the initial layers (i.e. the surface in contact with the rock salt substrate on which the film is grown) and final (top) layers of thick films ($>1000\text{Å}$). For this purpose, the reflection attachment was fixed in JEM-6A microscope and the specimen was positioned correctly with respect to the electron beam. The reflection stage allowed the following movements: rotation through 360° about the normal to the film surface, sideways movements to either side of the electron beam and a miximum tilt of 12° with respect to the electron beam. The elcctron accelerating voltage used was 80KV.

The film was first floated off the rock salt in distilled water, washed several times and then taken on a disc ($\sim$0.6 cm diameter) of microscopic slide in such a way that the surface which was in contact with the rock salt comes up for the reflection diffraction studies. The film on the disc was dried thoroughly and then pasted with the specimen holder (metallic) by aqua dag in such a way that there was

an electrical continuity (for discharging) between the film and the specimen holder. It was found very difficlut to put the film on the disc glass slide in the proper way without deforming the film shape. To get a true reflection it is necessary to use smooth flat surface. Hence extreme care was exercised so that the film surface was not deformed or buckled while taking on the disc slide. The film was grown on cleaved rock salt which is although smooth and flat, there was some degree of roughness in the surface of the film (which was in contact with rock salt) as indicated by the mixture of streaks and spots in the diffraction pattern (Fig. 6.2a). But the surface was not very rough otherwise spot patterns would appear because of large surface asperities. The film was grown under the epitaxial condition and its thickness was about 1100Å. The diffraction pattern (Fig. 6.2a) clearly indicates the f.c.c. single crystal structure while that of Fig. 6.2c (which is taken from the top surface of the same film) shows clearly the polycrystalline h.c.p. metallic structure. The diffraction pattern from the top of another film of 650Å is shown in Fig.6.2b which shows the existence of both f.c.c. dihydride and h.c.p. metal while the diffraction pattern from the bottom surface is similar to that of Fig. 6.2a. These observations provide more support for our previous results and are consistent withthe results of Grunbaum and Kremer (1968) who studied the thickness dependence of phase changes in Cobalt films by RHEED. It is to be noted that the penetration of the electrons for 80KV and at an angle of incidence between one or two degreed did not exceed 6 or 7Å. It is also worth noting that the accuracy of RHEED for identification of a solid phase is much less than that of transmission because of refraction effects and the loss in resolution due to limiting penetration of the electron beam into a smooth surface introduce an uncertainty of the

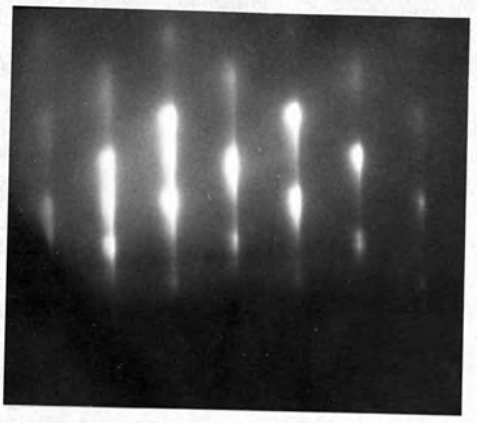

(a) RHEED pattern from the initial layers of a 1100Å film, showing the single crystal f.c.c. dihydride structure.

(b) RHEED pattern from the top surface of 650Å film, grown epitaxially, showing the co-existence of f.c.c. dihydride and h.c.p. metal.

(c) RHEED pattern from the top surface of 1100Å film, showing the h.c.p. metallic structure.

Figure 6.2 RHEED patterns of Gd films.

true position of the diffraction rings or spots relative to the centre. Although the lattice parameter measurements could not be done accurately by this technique, the diffraction patterns from the top and bottom surface of the films of similar thickness (grown under identical conditions) clearly distinguish the crystal structures and allow the conclusion that thin films are f.c.c. dihydrides and thick films ($>1000\text{Å}$) are h.c.p. metal.

6.7. Films grown in uhv.

A few films of gadolinium and terbium grown in ultra-high vacuum (uhv) at 2×10^{-10} torr on carbon film have been studied by transmission electron diffraction and microscopy. The main purpose was to see whether there is any structural difference in these films from those grown in o.h.v. The d-spacing measurement of the film have been carried out from the diffraction pattern of the films of different thickness. The results were found to be in general agreement with those grown in (o.h.v.) at higher pressures $\sim 10^{-6}$ torr, with a slight variation of lattice parameter. For example the lattice parameter of 200Å film grown from gadolinium was found to be $a_o = 5.310 \pm 0.005$Å, i.e. an increment of 0.002Å. The same increment in lattice parameter was found for terbium films also. This small increment in lattice parameter can be satisfactorily explained on the basis of non-stoichiometry of rare earth dihydrides (section 2.2., chapter 2.) Since the gadolinium dihydride phase exists for H/M atomic ratios in the range 1.82 - 2.30, it is likely that although the films grown in uhv are expected to contain less amount of hydrogen, they formed dihydrides. It is also seen from Fig. 2.4., chapter 2 that for DyH_2 there is a slight increment in lattice parameter for a slight decrease in H/M ratio. Hence it is concluded that although the lattice parameter increased slightly because of slightly decreased H/M ratio, thin

films ($\lesssim 250$Å) grown in uhv formed face-centred-cubic dihydrides. Gasgnier etal (1974) also found that thin films grown in uhv have f.c.c. dihydride structure. Thicker films grown in uhv have h.c.p. metallic structure like that of ohv films. The electron micrograph of a 250Å gadolinium dihydride film is shown in Fig. 6.3. Some nucleation features of terbium dihydride grown in uhv are shown in section 6.11.

6.8. Analysis of gadolinium films for oxygen, hydrogen and nitrogen gas by mass spectrometer.

An impurity analysis has been made for oxygen, hydrogen and nitrogen gas contained in gadolinium film of about 200Å thick grown on rock salt by using vacuum fusion AEIMSIO metallurgical mass spectrometer in Fulmer Research, Slough, Berks.

The most widely adopted analytical technique for impurity analysis in thin films is that of vacuum fusion, in which the sample is dissolved under vacuum in a bath of molton metal contained in a graphite crucible. The films were separated from the rock salt by dissolving in water and then dried thoroughly before putting in the furnace. The reactions that take place are summarised below:

1) Hydrides are decomposed and hydrogen evolved.
2) Oxides are reduced in a complex reaction with the dissolved graphite to give carbon monoxide.
3) Nitrides are decompossed with the evolution of nitrogen.

In the (metallurgy) MSIO, the gases evolved as a result of the vacuum fusion of the sample are pumped as rapidly as possible from the vicinity of the crucible into the reservoir section. The mass spectrometer monitors these gases through a metrosil leak. The complete instrument comprises four sections - the induction heater, the furnace, the reservoir and the analyser. The furnace section consists of a vacuum lock for sample admission, a sample storage

magazine and the furnace tube assembly which includes the graphite crucible. The gases evolved are transferred rapidly to the reservoir section. This is a previously evacuated volume, now sealed off from its pumps, in which the gases are collected. A small percentage of the gases passes through a leak into the continuously pumped analyser section. The conduction of this leak is chosen so that the reservoir pressure does not change significantly during the period in which an analysis is made. The mass spectrometer thus monitors pressure changes in the resevoir and hence, after calibration, the quantity of gases released by vacuum fusion can be measured.

The following results were obtained

oxygen, 1840 p.p.m. by weight i.e. 1.76 at %

hydrogen, 5290 p.p.m. by weight i.e. 82.5_2 at %.

nitrogen — no traces were found.

These results confirm the high gettering effect of gadolinium for hydrogen and are consistent with the structures of the films as investigated in chapter 5.

6.9. Oxidation.

A few experiments have been conducted to study the oxidation of gadolinium films. As is obvious from the foregoing sections, the films grown on rock salt or carbon films are free from oxides. But it was observed that the use of a strong beam of electrons led to oxidation of gadolinium films ($\sim$300Å) possibly because of the heating effect of the beam. Fig. 6.4a shows the micrograph obtained after such oxidation. As may be seen from the structure of the film, the oxidation process is accompanied by a considerable increase in grain size. If the electron beam is kept at full intensity, the oxide crystals increase in grain size to such an extent that holes develop and the film eventually ruptures. It was also observed that annealing the

film of about 400Å, at about 600°C for four hours in a furnace causes oxidation together with the increase in the amount of hydride but the film later is converted completely to cubic c-type sesqui-oxides (Gd_2O_3) when heated over night. This result was in good agreement with that of Gasgnier etal (1974) and Murr (1967). The electron micrograph of a film after four hours of annealing is shown in Fig. 6.4b.

6.10. Decoration studies by gadolinium dihydride films.

The decoration pattern of the steps on the air cleaved rock salt has been studied by gadolinium dihydride films. It was observed that when gadolinium dihydride was deposited onto a rock salt cleavage surface, there is a preferential nucleation at steps on the substrate surface. The most striking feature of the nucleation of a gadolinium deposit on a freshly cleaved rock salt surface is the formation of greater numbers of nuclei along the edge surface steps compared with regions which are atomically smooth. It was also observed that the nuclei formed in the centre of the cleavage step are smaller than those on the smooth surface but the difference between them was not so high as in the case of Basset (1958). This preferential nucleation very effectively decorates cleavage steps which are made visible as chains of closely spaced gadolinium dihydride particles. Typical patterns of cleavage steps are shown in Fig. 6.5a, decorated with gadolinium dihydride deposit of about 20Å average thickness backed by carbon film of about 150Å. The crystallite size was about 110Å. In Fig. 6.5a many single steps are observed following a curved of a 'U' or elongated 'S' shape. A number of single chains of nuclei which are parallel also observed (Fig. 6.5b.) Many single steps are observed following a wandering path eventually to join up with a larger cleavage step (Fig. 6.5c).

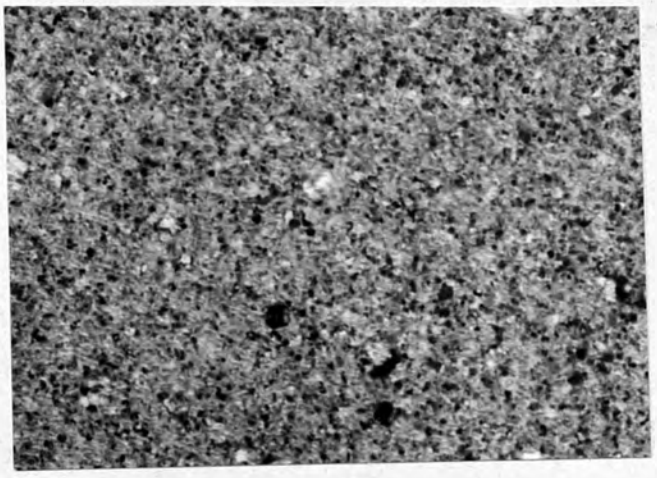

Fig. 6.3. Electron micro graph of 250Å GdH_2 film grown in uhv (x 20,000)

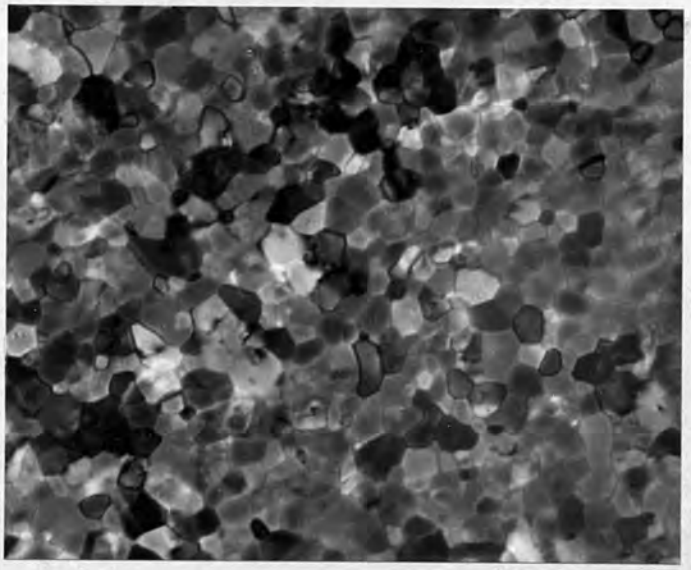

(a) Gd_2O_3 formed by strong electron beam, showing the large grain size (x 7,000)

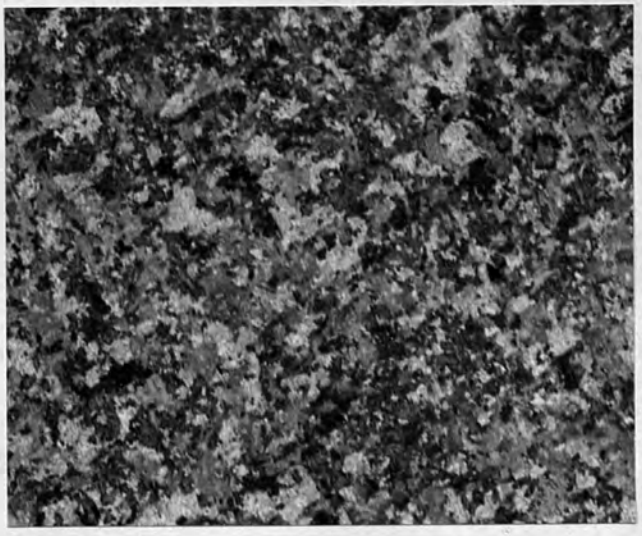

(b) Annealing the Gd film of 400Å at 600°C for 4 hours caused oxidation (x 10,000)

Fig. 6.4. Electron micrograph of Gd films after oxidation.

(a) Thickness $\simeq$ 20Å

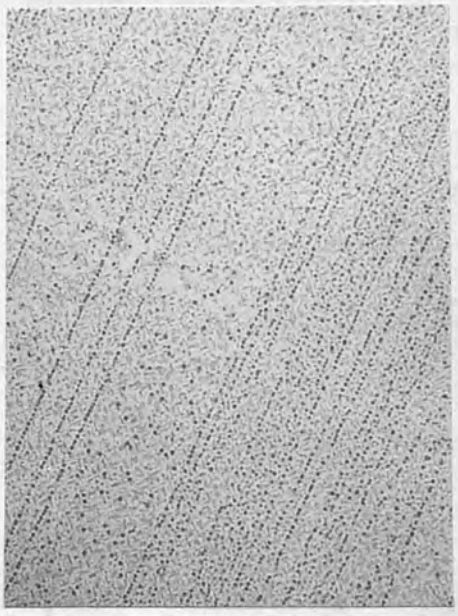

(b) Thickness $\simeq$ 20Å

(c) Thickness $\simeq$ 20Å

Figure 6.5. Decoration of cleaved rock salt by GdH_2 (x 40,000)

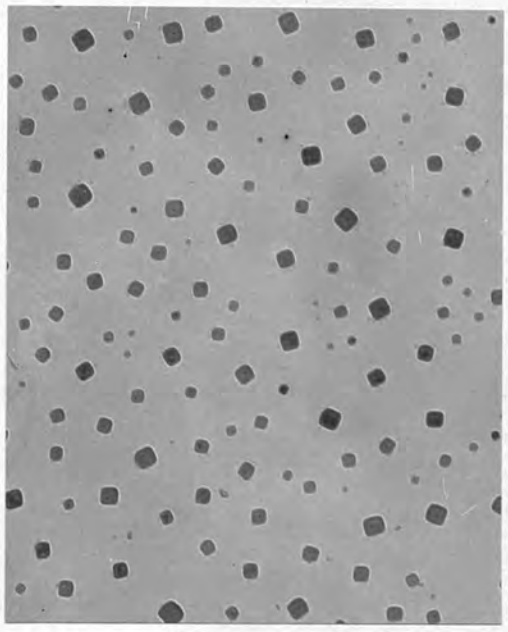

(a) Thickness ≃ 15Å, nuclei are isolated (x 16,000)

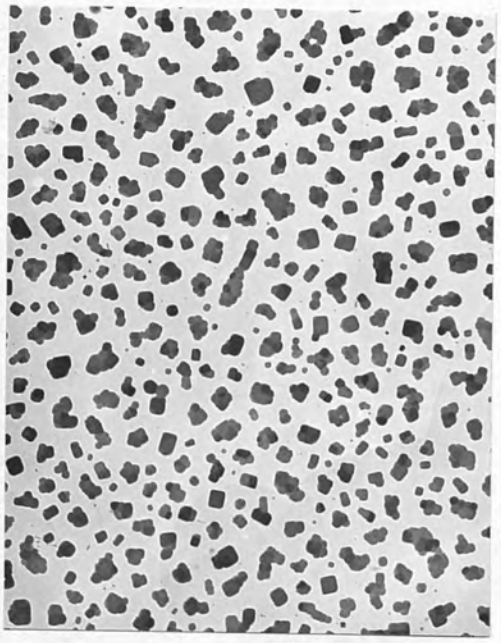

(b) Thickness ≃ 30Å cluster-like structure (x 10,000)

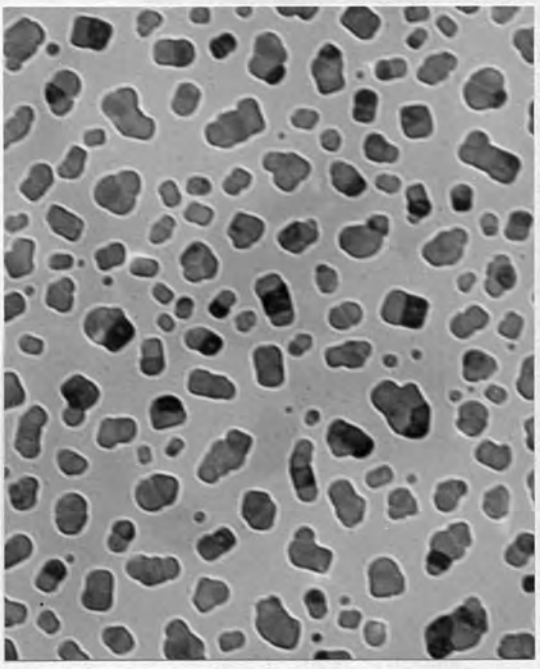

(c) Thickness ≃ 45Å (x 16,000)

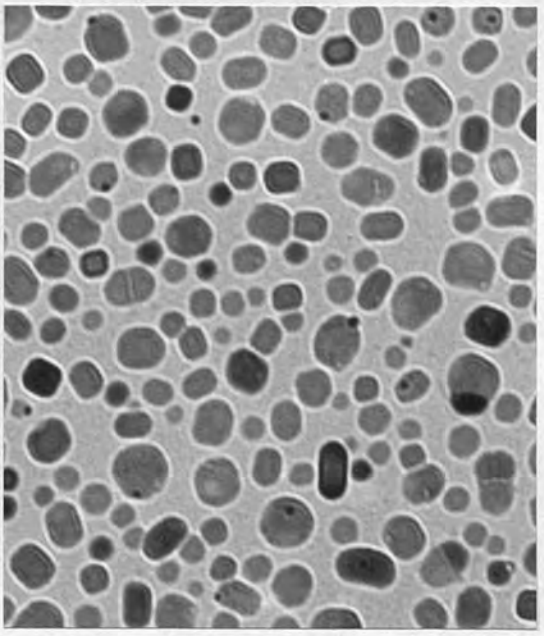

(d) Thickness ≃ 55Å liquid-like coalescence (x 16,000)

Figure 6.6. Nucleation stages of gadolinium dihydride deposit on carbon films in ohv.

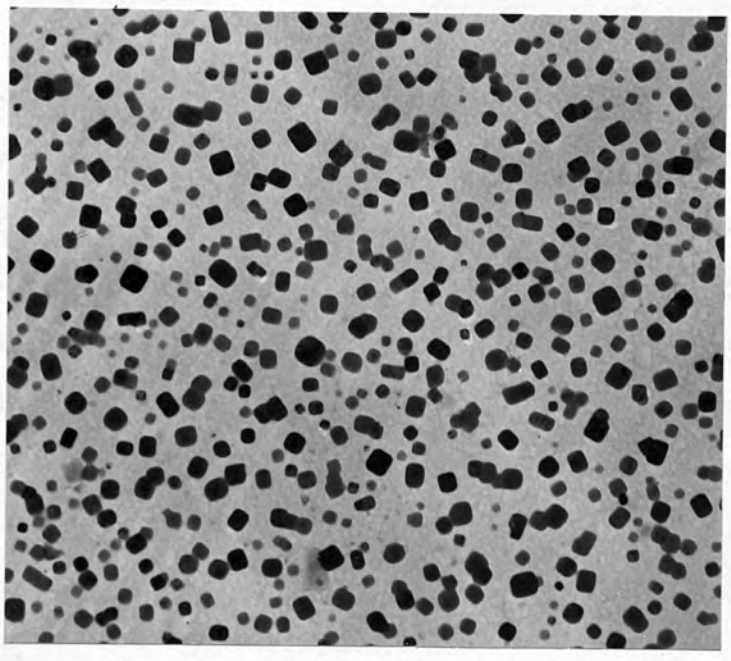

(a) Thickness $\simeq$ 25Å

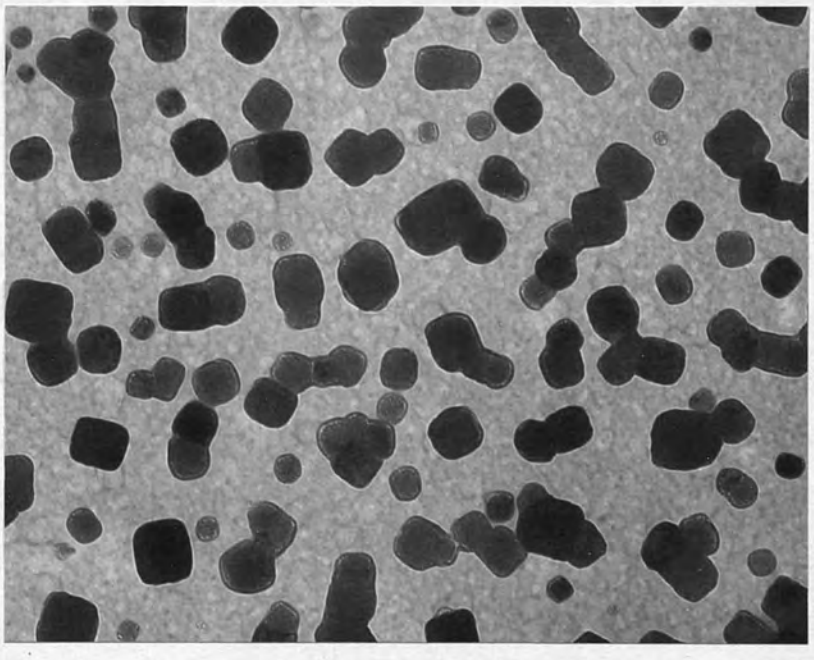

(b) Thickness $\simeq$ 40Å

Figure 6.7. Nucleation stages of GdH_2 on carbon films in uhv (x 16,000)

At lower substrate temperature the decoration was not observed; probably the crystallites were being washed away when film was separated from rock salt. This feature indicated a strong bonding between rock salt and gadolinium dihydride and weaker bonding between carbon and gadolinium dihydride. The essential conditions for the decoration obtained by GdH_2 was that the substrate temperature should be raised to 400°C. It was of course found very difficult to get good decoration with GdH_2. Attempts were made with TbH_2 also but having no success.

6.11. Nucleation.

Attempts have been made to study the sequence of growth of gadolinium and terbium dihydride film from the initial stage to the final continuous film. Observations have been made on gadolinium and terbium dihydrides deposited on transparent carbon films at elevated temperature. This process avoids the stripping of the deposit from the substrate. Of course trials have been made to grow ultra-thin gadolinium and terbium dihydrides on rock salt and coated with carbon to study the nucleation but without success except that of decoration for gadolinium dihydrides.

The sequence of events which occurs as the film thickness is increased has been shown in Fig. 6.6. At a mean thickness of about 15Å, very small three dimensional isolated nuclei are observed (Fig. 6.6a). The distribution of the particles are random but most of them have cubic morphology, ⟨001⟩ zone axis perpendicular to film. The particle size varied from 60Å to 150Å. As the thickness increased (30Å), the individual nuclei (two, three, four etc.) coalesce together, forming an interesting cluster-like structure (Fig. 6.6b.), increasing the size of the crystallite and decreasing the density of

individual nuclei. The same trend continued forming an island-like (agglomerated) structure when the number of separate crystallites reduced (Fig.6.6c). It can be noticed from Fig. 6.6b. that although the coalescence took place, the individual nuclei did not loose their identity until the thickness was increased to 60Å (Fig. 6.6d) where the coalescence was liquid-like as was observed by Pashley etal (1964) for the nucleation of gold on carbon films. Coalescence by 'bridging' was also observed in Fig.6.6b. This mechanism (Adamsky and LeBlanc, 1956), apparently resulted from preferential trapping of subcritical clusters in the region between two closely spaced nuclei. The carbon substrate was heated up to 250°C which helped the recrystallization during coalescence. The film became continuous at about 80Å.

It is believed that initially the increase in size of the nuclei occurs both by the receipt of new deposit atoms, and by receipt from neighbouring nuclei which eventually disappear. In the subsequent stages, increase in the size of the separate crystallites occurs also by the growing together of near neighbouring nuclei, until finally this mechanism is the predominant one, when no very small nuclei remain. In general, the following characteristic sequential growth stages were observed for both gadolinium and terbium dihydride films: 1) nucleation, 2) growth and coalescence of nuclei into cluster and then into larger islands, and 3) coalescence of islands to form a continuous film.

The nucleation of gadolinium dihydride in uhv on carbon film is shown in Fig. 6.7. The growth sequence in the same as in ohv.

CHAPTER 7.

EXPERIMENTAL DETAILS OF THE ELECTRICAL MEASUREMENTS.

7.1. Introduction.

The experimental details of the electrical measurements made on polycrystalline rare earth hydride films of the thickness range 70 - 1000Å are described in this chapter. All the measurements were made in vacuum in order to avoid possible atmospheric attack on the film (Curzon and Chlebeck,1974), which might change the resistivity. The vacuum system used for this purpose was Edwards E3 (described in chapter 4). The purity of the rare earth metals evaporated was 99.9% and evaporated from electrically heated spirally wound tungsten filaments. The evaporation conditions were the same as mentioned in chapter 4.

7.2. The substrates.

Soda glass microscope slides (7.6 x 2.5 x 0.1 cm^3) were used as substrates throughout this work. Glass substrates were used not only because of the high electrical insulation of glass, which is so essential to the measurement of resistance of the deposit film, but also because glass is in itself an excellent substrate material and can be cleaned to a higher degree than is possible with other substrates. The cleanliness of the substrate surface is extremely important in order to prevent dust particles from roughening the surface, and grease-like materials, absorbed water etc. from contaminating the film.

The substrate was first selected for its freedom from scratches by examination under a bright light source. It was then rubbed several times with cotton wool to remove any visible dirt or foreign particles and then blown with dry nitrogen. The substrate was then placed in a beaker of degreasing agent (DECON 90) in an inclined position and cleaned ultra-sonically for 30 minutes.

The degreasing agent was then displaced with distilled water and the substrate was rinsed for fifteen minutes. It was than clamped into a crocodile clip attached to a stand for drying in a stream of hot air. When the substrate was dry, it was rubbed again several times by cotton wool until it became shining. Prior to installation in the vacuum chamber, dry nitrogen was blown across the slide surface to complete the drying. The glass slides were handled very carefully wearing ploythene gloves during the cleaning procedure.

7.3. Electrical Contacts.

The means of making reliable electrical contacts to the films is always a problem, and initial difficulties of intermittent contact, experienced with flat crocodile clips and silver paint were overcome by constructing four spring loaded flat ended copper rods (0.25 cm diameter) fixed with the mask (Fig.7.1) in such a way that they could be easily adjusted to make good electrical contact with the predeposited nichrome electrode on the substrate (described later). This system was found to give satisfactory ohmic contact to the film in the temperature range 77°K - 573°K.

The mask for making the substrate electrode is shown in Fig.7.2. Gold and silver films of about 1500A° thick were at first vacuum evaporated onto the substrate to form the contact electrodes, but they were not found very successful for the following reasons:

a) they become partly detached when the substrate again cleaned ultrasonically.

b) they become broken sometimes with slight movement of the spring loaded contact rods.

c) they develop higher contact potential differences for the rare earth dihydride deposits.

The above mentioned difficulties were overcome by depositing a 1500A° nichrome film on the substrate. These nichrome electrodes were found

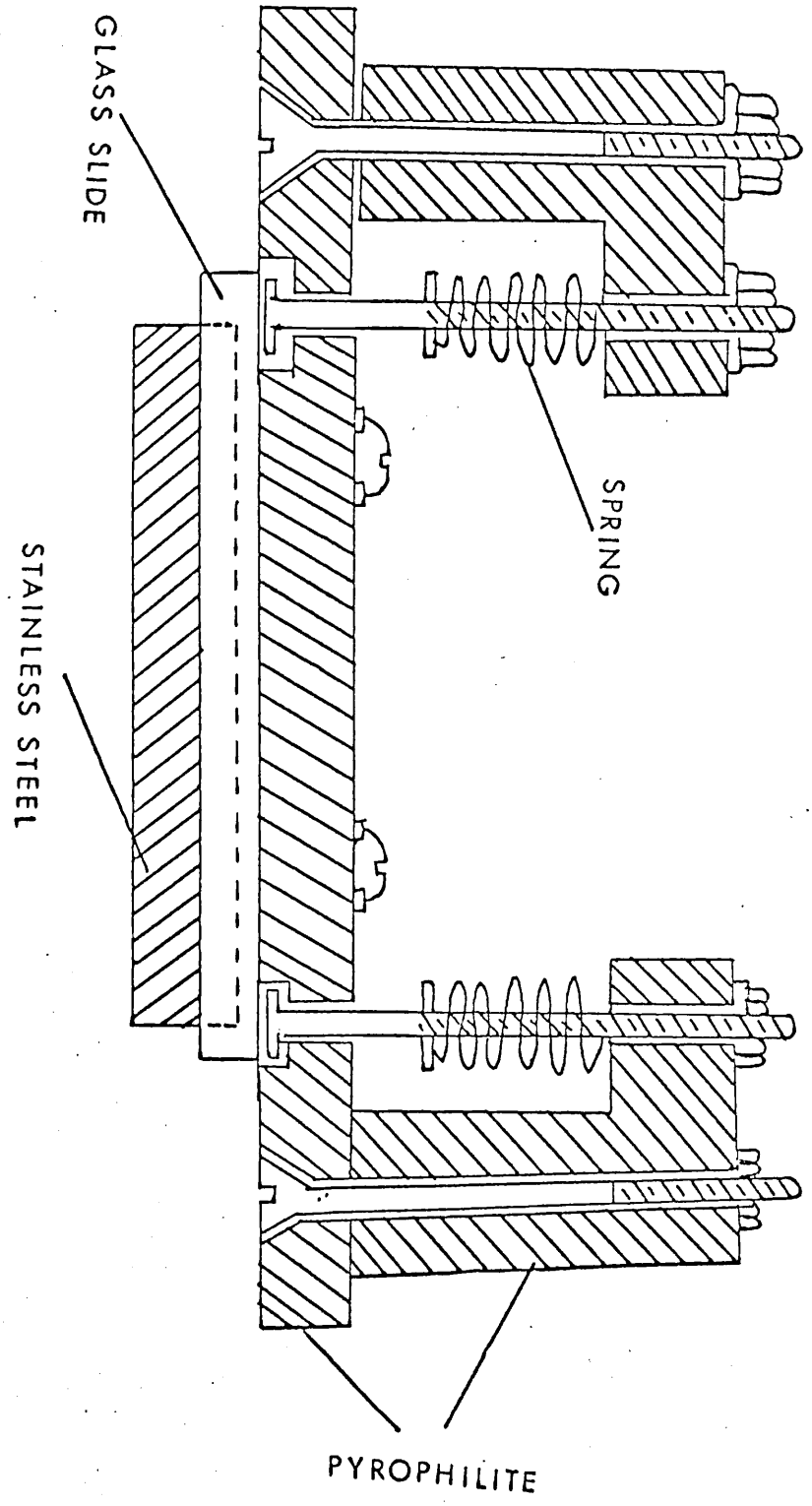

Fig. 7.1. Spring loaded electrods fixed with the mask on the jig.

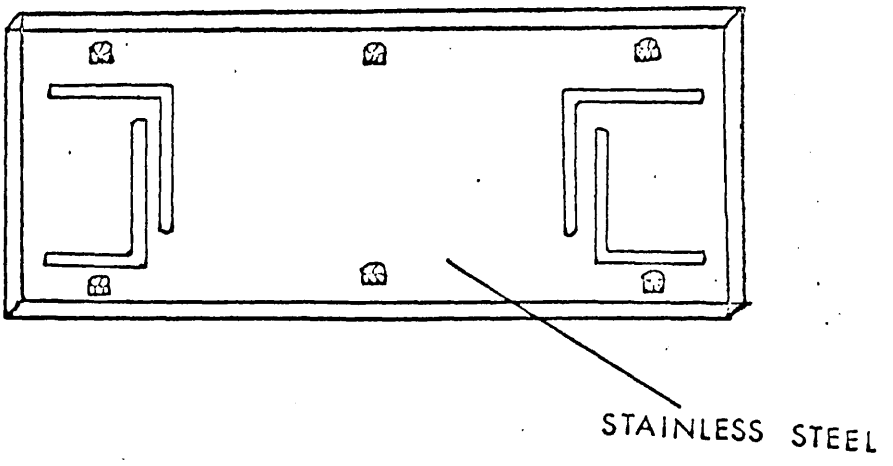

Fig. 7.2. Mask for making the nichrome electrodes on the substrate.

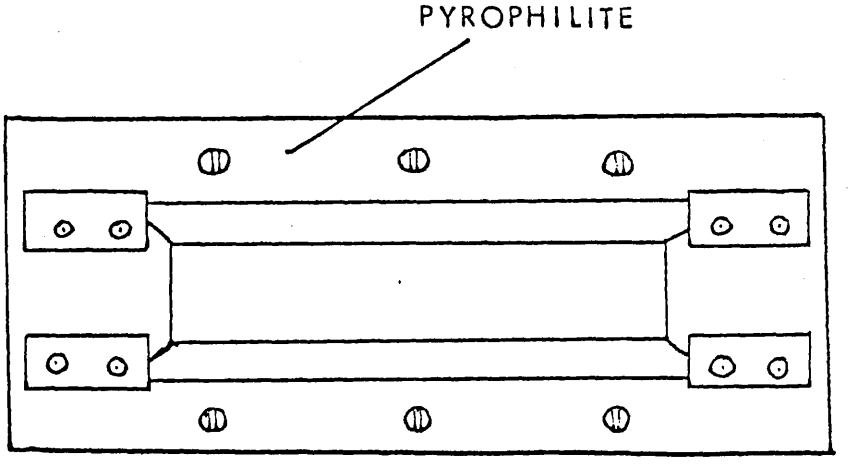

Fig. 7.3. Mask for depositing the film.

very effective because they remained intact when the substrate was cleaned ultra-sonically and also when brought in contact with the spring loaded contact rods. Contact potential differences were also minimised because the resistivity of nichrome is close to those of rare earth dihydrides. The nichrome electrodes were so strong that they could not be removed without scratching the glass base, and could be repeatedly polished to remove grease or dirt. Total lead and contact resistance was found to be 0.05 ohm. The contacts to the film were made by evaporating the rare earth dihydride films over the predeposited nichrome electrodes.

7.4. Masks.

The conventional four-probe method has been used to measure the resistance of the films. In general, the separation of the potential probes on the sample defines the sample length. In the case of bulk specimen, the probes used are very fine point contacts but in thin films, the potential contacts must necessarily have a finite area because they must be evaporated onto the substrate by means of a mask. Two separate masks were used in this work, one for low temperature measurement and another for high temperature measurement is made of pyrophilite (Fig. 7.3). The mask used for low temperature (liquid nitrogen) is made of perspex, and the shape of which is the same as high temperature one. The voltage and current probes on the film are 0.3 cm apart and 0.1 cm in width. The inner edges of the masks were made very sharp so that the film edges became sharp also. The sample area is 6.2×1.3 cm^2.

7.5. Procedure of the film growth.

Immediately after cleaning, the substrate was placed on a stainless steel jig covered with the mask for the deposition of the nichrome electrodes. The nichrome evaporation was carried out normally in the region of 8×10^{-6} torr. Following this deposition the substrate was removed from the chamber and cleaned again for the rare earth

hydride film deposition. For this purpose the substrate was placed under another mask (either pyrophilite or perspex) which shielded part of the predeposited contact electrodes and allowed the rare earth hydride film to deposit on the substrate and also over lay part of the contact electrodes. A moveable shutter was used so that evaporation could be started and stopped at any desired time.

Before placing the substrate in the chamber for final evaporation it was ensured that the spring-loaded electrode leads were in good contact with the predeposited nichrome electrdes on the substrate. Also other electrical connections were checked before putting the whole jig inside the vacuum chamber. When the substrate was under vacuum, the temperature of the substrate was raised to 150°C and maintained for one and a half hours to degas the substrate. At the end of this time the substrate was cooled to room temperature and the evaporation was carried out. The filament was thoroughly outgassed by passing a moderate current through it beforehand.

At the start of the evaporation, the metal vapour was prevented from condensing on the substrate by using a moveable shutter, until the gettering of residual gases was complete.

7.6. Film thickness

The film thickness was estimated by the Tolansky multiple beam interferometry method in the same way as for the structural studies described in chapter 4. The deposition rates used were the same for different materials as mentioned in section 5.7, chapter 5. So long as the distance from the source to the substrate and the current through the filament were kept constant, the deposition rates were found to be constant (from time VS thickness curve) within $\pm$ 5Å. Film thickness, although estimated from the deposition rates, were checked for every three runs by actual measurement by placing additional glass

slide (partly covered by razor blades) next to the experimental substrate. The values of the thickness quoted lie within ± 10Å.

7.7. Radiant heater.

Annealing of the films inside the vacuum chamber was performed by means of a specially constructed radiant heater shown in Fig.7.4. This heater was found very reliable and convenient especially for this work when the whole electrical measurements have been carried out insitu. The heater is cylindrical in shape, 11 cm in length and 6.8 cm in diameter and made of fused quartz. The substrate with the mask, fixed with the jig was placed inside the heater 4 cm below the window. The dimensions of the window were 8 x 2 cm^2 i.e. bigger than the film dimensions, so that a uniform deposition on the substrate could be possible. Nichrome wire has been spirally over the whole area (except window), used as the heating element. Alternating current up to 6 amps. was passed from a variac transformer through the nichrome wire attaining the temperature uniformly inisde the heater up to 320°C. It was found by placing the thermocouple junction at different positions inside the heater that a uniform temperature persists throughout the volume of the heater (within ± 2°C). This was a great advantage of this heater because it could provide uniform temperature through the film when annealing was conducted. A calibration curve (current VS temperature) has been drawn for the heater and is shown in Fig.7.5.

7.8. The cooling device.

The temperature between the ambient and liquid nitrogen were achieved by using a conduction cooled crystat, a very simple device constructed in the laboratory (Fig.7.6.). The main part of the device consist of a hollow rectangular copper block (dimensions 7 x 4 x 2.3 cm^3) having one inlet and one outlet tube for flowing liquid nitrogen. The copper block was constructed in such a way that

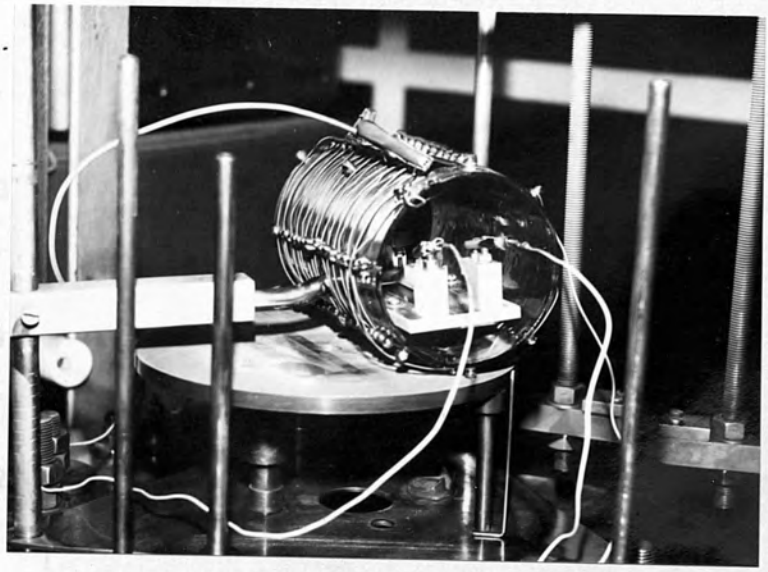

Figure 7.4. Radiant Heater

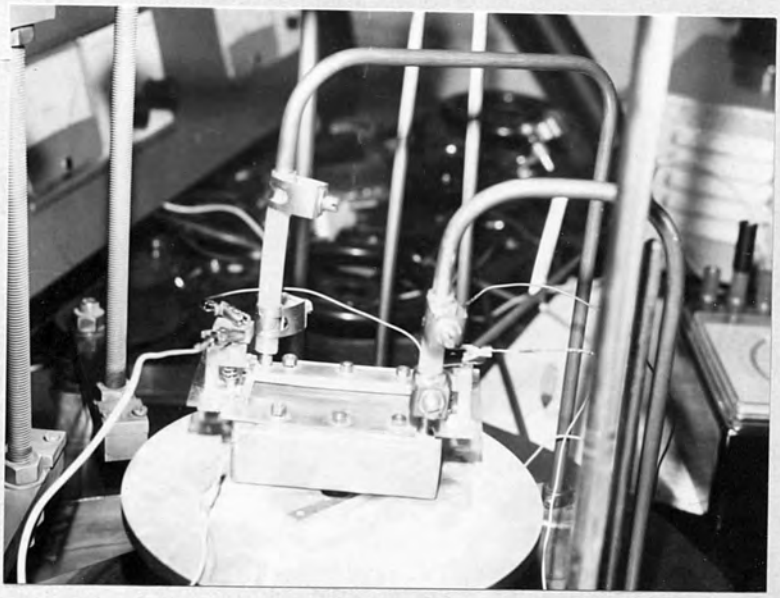

Figure 7.6. Cooling Device

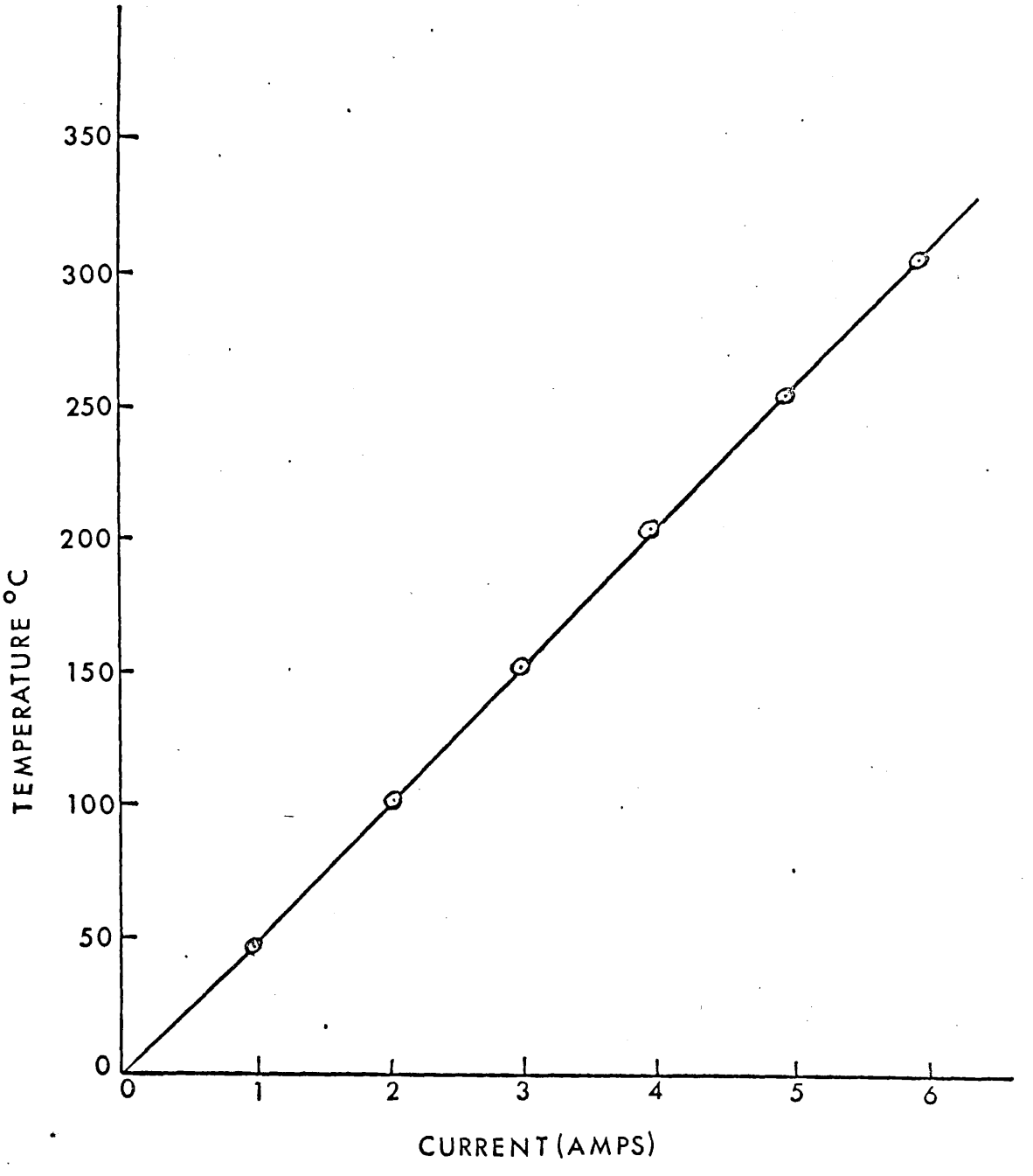

Figure 7.5. Calibration curve for radiant heater.

it was leak proof and sufficiently strong to stand against the atmospheric pressure when placed inside the vacuum. The top surface of the block also serves as the jig on which the glass slide is held in contact by pressing it with the mask by means of screws. The glass slide attains the temperature of the liquid nitrogen (passing through the block) by conduction. It was found that the temperature on the surface of the glass slide (i.e. on the film surface) differed by only $2^{\circ}C$ from that of the copper block. The inlet and outlet tubes (made of copper) passed through the base plate of the vacuum chamber by means of a feed through. The inlet tube has two sections: one inside the chamber having the internal diameter of 0.3 cm and the chamber having internal diameter of 1 cm, and at the top of which a funnel is fixed to pour liquid nitrogen. The position of the funnel is kept at a height of one and a half feet from the surface of the cooling chamber. The specimen attained the liquid nitrogen temperature ($77^{\circ}K$) within fifteen minutes. The liquid nitrogen was kept pouring from a flask at regular intervals while the measurement was carried out.

7.9. Measurement of temperature.

High temperature was measured by placing a Chromel-Alumel (T_1T_2) thermocouple inside the heater and recording it by means of a millivoltmeter with an accuracy of $\pm 5^{\circ}C$. Low temperature (liquid nitrogen) was measured by placing the copper-constantan thermocouple junction in contact with the glass substrate. The other two ends of the thermocouple were connected to a thermometer from which the temperature could be directly read. This thermometer has been specially built for liquid nitrogen temperature measurement and supplied with JEM-6A electron microscope. It has been graduated from $20^{\circ}C$ to $-200^{\circ}C$, having an accuracy of $\pm 3^{\circ}C$.

The thermocouple output connections were made to the metal-ceramic low current leads mounted on stainless steel flanges and brazed into the base plate.

7.10. Method of resistance measurement: The four-probe technique.

The resistance measurement in this work was carried out employing the conventional four-probe technique (Van der Pauw, 1958). The current-voltage characteristics were obtained by using a conventional d.c. arrangement (Green, 1969) shown in Fig. 7.7. A constant current in the range 200 - 500 μA was passed through the specimen between two probes, and the voltage

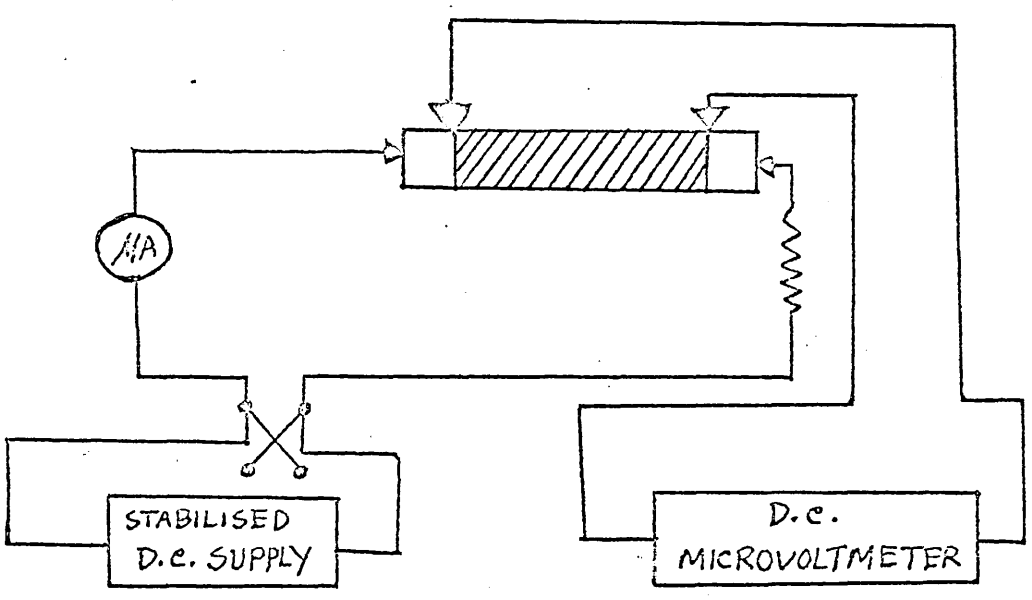

Fig. 7.7. schematic diagram of the d.c. apparatus for measuring the electrical resistance of rare earth hydride films. Effective film size is 5.2 x 1.3 cm^2 (shaded region).

developed between the other two probes was measured. The voltage across the two potential probes (which represents the actual film length 5.2 cm) was measured using a d.c. microvoltmeter (Dymar Type 721), sensitive to 100 μV and was suitable for the above range of current passing through the film. A fixed high resistor (10KΩ)

in series with the stabilised voltage source was used to limit the current through the film in the range 200 - 500μA. The currents were independent of load resistance and were highly stable. The current was measured with an electrometer (Keithley 610C) Sensitive to 10^{-14} amps.

The potential drop used to obtain the value of the resistance of the specimen between the potential probes is the average value obtained for both directions of current flow (although the difference was found to be negligibly small). This procedure eliminates, as far as possible, errors due to thermo-electric or rectification effects which may occur within the film due to inhomogeneities of structure, rectifying boundaries or other defects.

It should be mentioned that several spurious thin film effects may occur due to imperfect experimental technique employed to measure the I-V characteristics. In order to make sure that this was not so in the present case and that the observed I-V characteristics were truly representative of the rare earth hydride films, several checks were made. For example, the reliability of the experimental set up which led to the I-V characteristics reported in this work was checked by plotting the thickness dependence of the electrical resistivity of polycrystalline gold films and was found to yield results similar to those obtained by Chopra and Bob (1964). Also some improvements in the technique were employed in the present work such as for example, using spring-loaded pressure leads to contact the predeposited electrodes and using the evaporated nichrome electrodes instead of silver paint. The resistance of each film was obtained from its current-voltage characteristics and the corresponding resistivity was then evaluated from the geometry of the specimen. The resistivity value for a film of a particular thickness was found to be reproducible when the

observations were repeated on the films of the same thickness grown under identical conditions.

CHAPTER 8.

MEASUREMENT OF THE ELECTRICAL RESISTIVITY AND TEMPERATURE COEFFICIENT OF RESISTANCE OF GADOLINIUM, TERBIUM, DYSPROSIUM, HOLMIUM AND ERBIUM DIHYDRIDE FILMS.

8.1. Introduction.

The results obtained for the electrical resistivity (at 77°K and in the range 293-573°K) and the temperature coefficient of resistance of the polycrystalline films grown from Gd, Tb, Dy, Ho and Er of the thickness range 80 -1000Å are presented in this chapter. The mode of growth of the films and the experimental details have been described in chapter 7. The structures of the films have been determined by electron diffraction studies (chapter 5 and 6) and attempts have been made to correlate the dependence of the electrical resistivity and structures on thickness. The change of electrical resistivity due to the treatment of the film with hydrogen at 573°K has also been measured and a similar correlation sought between the resistivity and structural changes.

8.2. Resistivity of the films(80-1000Å) grown from gadolinium.

The thickness dependence, at room temperature, of the electrical resistivity of gadolinium dihydride films in the thickness range 80-250Å is shown in Fig. 8.1. The films of this thickness range are f.c.c. gadolinium dihydrides as determined earlier. The resistivity of the films of thickness less than 80Å could not be measured reliably. Such very thin films have discontinuous structures (as revealed by electron microscopy - sections 5.7.1., chapter 5) and the conduction phenomenon is very complicated (Morris, 1972). The curve shown in Fig. 8.1. is reproducible within experimental error. Although apparently the curve exhibits characteristics similar to other known results of the thickness dependence of electrical resistivity, it will be clear later on that the overall behaviour is curious indeed. The

non-stoichiometric characteristics of the rare earth dihydride (sections 2.2., chapter 2) and the lack of knowledge of the exact composition (i.e. H/Gd atomic ratio) of the film made it difficult to explain exactly the behaviour of resistivity VS thickness curve. However attempts have been made to put forward arguments and evidence to explain the characteristic on the basis of the bulk dihydride resistivity, our own structural investigations and the observed resistivity values.

The thickness dependence at room temperature, of the electrical resistivity of the films of thickness range 250-1000Å is shown in Fig. 8.2. Structural analysis of the films (250-850Å) showed the co-existence of f.c.c. dihydride and h.c.p. metal. As may be seen from the curve, the resistivity increases with the thickness, which exhibits characteristics different from other known results on the thickness dependence of electrical resistivity (Chopra etal 1963, Chaudhuri and Pal, 1975). To explain the dependence of the electrical resistivity on thickness (80-1000Å) and to correlate them with structural phase, it is convenient to show the thickness dependence of resistivity by a single curve (Figure 8.3., solid line). An examination of the curve shows its anomalous behaviour. The characteristic features of the resistivity-thickness curve for thin film of the thickness range (80-1000Å) are

i. the resistivity has a minium value of 112 $\mu\Omega$-cm at a film thickness of about 250Å and increases for thinner films.

ii. an abnormal increase occurs in the resistivity of the films thicker than 250Å and continues to increase until it becomes nearly constant at 1000Å. The above features clearly indicate the anomalous resistivity behaviour of the gadolinium dihydride films. An interesting feature of the experimental results is that the resistivity of a 250Å

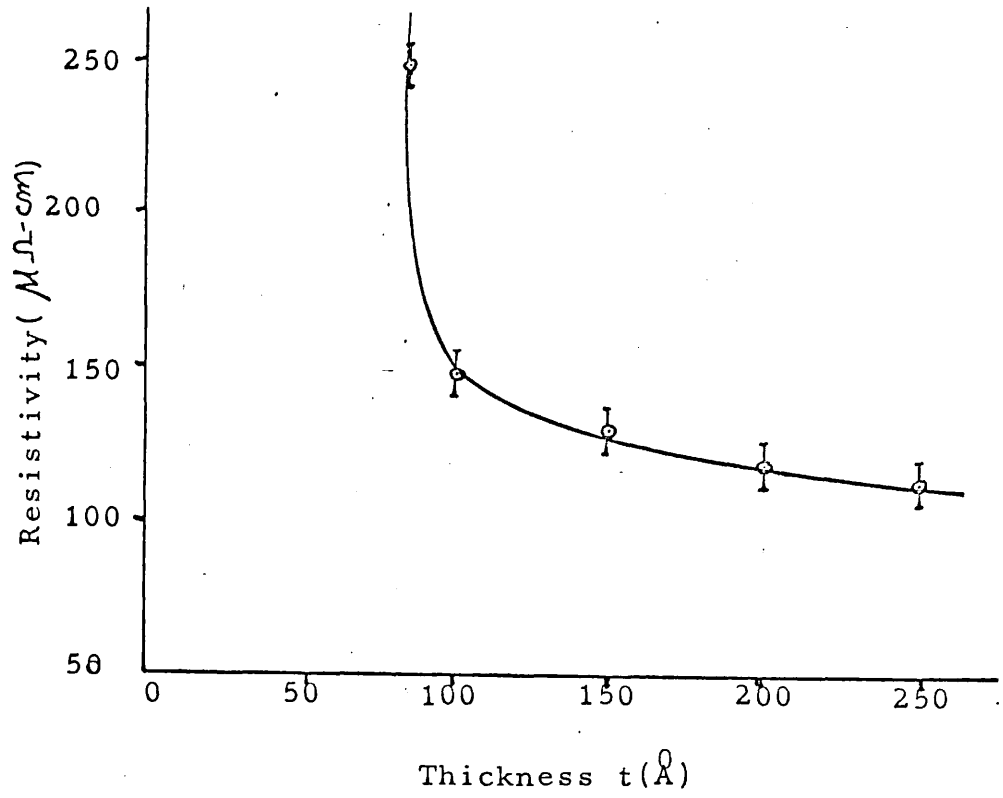

Figure 8.1. Room temperature thickness dependence of resistivity of gadolinium dihydride films.

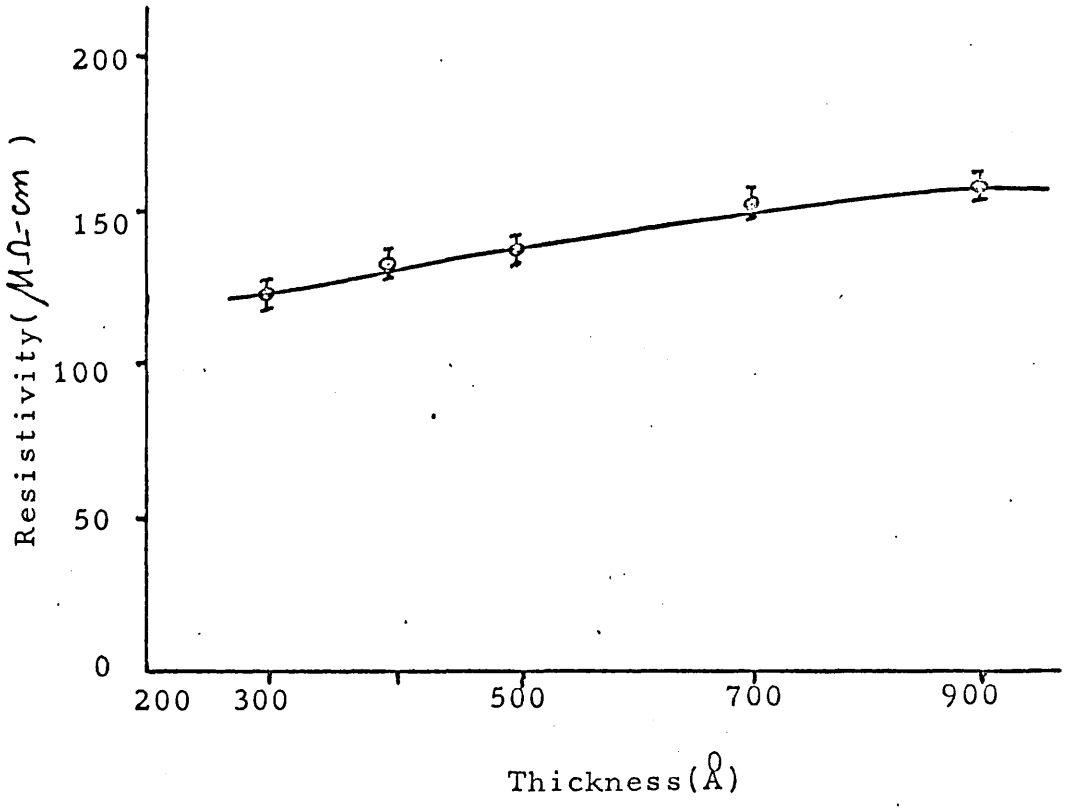

Figure 8.2. Room temperature thickness dependence of resistivity of the films grown from Gd(250-900Å).

film (112 $\mu\Omega$-cm) is less than that of the parent metal (for bulk Gd, ρ = 134 $\mu\Omega$-cm). This shows clearly that a 250Å film (gadolinium dihydride) is a better electrical conductor than the parent metal, which is consistent with the conduction behaviour of bulk gadolinium dihydride (Heckman, 1964). In the bulk gadolinium-hydrogen system, the f.c.c. dihydride phase exists in the composition range H/Gd=1.82-2.3, and the resistivity values for this composition range vary widely e.g. 57 $\mu\Omega$-cm for H/Gd = 1.8 and 454 $\mu\Omega$-cm for H/Gd = 2.2 (Heckman, 1969). Two important features of Heckman's results are:

1) the minimum resistivity (57 $\mu\Omega$-cm) was observed at the boundary of the single phase (f.c.c. dihydride) and mixed phase (f.c.c. dihydride + h.c.p. metal).
2) the resistivity increases again with decreasing hydrogen content in the mixed phase region e.g. 66 $\mu\Omega$-cm forH/Gd = 1.5.

The present experimental values of the resistivity can be discussed in the light of the above two features. As may be seen from Figure 8.3 the resistivity of the film in the thickness range 250-850Å (which have mixed phases - f.c.c. dihydride + h.c.p. metal) are higher than 112 $\mu\Omega$-cm, which is consistent with feature (2). Our structural investigations indicated that a film of thickness 250Å is at the boundary between single (f.c.c. dihydride) and mixed phases, and therefore has minimum resistivity value (112 $\mu\Omega$-cm), in agreement with feature (1). Although the crystal structure of a 250Å film has been determined to be f.c.c. dihydride, it was not possible to know the exact composition (i.e. H/Gd atomic ratio) of the film. However, it would not be unreasonable to assume from the resistivity behaviour that the composition of 250Å film was around H/Gd = 1.8.

The increase in resistivity with decreasing thickness in the range 80-250Å might be explained in either of the two ways:

i) thinner films are usually discontinuous and contain higher densities of defects; hence their residual resistivity and consequently the total resistivity become progressively higher or the thickness approach to the lower region (Bist and Srivastava, 1973).

ii) it is well known that the resistivity of gadolinium dihydride (bulk) is dependent on its non-stoichiometric composition (Fig.3.4. chapter 3), so it is possible that thin films in the range 80-250Å may have slightly varying composition (i.e. increase of H/Gd with decreasing thickness) which caused the increase in resistivity.

Of the above two, the later is more acceptable in the present case because it is consistent with the resistivity characteristic of bulk gadolinium dihydride and our own structural investigations, whereas the former is contradictory to our electron microscopic studies, because it was found that films thicker than 80Å were always continuous. The sharp rise in resistivity below 80Å thickness is not surprising because the films have discontinuous structure and such an increase in resistivity is expected (Maissel, 1970).

As the thickness of the film was increased to 1000Å (which is almost completely h.c.p. metal), the resistivity attained a nearly constant value (159 $\mu\Omega$-cm). This value is consistent with the known value for bulk gadolinium (134 $\mu\Omega$-cm). The somewhat higher values of resistivity for the thicker films compared with the bulk metal can be attributed to inherent film defects which are always present even in comparatively thick "as grown" films. It is known that for thick Al films ($\sim$1500Å), the resistivity is about 75% greater than the resistivity of the bulk material (Jayadevaiah and Kirby, 1969), and for thick Au films ($\sim$ 1000Å) the resistivity is about 10% greater than

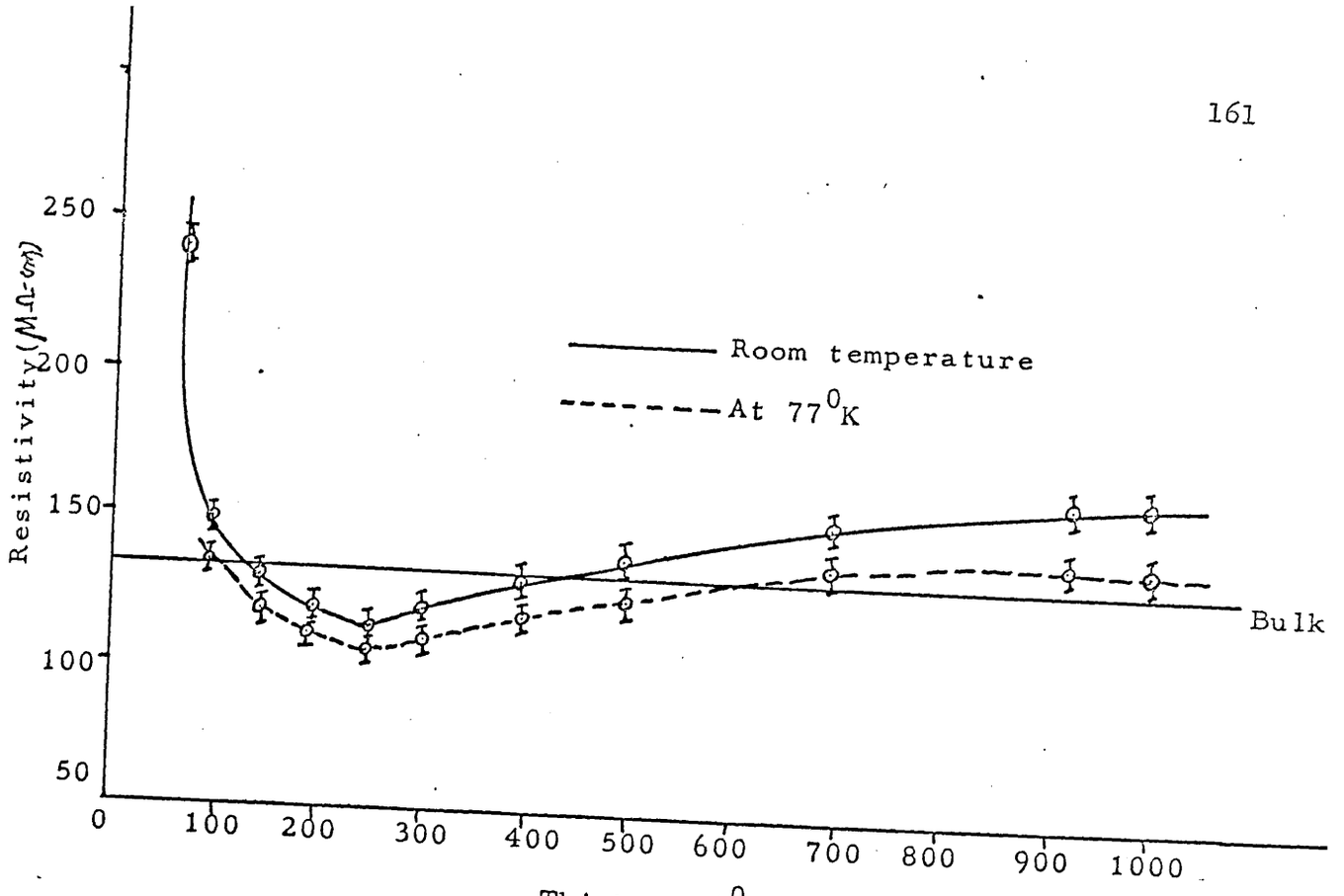

Figure 8.3.Thickness dependence of resistivity of the films (70-1000Å)grown from gadolinium.

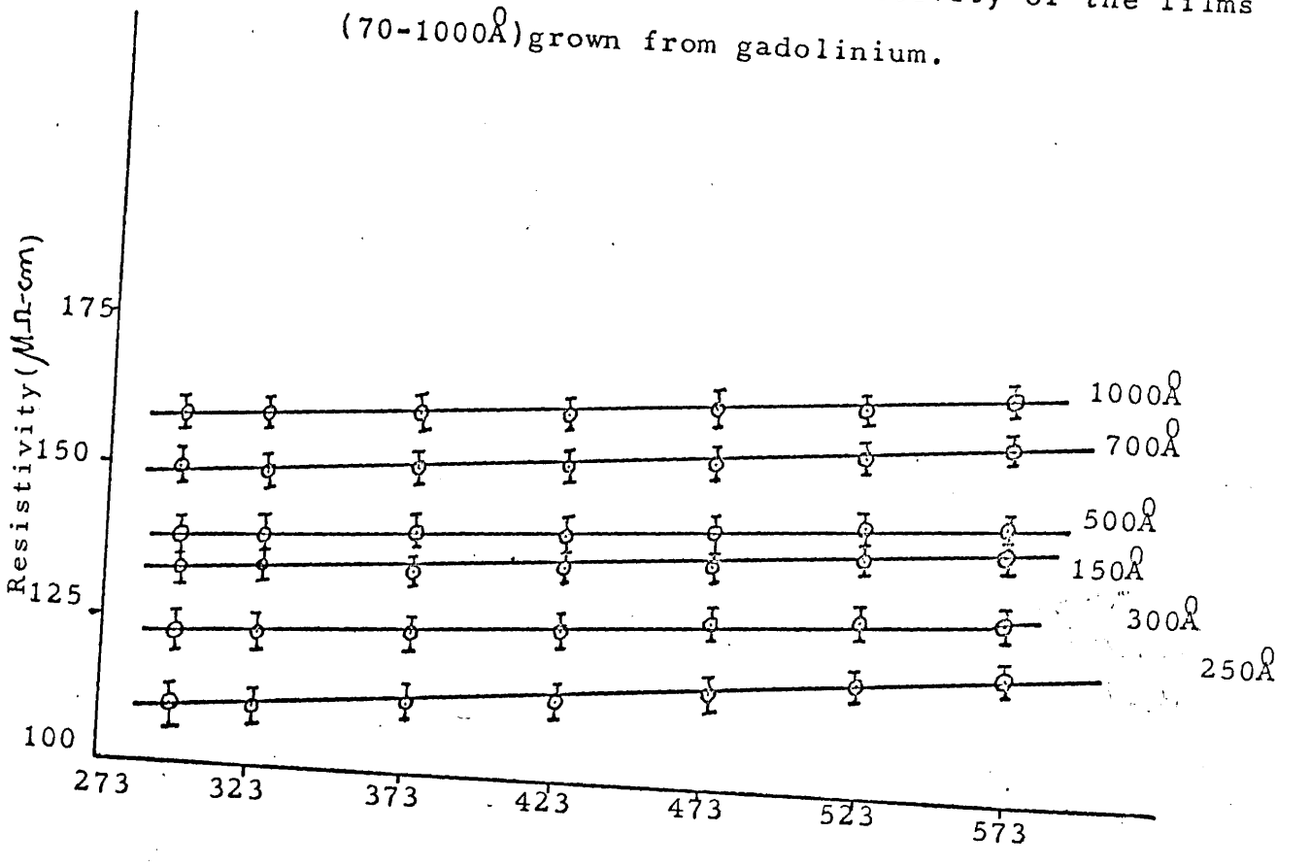

Figure 8.4.Variation of resistivity with temperature.

the bulk value (Chopra, 1969). In the light of these observations the present value of the resistivity of thick Gd films, which is about 19% higher than the bulk value, can be explained in terms of inherent film defects.

The resistivity of the film in the thickness range (80-1000Å) at 77°K is shown by the dotted curve of Fig. 8.3. The lower values of the resistivity at liquid nitrogen temperature are generally expected (Gillham,1955) and characterises the metallic nature of the films. It can be noted from the curve that there is noticeably lower resistivity for films of 900-1000Å thickness. This is also expected because gadolinium metal orders into a simple ferromagnetic phase below 293°K. But the decrease in resistivity of 900-1000Å thick films was not as high as was expected in bulk gadolinium (Colvin etal,1960). This is probably because the film was not completely h.c.p. metal. Gadolinium dihydrides (bulk) which are metallic conductors did show magnetic ordering at temperature 55°K (Wallace etal,1963). Unfortunately it was not possible to study the resistivity behaviour below 77°K because of the experimental difficulties.

8.2.1. Effect of temperature on resisitivity.

Measurements of the variation of resistance with temperature were made for 6 films ranging from 150Å to 1000Å. Typical data are shown in Fig. 8.4. in which the resistivity of the films has been plotted as a function of temperature for heating rate 2-3°K/min. The resistivity was measured over the temperature range 293-573°K at intervals of 50°K. The increase in resistivity with temperature was found to be linear for films thicker than 150Å. The general behaviour of the temperature dependence of resistivity indicates the conduction as metallic (Chaudhuri and Pal, 1975).

8.2.2. Temperature coefficient of resistance(TCR)

The temperature coefficient of resistance of the films was measured in the range 293-353^{0}K by thermally cycling the films to allow for small changes in their electrical characteristics.The observed TCR values are recorded in table 8.1.(Appendix-2,P-218).There are no other TCR data available(even on bulk material)for comparison(I hope ours are correct).

8.2.3. Change of resistance due to hydrogen treatment.

A sharp rise in resistance was observed when a stream of hydrogen was continuously passed over the heated(300^{0}C)thin gadolinium dihydride films(80-250$\mathring{A}$).The pressure in the chamber before and after admitting hydrogen was 5×10^{-6}torr and 10^{-2}-10^{-3}torr respectively.The values of the resistivity of the films at 300^{0}C before and after treating with hydrogen are shown in table 8.2.(P-219)together with the values of the resistivity when the hydrogen-treated film was kept overnight inside the vacuum at room temperature.The sharp rise of resistivity when the film was heated for two hours at 300^{0}C in hydrogen is due to the conversion of metallic dihydrides to semiconducting trihydrides.This structural change has been observed by electron diffraction studies(section 6.2,chapter 6).It is ofcourse well known that in bulk material the heavy rare earth dihydrides are metallic,and trihydrides are semiconducting. The metallic conduction vanishes for the gadolinium-hydrogen system at H/Gd=2.3. Upon complete hydrogenation the conductivity falls by about five orders of magnitude with bulk Dy,Ho and Yb(Pebler and Wallace,1962). Similar observation has been made for Ce and La by Stalinski(1959),who obtained additional evidence for the non-metallic characteristics of these hydrides by noting that their resistivities decreased with increasing temperature.In the present work,the increase in resistance was not as high as for bulk Dy,Ho and Yb trihydrides(Pebler and Wallace'62)

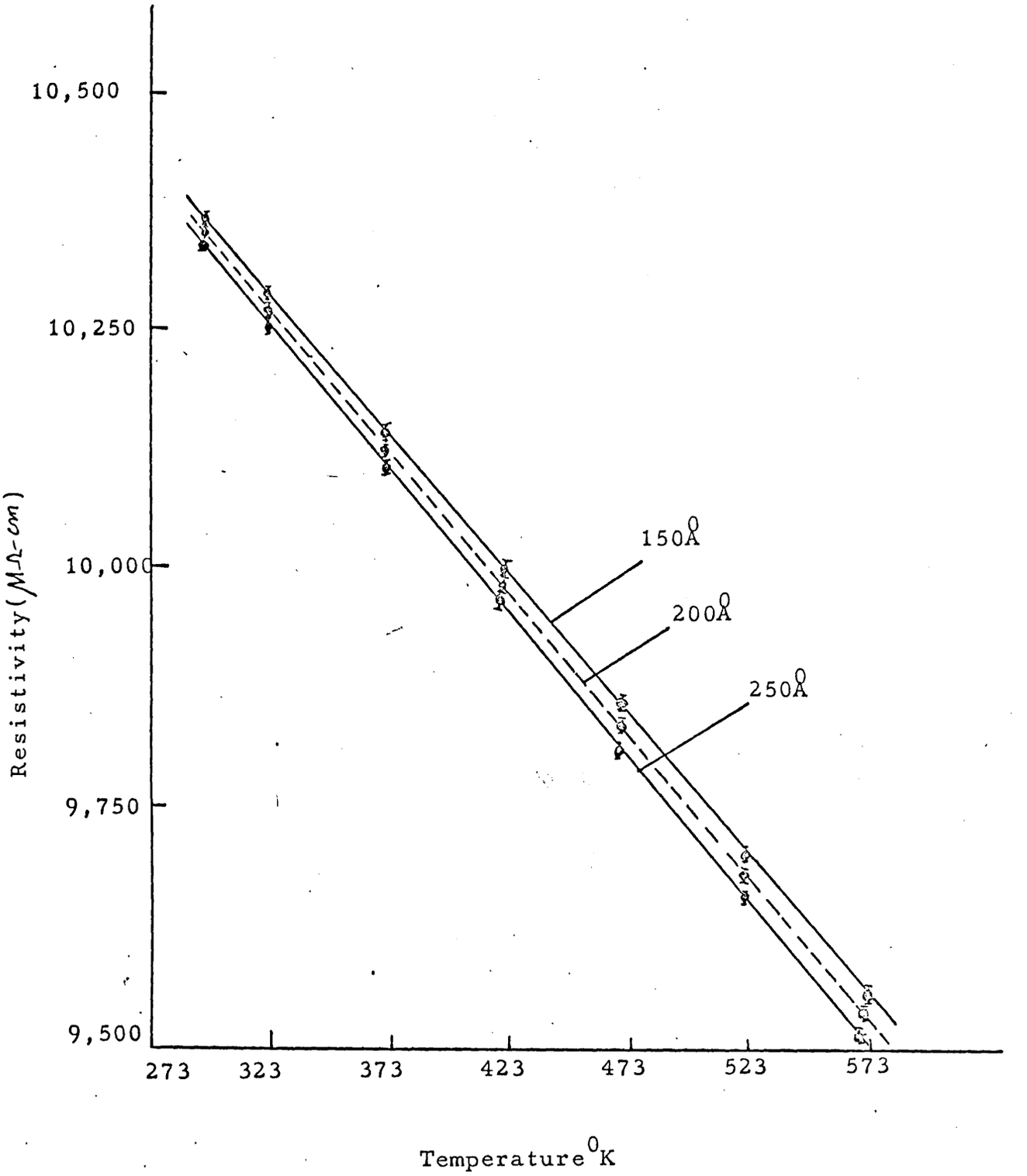

Figure 8.5. Variation of resistivity with temperature of GdH_3 films.

probably because the film was not fully hydrogenated and some oxides were formed (as revealed by electron diffraction studies section 6.2. chapter 6). However, the films display semiconducting characteristics by the decrease of resistance with the increase of temperature and consequently having negative TCR. The temperature dependence of resistivity of such films is shown in Fig. 8.5. The TCR values are recorded in table 8.2. There are no existing data of the TCR values for bulk or film trihydrides. When the films of the thickness range 300-1000Å were treated with hydrogen in the same manner, there was little change in resistance. This happened because the film was not converted to trihydrides (Section 6.2., chapter 6.).

8.3. Resistivity of the films (80-950Å) grown from terbium.

The thickness dependence, at room temperature, of the electrical resistivity of terbium dihydride films in the thickness range 80-230Å is shown in Fig. 8.6. The resistivity of the films thinner than 80Å could not be measured reliably because of their discontinuous structures. The curve of Fig.8.6. is reproducible within experimental error. The room temperature thickness dependence of the electrical resistivity of the films of thickness range 250-950Å is shown in Fig. 8.7. (The structures of 250-850Å were determined by electron diffraction to be a mixture of f.c.c. dihydride and h.c.p. metal. As may be seen from the curve, the resisitivity increases with the thickness, exhibiting characteristics similar to that of the films grown from Gd but different from other known results on the thickness dependence of electrical resistivity. Combining Figs. 8.6 and 8.7 into a single curve (Fig. 8.8.), emphasises its anomalous behaviour. The characteristics feature of the resistivity-thickness curve for thin films of the thickness range 80-950Å are:

i. the resistivity has a minimum value of 97 $\mu\Omega$-cm at a film

thickness of 230Å and increases for thinner films.

ii. an abnormal increase occurs in the resistivity of the films thicker than 230Å and continues to increase until becomes nearly constant at 950Å.

The above features are quite similar to that of gadolinium dihydride films. The resistivity of 230Å film (97 $\mu\Omega$-cm) is less than that of the parent metal (for bulk Tb, ρ = 114 $\mu\Omega$-cm). This indicates clearly that 230Å film (TbH_2) is better electrical conductor than parent metal, which is similar to the behaviour of gadolinium dihydride films (present work) and gadolinium dihydrides bulk (Heckman 1964). There are no other existing data on the electrical resistivity of terbium dihydrides. Although there are no resistivity data for the Tb - H system, the present experimental values of the resistivity may be explained by assuming similar behaviour to that of the Gd-H system (section 8.2.), since both the metals are chemically similar. In the bulk Tb-H system, the f.c.c. dihydride phase exists in the composition range H/Tb = 1.9 - 2.15. our structural investigations indicated that the films in the thickness range 80-230Å are f.c.c. dihydrides and a thickness of 230Å marks the boundary between single (f.c.c. dihydride) and mixed (f.c.c. dihydride + h.c.p. metal) phase and has the minimum resistivity value (97 $\mu\Omega$-cm). It may be seen from Fig. 8.8. that the resistivity of the films in the thickness range 230-850Å (which have mixed phases) are higher than 97 $\mu\Omega$-cm. The above features of the resistivity behaviour over the thickness range 80 - 850Å are similer to those of the Gd-H system. The increase in resistivity with the decrease of thickness in the range 80-230Å (which has continuous stucture) is due to the non-stoichiometric composition of terbium dihydride (in bulk, H/Tb = 1.9 - 2.15) which may exist over the above

thickness range. The sharp rise in resistivity below 80Å thickness is due to the discontinuous structure of the film. As the thickness of the films was increased to 950Å (which is almost h.c.p. Tb) the resistivity attained nearly a constant value (135 $\mu\Omega$-cm). This value is in agreement with the known bulk resistivity (114 $\mu\Omega$-cm). The somewhat higher values 15% of resistivity for the thicker films compared with the bulk metal can be attributed to inherent film defects such as point defects, vacancies, grain boundaries, dislocations etc. The resistivity of the film in the thickness range (80-950Å) at 77°K is shown by the dotted curve of Fig. 8.8. The general behaviour of the resistivity at liquid nitrogen temperature is similar to that of the films grown from gadolinium. The Néel point and ferromagnetic Curie point of Tb metal are 235°K and 221°K respectively. Colvin etal (1960) observed anomalies at the above temperatures in the resistivity curves for bulk Tb. A similar behaviour is expected for thick (950Å) films also (Lodge 1970, studied both 405Å and 2120Å film but observed the above feature only in 2120Å film). In the present study, slightly detectable anomalies were observed at 232°K and 220°K only for the thickest film (950Å) studied.

8.3.1. Effect of temperature on resistivity.

Measurements of the variation of resistance with temperature were made for 6 films ranging from 150Å to 950Å. Typical heating curves are shown in Fig. 8.9. in which the resistivity of the films has been plotted as a function of temperature for heating rate 2-3°K/min. The resistivity was measured in the temperature range 293-573°K at intervals of 50°K. The increase in resistivity with temperature was found to be linear for films thicker than 150Å. The general behaviour of the temperature dependence of resistivity indicates metallic

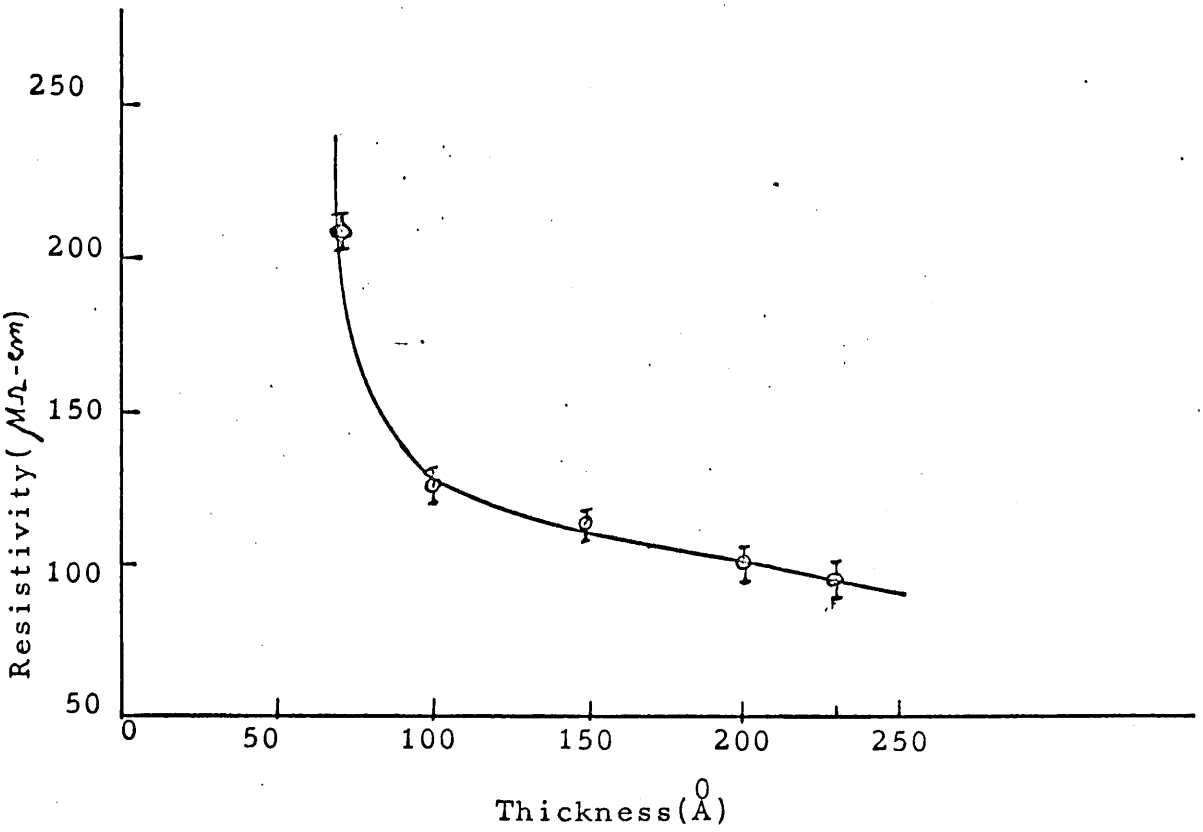

Figure 8.6. Room temperature thickness dependence of resistivity of terbium dihydride films.

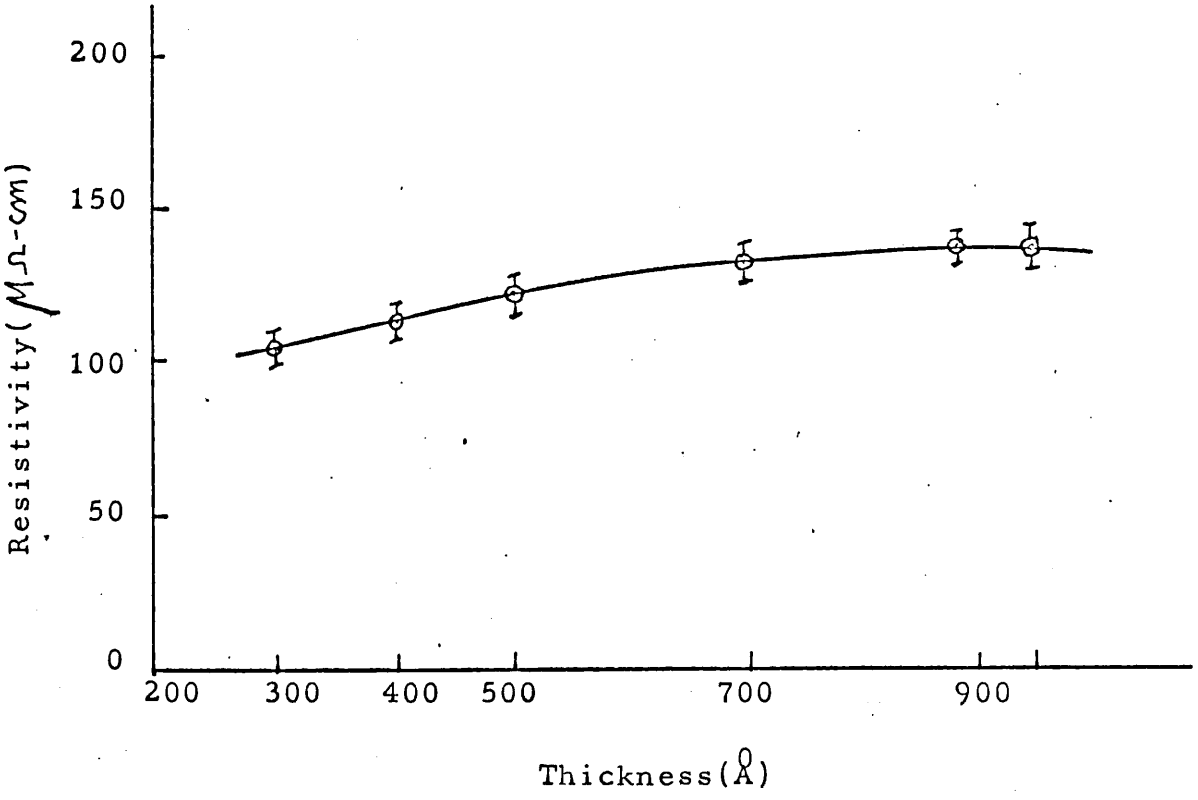

Figure8.7. Room temperature thickness dependence of resitivity of the films(300-950Å)grown from Tb.

conduction behaviour similar to that of the films grown from gadolinium.

8.3.2. Temperature coefficient of resistance.

The temperature coefficient of resistance of the films was measured in the range 293-353°K and the values are shown in table 8.3. There are no existing TCR data available for Tb-H system.

8.3.3. Change of resistance due to hydrogen treatment.

When a stream of hydrogen (pressure in the chamber 10^{-2} - 10^{-3} torr) was continuously passed through heated films of terbium dihydrides (80 - 230Å), an abrupt increase in resistivity was observed. The films were heated at 300°C for two hours. The values of the resistivity before and after hydrogen treatment is shown in table 8.4. The sharp rise in resistivity when the films were heated in hydrogen is due to the conversion of the metallic dihydrides to semiconducting trihydrides. This structural change has been established by the electron diffraction studies (section 6.2. Chapter 6). The effect of temperature on the resistivity of the trihydride films is shown in Figure 8.10. It may be seen from the curve that the resistivity decreases with increasing temperature, having negative temperature coefficient of resistance, which characterises the semiconducting nature of the film. The TCR values are shown in table 8.4. There are no existing data of either resistivity or TCR for terbium trihydrides. Films of the thickness range 300-950Å when treated with hydrogen in the same way, there was little change in resistance because they were not converted to trihydrides (section 6.2. chapter 6.).

8.4. Resistivity of the films (75-900Å) grown from dysprosium.

The variation of electrical resistivity with thickness at room temperature of dysrosium dihydride films (75-200Å) is shown in Fig. 8.11. The structure of the films of this thickness range has been determined carlier (section 4.1.). Films thinner than 75Å have discontinuous

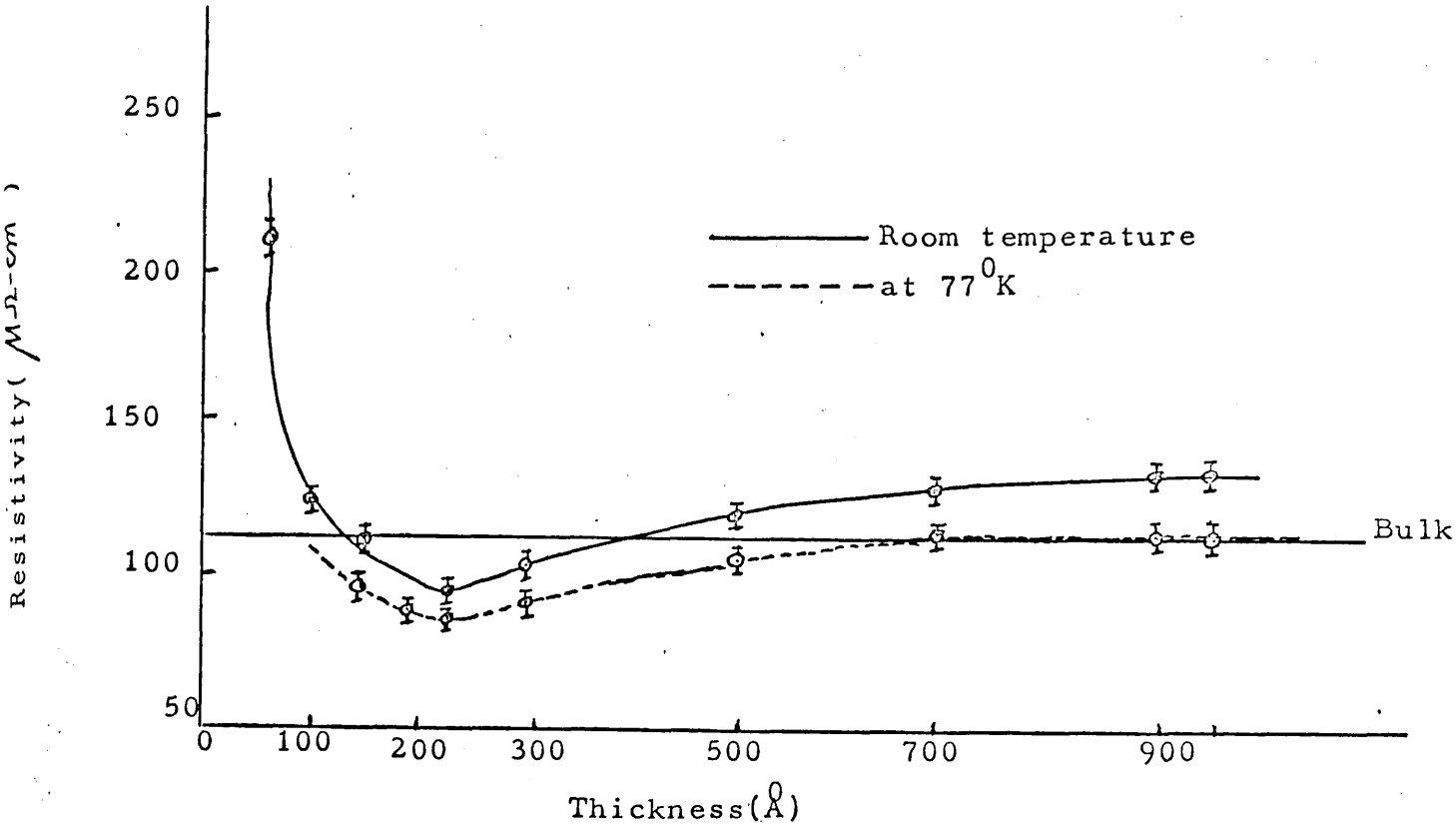

Figure 8.8. Thickness dependence of resistivity of the films (70-950Å) grown from terbium.

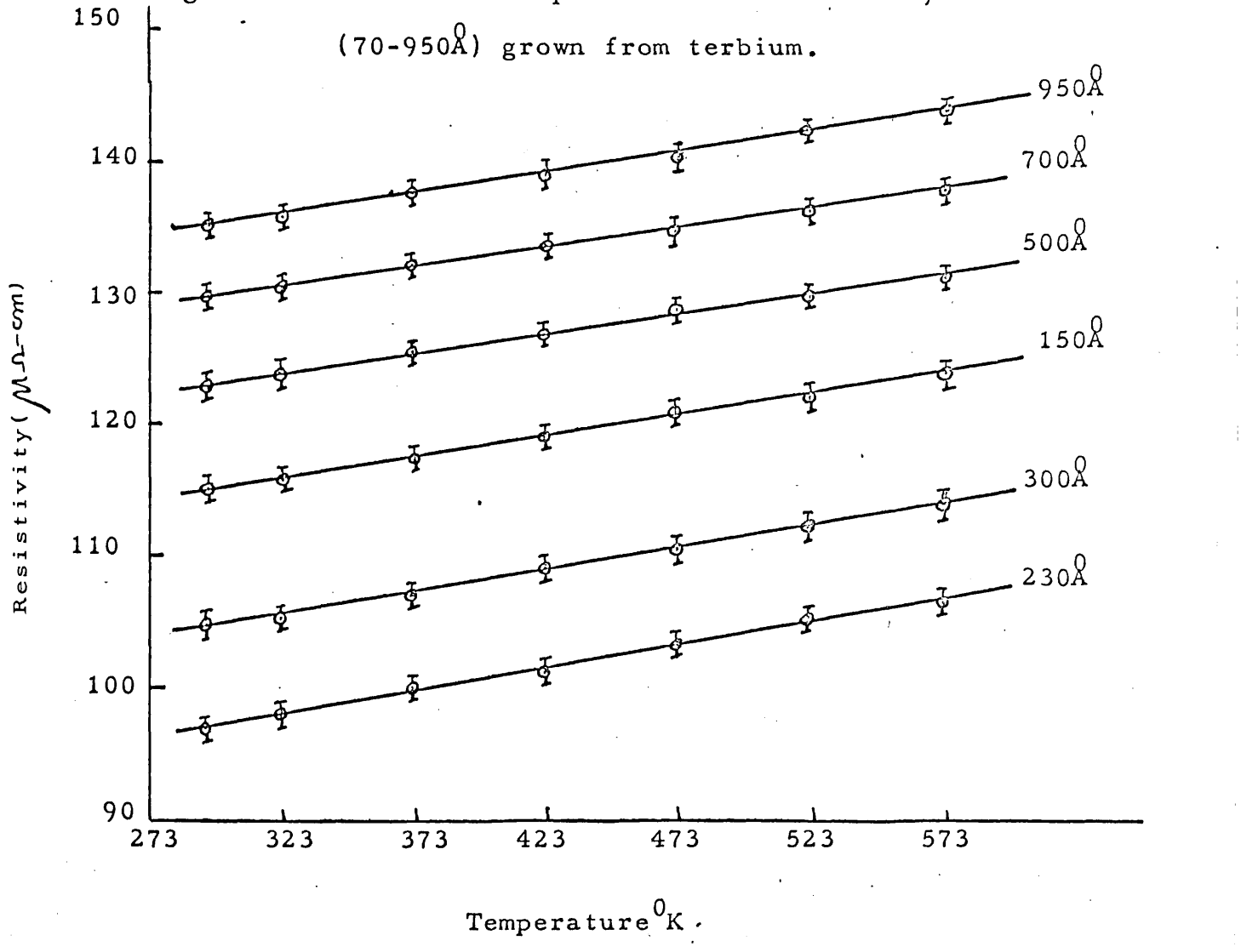

Figure 8.9. Variation of resistivity with temperature

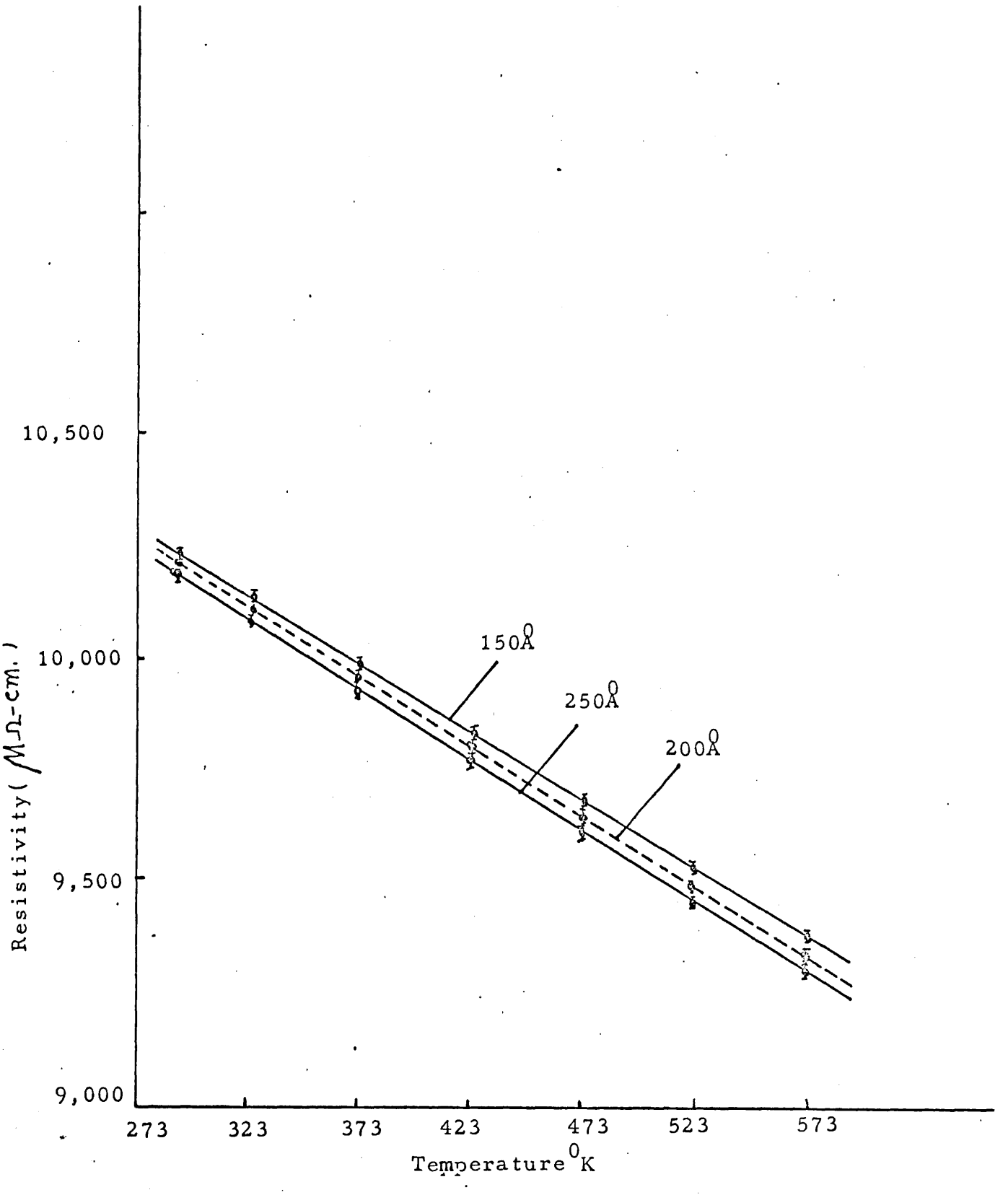

Figure 8.10. Variation of resistivity with temperature of TbH_3 films.

structure so their resistivities could not be measured reliably. The room temperature thickness dependence of the electrical resistivity of the films of the thickness range 200-900Å is shown in Fig.8.12. (the structures of 200-800Å showed the co-existence of f.c.c. dihydride and h.c.p. metal). It may be seen from the curve that the resistivity increases with thickness which shows characteristics similar to that of Gd and Tb films but different from other known results on the thickness dependence of electrical resistivity (Chopra and Bob,1964). To explain the dependence of the electrical resistivity on thickness (75-900Å) and to correlate them with structural phases, it is convenient to show the thickness dependence of resistivity by a single curve (Fig. 8.13, solid line) The main two features of the curve are:

i) the resistivity has a minimum value of 85 $\mu\Omega$-cm at a film thickness of 200Å and increases for thinner films.

ii. An abnormal increase occurs in the resisitivity of the films thicker than 200Å and continues to increase until becoming nearly constant at 900Å.

These features are similar to those observed in Gd and Tb films. The 200Å film (dysprosium dihydride)is a better electrical conductor than dysprosium metal itslef (for bulk Dy, ρ = 92 $\mu\Omega$-cm), which is similar to the behaviour of gadolinium and terbium dihydride films. No other data exists on the electrical resistivity of Dy-H system.

Our structural investigations showed that films of the thickness range 75-200Å are f.c.c. dihydrides but since the f.c.c. dihydride phase in bulk material exists over the composition range $H/_{Dy}$ = 1.94 - 2.08, the variation of resistivity over the thickness range (75-200Å) is due to the slightly varying composition in their structure (assuming the similar behaviour as that of gadolinium dihydride Heckman 1964). Lowest resistivity occurs at about 200Å thickness and is the boundary.

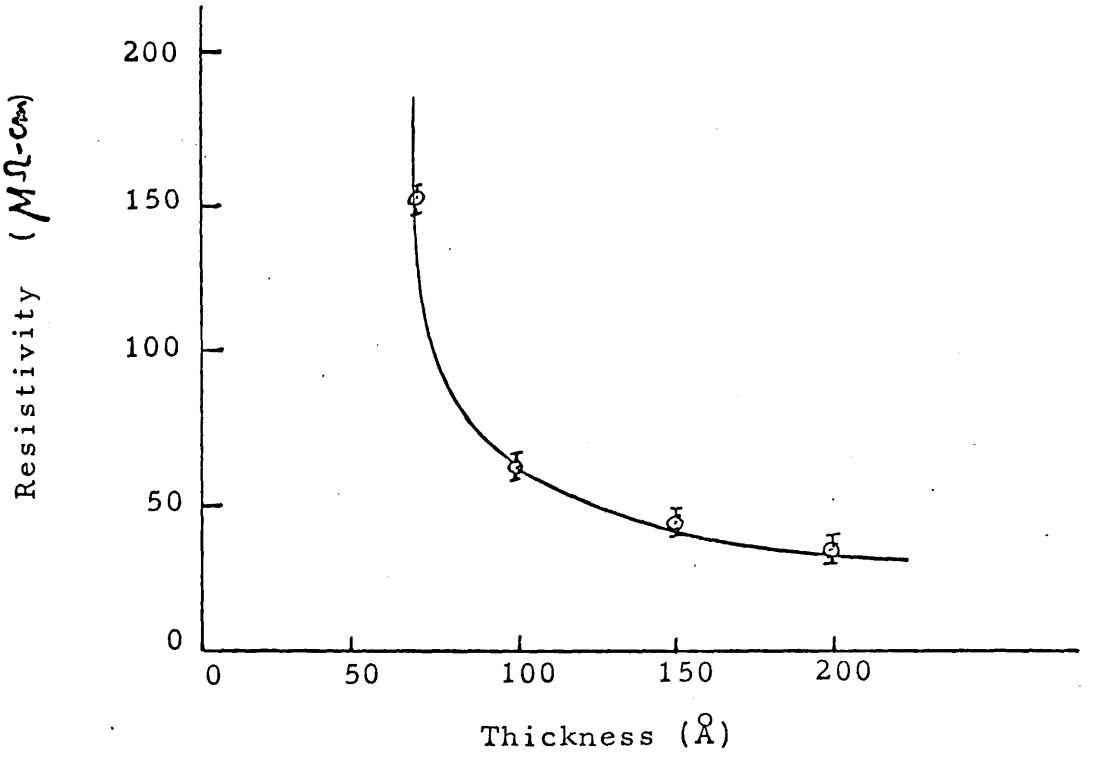

Figure 8.11 Room temperature thickness dependence of resitivity of dysprosium dihydride film,

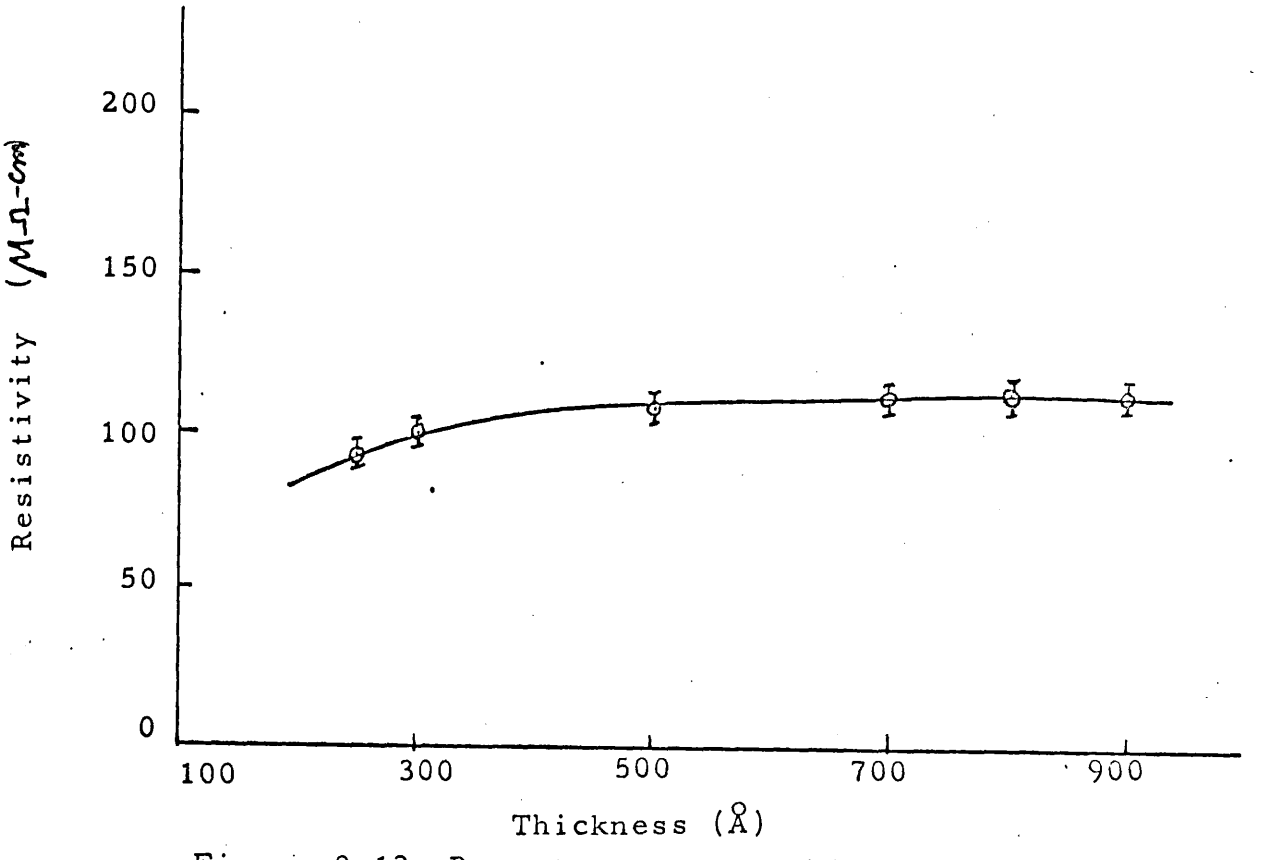

Figure 8.12 Room temperature thickness dependence of resistivity of films (200 - 900Å) grown from dysprosium.

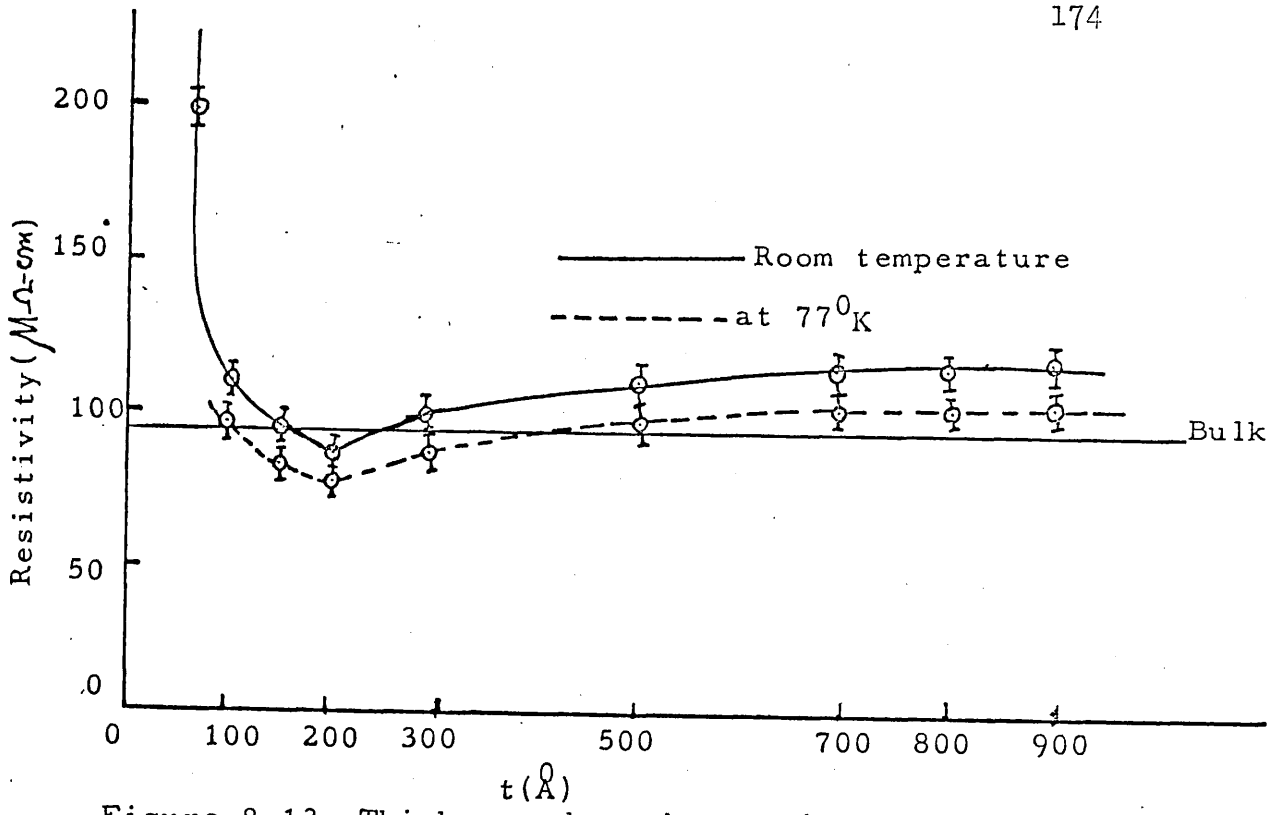

Figure 8.13. Thickness dependence of resistivity of the films(70-900Å)grown from dysprosium

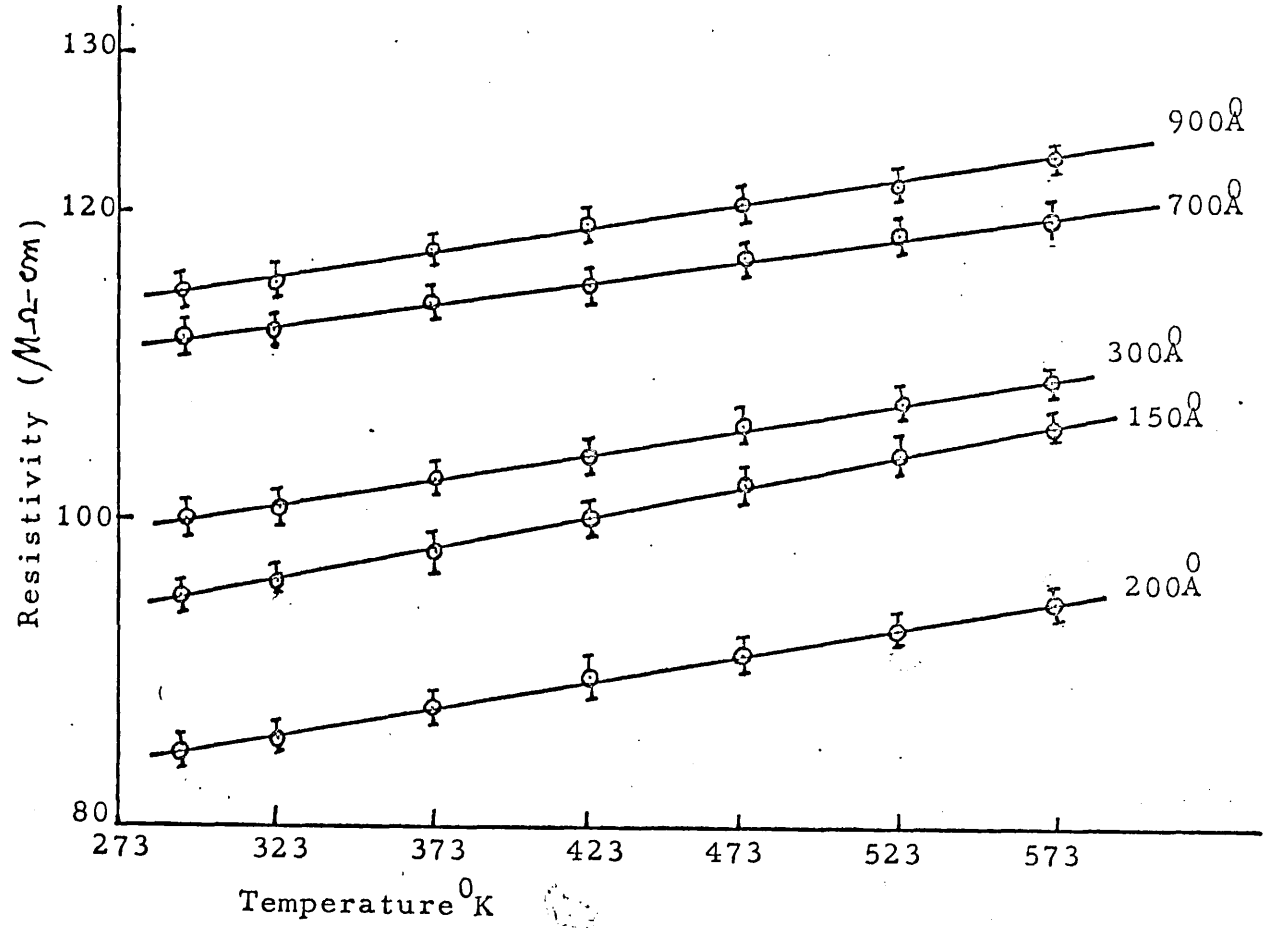

Figure 8.14. Variation of resistivity with temperature.

between single and mixed phases. This is in agreement with Heckman, (1964). It may also be seen from Fig. 8.13 that the resistivity of the films in the thickness range 200-800Å (which have mixed phases) are higher than 85 $\mu\Omega$-cm. As the thickness of the film was increased to 900Å (which is dominated by h.c.p. metallic structure) the resistivity attained a nearly constant value (115 $\mu\Omega$-cm). This value agrees with the known bulk resistivity (92 $\mu\Omega$-cm). This higher values of resistivity for thicker films compared with the bulk metal may be attributed to inherent film defects. The sharp rise in resistivity below 75Å thickness is due to the discontinuous structure of the film.

The resistivity of the film in the thickness range (75-900Å) at 77°K is shown by the dotted curve of Figure 8.13. The general behaviour of the resistivity at liquid nitrogen temperature is similar to that of Gd and Tb films. The Néel point and ferromagnetic Curie point of Dy metal are 184°K and 85°K respectively. In the present study, slightly detectable anomalies were observed at 183°K and 84 °K only for the thickest film (900Å) studied. The effect was not prominent probably because the film was not completely metallic and thick enough (the Néel temperature of DyH_2 is 8°K)

8.4.1. Effect of temperature on resistivity.

The temperature dependence of resistivity has been observed for 5 films ranging from 100 to 900Å. The variation of resistivity with temperature is shown in Fig. 8.14. The resistivity was measured in the temperature range 293-573°K at intervals of 50°K and the heating rate was 2-3°K/min. The increase in resistivity with temperature was found to be linear for films thicker than 100Å and generally indicates metallic conduction.

8.4.2. Temperature coefficient of resistance.

The TCR values of the films were measured in the range 293-353°K and are shown in table 8.5.

8.4.3. Change of resistance due to hydrogen treatment.

When dysprosium dihydride films (75-200Å) were heated at 300°C for two hours in hydrogen, the resistivity increased sharply as shown in table 8.6. This sharp increase in resistivity is due to the conversion of the metallic dihydrides to semiconducting trihydrides. The increase in resistivity for DyH_3 was observed to be greater than those of GdH_3 and TbH_3. The change in structure (from dihydrides to trihydrides) has been studies by electron diffraction (section 6.2, chapter 6) for Gd and Tb films and similar behaviour is expected for Dy films. The effect of temperature on resistivity of the DyH_3 film is shown in Fig. 8.15, which characterises the semiconducting nature of the films. Films of the thickness range 200-900Å, when treated similarly with hydrogen, showed similar behaviour to that of Gd and Tb films.

8.5. Resistivity of the films (100-900Å) grown from holmium.

The thickness dependence at room temperature of the electrical resistivity of holmium dihydride films in the thickness range 100-220Å is shown in figure 8.16. As may be seen from the figure the resistivity increased sharply below 100Å because of the discontinuous structure of the film. The room temperature thickness dependence of the electrical resistivity of the films in the thickness range 200-900Å (the structure of 200-800Å films consist of both f.c.c. dihydride and h.c.p. metal), is shown in figure 8.17. It may be noted from the figure (8.17) that the resistivity increased with the thickness which is similar to Gd, Tb, Dy films. To explain the dependence of the electrical resistivity on thickness (100-900Å) and to correlate them with structural phases, it is convenient to show both Figs. 8.16 and 8.17

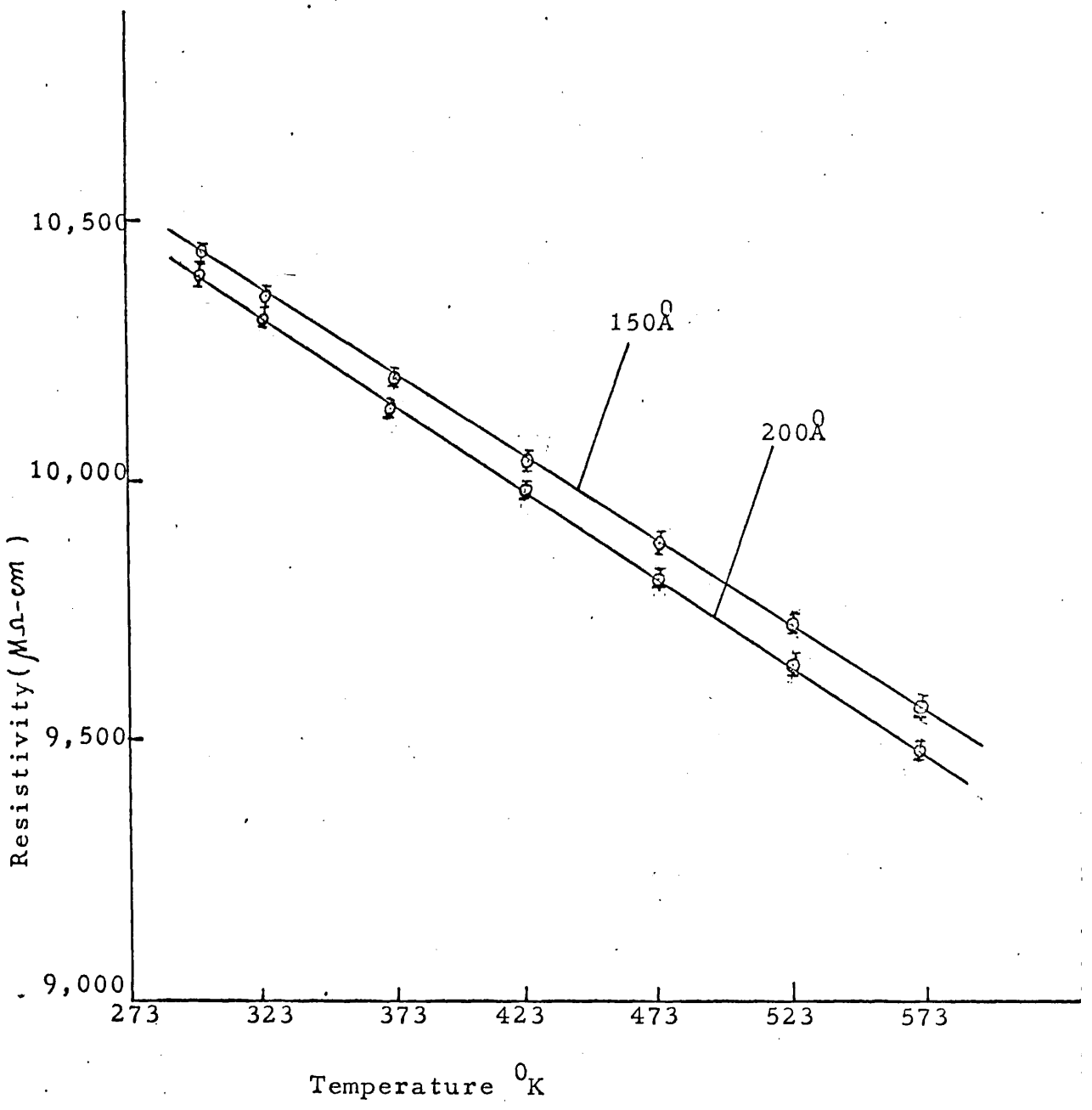

Figure 8.15. Variation of resistivity with temperature of DyH_3 films.

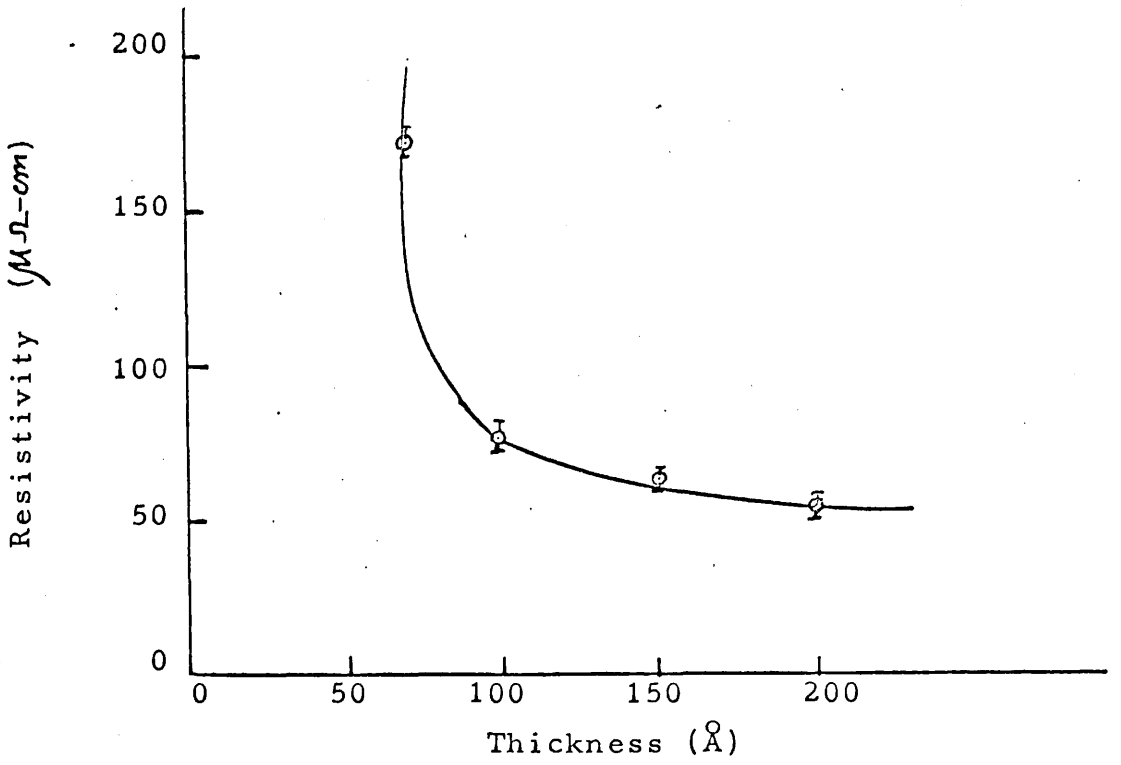

Figure 8.16 Room temperature thickness dependence of resistivity of holmium dihydride film.

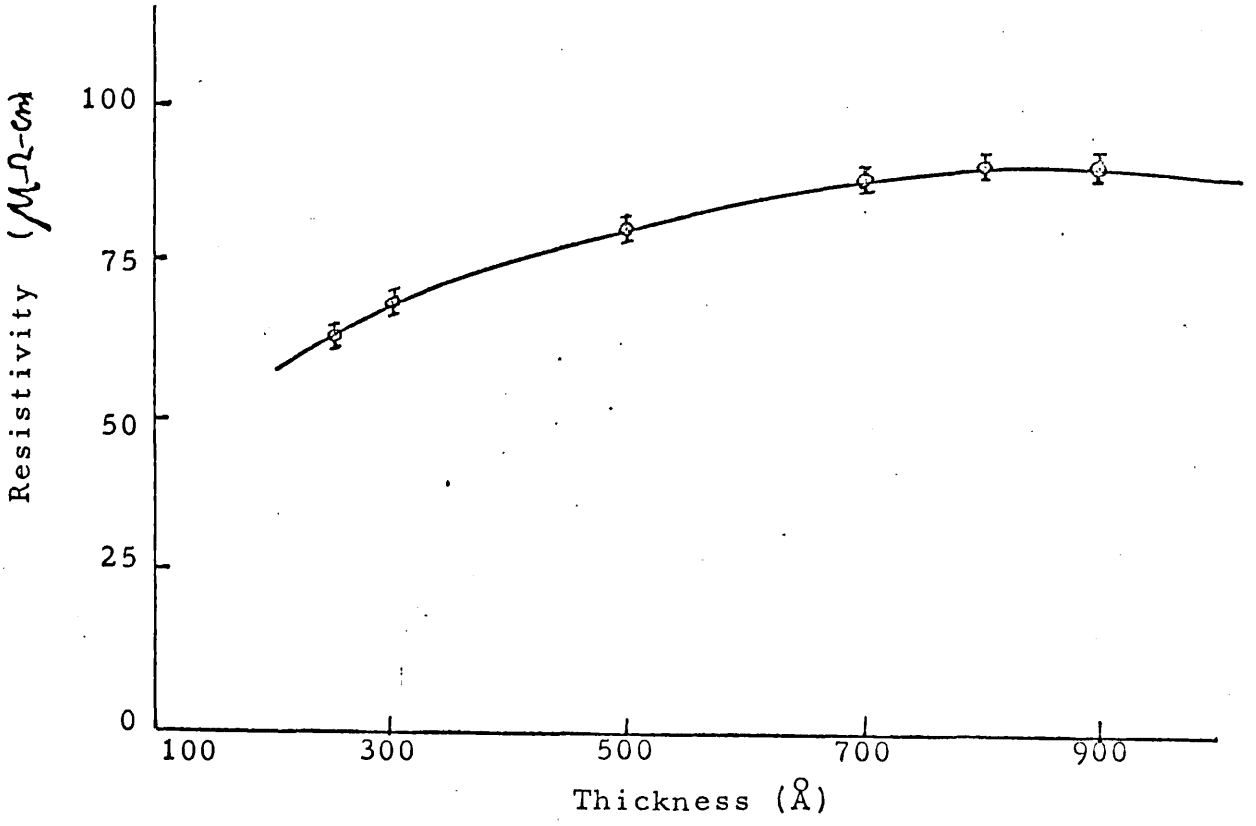

Figure 8.17 Room temperature thickness dependence of the films grown from holmium.

on a single diagram (Fig. 8.18.). The characteristic features of the curves are:

i. The resistivity has a minimum value of 56 $\mu\Omega$-cm at a film thickness of 200Å and increases for thinner films.

ii. An abnormal increase occurs in the resistivity of the films thicker than 200Å and continues to increase until became nearly constant at 900Å.

These two features are similar to those observed in Gd, Tb and Dy films but the minimum resistivity value, obtained was low compared to the others. The interesting feature of the experimental results is that the resistivity of 200Å films (56 $\mu\Omega$-cm) is less than that of Ho metal (ρ = 81 $\mu\Omega$-cm). Like the Gd-H system, the bulk holmium dihydride phase exists in the composition range $^{H}/_{H_o}$ = 1.95 - 2.24, and the resistivity values varies over the composition range having the minimum value 25 $\mu\Omega$-cm at $^{H}/_{H_o}$ = 1.9. The variation in resistivity over the thickness range 100-200Å (f.c.c. dihydride) is due to their slightly varying compositions (the resistivity increases with increasing hydrogen content within the dihydride range). From the structural investigations (section 5.5.1.) it was found that 200Å thickness indicates the boundary between single (f.c.c.) and mixed (f.c.c. and h.c.p.) phases. The resistivity measurements have correlated this feature. Films in the thickness range 200-800Å have mixed phases and the variation of resistivity over the thickness range is due to varying compositions of the films (the resistivity increases with decreasing hydrogen content). As the thickness of the film was increased to 900Å (which is almost h.c.p.H_o) the resistivity attained nearly a constant value (93 $\mu\Omega$-cm). This value is consistent with the known bulk resistivity (81 $\mu\Omega$-cm).

The resistivity of the film in the thickness range (100-900Å)

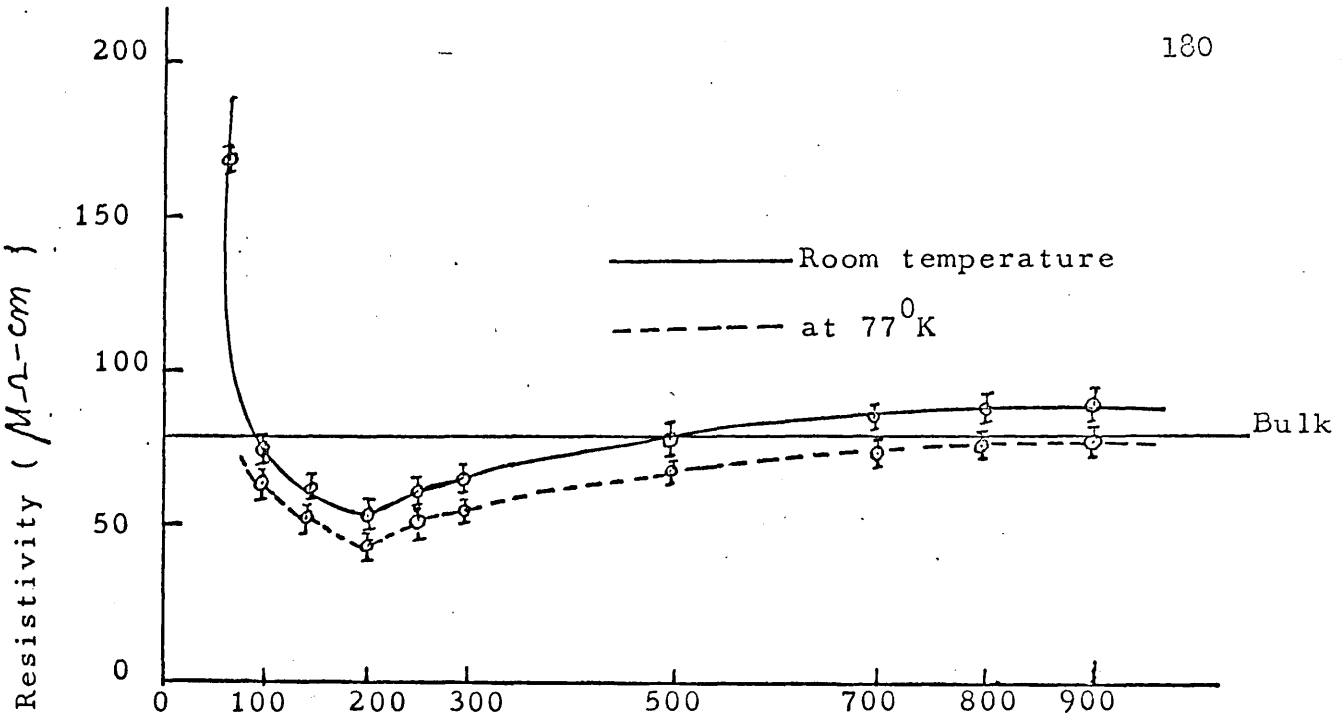

Fig.8.18. Thickness dependence of resistivity of the films(70-900Å) grown from holmium.

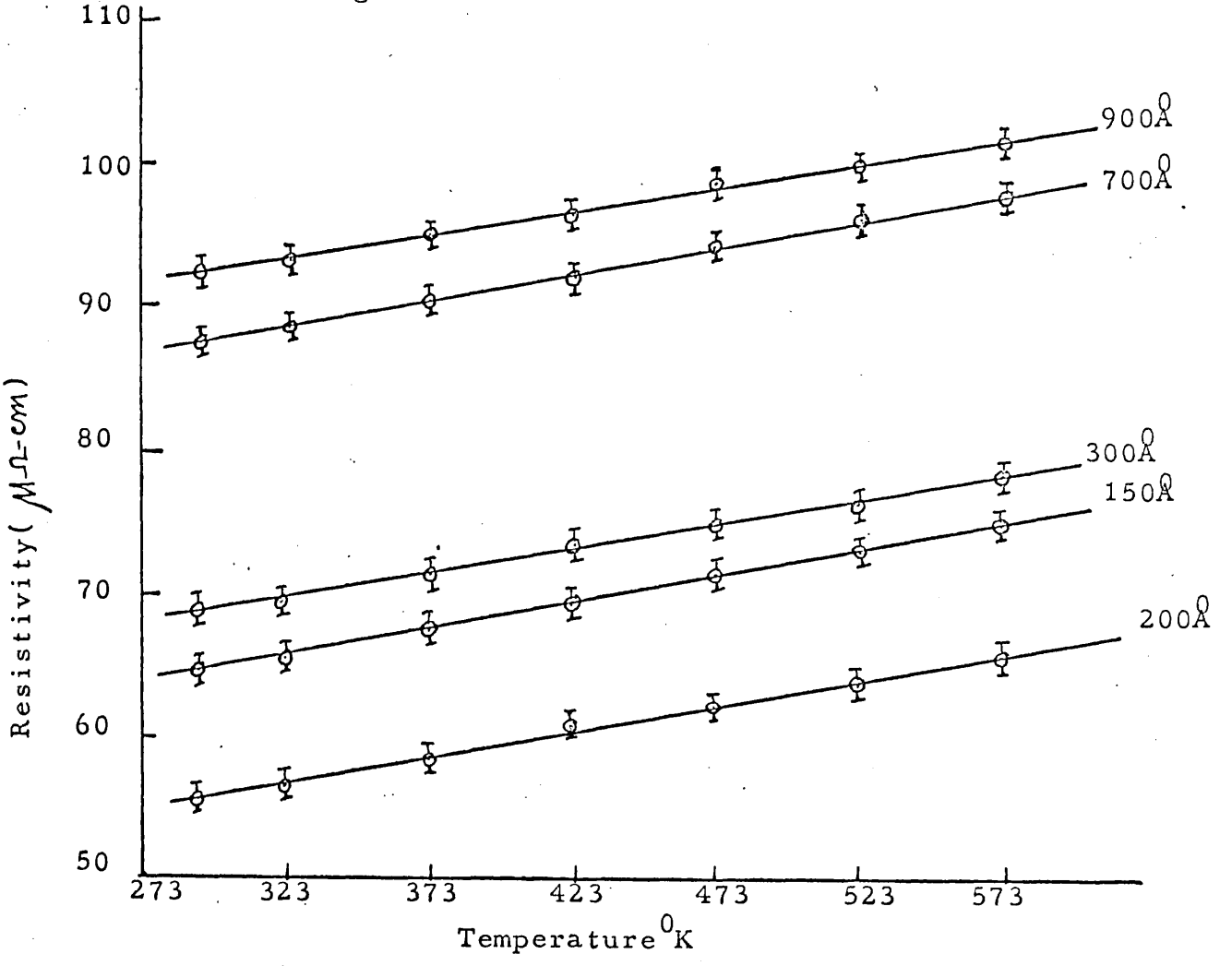

Figure 8.19. Variation of resistivity with temperature

at 77°K is shown by the dotted curve of Fig. 8.18. The general behaviour of the resistivity curve indicates the metallic nature and is similar to those of Gd, Tb and Dy films, but the anomaly noticed at the Néel temperature (135°K) for 900Å film was very weak.

8.5.1. Effect of temperature on resistivity.

Measurements of the variation of resistance with temperature were made for 5 films of thickness 150Å, 200Å, 300Å, 700Å and 900Å (Fig. 8.19). The resistivity was measured in the temperature range 293-573°K at intervals of 50°K. The increase in resistance with temperature was found to be linear.

8.5.1. Temperature coefficient of resistance.

The temperature coefficient of resistance of the films were measured in the range 293-353°K and the values are shown in table 8.7. There are no existing TCR data available for H_o-H system.

8.5.3. Change of resistance due to hydrogen treatment.

When holmium dihydride films (100-200Å) were heated for two hours at 300°C in hydrogen, the resistivity of the films increased sharply. Table 8.8 shows the resistivity before and after hydrogen treatment. This sharp increase in resistivity is due to the conversion of the metallic dihydrides to the semiconducting trihydrides (assuming the similar structural change as that of Gd and Tb dihydrides). The increase in resistance due to the conversion of H_oH_2 to H_oH_3 was greater than those of GdH_3 and TbH_3. The change of resistivity with temperature of the HoH_3 films is shown in Fig. 8.20. As may be seen from the figure, the resistivity decreases with increasing temperature which indicates semiconducting nature of HoH_3. The TCR values are shown in table 8.8.

8.6. Resistivity of the films (80-900Å) grown from erbium.

The dependence of electrical resistivity on thickness of erbium

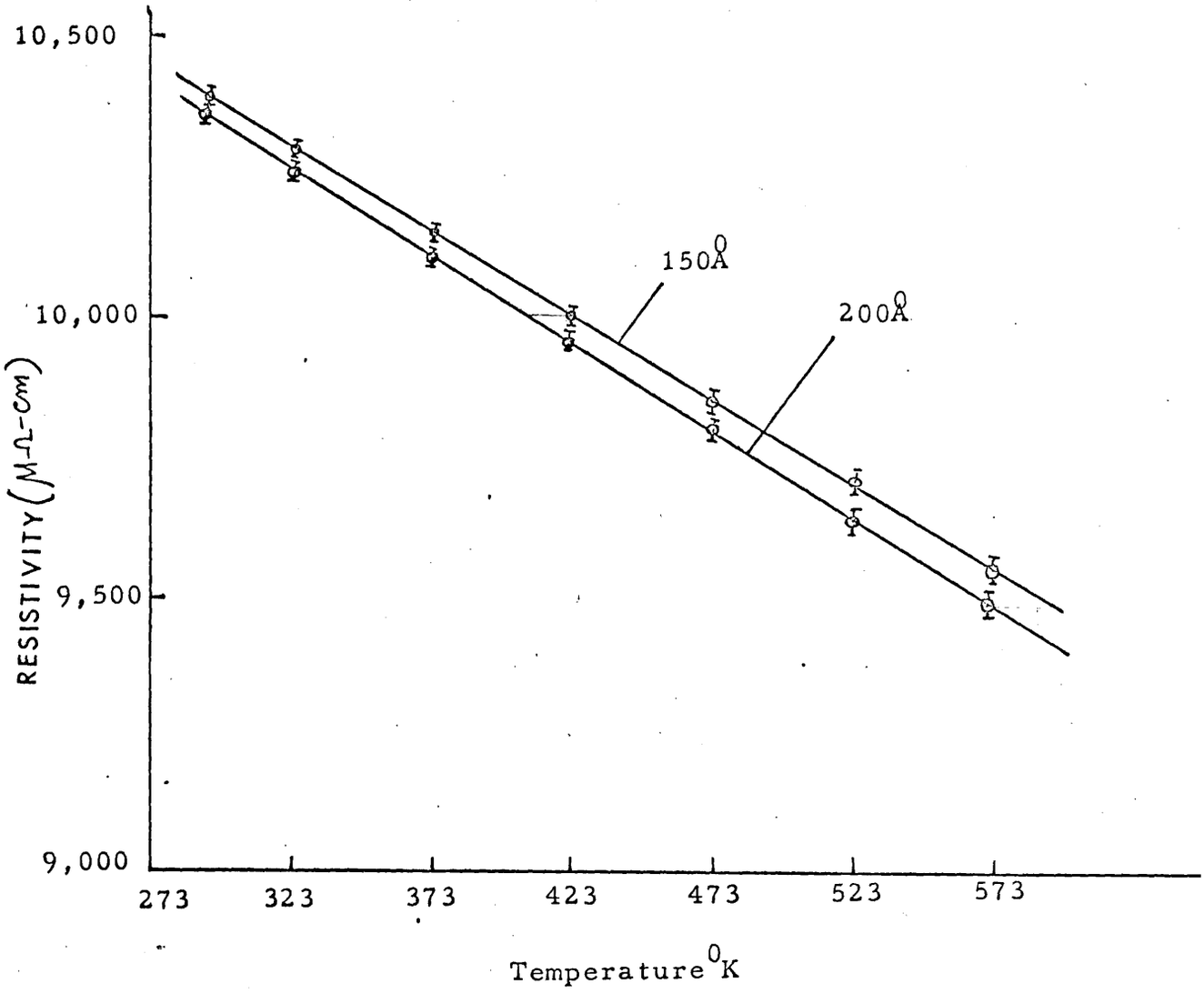

Figure 8.20. Variation of resistivity with temperature of HoH_3 films.

dihydride films in the range 80-210Å at room temperature is shown in Fig. 8.21. Films thinner than 80Å had discontinuous structures so their resistivities could not be measured reliably. The thickness dependence, at room temperature, of the electrical resistivity of the films in the thickness range 210-900Å is shown in Fig.8.22. Putting Figs. 8.21 and 8.22 together on a single diagram, the resultant curve for the thickness dependence of resistivity of films in the range 80-900Å is shown in Fig. 8.23. The characteristic features of the curves are:

i. the resistivity has a minimum value of 75 $\mu\Omega$-cm at a film thickness of 250Å and increases for thinner films.

ii. an abnormal increase occurs in the resistivity of the films thicker than 210Å and continues to increase until it becomes nearly constant at about 900Å.

The interesting feature is that the resistivity of 150Å, 200Å films are less than that of bulk erbium metal (ρ = 86 $\mu\Omega$-cm). Such results are surprising but consistent with the resistivity measurements of bulk erbium dihydride (Heckman, 1969), for H/Er = 1.8, ρ = 26 $\mu\Omega$-cm and H/Er = 1.9, ρ = 55 $\mu\Omega$-cm. The increase in resistivity over the thickness range 250-800Å (mixed phase) is due to the variation of composition (resistivity increases with decreasing hydrogen content.) Similarly the increase in resistivity over the thickness range 210-80Å (f.c.c. dihydride) is due to the non-stoichiometric composition of the dihydrides (resistivity increases with the increase of hydrogen content). As the thickness of the film was increased to 900Å (which is almost h.c.p. metal), the resistivity attained nearly a constant value (108 $\mu\Omega$-cm). This value is in agreement with the known bulk resistivity (86 $\mu\Omega$-cm). The somewhat higher values (~ 20%)

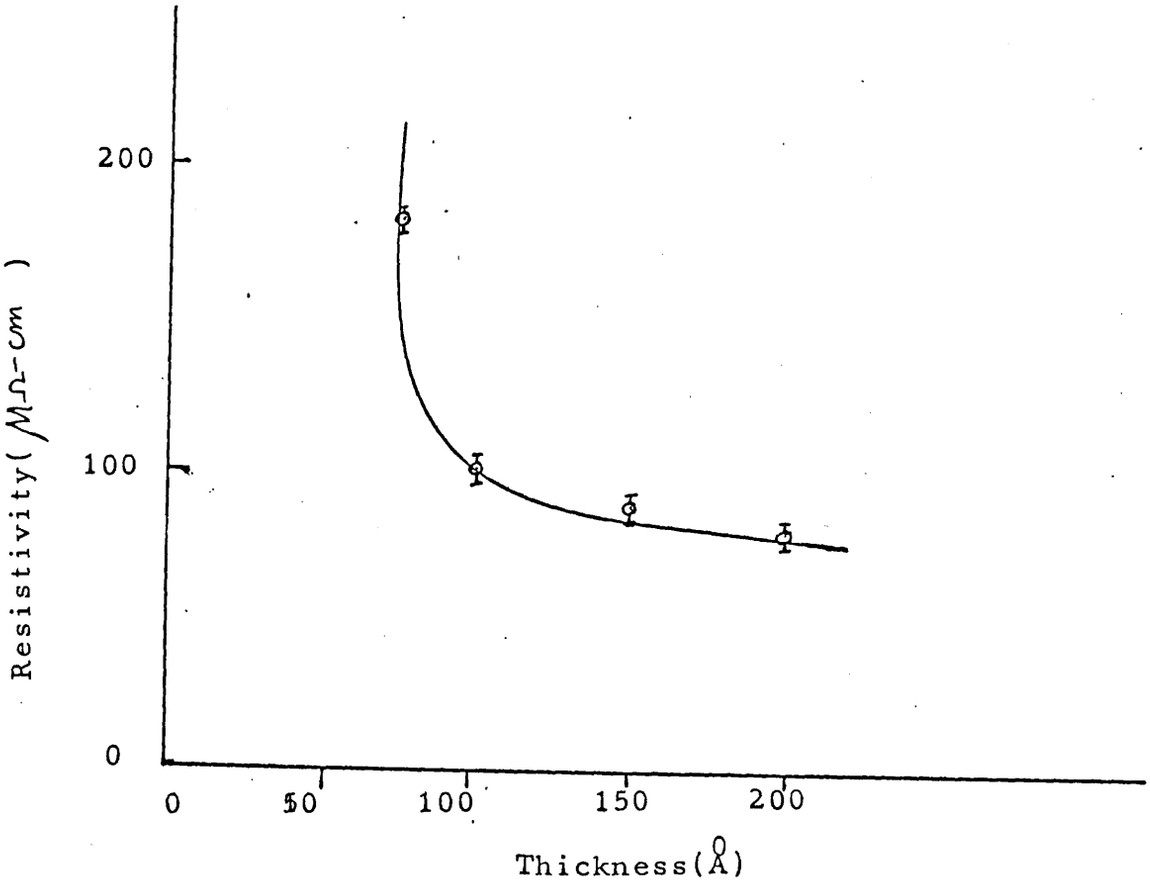

Figure 8.21. Room temperature thickness dependence of resistivity of erbium dihydride films.

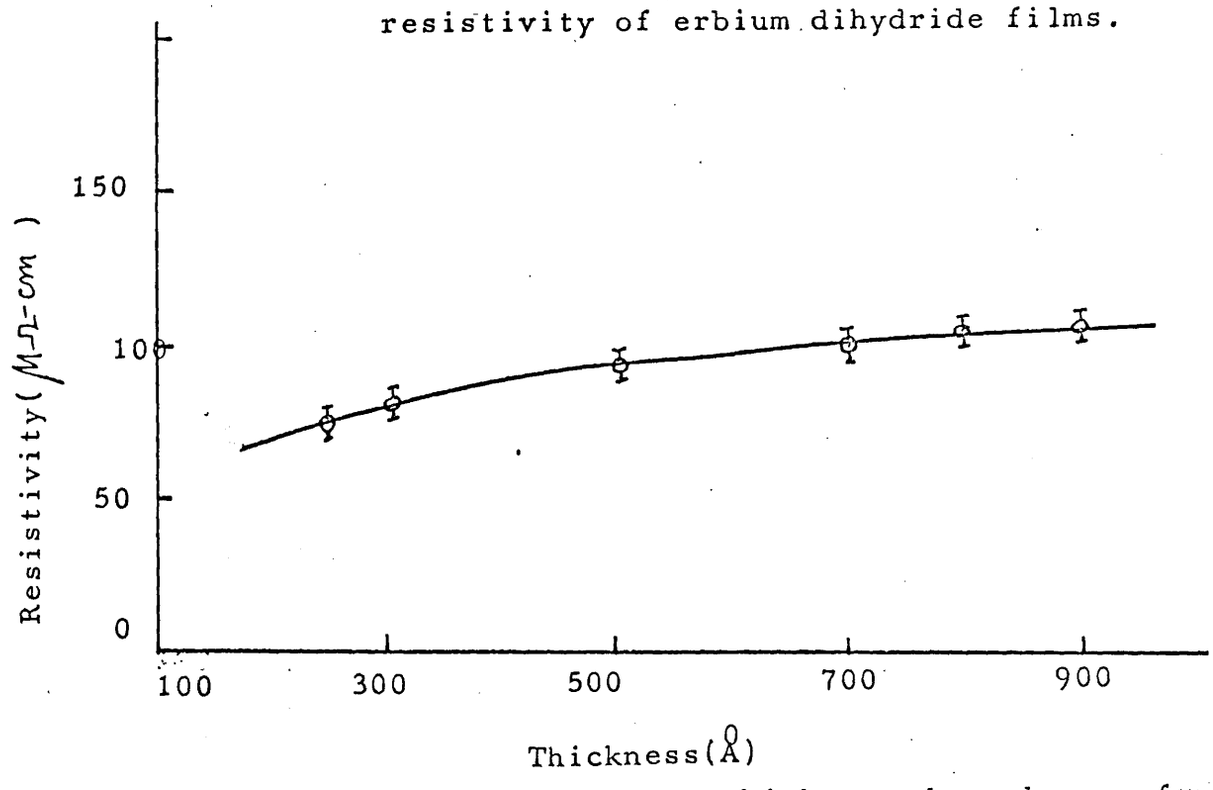

Figure 8.22. Room temperature thickness dependence of resistivity of films(70-900Å)grown from erbium.

of resistivity for the thicker films compared with the bulk metal can be attributed to inherent film defects.

The resistivity of the film in the thickness range 80-900Å at 77°K is shown by the dotted curve of Fig. 8.23. The general behaviour of the resistivity at liquid nitrogen temperature is similar to the films grown from Gd, Tb, Dy and Ho. The Néel point of erbium metal is 85°K but in the present study no anomaly was observed even for the thickes film (900Å) studied.

8.6.1. Effect of temperature on resistivity.

The tempeature dependence of resistivity have been observed for 5 films of thickness ranging from 150-900Å. The variation of resistivity with temperature is shown in Fig. 8.24. The resistivity was measured in the temperature range 293-573°K at intervals of 50°K, the heating rate was 2-3°K/min. The increase in resistivity with temperature was found to be linear and in general agreement with the behaviour of metallic conductions.

8.6.2. Temperature coefficient of resistance.

The TCR values of the films were measured in the temperature range 293-353°K and are recorded in table 8.9. There are no existing TCR data available for the Er-H system.

8.6.3. Change of resistance due to hydrogen treatment.

When erbium dihydride films (80-210) were heated at 300°C for two hours in hydrogen presence the resistivity increased sharply. The values of the resistivity before and after hydrogen treatment are shown in table 8.10. The increase in resistivity is due to the conversion of metallics dihydrides to semiconducting trihydrides. Although the structural studies of the hydrogen treated Er dihydride films have not been performed, the above inference is made from the resistivity behaviour and assuming similar characteristics as those of

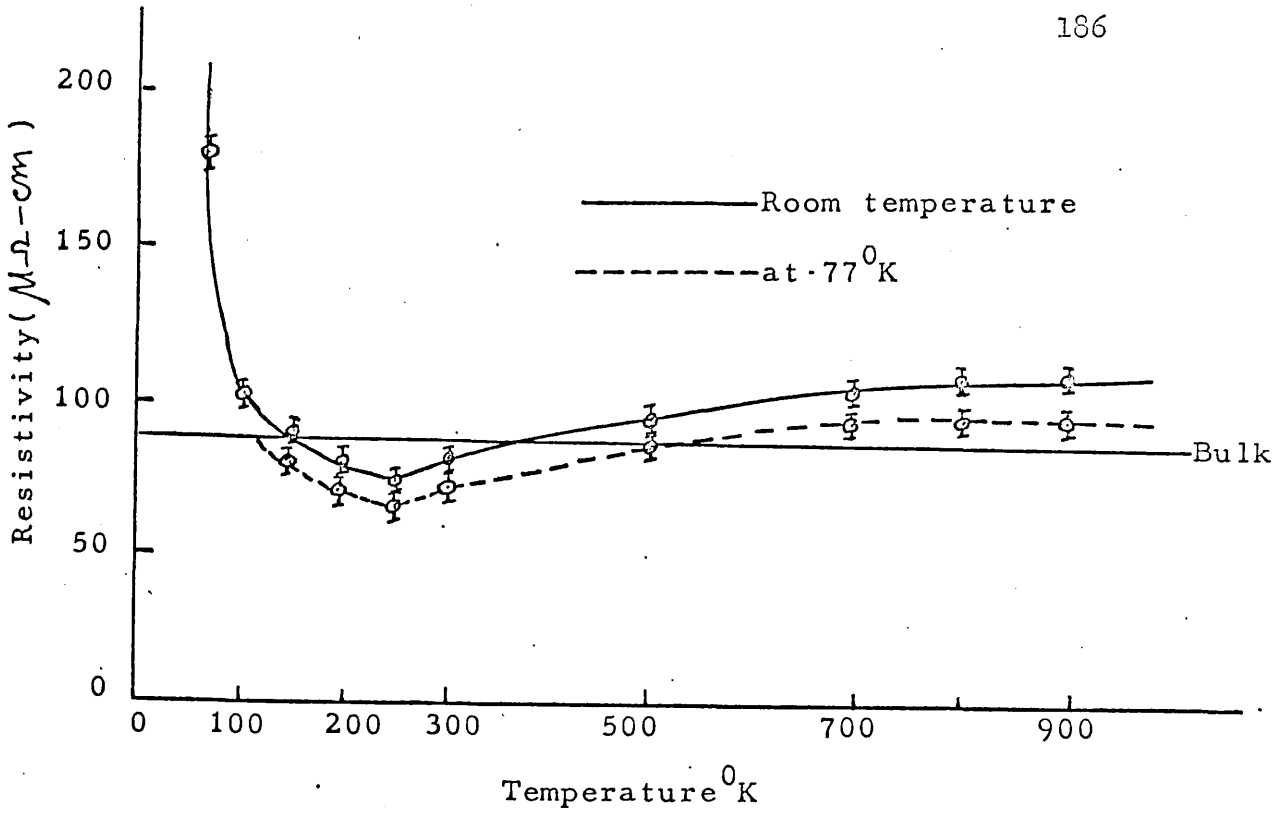

Figure 8.23. Thickness dependence of the resistivity of the films(70-900Å) grown from erbium.

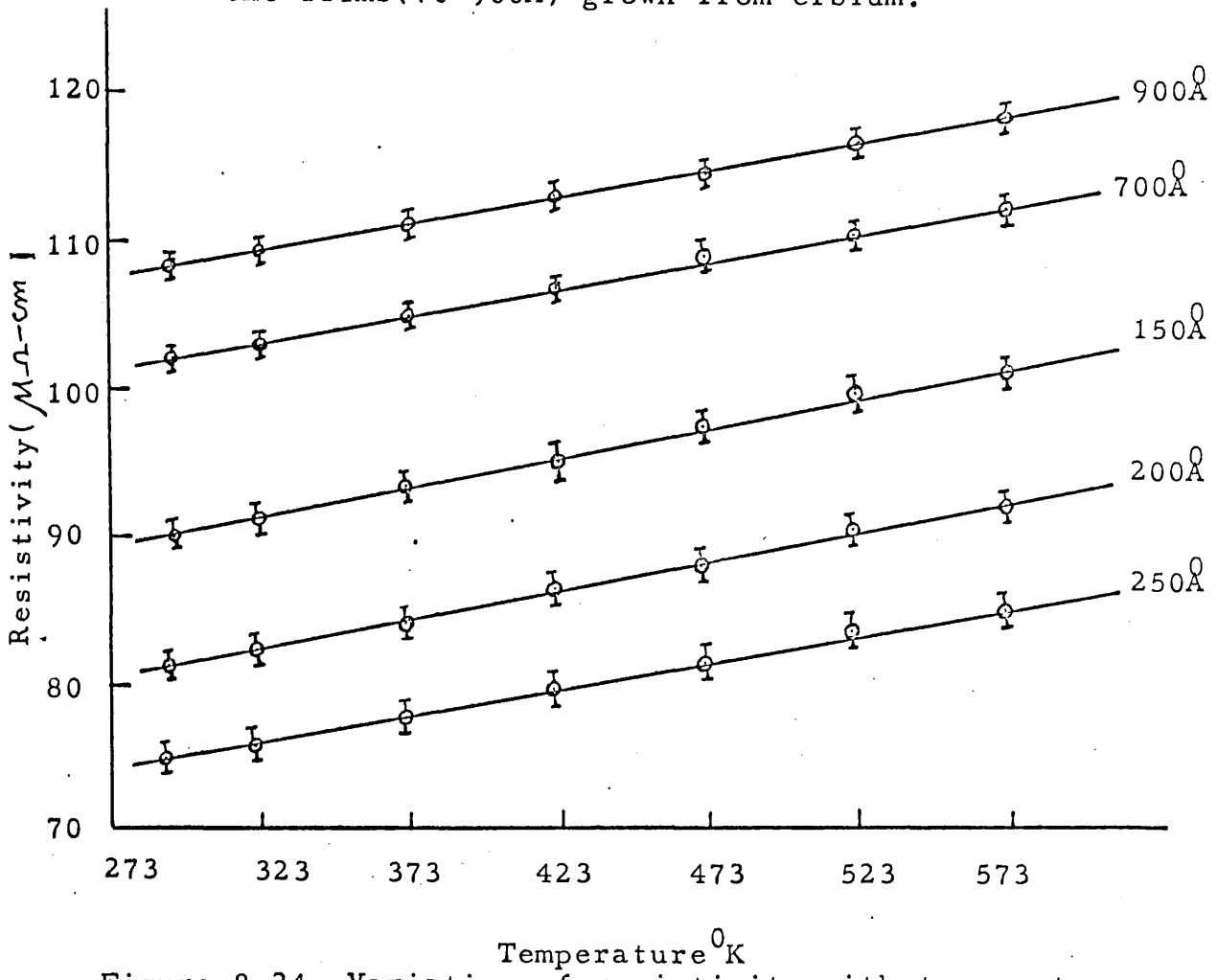

Figure 8.24. Variation of resistivity with temperature.

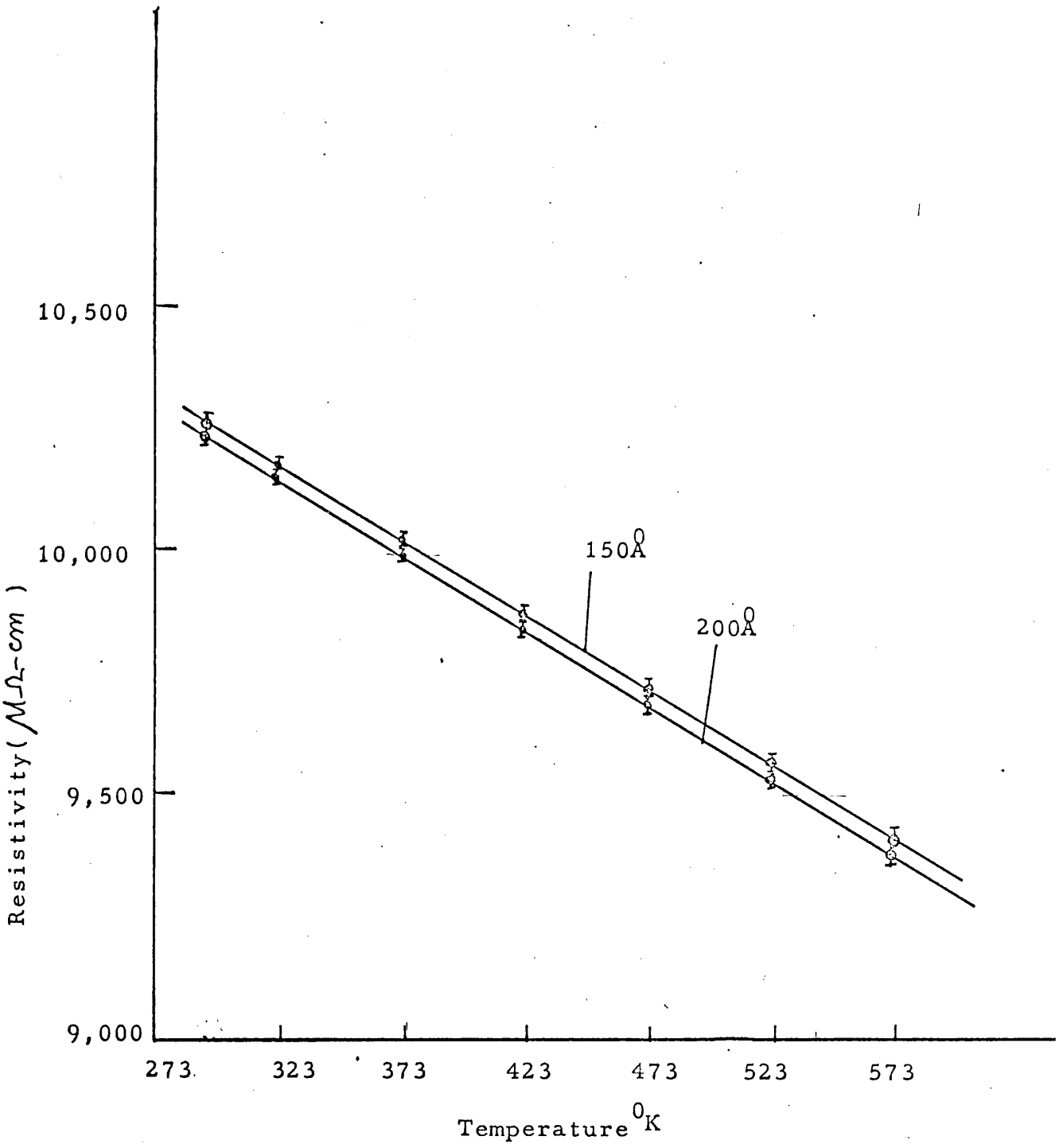

Figure 8.25. Variation of resistivity with temperature of ErH_3 films.

Gd and Tb dihydride films. The temperature dependence of resistivity of ErH_3 films are shown in Figure 8.25. which shows clearly the semi-conducting characteristic. The TCR values are recorded in table 8.10.

8.7. DISCUSSION.

Generally, the variation of resistivity with thickness of the films of noble and transition metals are in accordance with the Fuchs-Sondheimer theory of size affected conduction (Anderson, 1966, Chopra, 1969, Hass and Thun, 1971, Heavens 1970, Maissel and Glang, 1970), the salient feature being the increase in the resistivity of the film with decreasing thickness, which becomes very pronounced for films of thickness less than the mean free path. However, the results obtained for the thickness dependence of electrical resistivity of the rare earth dihydride films are at variance with the Fuchs-Sondheimer theory of size affected conduction and are interesting because the resistivity decreases with decreasing thickness (900-250Å), whereas, on the basis of surface scattering considerations, the resistivity should increase. Another curious feature of the results is that the resistivity of the films of limiting thickness (say for GdH_2, 250Å) is less than the bulk parent metal.

Evidently the observed features of the resistivity of the dihydride films can be explained if factors other than that covered by the Fuchs-Sondheimer theory (i.e. surface scattering) are taken into account. A convenient way to discuss the total electrical resistivity of thin films in terms of its different components (Matthiessen's rule). Accordingly, the resistivity ρ_F of a film is given by the equation

$$\rho_F = \rho_T + \rho_d + \rho_s + \rho_m$$

(these terms already defined in section 3.4.1., chapter 3).

The non-magnetic part of the resistivity, i.e. components ρ_T, ρ_d and ρ_s depend upon the structural phase of the film (James etal, 1952), Marcinkowski and Hopkins, 1968). Since the structures of the films (70-1000Å) studied are highly dependent on thickness, the above effect may play a role in the resistivity behaviour. Also the anomalous resistivity behaviour can be explained quite satisfactorily on the basis of the non-stoichiometric composition and consequently on the thickness dependence of the structural phase of dihydride films. As has been discussed in chapter 3 section 3.3., the resistivity of bulk dihydrides are highly dependent on the non-stoichiometric compostion and it is evident from the present experimental results that the resistivity depends on the structural phase (which is again dependent on film thickness, chapter 5). The resistivity results are quite in agreement with the behaviour of the bulk resistivity (although heavy rare earth dihydride bulk results are few and there have been more work on light rare earth dihydrides,) satisfying both anionic and protonic model.

8.8. Conclusion.

It follows from the above that the effective thickness dependence of the resistivity of thin rare earth dihydride films can be assumed to arise from a superposition of several factors, namely, the usual surface scattering component ρ_s, structural phase change, non-stoichiometric composition of the dihydride phase and the co-existence of dihydride and metallic phase in certain thickness ranges. The changes of resistivity on annealing the dihydride films in hydrogen presence support the conclusion that the films became converted to semiconducting trihydrides having negative temperature coefficient of resistance.

CHAPTER 9.

CONCLUSIONS, DISCUSSION OF THE RESULTS AND SOME SUGGESTIONS FOR FURTHER WORK.

A detailed study has been made of the thickness dependence of the structure of the films grown (either monocrystalline or polycrystalline) from Gd, Tb, Dy, Ho and Er on different substrates (rock salt, mica and carbon) and under various growth conditions. The general conclusion is that the films grown from these metals form respective dihydrides (f.c.c.) when the thickness is less than 200Å. The structure of the films is dominated by the h.c.p. metallic phase when the thickness exceeds 900Å. Films in the intermediate thickness range (200-900Å) show the co-existence of f.c.c. dihydride and the h.c.p. metallic phase.

It is well known that the rare earth metals are highly reactive towards atmospheric gases (Gasgnier etal 1974, Spedding and Beaudry 1971, and Müller, Singh and Surplice 1972). All the metals studied in the present work were found to act as getters. This, together with the results of our structural studies (including the results of the hydrogen-treatment of the films), confirms that rare earth metals especially when evaporated in thin film form have a high sorption capacity for hydrogen. Mass spectrometric analysis of gadolinium films (section 6.8 chapter 6) also supported this suggestion. A reasonable hypothesis, for the structure/thickness behaviour of the films studied, is suggested as follows. Very thin films, which involve a relatively small amount of metal react readily with the residual hydrogen in the vacuum chamber or with the absorbed (or adsorbed) gases in the substrate, forming a thin coherent dihydride film shortly after the metal is deposited. The nucleation of the hydride takes place on the substrate, immediately after the deposit

of the first layers of metal. For very thin films, the metal is rapidly converted. As the films become thicker, the thin surface layer of hydride is overlaid by the h.c.p. metallic structure and so is not detected against the dominant phase. This is the first reported work on the epitaxial growth of Gd, Tb, Dy, Ho and Er dihydride films. Further studies in this field might usefully be made, using vacuum-cleaved rock salt substrates and ultra high vacuum evaporation. Analysis of the composition and proportions of the residual gases in the system, by mass spectrometry would also be useful.

There has been only limited information on the exact composition of the dihydride film throughout this work. The non-stoichiometric composition of the rare earth dihydride phase a well known character of bulk materials, but the precise stoichiometry of the specimens could not be exactly determined by the present structural studies, although some evidence has been obtained from the electrical measurements (discussed later). There is a good prospect for further work to study the stoichiometry of the composition of the rare earth dihydride films. This could be done by using a specially designed vacuum system in which a gas dosing system is incorporated (Müller etal, 1972). In this system it would be possible to know the H/M atomic ratio by measuring the amount of gas taken up by the film, the mass of the film and its surface area. The number of gas atoms in each dose might be calculated from the known volume of the gas reservoir and the initial and final pressure at the reservoir.

The change of structural phase with thickness has been satisfactorily correlated with the resistivity behaviour of the hydride films. At present there are no other data for the

resistivity of dihydride films of rare earths, but as mentioned in section 3.3 chapter 3, there are a few resistivity data for bulk materials. The resistivities of bulk Gd, Ho and Er dihydrides suggest that the conduction is metallic, highly dependent on the non-stoichiometric composition of the dihydride phase, and that at the boundary of the single (f.c.c. dihydride) and mixed (f.c.c. dihydride + h.c.p. metal) phases, the dihydrides are better electrical conductors than the parent metal. This anomalous behaviour of the resistivity has also been observed in the present study for thin films. For example, in the case of a 250Å GdH_2 film, the resistivity is 112 $\mu\Omega$-cm, which is lower than the parent metal (bulk Gd, ρ = 134 $\mu\Omega$-cm). The general behaviour of the resistivity is in agreement with the structural studies and bulk resistivity.

The trihydrides (when formed by annealing in hydrogen) show semiconducting characteristics, having negative TCR values. The resistivity and TCR values are the only available data for films at the present time. Further studies could be made on the electrical resistivity by varying the composition (H/M ratio) of the film, extending up to the trihydride phase. It would also be worthwhile to extend the work down to liquid helium temperatures, because the bulk heavy rare earth dihydrides show magnetic ordering at temperatures ranging from 8°K for HoH_2 and DyH_2, to 40°K for TbH_2 and to 21°K for GdH_2.

REFERENCES

REFERENCES

Adamasky, R.F. and R. Leblanc, J. Vac. Sci. Tech. 2 (1965) 79

Aminoff, G and Broome, B., Nature 137 (1936) 995

Anderson, J.C. "Use of thin films in physical investigations, Academic Press (1966).

Basset, G.A., J.W. Menter and D.W. Pashley in "Structure and properties of thin films" by Neugebaner etal John Willey and Sons, N.Y. (1959) 11

Basset, G.A. 4th conf. on electron microscopy (1958) 512

Becker, R. and W. Doring, Ann.Physik 24 (1935) 719

Bist, B.M.S. and Srivastava, O.N. Phys. Stat. Solidi 7 (1971) K9

Bist, Kumar, J. and Srivastava, Phys. Stat. Solidi 14 (1972) 197

Bos, W.G. and Gayer, K.H., J.Nuclear Mat. 18 (1966) 1

Bradley, D.E., Brit, J. Appl.Phys. 5 (1954) 65

Bruck, L., Ann. Physik, 26 (1936) 233

Campbell, D.S. and Stirland, D.J., Phil. Mag. 9 (1964) 100, 703

Chakraverty and G.M. Pound, Acta Met. 12 (1964) 851

Chaudhuri, S. and A.K. Pal, J. Phys. D 8 (1955) 1311

Chopra, K.L., Randlett and Duff, Phil. Mag 16 (1967) 261

Chopra, K.L. and Randlett, M.R. J.Appl. Phys. 39 (1968) 1874

Chopra, K.L. Bob, L.C. and Francombe, J. Appl. Phys. 34 (1963) 1699

Chopra, K.L. "Thin Film Phenomenon" (1969) McGraw Hill, N.Y.

Cochrane, W. Proc.Phys.Soc. 48 (1936) 723

Coffinberry, A.S. and Ellinger, U.S.A. Rep. A/Conf. 8/P/826 (1957)

Colvin, R.V., Legvold and Spedding, F.H. Phys. Rev. 120 (1960) 741

Curzon, A.E. and Chlebek, H.G., J.Less Common Metals 32 (1973b) 365

Curzon, A.E. and Chlebek, H.G., J. Phys.F. 3 (1973) L176

Curzon, A.E. and Chlebek, H.G., J. Phys. F. 3 (1973a) 1

Curzon, A.E. and Chlebek, H.G., J.Less Common Metals 27 (1972) 411

Curzon, A.E. and Singh, O., J.Less Common Metals 39 (1975a) 227

Curzon, A.E. and Singh, O., J.Phys. D. 8 (1975b) 1704

Daou, J.N. Compt. Rend 247 (1958) 1595

Daou, J.N., Compt. Rend 252 (1961) 80

Davisson, C. and Germer, L.H., Phys. Rev. 30 (1927) 707

Engel, O.G., J.Chem.Phys. 20 (1952) 1174

Engel, O.G., J.Res. NBS, 50 (1953) 249

Ellinger, F.H., J.Am.Chem.Soc. 78 (1956) 1085

Finch, G.I. and Quarrell, A.G. Proc. Roy.Soc. A141 (1933) 398

Frank, F.C. and Van der Merwe. Proc. Roy.Soc. A198 (1949) 216

Frank, F.C. Proc.Roy.Soc. A200 (1949) 125

Frankenheim, M.L., Ann.Phys. 37 (1936) 516

Freedman, J.F., J.Appl.Phys. 33 (1962) 1148

Fuchs, K., Proc. Cambridge Phil. Soc. 34 (1938) 100

Gasgnier, M., etal J.Less Common Metals 34(1974)131

Gillham, E.J., Preston, J.S. and B. Williams, Phil.Mag. 46 (1955) 1051

Grunbaum, E. and Kremer, G., J.Appel.Phys. 39 (1968) 347

Hass, G. and R.H. Thun (eds.) Physics of thin films vol. 6 (1971) 82

Heavens,O.S. Thin Film Physics (1970) Methuen& Co,London

Heavens, O.S. and Pandeya. Nature 181 (1958) 1394

Heckman, R.C. Sandia Corporation (1964) Sc-R-64-136

Heckman, R.C., J.Chem.Phys. 46 (1967) 2158p2958

Heckman, R.C., Sandia Corporation report No. Sc-RR-69-571 (1969) 8

Heckman and Hills, Sandia Corporation (1965)

Hardcastle, K.l., Ph.D. Thesis (1961) - 80

Hirth, J.P., Hruska and Pound, "Single Crystal Films"
edited by Francombe and Sato (1964)

Ino, S. Watanabe and Ogawa, J. Phys.Soc. Japan 19 (1964) 881

Jaunet, J. and C. Sella, Bull. Soc. Franc. Miner. Crist. 87 (1964) 393

James, W.R. Legvold and Spedding, Phys.Rv. 88 (1952) 1092

Jayadevaiah, T.S. and R.E. Kirby, Appl.Phys. lett. 15 (1969) 150

Jones, J.P. Proc.Roy.Soc. London A 284 (1965) 469

Khan, I.H., Mater Rs. Bull. 4 (1969) S 285

Kirchner and Cramer, Ann.Physik. 33 (1938) 138

Kubota, Y. and Wallace, W.E., J.Appl.Phys. 33 (1962) 1348

Lewis, B., Thin solid films, 1 (1967) 85

Lewis, B. and D.S. Campbell, J.Vac.Sci.Tech. 4 (1967) 209

Libowitz, G.G., Solid state chem. of binary metal hydrides. (1965)
Benjamin Inc. N.Y. P.40.

Libowitz, G.G., "Metal hydrides" Academic Press (1968) P390

Libowitz, G.G. and T.R.P. Gibb, J.Chem.Phys. (1956) Vol. 60. P510

Lodge, F.M.K., Physis Abstract No. 51175, 1970

Lucas, L.N.D. Proc.Phys.Soc. A64 (1951) 943

Matthews, J.W., Phil.Mag. 12 (1965a) 1143

Matthews, J.W., Phil.Mag. 7 (1962) 415

Matthews, J.W., J.Vac.Sci.Tech. 3 (1966) 133

Matthews, J.W., Phys. Thin Films 4 (1967) 137

Marcinkowski, M.J. and E.H. Hopkins, Trans. Metall.Soc.AIME, 242 (1968) 579

Maissel, L.I. and R.Glang, "Hand Book of Thin Film Technology" (1970)

Menzer, G., Naturwiss. 26 (1938) 385

Menzer, G., Z. Krist., 99 (1938) 378

Menzer, G., Z Krist., 99 (1938) 410

Miyake, S. Soc.Pap. Inst.Phys. Chem.Res.Japan 1938 (34) P565

Miller, R.F. Ph.D. Thesis, London University, 1962

Moazed, K.L., "Use of thin films in physical investigations"
edited by J.C. Anderson P203 (1966) Academic Press, N.Y.

Morris, J.E., Thin solid films, II (1972) 81

Mugge, O., Neves Jarbuch fur Mineralogie, Beilage-Band 16 (1903) P335

Mulford, R.N.R. AECU - 3813 (1958)

Mulford, R.N.R. AECU - 3945 (1959)

Mulford, R.N.R. and Holley, C.E. - J.Phys.Chem. 59 (1955)

Murr, L.E., Phys.Stat. Solidi 24 (1967) 135

Müeller, W.M., Blackledge and Libowitz, "Metal hydrides"
Academic Press (1968) P390

Müller, J. Singhand Surplice, J.Phys. D. 5 (1972) 90

Newman, R.C. and Pashley, D.W., Phil.Mag. 46 (1955) 917

Otsuka, K. and C.M. Wayman. Phys.Stat.Solidi. 22 (1967) 559

Pashley, D.W., Advan. Phys. 5 (1956) 173

Pashley, D.W., Phil.Mag. 4 (1959) 316

Pashley, Stowell, Jacobs and Law, Phil.Mag. 10 (1964) 127

Pashley, D.W., Advan.Phys. 14 (1965) 327

Pashley, D.W., "Epitaxial growth", Part A, edited by
J.W. Matthews (1975) 1

Pebler, A and Wallace, W.E., J.Phys.Chem. 66 (1962) 148

Pound, G.M. and J.P. Hirth. "Dayton International Symposium on
Evaporation and Condensation of Solids"(1963)

Pound, Simnad and Yong, J.Chem.Phys. 22 (1954) 1215

Rai, K.N. and Srivastava, O.N., Mater. Sci.Eng. 8 (1971) 341

Raether, H., Optik. 1 (1946) 296

Raether, H., Ergeb. Exakt. Naturw. 24 (1951) 54

Rhodin, T.N. and Walton, "Metal Surfaces" (1962) P259

Rhodin, T.N. and Walton, "Single crystal films" (1964) 31 Pergaman Press

Rhodin, T.N., in J.C. Anderson's "Use of thin films in physical
investigation" P187 (1966(Academic Press

Rossi, A. Nature 133 (1934) 174

Royer, L. Bull. Soc. Franc. Mineral, 51 (1928) 7

Sella and Trillat in "Single crystal films" by Francombe and Sato P201 (1964)

Singh, B., Müller and Surplice, Nederlands Tijdschrift Voor Vacuumtechniek 8 (1970) 109

Schrey, F., Mathis, Payne and Murr, Thin solid films 5 (1970) 29

Schlier and Farnsworth, J. Phys.Chem.Solids 6 (1958) 271

Shirai, S., and Fukada, J.Phys.Soc.Japan 17 (1962) 1018

Shinozaki, S. and Sato, J.Appl.Phys. 36 (1965) 2320

Spedding, F.H. and B.J. Beaudry, J.Less Common Metals 35 (1971) 61

Stalinski, B., Bull Acad.Polon.Sci. 7 (1959) 269

Sandheimer, E.H., Advan.Phys. 1 (1952) 1

Sturdy and Mulford, J.Am.Chem.Soc. 78 (1956) 1083

Stirland, D.J., Appl.Phys. letter 8 (1966) 326

Taylor, K.N.R., Physics of rare earth solids, Chapman and Hall (1972)

Thomson and Reid, Nature 119 (1927) 80

Tolansky, S. "Multiple beam interferrometry of surfaces and films" (1948)

Uyeda, R. Proc.Phys-Math.Soc. Japan 24 (1942) 809

Van der Merwe, J.H. Discussions Faraday Soc. No.5 (1949) 201

Van der Pauw, L.J. Philips Res. Rep. 13 (1958) 1

Volmer, M and Weber, Z.Phys.Chem. 119 (1925) 277

Volmer, M. (1939) "Kinetik der Phasenbildung"

Walton, D. Phil.Mag. 7 (1962) 1671

Walton, D. J.ChemPhys. 37 (1962) 2182

Walton, Rhodin and Rollins, J.Chem.Phys. 38 (1963) 2698

Wallerant, F. Bull.Soc.Franc. Mineral 25 (1902) 180

Wanmer, F.E. Lawless, J.Vac.Sci.Tech. 6 (1969) 588

Wallace, Kubota and Zanowick, Advan.Chem.Ser. 39 (1963) 122

Wallace, W.E. Berchte der Bunsen Gessellschaff fur Physikalikh Chem. (1972) P832

Yakel, H.L. Cavin and Steele - ORNL-2839 (1959) 49

APPENDIX 1

DATA FOR FILMS GROWN FROM Gd

Table 1 Thickness (t) = 200Å, Filmgrown on (100) rock salt.

hkl	d_{obs}	GdH_2 f.c.c.		Gd. f.c.c.		Gd_2O_3 b.c.c.	
		d_{cal}	hkl	d_{cal}	hkl	d_{cal}	hkl
200	2.657	2.651	200	2.542	200	5.39	200
220	1.879	1.873	220	1.795	220	3.81	220
400	1.328	1.322	400	1.273	400	2.69	400
420	1.188	1.185	420	1.136	420	2.41	420
440	0.939	0.937	440	0.901			

Table 2. t = 180Å. Film grown on (110) rock salt.

hkl	d_{obs}	GdH_2 f.c.c.		Gd. f.c.c.		Gd_2O_3 b.c.c.	
		d_{cal}	hkl	d_{cal}	hkl	d_{cal}	hkl
111	3.068	3.062	111	2.931	111		
200	2.657	2.651	200	2.542	200	5.39	200
220	1.879	1.873	220	1.795	220	4.40	211
311	1.602	1.598	311	1.532	311	3.81	220
222	1.534	1.530	222	1.464	222	3.41	310
333	1.023	1.020	333	0.971	333	3.11	222

Table 3. t = 220Å. Film grown on (111) rock salt.

hkl	d_{obs}	GdH_2 f.c.c.		Gd. f.c.c.		Gd h.c.p.	
		d_{cal}	hkl	d_{cal}	hkl	d_{cal}	hk.l
220	1.877	1.873	220	1.795	220	1.812	11.0
						1.631	01.3

Table 4. $t = 150\text{Å}$. Polycrystalline film grown on rock salt and carbon film.

Ring Nos.	d_{obs}	GdH_2 f.c.c.		Gd f.c.c.		Gd h.c.p.		Gd_2O_3		GdH_3 h.c.p.	
		d_{cal}	hkl	d_{cal}	hkl	d_{cal}	hk.l	d_{cal}	hkl	d_{cal}	hk.l
1	3.063(3.064)	3.062	111	2.931	111	3.135	01.0	7.63	110	3.224	01.0
2	2.653(2.654)	2.651	200	2.542	200	2.886	00.2	5.39	200	3.356	00.2
3	1.875(1.876)	1.873	220	1.795	220	2.761	01.1	4.40	211	2.901	01.1
4	1.599(1.600)	1.598	311	1.532	311	2.143	01.2	3.81	220	2.328	01.2
5	1.531(1.532)	1.530	222	1.464	222	1.816	11.0	3.41	310	1.862	11.0
6	1.325(1.326)	1.322	400	1.273	400	1.631	01.3	3.11	222	1.831	01.3
7	1.186(1.186)	1.185	420	1.136	420			2.88	321		

Table 5. $t = 450\text{Å}$. Film grown on (100) rock salt.

Ring Nos.	d_{obs}	GdH_2 f.c.c.		Gd f.c.c.		Gd h.c.p.		Gd_2O_3		GdH_3 h.c.p.	
		d_{cal}	hkl	d_{cal}	hkl	d_{cal}	hk.l	d_{cal}	hkl	d_{cal}	hk.l
1	3.137	3.062	111	2.931	111	3.135	01.0	7.63	110	3.224	01.0
2	3.064	2.651	200	2.542	200	2.886	00.2	5.39	200	3.356	00.2
3	2.887	1.873	220	1.795	220	2.761	01.1	4.40	211	2.901	01.1
4	2.654	1.598	311	1.532	311	2.143	01.2	3.81	220	2.328	01.2
5	2.145	1.530	222	1.464	222	1.816	11.0	3.41	310	1.862	11.0
6	1.876	1.322	400	1.273	400	1.631	01.3	3.11	222	1.831	01.3
7	1.621										

Table 6. $t = 550\text{Å}$. Film grown on (110) rock salt.

Ring Nos.	d_{obs}	GdH_2 f.c.c.		Gd f.c.c.		Gd h.c.p.		Gd_2O_3		GdH_3 h.c.p.	
		d_{cal}	hkl	d_{cal}	hkl	d_{cal}	hk.l	d_{cal}	hkl	d_{cal}	hk.l
1	3.136	3.062	111	2.931	111	3.135	01.0	7.63	110	3.224	01.0
2	3.065	2.651	200	2.542	200	2.886	00.2	5.39	200	3.356	00.2
3	2.886	1.873	220	1.795	220	2.761	01.1	4.40	211	2.901	01.1
4	2.655	1.598	311	1.532	311	2.143	01.2	3.81	220	2.328	01.2
5	2.144	1.530	222	1.464	222	1.816	11.0	3.41	310	1.862	11.0
6	1.876	1.322	400	1.273	400	1.631	01.3	3.11	222	1.831	01.3
7	1.817										

Table 7. t = 600Å. Film grown on (111) rock salt.

Ring Nos.	d_{obs}	GdH_2 f.c.c.		Gd f.c.c.		Gd h.c.p.		Gd_2O_3		GdH_3 h.c.p.	
		d_{cal}	hkl	d_{cal}	hkl	d_{cal}	hk.l	d_{cal}	hkl	d_{cal}	hk.l
1	3.136	3.062	111	2.931	111	3.135	01.0	7.63	110	3.224	01.0
2	3.066	2.651	200	2.542	200	2.886	00.2	5.39	200	3.356	00.2
3	2.887	1.873	220	1.795	220	2.761	01.1	4.40	211	2.901	01.1
4	2.654	1.598	311	1.532	311	2.143	01.2	3.81	220	2.328	01.2
5	2.144	1.530	222	1.464	222	1.816	11.0	3.41	310	1.862	11.0
6	1.876	1.322	400	1.273	400	1.631	01.3	3.11	222	1.831	01.3
7	1.817										

Table 8. t = 450Å. Polycrystalline film grown on rock salt and carbon film

Ring Nos.	d_{obs}	GdH_2 f.c.c.		Gd f.c.c.		Gd h.c.p.		Gd_2O_3		GdH_3 h.c.p.	
		d_{cal}	hkl	d_{cal}	hkl	d_{cal}	hk.l	d_{cal}	hkl	d_{cal}	hk.l
1	3.136	3.062	111	2.931	111	3.135	01.0	7.63	110	3.224	01.0
2	3.064	2.651	200	2.542	200	2.886	00.2	5.39	200	3.356	00.2
3	2.887	1.873	220	1.795	220	2.761	01.1	4.40	211	2.901	01.1
4	2.654	1.598	311	1.532	311	2.143	01.2	3.81	220	2.328	01.2
5	2.143	1.530	222	1.464	222	1.816	11.0	3.41	310	1.862	11.0
6	1.875	1.322	400	1.273	400	1.631	01.3	3.11	222	1.831	01.3
7	1.817										

Table 9. t = 950Å. Film grown on (111) rock salt.

hk.l	d_{obs}	GdH_2 f.c.c.		Gd f.c.c.		Gd h.c.p.		Gd_2O_3 b.c.c.		GdH_3 h.c.p.	
		d_{cal}	hkl	d_{cal}	hkl	d_{cal}	hk.l	d_{cal}	hkl	d_{cal}	hk.l
01.0	3.136	3.062	111	2.931	111	3.135	01.0	7.63	110	3.224	01.0
		2.651	200	2.542	200	2.886	00.2	5.39	200	3.356	01.2
		1.873	220	1.795	220	2.761	01.1	4.40	211	2.901	01.1
		1.598	311	1.532	311	2.143	01.2	3.81	220	2.328	01.2
11.0	1.817					1.816	11.0	3.41	310	1.862	11.0

Table 10. t = 920Å. Polycrystalline film grown on rock salt.

Ring Nos.	d_{obs}	GdH_2 f.c.c.		Gd f.c.c.		Gd h.c.p.		Gd_2O_3		GdH_3 h.c.p.	
		d_{cal}	hkl	d_{cal}	hkl	d_{cal}	hk.l	d_{cal}	hkl	d_{cal}	hk.l
1	3.136	3.062	111	2.931	111	3.135	01.0	7.63	110	3.224	01.0
2	3.065	2.651	200	2.542	200	2.886	00.2	5.39	200	3.356	00.2
3	2.887	1.873	220	1.795	220	2.761	01.1	4.40	211	2.901	01.1
4	2.762	1.598	311	1.532	311	2.143	01.2	3.81	220	2.328	01.2
5	2.144	1.530	222	1.464	222	1.816	11.0	3.41	310	1.862	11.0
6	1.817	1.322	400	1.273	400	1.631	01.3	3.11	222	1.831	01.3
7	1.632										

DATA FOR TERBIUM HYDRIDE FILMS.

Table 11 t = 180Å. Film grown on (100) rock salt.

hkl	d_{obs}	TbH_2 f.c.c.		Tb f.c.c.		Tb_2O_3 b.c.c.	
		d_{cal}	hkl	d_{cal}	hkl	d_{cal}	hkl
200	2.626	2.623	200	2.501	200	5.35	200
220	1.857	1.855	220	1.763	220	3.78	220
400	1.312	1.311	400	1.252	400	2.67	400
420	1.174	1.173	420	1.134	420	2.39	420
440	0.928	0.927	440	0.891	440	1.89	440

Table 12. t = 200Å. Film grown on (110) rock salt.

hkl	d_{obs}	TbH_2 f.c.c.		Tb f.c.c.		Tb_2O_3 b.c.c.	
		d_{cal}	hkl	d_{cal}	hkl	d_{cal}	hkl
111	3.032	3.028	111	2.891	111		
200	2.626	2.623	200	2.501	200	5.35	200
220	1.858	1.853	220	1.763	220	4.36	211
311	1.583	1.582	311	1.502	311	3.78	220
222	1.515	1.514	222	1.445	222	3.38	310
333	1.016	1.014	333	0.961	333	3.09	222
440	0.928	0.927	440	0.891	440		

Table 13. t = 190Å. Film grown on (111) rock salt.

hkl	d_{obs}	TbH_2 f.c.c.		Tb f.c.c.		Tb h.c.p.	
		d_{cal}	hkl	d_{cal}	hkl	d_{cal}	hk.l
						1.799	11.0
220	1.858	1.855	220	1.763	220		
						1.619	01.3

Table 14. t = 200Å. Polycrystalline film grown on rock salt and carbon film.

Ring Nos.	d_{obs}	TbH_2 f.c.c.		Tb f.c.c.		Tb h.c.p.		TbH_3 h.c.p.	
		d_{cal}	hkl	d_{cal}	hkl	d_{cal}	hk.l	d_{cal}	hk.l
1	3.032(3.031)	3.028	111	2.891	111	3.113	01.0	3.201	01.0
2	2.626(2.625)	2.623	200	2.501	200	2.843	00.2	3.329	00.2
3	1.857(1.856)	1.855	220	1.763	220	2.740	01.1	2.880	01.1
4	1.584(1.583)	1.582	311	1.502	311	2.101	01.2	2.301	01.2
5	1.515(1.515)	1.514	222	1.445	222	1.799	11.0	1.850	11.0
6	1.016(1.015)	1.014	333	0.961	333	1.619	01.3	1.824	01.3
7									

Table 15. t = 650Å. Film grown on (100) rock salt.

Ring Nos.	d_{obs}	TbH_2 f.c.c.		Tb f.c.c.		Tb h.c.p.		TbH_3 h.c.p.	
		d_{cal}	hkl	d_{cal}	hkl	d_{cal}	hk.l	d_{cal}	hk.l
1	3.116	3.028	111	2.891	111	3.113	01.0	3.201	01.0
2	3.031	2.623	200	2.501	200	2.843	00.2	3.329	00.2
3	2.845	1.855	220	1.763	220	2.740	01.1	2.880	01.1
4	2.626	1.582	311	1.502	311	2.101	01.2	2.301	01.2
5	2.103	1.514	222	1.445	222	1.799	11.0	1.850	11.0
6	1.857	1.311	400	1.252	400	1.619	01.3	1.824	01.3
7	1.801								

Table 16. t = 600Å. Film grown on (110) rock salt.

Ring Nos.	d_{obs}	TbH_2 f.c.c.		Tb f.c.c.		Tb h.c.p.		TbH_3 h.c.p.	
		d_{cal}	hkl	d_{cal}	hkl	d_{cal}	hk.l	d_{cal}	hk.l
1	3.115	3.028	111	2.891	111	3.113	01.0	3.201	01.0
2	3.031	2.623	200	2.501	200	2.843	00.2	3.329	00.2
3	2.845	1.855	220	1.763	220	2.740	01.1	2.880	01.1
4	2.625	1.582	311	1.502	311	2.101	01.2	2.301	01.2
5	2.103	1.514	222	1.445	222	1.799	11.0	1.850	11.0
6	1.857	1.311	400	1.252	400	1.619	01.3	1.825	01.3
7	1.801								

Table 17 t = 550Å. Film grown on (111) rock salt.

Ring Nos.	d_{obs}	TbH_2 f.c.c.		Tb f.c.c.		Tb h.c.p.		TbH_3 h.c.p.	
		d_{cal}	hkl	d_{cal}	hkl	d_{cal}	hk.l	d_{cal}	hk.l
1	3.114	3.028	111	2.891	111	3.113	01.0	3.201	01.0
2	3.032	2.623	200	2.501	200	2.843	00.2	3.329	00.2
3	2.844	1.855	220	1.763	220	2.740	01.1.	2.880	01.1
4	2.625	1.582	311	1.502	311	2.101	01.2	2.301	01.2
5	2.103	1.514	222	1.445	222	1.799	11.0	1.850	11.0
6	1.856	1.311	400	1.252	400	1.619	01.3	1.824	01.3
7	1.800								

Table 18. t = 500Å. Polycrystalline film grown on rock salt and carbon film.

Ring Nos.	d_{obs}	TbH_2 f.c.c.		Tb f.c.c.		Tb h.c.p.		TbH_3 h.c.p.	
		d_{cal}	hkl	d_{cal}	hkl	d_{cal}	hk.l	d_{cal}	hk.l
1	3.115(3.114)	3.028	111	2.891	111	3.113	01.0	3.201	01.0
2	3.031(3.030)	2.623	200	2.501	200	2.843	00.2	3.329	00.2
3	2.844(2.844)	1.855	220	1.763	220	2.740	01.1	2.880	01.1
4	2.625(2.624)	1.582	311	1.502	311	2.101	01.2	2.301	01.2
5	2.104(2.102)	1.514	222	1.445	222	1.799	11.0	1.850	11.0
6	1.857(1.856)	1.311	400	1.252	400	1.619	01.3	1.824	01.3
7	1.801(1.800)								

Table 19. t = 950Å. Film grown on (111) rock salt.

hk.l	d_{obs}	TbH_2 f.c.c.		Tb f.c.c.		Tb h.c.p.		TbH_3 h.c.p.	
		d_{cal}	hkl	d_{cal}	hkl	d_{cal}	hk.l	d_{cal}	hk.l
01.0	3.114	3.028	111	2.891	111	3.113	01.0	3.201	01.0
		2.623	200	2.501	200	2.843	00.2	3.329	00.2
		1.855	220	1.763	220	2.740	01.1	2.880	01.1
		1.582	311	1.502	311	2.101	01.2	2.301	01.2
11.0	1.800					1.799	11.0	1.850	11.0
						1.619	01.3	1.824	01.3

Table 20. t = 930Å Polycrystalline film grown on rock salt.

Ring Nos.	d_{obs}	TbH_2 f.c.c.		Tb f.c.c.		Tb h.c.p.		TbH_3 h.c.p.	
		d_{cal}	hkl	d_{cal}	hkl	d_{cal}	hk.l	d_{cal}	hk.l
1	3.115	3.028	111	2.891	111	3.113	01.0	3.201	01.0
2	3.031	2.623	200	2.501	200	2.843	00.2	3.329	00.2
3	2.844	1.855	220	1.763	220	2.740	01.1	2.880	01.1
4	2.741	1.582	311	1.502	311	2.101	01.2	2.301	01.2
5	2.102	1.514	222	1.445	222	1.799	11.0	1.850	11.0
6	1.800	1.311	400	1.252	400	1.619	01.3	1.824	01.3
7	1.620								

DATA OF DYSPROSIUM HYDRIDE FILMS

Table 21. t = 170Å. Film grown on (100) rock salt.

hkl	d_{obs}	DyH_2 f.c.c.		Dy f.c.c.	
		d_{cal}	hkl	d_{cal}	hkl
200	2.604	2.602	200	2.485	200
220	1.841	1.839	220	1.757	220
400	1.302	1.300	400	1.242	400
420	1.164	1.163	420	1.111	420
440	0.921	0.919	440	0.878	440

Table 22. t=150Å. Film grown as polycrystalline on rock salt.

Ring Nos.	d_{obs}	DyH_2 f.c.c.		Dy f.c.c.		Dy h.c.p.		DyH_3 h.c.p.	
		d_{cal}	hkl	d_{cal}	hkl	d_{cal}	hk.l	d_{cal}	hkl
1	3.006	3.002	111	2.869	111	3.105	01.0	3.179	01.0
2	2.604	2.602	200	2.485	200	2.821	00.2	3.307	00.2
3	1.841	1.839	220	1.757	220	2.720	01.1	2.865	01.1
4	1.570	1.568	311	1.498	311	2.088	01.2	2.291	01.2
5	1.503	1.501	222	1.434	222	1.793	11.0	1.835	11.0
6	1.302	1.300	400	1.242	400	1.608	01.3	1.811	01.3

Table 23. t = 500Å. Film grown on (100) rock salt.

Ring Nos.	d_{obs}	DyH_2 f.c.c.		Dy f.c.c.		Dy h.c.p.		DyH_3 h.c.p.	
		d_{cal}	hkl	d_{cal}	hkl	d_{cal}	hk.l	d_{cal}	hkl
1	3.107	3.002	111	2.869	111	3.105	01.0	3.179	01.0
2	3.005	2.602	200	2.485	200	2.821	00.2	3.307	00.2
3	2.823	1.839	220	1.757	220	2.720	01.1	2.865	01.1
4	2.603	1.568	311	1.498	311	2.088	01.2	2.291	01.2
5	2.089	1.501	222	1.434	222	1.793	11.0	1.835	11.0
6	1.840	1.300	400	1.242	400	1.608	01.3	1.811	01.3
7	1.794								

Table 24. $t = 500\text{Å}$. Polycrystalline film grown on rock salt.

Ring Nos.	d_{obs}	DyH_2 f.c.c.		Dy f.c.c.		Dy h.c.p.		DyH_3 h.c.p.	
		d_{cal}	hkl	d_{cal}	hkl	d_{cal}	hk.l	d_{cal}	hk.l
1	3.106	3.002	111	2.869	111	3.105	01.0	3.179	01.0
2	3.004	2.602	200	2.485	200	2.821	00.2	3.307	00.2
3	2.822	1.839	220	1.757	220	2.720	01.1	2.865	01.1
4	2.603	1.568	311	1.498	311	2.088	01.2	2.291	01.2
5	2.089	1.501	222	1.434	222	1.793	11.0	1.835	11.0
6	1.840	1.300	400	1.242	400	1.608	01.3	1.811	01.3
7	1.794								

Table 25. $t = 900\text{Å}$. Polycrystalline film grown on rock salt.

Ring Nos.	d_{obs}	DyH_2 f.c.c.		Dy f.c.c.		Dy h.c.p.		DyH_3 h.c.p.	
		d_{cal}	hkl	d_{cal}	hkl	d_{cal}	hk.l	d_{cal}	hk.l
	3.106	3.002	111	2.869	111	3.105	01.0	3.179	01.0
	3.005	2.602	200	2.485	200	2.821	00.2	3.307	00.2
	2.822	1.839	220	1.757	220	2.720	01.1	2.865	01.1
	2.721	1.568	311	1.498	311	2.088	01.2	2.291	01.2
	2.089	1.501	222	1.434	222	1.793	11.0	1.835	11.0
	1.794	1.300	400	1.242	400	1.608	01.3	1.811	01.3
	1.609								

DATA OF HOLMIUM HYDRIDE FILMS

Table 26. t = 150Å. Film grown on (100) rock salt.

hkl	d'_{obs}	HoH_2 f.c.c.		Ho f.c.c.	
		d_{cal}	hkl	d_{cal}	hkl
200	2.585	2.582	200	2.471	200
220	1.828	1.825	220	1.750	220
400	1.293	1.291	400	1.237	400
420	1.156	1.154	420	1.106	420
440	0.915	0.913	440	0.875	440

Table 27 t=130Å. Film grown as polycrystalline on rock salt and carbon film.

Ring Nos.	d_{obs}	HoH_2 f.c.c.		Ho f.c.c.		Ho h.c.p.		HoH_3 h.c.p.	
		d_{cal}	hkl	d_{cal}	hkl	d_{cal}	hk.l	d_{cal}	hk.l
1	2.986(2.987)	2.982	111	2.857	111	3.093	01.0	3.153	01.0
2	2.586(2.587)	2.582	200	2.471	200	2.808	00.2	3.282	00.2
3	1.827(1.828)	1.825	220	1.750	220	2.709	01.1	2.842	01.1
4	1.559(1.560)	1.557	311	1.492	311	2.078	01.2	2.273	01.2
5	1.493(1.494)	1.491	222	1.428	222	1.786	11.0	1.821	11.0
6	1.293(1.294)	1.291	400	1.237	400	1.601	01.3	1.796	01.3
7		1.154	420	1.106	420				

Table 28. t=500Å. Film grown on (100) rock salt.

Ring Nos.	d_{obs}	HoH_2 f.c.c.		Ho f.c.c.		Ho h.c.p.		HoH_3 h.c.p.	
		d_{cal}	hkl	d_{cal}	hkl	d_{cal}	hk.l	d_{cal}	hk.l
1	3.096	2.982	111	2.857	111	3.093	01.0	3.153	01.0
2	2.987	2.582	200	2.471	200	2.808	00.2	3.282	00.2
3	2.811	1.825	220	1.750	220	2.709	01.1	2.842	01.1
4	2.587	1.557	311	1.492	311	2.078	01.2	2.273	01.2
5	2.080	1.491	222	1.428	222	1.786	11.0	1.821	11.0
6	1.829	1.291	400	1.237	400	1.601	01.3	1.796	01.3
7	1.789	1.154	420		420				

Table 29. $t = 450\text{Å}$. Polycrystalline film grown on rock salt.

Ring Nos.	d_{obs}	HoH_2 f.c.c.		Ho f.c.c.		Ho h.c.p.		HoH_3 h.c.p.	
		d_{cal}	hkl	d_{cal}	hkl	d_{cal}	hk.l	d_{cal}	hk.l
1	3.096	2.982	111	2.857	111	3.093	01.0	3.153	01.0
2	2.985	2.582	200	2.471	200	2.808	00.2	3.282	00.2
3	2.808	1.825	220	1.750	220	2.709	01.1	2.842	01.1
4	2.584	1.557	311	1.492	311	2.078	01.2	2.273	01.2
5	2.079	1.491	222	1.428	222	1.786	11.0	1.821	11.0
6	1.826	1.291	400	1.237	400	1.601	01.3	1.796	01.3
7	1.787								

Table 30. $t = 870\text{Å}$. Polycrystalline film grown on rock salt.

Ring Nos.	d_{obs}	HoH_2 f.c.c.		Ho f.c.c.		Ho h.c.p.		HoH_3 h.c.p.	
		d_{cal}	hkl	d_{cal}	hkl	d_{cal}	hk.l	d_{cal}	hk.l
1	3.094	2.982	111	2.857	111	3.093	01.0	3.153	01.0
2	2.983	2.582	200	2.471	200	2.808	00.2	3.282	00.2
3	2.809	1.825	220	1.750	220	2.709	01.1	2.842	01.1
4	2.710	1.557	311	1.492	311	2.078	01.2	2.273	01.2
5	2.079	1.491	222	1.428	222	1.786	11.0	1.821	11.0
6	1.787	1.291	400	1.237	400	1.601	01.3	1.796	01.3
7	1.602								

DATA OF ERBIUM HYDRIDE FILMS

Table 31 t = 160Å. Film grown on (100) rock salt.

hkl	d_{obs}	ErH_2 f.c.c.		Er f.c.c.	
		d_{cal}	hkl	d_{cal}	hkl
200	2.564	2.561	200	2.461	200
220	1.814	1.811	220	1.739	220
400	1.282	1.280	400	1.230	400
420	1.146	1.145	420	1.102	420
440	0.906	0.905	440	0.869	440

Table 32 t=170Å. Polycrystalline film grown on rock salt.

Ring Nos.	d_{obs}	ErH_2 f.c.c.		Er f.c.c.		Er h.c.p.		ErH_3 h.c.p.	
		d_{cal}	hkl	d_{cal}	hkl	d_{cal}	hk.l	d_{cal}	hk.l
1	2.961	2.957	111	2.842	111	3.077	01.0	3.135	01.0
2	2.565	2.561	200	2.461	200	2.791	00.2	3.263	00.2
3	1.814	1.811	220	1.739	220	2.694	01.1	2.826	01.1
4	1.547	1.544	311	1.483	311	2.067	01.2	2.260	01.2
5	1.480	1.478	222	1.420	222	1.777	11.0	1.810	11.0
6	1.282	1.280	400	1.230	400	1.591	01.3	1.787	01.3
7	1.147	1.145	420	1.102	420				

Table 33. t = 600Å. Film grown on (100) rock salt.

Ring Nos.	d_{obs}	ErH_2 f.c.c.		Er f.c.c.		Er h.c.p.		ErH_3 h.c.p.	
		d_{cal}	hkl	d_{cal}	hkl	d_{cal}	hk.l	d_{cal}	hk.l
1	3.079	2.957	111	2.842	111	3.077	01.0	3.135	01.0
2	2.960	2.561	200	2.461	200	2.791	00.2	3.263	00.2
3	2.793	1.811	220	1.739	220	2.694	01.1	2.826	01.1
4	2.564	1.544	311	1.483	311	2.067	01.2	2.260	11.2
5	2.069	1.478	222	1.420	222	1.777	11.0	1.810	11.0
6	1.813	1.280	400	1.230	400	1.591	01.3	1.787	01.3
7	1.778								

Table 34 t = 550Å. Polycrystalline film grown on rock salt.

Ring Nos.	d_{obs}	ErH_2 f.c.c.		Er f.c.c.		Er h.c.p.		ErH_3 h.c.p.	
		d_{cal}	hkl	d_{cal}	hkl	d_{cal}	hk.l	d_{cal}	hk.l
1	3.078	2.957	111	2.842	111	3.077	01.0	3.135	01.0
2	2.959	2.561	200	2.461	200	2.791	00.2	3.263	00.2
3	2.793	1.811	220	1.739	220	2.694	01.1	2.826	01.1
4	2.563	1.544	311	1.483	311	2.067	01.2	2.260	01.2
5	2.068	1.478	222	1.420	222	1.777	11.0	1.810	11.0
6	1.812	1.280	400	1.230	400	1.591	01.3	1.787	01.3
7	1.778								

Table 35 t = 900Å. Polycrystalline film grown on rock salt.

Ring Nos.	d_{obs}	ErH_2 f.c.c.		Er f.c.c.		Er h.c.p.		ErH_3 h.c.p.	
		d_{cal}	hkl	d_{cal}	hkl	d_{cal}	hk.l	d_{cal}	hk.l
1	3.078	2.957	111	2.842	111	3.077	01.0	3.135	01.0
2	2.959	2.561	200	2.461	200	2.791	00.2	3.263	00.2
3	2.793	1.811	220	1.739	220	2.694	01.1	2.826	01.1
4	2.695	1.544	311	1.483	311	2.067	01.2	2.260	01.2
5	2.068	1.478	222	1.420	222	1.777	11.0	1.810	11.0
6	1.778	1.280	400	1.230	400	1.591	01.3	1.787	01.3
7	1.592								

Caption for the tables.

d_{obs} = observed d - spacings.

d_{cal} = calculated d-spacings

For h.c.p. Gd*, a = 5.770, c = 3.627 Å

For h.c.p. Tb , a = 5.686, c = 3.599 Å

For h.c.p. Dy, a = 5.642, c = 3.586 Å

For h.c.p. Ho, a = 5.616, c = 3.572 Å

For h.c.p. Er, a = 5.582, c = 3.554 Å

For b.c.c. Gd_2O_3, a_o = 10.79Å

For b.c.c. Tb_2O_3, a_o = 10.70Å

* Taylor (1970)

Table 36.

t = 200Å, gadolinium dihydride film trated with H_2 when converted to h.c.p. GdH_3.

Ring Nos.	d_{obs}	GdH_2 f.c.c.		Gd h.c.p.		GdH_3 h.c.p.		Gd_2O_3 b.c.c.	
		d_{cal}	hkl	d_{cal}	hk.l	d_{cal}	hk.l	d_{cal}	hkl
1	4.407	3.062	111	3.135	01.0	3.356	00.2	7.631	110
2	3.358	2.651	200	2.886	00.2	3.224	01.0	5.393	200
3	3.226	1.873	220	2.761	01.1	2.901	01.1	4.404	211
4	2.902	1.604	311	2.143	01.2	2.328	01.2	3.812	220
5	2.652	1.536	222	1.816	11.0	1.862	11.0	3.418 3.119	310 222
6	2.329	1.322	400	1.631	01.3	1.831	01.3	2.885 2.690	321 400
7	2.127							2.544 2.410	411 420
8	1.863							2.205 2.126	422 510

Caption for the table.

For GdH_3 , a = 3.73 , c = 6.71

APPENDIX 2

Table 8.1

Thickness of the films (Å)	Temperature coefficient of resistance /°K over the range 293-353°K
150	0.000123
250	0.000148
300	0.000136
500	0.000123
700	0.000110
1000	0.00010

Table 8.3

Thickness of the films (Å)	Temperature coefficient of resistance /°K over the range 293-353°K.
150	0.00021
230	0.00022
300	0.00024
500	0.00023
700	0.00022
950	0.00018

Table 8.5

Thickness of the films (Å)	Temperature coefficient of resistance /°K over the range (293-323°K.
150	0.00034
200	0.00038
300	0.00033
700	0.00021
900	0.00021

Table 8.2.

Thickness of the film in (Å)	Resistivity at room temperature before treating with H_2 ($\mu\Omega$-cm)	Resistivity when the films were heated in H_2 for 2 hours at 300°C ($\mu\Omega$-cm)	Resistivity when the hydrogen treated films were kept overnight in vacuo ($\mu\Omega$-cm)	Temperature coefficient of resistance /°K of GdH_3 over the temperature range (293-353°K)
150	133	10,213	10,362	-0.000360
200	122	10,198	10,351	-0.000299
250	112	10,186	10,337	-0.000302

Table 8.4.

Thickness of the film(Å)	Resistivity at room temperature before treating with H_2 ($\mu\Omega$-cm)	Resistivity when the films were heated in H_2 for 2 hours at 300°C ($\mu\Omega$-cm)	Resistivity when the hydrogen treated films were kept overnight in vacuo ($\mu\Omega$-cm)	TCR of TbH_3 /°K over the range 293 - 353°K
150	115	10,078	10,226	-0.000310
200	104	10,059	10,208	-0.000318
230	97	10,045	10,192	-0.000338

Table 8.6.

Thickness of the film (Å)	Resistivity at room temperature before treating with hydrogen ($\mu\Omega$-cm)	Resistivity when the films were heated in H_2 for 2 hours at 300°C ($\mu\Omega$-cm)	Resistivity when the hydrogen treated films were kept overnight in vacuo ($\mu\Omega$-cm)	TCR of DyH_3 /°K over the range (293-353°K)
150	95	10,287	10,434	-0.000288
200	85	10,267	10,412	-0.000293

Table 8.7.

Thickness of the films (Å)	Temperature coefficient of resistence /°K over the range 293-353°K
150	0.00044
200	0.00045
300	0.00043
700	0.00036
900	0.00035

Table 8.9.

Thickness of the films (Å)	Temperature coefficient of resistence /°K over the range (293-353°K)
150	0.00036
200	0.00035
250	0.00037
700	0.00032
900	0.00030

Table 8.8.

Thickness of the films (Å)	Resistivity at room temperature before treating with H_2 ($\mu\Omega$-cm)	Resistivity when the films were heated in H_2 for 2 hours at 300°C ($\mu\Omega$-cm)	Resistivity when the hydrogen treated films were kept overnight in vacuo ($\mu\Omega$-cm)	TCR /°K of MoH_3 over the range (293-353°K
150	65	10,247	10,392	-0.000297
200	56	10,239	10,385	-0.000312

Table 8.10.

Thickness of the film in (Å)	Resistivity at room temperature before treating with H_2 ($\mu\Omega$-cm)	Resistivity when the films were heated in H_2 for 2 hours at 300°C ($\mu\Omega$-cm)	Resistivity when the hydrogen treated films were kept overnight in vacuo ($\mu\Omega$-cm)	TCR /°K over the range 293-353°K
L50	90	10,119	10,265	-0.00031
200	81	10,102	10,249	-0.00032